Mikel De Prada Gil

Design, operation and control of novel electrical concepts for offshore wind power plants

Design, operation and control of novel electrical concepts for offshore wind power plants

Mikel De Prada Gil

PhD Thesis

Barcelona, June 2014

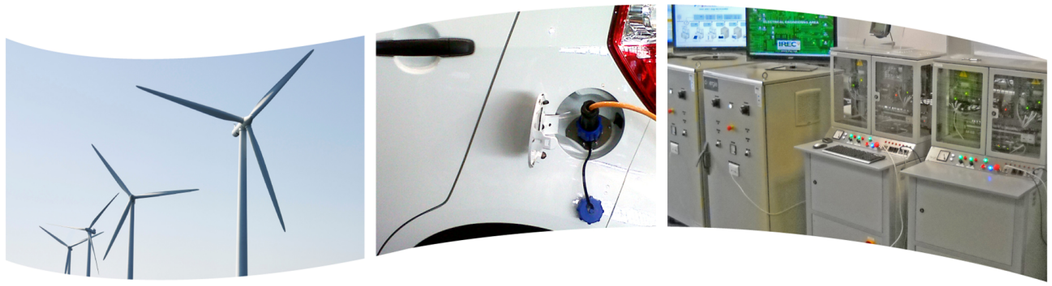

Electrical Engineering Department

UNIVERSITAT POLITÈCNICA DE CATALUNYA

Institut de Recerca en Energia de Catalunya

Catalonia Institute for Energy Research

Universitat Politècnica de Catalunya
Electrical Engineering Department

Institut de Recerca en Energia de Catalunya
Catalonia Institute for Energy Research

PhD Thesis

Design, operation and control of novel electrical concepts for offshore wind power plants

Author: **Mikel de Prada Gil**

Advisors: **Dr. Andreas Sumper**

Dr. Oriol Gomis–Bellmunt

Barcelona, April 2014

Catalonia Institute for Energy Research (IREC)
Electrical Engineering Research Area
Jardins de les Dones de Negre 1 2nd floor,
08930 Sant Adrià de Besòs, Barcelona, Spain

Printed in Barcelona by CPET, S.L.
First Print, April 2014

UNIVERSITAT POLITÈCNICA DE CATALUNYA
BARCELONATECH
Escola de Doctorat

Acta de qualificació de tesi doctoral

Curs acadèmic:

Nom i cognoms

Programa de doctorat

Unitat estructural responsable del programa

Resolució del Tribunal

Reunit el Tribunal designat a l'efecte, el doctorand / la doctoranda exposa el tema de la seva tesi doctoral titulada _____ _____.

Acabada la lectura i després de donar resposta a les qüestions formulades pels membres titulars del tribunal, aquest atorga la qualificació:

☐ NO APTE ☐ APROVAT ☐ NOTABLE ☐ EXCEL·LENT

(Nom, cognoms i signatura) President/a	(Nom, cognoms i signatura) Secretari/ària

(Nom, cognoms i signatura) Vocal	(Nom, cognoms i signatura) Vocal	(Nom, cognoms i signatura) Vocal

_____, _____ d'/de _____ de _____

El resultat de l'escrutini dels vots emesos pels membres titulars del tribunal, efectuat per l'Escola de Doctorat, a instància de la Comissió de Doctorat de la UPC, atorga la MENCIÓ CUM LAUDE:

☐ SÍ ☐ NO

(Nom, cognoms i signatura) Presidenta de la Comissió de Doctorat	(Nom, cognoms i signatura) Secretària de la Comissió de Doctorat

Barcelona, _____ d'/de _____ de _____

In memory of my father Enrique

Also to Valvanera, Victor and Merche

Abstract

Offshore wind is an emerging energy sector with a huge potential to be exploited in the near future. Offshore Wind Power Plants (OWPPs) are becoming increasingly relevant in Europe and worldwide due to several reasons such as the progressive saturation of propitious onshore sites (mainly in Europe), the lower visual and noise impact than their onshore counterparts and because the wind speeds are potentially higher and smoother at sea, which leads to higher wind power generation. Moreover, OWPPs have less space limitations constraints, so that it allows the possibility of using larger wind turbines.

The current trend points to significantly larger future offshore wind projects located further from shore forced by environmental and social aspects. Several studies have demonstrated that if the distance between an OWPP and its grid connection point at the Point of Common Coupling (PCC) exceeds a certain critical distance (approximately 55–70 km), HVDC transmission becomes a preferred solution over HVAC, since reduce cable energy losses and decrease reactive power requirements.

This trend towards increasing the OWPP size and its distance to shore is posing some technical, economic and political challenges that must be overcome to be fully competitive in the longer term compared to other energy sources. Today, there is an important concern about reducing the current Levelised Cost Of Energy (LCOE) of offshore wind projects by improving system reliability and availability, reducing O&M costs and/or increasing energy generation.

This thesis aims to propose novel electrical wind power plant concepts

more cost–effective than the existing ones and to comprehensive analyse their technical and economic feasibility. Specific challenges related to the design, optimisation, modelling, operation and control of these new concepts are addressed. All the concepts presented throughout this thesis, are focused on the collector grid of an offshore wind power plant, which encompasses all the necessary equipment to collect the power generated by the wind turbines and to export it to the offshore transmission HVDC platform.

The first novel wind power plant concept assessed can be applied to either an onshore or offshore wind power plant with a MVAC collection grid connected to the grid through either an HVAC or HVDC transmission link, whilst the rest of the OWPP configurations analysed are motivated by the presence of HVDC technology and its ability to electrically decouple the offshore wind power plant from the onshore power system.

Thus, the first wind power plant concept evaluated consists in operating some specific wind turbines at a non–optimum point in order to reduce the wake effect within the collection grid and, therefore, to maximise the energy yield by the whole wind power plant during its lifetime of the installation.

The following three OWPP concepts analysed arise thanks to the opportunity provided by HVDC technology to operate the collection grid at variable frequency. Thus, the second proposed OWPP concept investigated is based on removing the individual power converter of each wind turbine and connecting a synchronous generator–based OWPP (or a wind turbine cluster) to a single large power converter which operates at variable frequency. Likewise, the third OWPP configuration assessed deals with (i) the optimisation of this aforementioned concept and (ii) the proposal of an hybrid MVAC/MVDC OWPP concept for the offshore collection grid. Regarding the fourth OWPP design, it consists of a DFIG–based OWPP with reduced power converters (approximately 5% of rated slip) connected to a single HVDC substation. This proposal is analysed both static and dynamically by means of simulations.

Finally, the last novel OWPP concept presented in this thesis deals with the analysis of an entire offshore wind power plant in DC, with the aim of reducing the losses both in the inter–array and the export cable(s).

In general terms, all the novel OWPP concepts analysed suggest a good potential to be applied to future offshore wind power plants by reducing in all the cases the LCOE in comparison with the existing offshore wind power plants.

Resumen

La energía eólica marina es un sector emergente que se encuentra en plena expansión. Múltiples circumstancias tales como que cada vez sea más díficil encontrar lugares propicios en tierra (principalmente en Europa) para la instalación de parques eólicos, que a medida que el parque se aleja de la costa el impacto visual y auditivo es menor y que en el mar el viento sopla con más intensidad y de una manera más constante que en tierra, lo cual posibilita obtener una mayor generación de energía eólica, han provocado que cada vez existan más parques eólicos marinos.

Hoy en día, factores medioambientales y sociales están obligando a construir los parques eólicos marinos cada vez más alejados de la costa y se espera que esta tendencia continúe en los próximos años. Varios estudios han demostrado que a partir de una cierta distancia crítica entre el parque eólico y su punto de conexión a tierra (aproximadamente 55–70 km), la transmisión mediante alta tensión en corriente continua (ATCC) resulta una opción más interesante que a través de una transmisión en alta tensión de corriente alterna (ATCA), ya que las pérdidas en los cables se ven reducidas, así como los requerimientos de potencia reactiva.

Esta tendencia hacia construir parques eólicos marinos cada vez mayores y a ubicarlos más alejados de la costa, supone el tener que resolver cierto retos técnicos, económicos y políticos a fin de poder ser más competitivos en el futuro en comparación con otras fuentes de generación de energía. Hoy en día, existe una importante preocupación por tratar de reducir el elevado coste actual de la energía para los proyectos de eólica marina a base de mejorar la fiabilidad y disponibilidad del sistema, reducir costes de

operación y mantenimiento y/o incrementar la generación de energía.

Esta tesis tiene como objetivo proponer conceptos eléctricos novedosos, aplicados a parques eólicos marinos, que resulten más rentables que los existentes actualmente. Asimismo, esta tesis pretende analizar de una manera exhaustiva la factibilidad, tanto técnica como económica, de dichos conceptos. Asuntos tales como el diseño, la optimización, el modelaje, la operación y el control son presentes en la tesis. El alcance del trabajo se focaliza en la zona colectora de un parque eólico y, por lo tanto, no se analiza, el sistema de transmisión ni su integración a la red. Dicha zona comprende todo el equipamiento necesario para recolectar la potencia generada por los aerogeneradores y transmitirla a la plataforma marina de ATCC.

El primer concepto innovador de parque eólico evaluado puede ser aplicado tanto en parques situados en tierra como en el mar, que tengan una red colectora interna de corriente alterna en media tensión (MTCA) y un sistema de transmisión tanto ATCC o ATCA. Respecto al resto de configuraciones presentadas, stas vienen motivadas por la presencia de la tecnología ATCC y su capacidad para desacoplar eléctricamente la red interna del parque eólico del sistema eléctrico de potencia situado en tierra.

Así pues, la primera propuesta de parque eólico a analizar consiste en operar algunas máquinas concretas por debajo de su punto óptimo de operación a fin de poder reducir el efecto estela dentro del parque y poder así maximizar la potencia total extraída por el mismo.

Las tres siguientes configuraciones de parque analizadas se fundamentan en la posibilidad que ofrece la tecnología ATCC de poder operar la red interna del parque eólico a una frecuencia variable. En base a este nuevo concepto, la segunda propuesta de parque investigada consiste en prescindir de los convertidores individuales de cada turbina y conectar todos los generadores síncronos del parque eólico (o un simple grupo de máquinas) directamente al convertidor central, el cual opera a frecuencia variable. El tercer diseño de parque eólico se basa en una topología híbrida dentro del parque combinado MTCA y MTCC. Esta configuración surge de optimizar la propuesta anterior de parque eólico. Asimismo, la cuarta propuesta a analizar estudia la posibilidad de tener un parque consistente en generadores de inducción doblemente alimentados conectados a un convertidor común de tensión controlada situado en la plataforma marina, en el cual los convertidores de cada máquina sean de un tamaño menor a lo habitual (aproximadamente a un deslizamiento nominal de un 5%). Este sistema es analizado en detalle tanto estática como dinámicamente.

Finalmente, el último concepto que se presenta en esta tesis analiza la posibilidad de considerar un parque eólico marino completamente (trans-

misión y red interna del parque) constituido mediante tecnologa en CC, con el fin de poder reducir las pérdidas tanto en la red interna del parque como en el cable de exportación.

En términos generales se puede concluir que todos los conceptos propuestos a lo largo de esta tesis sugieren un gran potencial para poder ser aplicados en futuros parques eólicos marinos, ya que su coste de energía se ve reducido en comparación con los parques eólicos existentes hoy en día.

Acknowledgements

This work has been carried out at the Electrical Engineering Research Area (EERA) of Catalonia Institute for Energy Research (IREC). This thesis has been financially supported by IREC through the 01/10 WIND ENERGY grant.

First of all, I would like to express my sincere gratitude to my advisors Dr. Andreas Sumper and Dr. Oriol Gomis-Bellmunt for the supervision, guidance and support they gave me, as well as, for their always useful scientific and personal advices throughout this thesis. Also, I would like to say thank you to all my colleagues and ex–colleagues from IREC (Miguel C., Lluís, Emer, Ignasi, Manel, Ramon, Gerard, Alba, Manuel, Albert, Moussa, Oriol, Oscar, Joaquim, Anna, Rajai, Frieder, Miguel A., Carla and Santi) for their help and friendship. Specially, I am extremely grateful to José Luis, Francisco, Lucía, Cristina, Fernando, Jordi, David B., David L. and Lázaro for their invaluable support at all times and their always helpfulness and patience, and friendship as well.

Likewise, I would like to show my thankfulness to the people of National Renewable Energy Laboratory (NREL) and the University of Colorado Denver (UCD) by graciously welcoming me during my stay there and for giving me the opportunity to live this great experience. Specially, I greatly appreciated the help of Dr. Eduard Muljadi, Dr. Fernando Mancilla–David, Dr. Mohit Singh and Irving Paul Girsang. I could not forget to thank Deborah and Lili for their warm hospitality throughout my stay and for all the good times we spent together.

I would like to also acknowledge the support received by CITCEA–UPC and the collaboration of Alstom Wind during the first stage of this research.

Finally, I would like to thank my family for their continuous support and for giving me encouragement whenever I needed it. I would like to thank specially to Cesar and Gloria for their substantial help and to my mum Valvanera, my brother Victor and my girlfriend Merche for their infinite patience and support.

Contents

List of Tables

List of Figures

Acronyms

AIS	Air Insulated Switchgear
CAPEX	CAPital EXpenditures
CFD	Computational Fluid Dynamics
CPI	Consumer Price Index
DFIG	Doubly Fed Induction Generator
DICOPT	DIscrete and Continuous OPTimizer
ECMFW	European Centre for Medium Range Weather Forecasts
EEA	European Economic Area
EENS	Expected Energy Not Supplied
EIA	Energy International Agency
EPR	Ethylene propylene rubber
EWEA	European Wind Energy Association
FEED	Front End Engineering and Design
FRCWT	Full Rate Converter Wind Turbine
GAMS	General Algebraic Modeling System
GIS	Gas Insulated Switchgear
GSC	Grid Side Converter
HVAC	High Voltage Altern Current
HVDC	High Voltage Direct Current
LCC–HVDC	Line Commutated Converter–High Voltage Direct Current

LCOE	Levelised Cost Of Energy
LV	Low Voltage
MI	Mass Impregnated
MINLP	Mixed Integer Non Linear Programming
MMCC	Modular Multilevel Cascaded Converter
MPC	Multiple Power Converter
MPPT	Maximum Power Point Tracking
MTTR	Mean Time To Repair
MV	Medium Voltage
NREAP	National Renewable Energy Action Plan
NSTDA	Number of Standard Deviations Analysed
NWCA	Number of Wind Conditions Analysed
NWPPA	Number of Wind Power Plants Analysed
OWPP	Offshore Wind Power Plant
PCC	Point of Common Coupling
PMSG	Permanent Magnet Synchronous Generator
RSC	Rotor Side Converter
SCADA	Supervisory Control And Data Acquisition
SCIG	Squirrel Cage Induction Generator
SLPC–CF	Single Large Power Converter–Constant Frequency
SLPC–VF	Single Large Power Converter–Variable Frequency
SRA	Strategic Research Agenda
TPWind	European Wind Energy Technology Platform
VSC–HVDC	Voltage Source Converter–High Voltage Direct Current
WECS	Wind Energy Conversion System
WPP	Wind Power Plant
WRIG	Wound Rotor Induction Generator
WRSG	Wound Rotor Synchronous Generator
WT	Wind Turbine
XLPE	Cross Linked Polyethylene

1 Introduction

In the last decades, renewable energy have experienced significant growth worldwide mainly due to global environmental concern and a commitment by industrialized countries to meet binding targets for greenhouse gas emission reduction agreed under the Kyoto protocol [1]. In Europe, the decision of the Member States to commit to renewable energies has been reinforced by the 20–20–20 target set by the European Commission, which aims to reduce EU greenhouse gas emissions by 20% from 1990 levels, a 20% improvement in the EUs energy efficiency and to reach, at least, 20% of its energy consumption from renewable sources by 2020 [2].

These ambitious renewable energy targets are expected to be even higher beyond 2020. Looking at a long term scenario, the EU energy policy 2020–2050 aims to achieve 80–95% greenhouse gas emissions reductions by 2050 compared to 1990 levels, by moving to a zero–carbon power system, where a 100% of Europe's electricity is provided by renewable energy [3]. According to the strategic research agenda (SRA) set by the European Wind Energy Technology Platform (TPWind), wind energy will play a decisive role in order to meet this challenge [4].

Wind energy is one of the fastest growing resources for electricity generation in recent years. According to [5], global cumulative installed wind capacity grew from 6.1 GW in 1996 to 318.137 GW at the end of 2013. This remarkable growth has led to wind power sector playing an increasingly important role in the energy mix. Nowadays, the wind power generation capacity all over the world is enough to cover almost 4% of the global electricity demand [6] and in some countries such as Denmark, Portugal or Spain, wind power penetration level is particulary noteworthy (Denmark 30%, Portugal

20% and Spain 16.3%, by the end of 2012 [7]).

Offshore wind is a promising energy source which has attracted worldwide attention in recent years as a consequence of various circumstances, such as the lack of available onshore locations (mainly in Europe), the potentially higher and more constant wind speeds at sea than their onshore counterparts (enabling a greater wind power generation) and the fact that space limitations offshore are a less critical issue than inland, which allows the possibility of using larger wind turbines [8, 9]. Figure 1.1 depicts the wind speeds in European Economic Area (EEA) countries, based on data reported in [10].

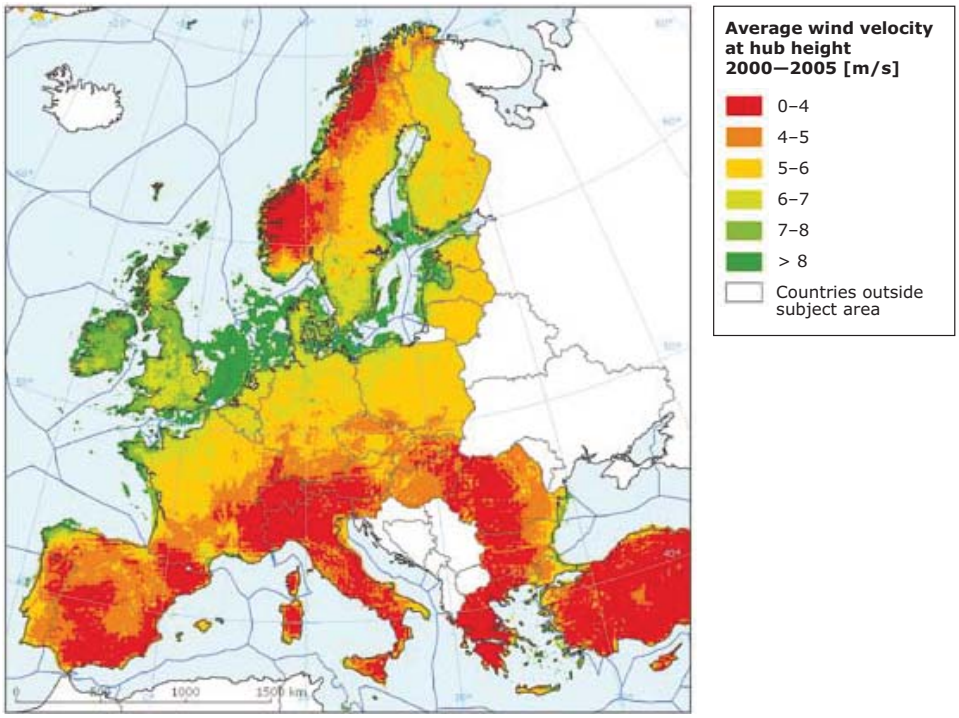

Figure 1.1: European Centre for Medium–Range Weather Forecasts (ECMFW) wind field data after correction for orography and local roughness (80 m onshore, 120 m offshore) [10].

To date, Europe (especially the UK) is the world leader in offshore wind power, accounting for approximately 90% of the global cumulative installed offshore wind capacity [6]. Figure 1.2 shows both cumulative and annual offshore wind installations in Europe from 1993 to end of 2013 [11].

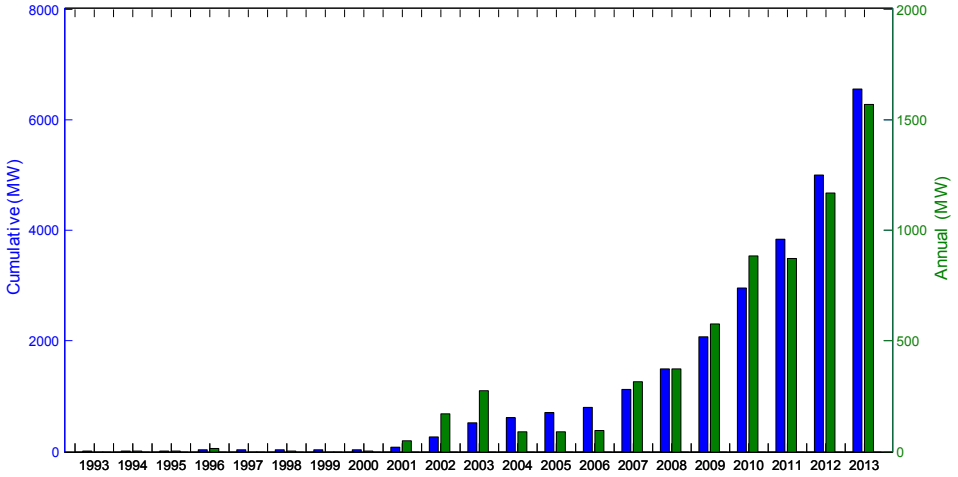

Figure 1.2: Cumulative and annual offshore wind installations in EU [11].

As it can be noted, cumulative offshore wind capacity at the end of 2013 reached 6562 MW, which would be enough to cover up to 0.7% of European electricity consumption in a normal wind year [11]. Although this figure is still far from reaching onshore wind sector and it is lagging slightly behind the objectives set by EU Member States in their National Renewable Energy Action Plans (NREAPs) [6], a substantial growth of offshore wind is expected to be seen as a result of the ambitious targets intended to be carried out not only by Europe but also by China, Japan, Korea and USA [9, 12]. In particular, EWEA forecasts that by 2020, 40 GW offshore wind capacity could be operational in European waters and that by 2030 it could reach 150 GW, meeting 14% of the EUs total electricity consumption [13].

Thus far, most of the existing offshore wind farms are of a relatively small up to medium sized rating (up to few hundreds MW), and are close enough to the shore that it is feasible transmit the power through HVAC submarine cables. However, offshore wind farms are increasingly larger in size and located further away from shore, forced by environmental and social aspects, which is leading towards the utilization of HVDC technology. Several studies have demonstrated that if the distance between an offshore wind farm and its grid connection point at the Point of Common Coupling (PCC) exceeds a certain critical distance (approximately between the range of 55-70 km depending on the power ratings of the wind farm), HVDC transmission becomes the most suitable solution, since it reduces cable energy losses and decreases reactive power requirements [14–16].

The higher penetration of wind power into the utility networks have encouraged the use of power electronic converters, in order to smooth the operational concerns that may arise due to the intermittent nature of wind and to facilitate the grid integration of Wind Energy Conversion Systems (WECS) [17–23]. Thereby, power converters play a very important role as an enabling technology to operate at variable speeds [24–27], providing more effective energy capture than their fixed speed counterparts [28,29]. In addition, the inclusion of power converters as an interface between the generator and the AC grid has enabled wind farms to operate similarly as conventional generation units do. Thus, wind power facilities can be considered as wind power plants (WPPs) [20,30,31], so that they are capable not only to generate active power, but also to provide support for grid voltage [32,33] and frequency [34–36], hence contributing to power system stability [37–41]. For offshore wind applications, Voltage Source Converters VSC–HVDC are preferred over Line Commutated Converters LCC–HVDC as they can be connected to weak grids, since they do not rely on the AC system to support their operation and they have less filter requirements, enabling a reduction in the size of the substation [42, 43]. Table 1.1 presents various examples of offshore wind projects with VSC–HVDC technology. As it is shown, the Modular Multilevel Cascaded Converter (MMCC) topology is the most employed option for grid connection of OWPPs with VSC–HVDC, since it results in a very small harmonic content and low filter requirements by using multiple switching modules which synthesise a high quality sinusoidal voltage waveform [44].

Table 1.1: Overview of offshore wind projects with VSC–HVDC [44, 45].

OWPP name	**Installation year**	**Manufacturer**	**Capacity (MW)**	**Converter topology**
BorWin 1	2009	ABB	400	2–level
BorWin 2	2013	Siemens	800	MMCC
HelWin 1	2013	Siemens	576	MMCC
DolWin 1	2013	ABB	800	MMCC
SylWin 1	2014	Siemens	864	MMCC
HelWin 2	2015	Siemens	800	MMCC
DolWin 2	2015	ABB	900	MMCC
DolWin 3	2017	Alstom	800	MMCC

The trend towards constructing larger wind turbines and locating the offshore wind power plants (OWPPs) increasingly further from shore (which usually leads to deeper waters) is posing technical, economic and political challenges that must be overcome to be fully competitive in the longer term

compared to other types of electricity generation. According to [46], the current Levelised Cost Of Energy (LCOE) for offshore wind power is estimated to be between 119 and 194 €/MWh, whilst for onshore wind it ranges from 45 and 107 €/MWh. These figures highlights the necessity for cost reduction, which can be achieved, inter alia, through a commitment from government and industry to encourage the planning and development tasks carried out in the early stage of any offshore wind project. An important task within all these activities corresponds to electrical OWPP design. This aims to reduce LCOE by improving system reliability and availability, reducing O&M costs and/or increasing energy generation.

1.1 Research motivations and objectives

Today, academic researchers and industry investigate new wind power plant designs seeking for more cost–effective alternatives and aiming to acquire a more competitive offshore wind energy sector within the electricity market [47–61].

One possible approach in the attempt of reducing the LCOE is to step up the voltage level in the OWPP collection grid from the conventional 33–36 kV to 48 kV [62] or 66–72 kV [62–65]. Thereby, the overall losses of the system are reduced (especially important as the number and rated power of wind turbines increase) whilst the cost of the components (in general terms) becomes more expensive. Likewise, taking advantage of HVDC technology and its ability to electrically decouple the OWPP from the onshore power system, other innovative concepts can be recently considered. The main objective of this thesis is to propose novel electrical designs for wind power plants more cost–effective than the existing ones and to comprehensively analyse their technical and economic feasibility. Specific challenges related to the design, optimisation, modelling, operation and control of these new concepts will be addressed in this thesis. All these novel topologies, except for the one presented in Chapter 3, are motivated by the presence of HVDC transmission systems for offshore wind power plants and its allowance to operate the wind power plant collection grid out of synchronism with the onshore electrical network (50 or 60 Hz). In the following, the specific goals of all the different innovative concepts evaluated throughout this thesis are summarized.

- To analyse the potential benefit of operating some wind turbines at a non–optimum point in the attempt of reducing the wake effect within a wind power plant, such that its total power output is maximised.

- To thoroughly assess the technical and economic feasibility (considering both the capital expenditures, CAPEX, and the operational and maintenance, O&M, energy costs) of a proposed WPP concept based on removing the individual power converter of each wind turbine and connecting a synchronous generator based WPP (or a wind turbine cluster) to a Single Large Power Converter which operates at Variable Frequency (SLPC–VF). Thereby, an unique VSC-HVDC converter is in charge of controlling the whole offshore wind power plant (or the WT cluster) and all the wind turbines operate at the same electrical frequency, which is dynamically changed.

- To investigate the influence of wind speed variability within the wind power plant, wind direction and wind farm size on power generation efficiency analysis of the SLPC–VF concept.

- To find the optimal design that minimises the total cost of a proposed hybrid AC–DC OWPP topology. This hybrid concept is based on the SLPC–VF design, but with the difference that the WPP is composed by several wind turbine clusters, so that each cluster is controlled by its respective power converter which operates at variable frequency in order to optimise its power generation. Thus, the optimisation model aims to determine the optimal number of power converters and offshore platforms needed, as well as their locations. In addition, the cable route connecting the wind turbines between each other is also intended to be optimised.

- To evaluate the impact of power converter size and wind speed diversity among turbines on wind power plant energy generation efficiency of a proposed WPP configuration which combines DFIG wind turbines with reduced size power converters and a single large VSC–HVDC converter which operates at variable frequency.

- To develop a coordinated control between the VSC–HVDC converter and the reduced back–to–back power electronic converters of each DFIG–based wind turbine in order to optimise its operation and to provide control capability for the wind power plant at a reduced cost.

- To analyse from the static and dynamic point of view the performance of this implemented control scheme.

- To carry out a technical and economic assessment of a new WPP configuration based on extending the DC nature of the high voltage

transmission to the collection grid and to consider the possibility of having an entire OWPP in DC.

1.2 Scope of the thesis and limitations

Aside from the novel control strategy for OWPPs presented in Chapter 3, which is addressed to the conventional WPP scheme, all the proposed innovative offshore wind power plants designs are based on the existence of VSC–HVDC transmission systems and the opportunity to modify the frequency or to use DC technology within the offshore collection grids. Although HVDC is the main trigger of this thesis, it is not based on HVDC technology itself but on the novel concepts designed for offshore wind power plants. This thesis focuses on the design and analysis of all these concepts within the WPP collection grid and does not consider grid integration and transmission aspects. Relevant issues such as stability, protection, interaction with the mechanical system, control and experimental implementation are out of the scope.

1.3 Thesis contributions

The main contributions of the thesis are summarized below along with their associated publications:

- A new concept for WPP operation based on operating the appropriate wind turbines at non–optimum points and reducing, therefore, the wake effect within the WPP, that maximizes its total power generated. Thereby, the energy yield by the WPP over its lifetime is increased compared to that obtained by operating the WPP using the conventional control strategy (which aims to maximise each individual turbine according to a MPPT approach) [J7].
- A new tool (described in Appendix B) targeted to analyse, from the technical and economic point of view, the cost–effectiveness of the proposed WPP concept presented in Chapter 4 in comparison with the conventional WPP design. The tool includes a comprehensive wake model considering single, partial and multiple wakes for any wind power plant layout and any wind conditions (wind speeds and directions) and it has been used not only in Chapter 4, but also in Chapters 3, 6 and 7. Besides, the tool considers variable frequency operation within the WPP collection grid (optimising its value depending on the

wind conditions) and takes into account both the steady state losses and the corrective and preventive maintenance losses for the technical analysis [J1, J2, J3, C1 and C4].

- A technical and economic assessment to quantify the possible benefit of the proposed SLPC–VF concept compared to a conventional WPP configuration. Likewise, the influence of the wind speed variability, wind direction and wind power plant layout on the power generation efficiency of the proposed WPP design, is also analysed [J1, J2, J3 and C1].

- The optimisation performed on the proposed hybrid AC/DC WPP concept presented in Chapter 5 and formulated as a MINLP problem. The model outputs the optimum number of both power converters and offshore collector platforms needed, their location, as well as, the optimum cable routing among wind turbines to minimise the total cost of the WPP [J4].

- A static and dynamic analysis of the proposed WPP concept based on reducing the power converter size of DFIG wind turbines connected to a single large VSC–HVDC operated at variable frequency. Moreover, the implementation of a coordinated control between the VSC–HVDC converter (centralised control) and the reduced power converters (5% of rated slip) of each DFIG–based wind turbines (local control) [C2 and J6].

- A technical and economic evaluation of considering an entire DC offshore wind power plant, i.e., not only the HVDC transmission but also the MVDC collection grid. Due to the uncertainty of DC technology, In addition, the sensitivity analysis carried out taking into consideration various parameters which may affect the technical and economic feasibility of DC OWPPs, for example, DC equipment efficiencies, DC component cost, OWPP rated power or export cable length [J5 and C3].

The publications indicated above are listed in Appendix A.

1.4 Thesis outline

This thesis has been divided into eight chapters organized as follows:

- **Chapter 2** presents a general overview about offshore wind power plants, focusing on its collection grid. The chapter includes a current status of OWPP projects in Europe, a brief description of the main components encompassed in a MVAC collection grid and an explanation of the OWPP electrical design methodology carried out during the planning and development tasks in the early stage of any offshore wind project.

- **Chapter 3** deals with the analysis of a new wind power plant design based on optimising the total power generated by the wind power plant, by operating some wind turbines at sub–optimum points and reducing the wake effect within the WPP.

- **Chapter 4** carries out a comprehensive technical and economic assessment of a novel WPP proposal consisting in removing the individual power converters of each wind turbine and connecting the entire WPP or a WT cluster to a Single Large Power Converter operated at Variable Frequency (SLPC–VF concept). This analysis is performed by using a new tool implemented for that purpose and detailed in Appendix B.

- **Chapter 5** proposes an AC/DC hybrid wind power plant concept and presents a MINLP optimisation model which aims to determine its optimal WPP design in terms of cost.

- **Chapter 6** is divided into two parts. In the first part of the chapter, the influence of power converter size and wind speed diversity within the wind power plant on the power extraction efficiency is evaluated from the static analysis point of view. In the second part, a coordinated control between the VSC–HVDC converter and the individual converters of each wind turbine is implemented. The dynamic performance of this novel WPP design is assessed by means of simulations and the results are compared to those obtained from the static analysis.

- **Chapter 7** assess the technical and economic feasibility of considering an entire wind power plant (transmission and collection grid) using DC technologies. The analysis is carried out for different wind power plant power ratings and different export cable lengths.

- Finally, some conclusions and future research lines arising from the thesis are drawn in **Chapter 8**.

In general terms, all the novel concepts presented throughout the thesis are addressed to the following OWPP schemes:

- OWPP with a MVAC collection grid and an HVAC or HVDC transmission link to shore (**Chapters 2 and 3**),
- OWPP with a MVAC collection grid and an HVDC transmission link to shore (**Chapters 4**, **5** and **6**),
- and OWPP with a MVDC collection grid and an HVDC transmission link to shore (**Chapter 7**).

1.5 PhD related work and activities

In this section, an overview of chronological PhD related work and activities that have been developed during this thesis are mentioned. Predoctoral activities started at April 2010 at the same time than a collaborative project with Alstom Wind, known as Windlider 2, was launched. The work developed in this project was addressed to the modelling a control of the ECO100 wind turbine using the PSS/E software. Derived from this project, the [C2] conference paper listed in Appendix A was published. Once this project finished, the so–called IX3 collaborative project with Alstom Wind began. The work performed for this project involved the development of heuristic algorithms to optimise the reactive power management within a wind farm. Meanwhile, the work carried out for the thesis evolved into the publication of two journal articles [J1] and [J2] and one conference paper [C1] related to energy capture analysis of wind power plants. From April 2012 to July 2012, the research stage in Denver CO (USA) at the National Renewable Energy Laboratory (NREL) and the University of Colorado Denver (UCD) took place. Throughout this period, the contribution of Type–2 wind turbines to sub–synchronous resonance (SSR) damping was investigated. One journal article [O4] and one conference paper [O2] arose from this research. Then, two more projects, Vendaval II (Alstom Wind) and KIC–OffWindTech (KIC InnoEnergy), were carried out. These collaborative projects resulted in the publication of the following three conference articles: [O1], [C3] (Vendaval II) and [O3] (KIC–OffWindTech). Vendaval II aimed to perform the Alstom Wind's roadmap and design of DC wind power plants, whilst the main objective of the KIC–OffWindTech project was to integrate four different tools developed by four partners (IREC, KUL, Tecnalia and TU/e) related to offshore wind integration into the utility network. During the last year of this thesis (2013–2014), five journal articles [J3], [J4], [J5], [J6] and [J7] and one

conference paper [O4] have been elaborated. Besides, this academic work has been combined with the participation in the project called Vendaval III, based on the design of a modular power converter of AC and DC wind power plants. Finally, I am coauthor of the patent application [P1] entitled "Harmonics mitigation in multiphase generator–conversion systems" arose from the Vendaval II project.

2 Offshore wind power plants

The aim of this chapter is to provide a general overview about offshore wind power plants, focusing on its collection grid area. First, the current status of the main offshore wind energy projects worldwide is presented. Then, a brief description of the main components encompassed within an MVAC collection grid is introduced. Likewise, the most common electrical connection designs for collection grids considered thus far, are shown. Finally, this chapter deals with the description of the electrical design performed in the conventional offshore wind power plants. Thus, the offshore platform electrical design of AC OWPPs connected with both HVAC and HVDC transmission systems is detailed, as well as, the current OWPP design methodology carried out during the planning and development tasks, is explained. The methodology focuses on explaining in detail the cable selection process and the technical assessment performed for an OWPP consisting of an AC collection grid and an HVDC transmission link to shore.

2.1 Current status of offshore wind energy projects

In the following, the current status of offshore wind power plant projects is presented. To date, Europe is leading the offshore wind energy market accounting for more than 90% of the worlds installed offshore wind capacity [8]. However, other non–European countries such as China and Japan are starting to play an important role in offshore wind owning an installed capacity of 389.6 MW and 25.3 MW, respectively [6]. Table 2.1 shows the cumulative offshore wind power plant installed capacity of 11 European countries

at the end of 2013, while Table 2.2 indicates the status of 22 offshore wind installations in Europe during 2013. Both tables refer to current statistics reported in [11].

Table 2.1: Cumulative installed capacity of European offshore wind power plants at the end of 2013 [11].

Country	**No. of OWPPs**	**No. of WTs**	**Capacity installed (MW)**
United Kingdom	23	1082	3681
Denmark	12	513	1271
Germany	13	116	520
Sweden	6	91	212
Belgium	5	135	571
Netherlands	4	124	247
Finland	2	9	26
Ireland	1	7	25
Norway	1	1	2
Spain	1	1	5
Portugal	1	1	2
TOTAL	**69**	**2080**	**6562**

Table 2.2: Summary of work carried out at European offshore wind power plants during 2013 [11].

OWPP name	**Country**	**Capacity (MW)**	**Status**
Thornton Bank II + III	Belgium	288	Fully grid connected
London Array	United Kingdom	630	Fully grid connected
Belwind Alstom demo	Belgium	6	Fully grid connected
Anholt	Denmark	400	Fully grid connected
Lincs	United Kingdom	270	Fully grid connected
BARD offshore 1	Germany	400	Fully grid connected
Karehamn	Sweden	48	Fully grid connected
Arinaga Quay (Demo)	Spain	5	Fully grid connected
Gunfleet Sands 3 (Demo)	United Kingdom	12	Fully grid connected
Teesside	United Kingdom	62	Fully grid connected
Northwind	Belgium	216	Partially completed
Gwynt y Mor	United Kingdom	576	Partially completed
West of Duddon Sands	United Kingdom	389	Turbines installed
Methil Demo	United Kingdom	7	Turbines installed
Riffgat	Germany	108	Turbines installed
Meerwind sud/ost	Germany	288	Turbines installed
Borkum West 2.1	Germany	200	Turbines installed
Humber Gateway	United Kingdom	219	Foundations installed
Baltic 2	Germany	288	Foundations installed
DanTysk	Germany	288	Foundations installed
Nordsee ost	Germany	295	Foundations installed
Global tech 1	Germany	400	Foundations installed

As it can be seen, the total installed capacity at the end of 2013 reached 6.562 MW, producing 24 TWh in a normal wind year. These figures cover 0.7% of the Europes total electricity consumption [11].

2.2 Components description within the AC offshore collection grid

Figure 2.1 shows the layout of the well–known Horns Rev offshore wind farm located in the North Sea (in Denmark). The dashed line delimits the area known as offshore collection grid. In this section, a brief description of the main components encompassed within an AC offshore collection grid, is presented.

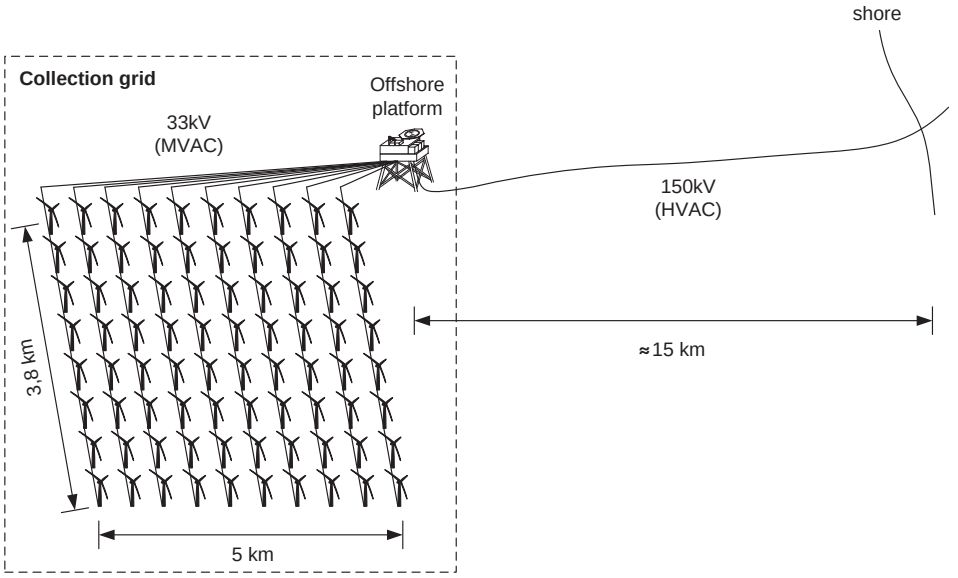

Figure 2.1: Horns Rev offshore wind farm layout.

2.2.1 Wind turbine types

To date, the most commonly applied wind turbine configurations can be mainly classified into the following four types, according to their ability to control speed [17]:

- Type A: fixed speed wind turbine
- Type B: Partial variable speed wind turbine
- Type C: Variable speed wind turbine with partial rate converter
- Type D: Variable speed wind turbine with full rate converter

The last two concepts associated to variable speed operation are leading the wind turbine market today.

Type A: Fixed speed wind turbine

Figure 2.2 shows a fixed speed wind turbine. It consists of a Squirrel Cage Induction Generator (SCIG) connected directly to the grid by means of a LV/MV transformer. A capacitor bank is usually provided to compensate the need of the SCIG to absorb reactive power from the electrical network to be magnetized. It generally also contains a thyristor–based soft starter to smooth the grid connection of the machine by reducing the large currents that occur when it is started–up. Regarding its power limiting system implemented this wind turbine configuration can be classified in passive or active stall and pitch [17].

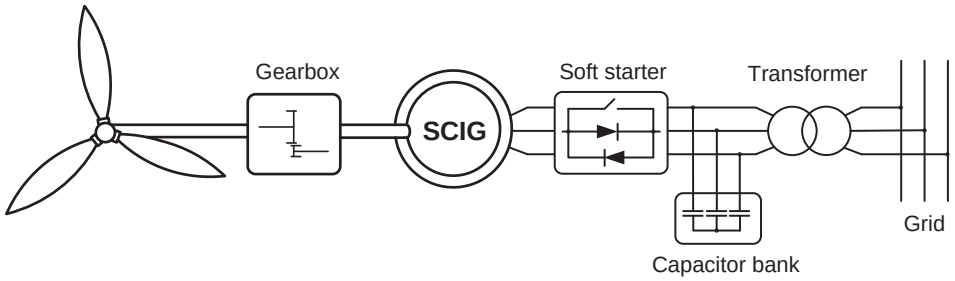

Figure 2.2: Fixed speed wind turbine with SCIG.

The main advantages of Type A wind turbine are its relatively low production costs, its robustness and reliability and its simplicity in terms of control and construction [66]. These propitious features became it so popular during the 1980s and 1990s [17]. However, the fixed speed wind turbine configuration presents some main drawbacks. Firstly, this wind turbine type operates at a constant speed determined by the frequency of the supply grid, the gearbox ratio and the generator design. Thereby, maximum power generation can only be achieved at the one particular wind speed for which the turbine has been designed for. Secondly, this fixed speed operation coupled with the fluctuant behavior of the wind brings about mechanical stress in the rotor shaft which can lead to possible failures of the drive train and undesirable power fluctuations on the electrical grid. Moreover, other disadvantage of fixed speed wind turbines is its inability to provide voltage and frequency support to the grid and fault ride through capability.

Type B: Partial variable speed wind turbine

Figure 2.3 shows the Type–2 wind turbine model employing a Wound Rotor Induction Generator (WRIG) with an external rotor resistance (R_{ext}) connected to the rotor winding terminals by means of power converter and the stator directly connected to the grid. As previous Type A wind turbine, it usually includes a bank capacitor and a soft starter for reactive power compensation requirements and a smoother grid connection, respectively.

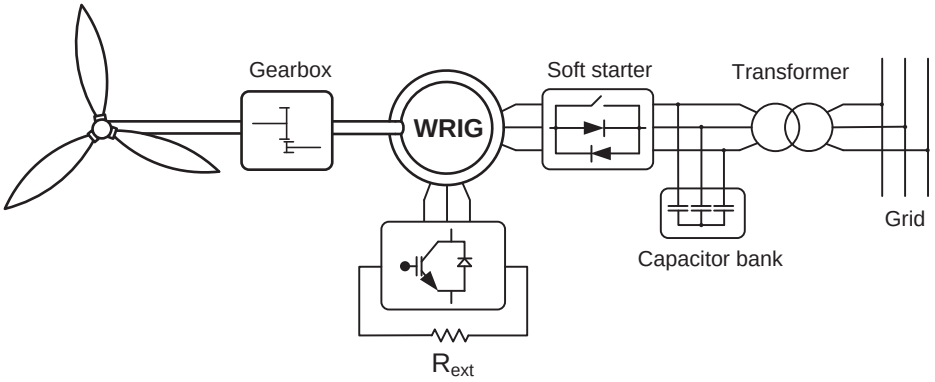

Figure 2.3: Partial variable speed wind turbine with WRIG and adjustable external rotor resistance.

This technology, commercialized under the name of Optislip by the Danish manufacturer Vestas, are capable to regulate a slip range of 0–10% above synchronous speed by adjusting the external rotor resistance. This range is limited by the excessive power that is dissipated in the external resistor. Thus, these wind turbines partially improve their power extraction efficiency and can help to enhance power quality. Nevertheless, they still have mainly the same drawbacks as the fixed speed concept.

Type C: Variable speed wind turbine with partial rate converter

The Type C wind turbine, also known as Doubly Fed Induction Generator (DFIG), consists of a WRIG with the stator windings connected to the grid by means of a step–up transformer and the rotor connected through a power converter (rated at approximately 30% of the nominal power of the generator), as it is shown in Figure 2.4. In this case, the reactive power compensation and the smoother grid connection is performed by the back–to–back converter.

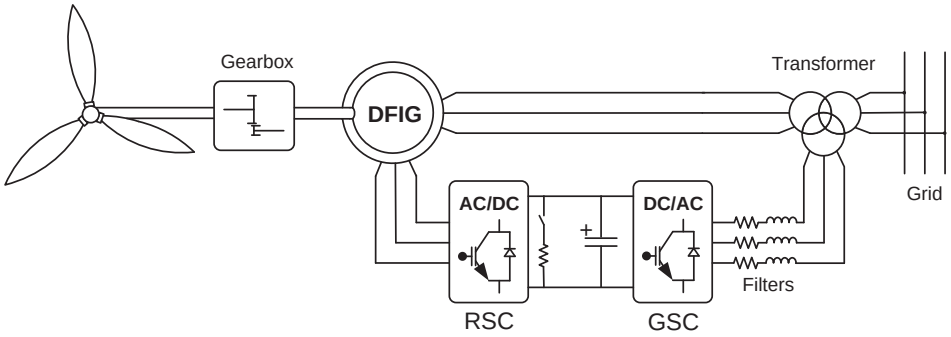

Figure 2.4: Variable speed wind turbine with DFIG.

This configuration allows to control the machine in a wider speed range than the Type B wind turbine (typically from -40% to 30% of the synchronous speed), so that the power flow through the rotor can be bidirectional. Below synchronous speed, the rotor power flows from the grid to the rotor winding, whilst above synchronous speed the rotor power flows from the rotor winding to the grid. Although this wind turbine type can contribute to the power system stability enhancement by providing ancillary services to the grid, the fact that the stator winding is directly connected to the grid complicates a proper ride through operation in the case of grid faults [17]. Likewise, the other main drawback of this wind turbine concept is the need to use slip rings to extract the power from the rotor, since these are the possible causes of machine operation failures [17].

Type D: Variable speed wind turbine with full rate converter

Figures 2.5(a) and 2.5(b) show two different configurations of Type D wind turbines, also known as Full Rate Converter Wind Turbines (FRCWT). In both cases, the generator is connected to the grid by means of a full rate power converter, which electrically decouples the machine from the grid. This concept can be implemented either by employing a SCIG (Figure 2.5(a)) or by using a Permanent Magnet Synchronous Generator (PMSG) or a Wound Rotor Synchronous Generator (WRSG) without a gearbox obtaining a direct drive system (Figure 2.5(b)).

The advantage of this wind turbine type is that maximum power extraction efficiency can be achieved regardless of the wind speed by the inclusion of the full power converter. Moreover, voltage and frequency support, as well as fault ride through capability, can be provided by a proper control of

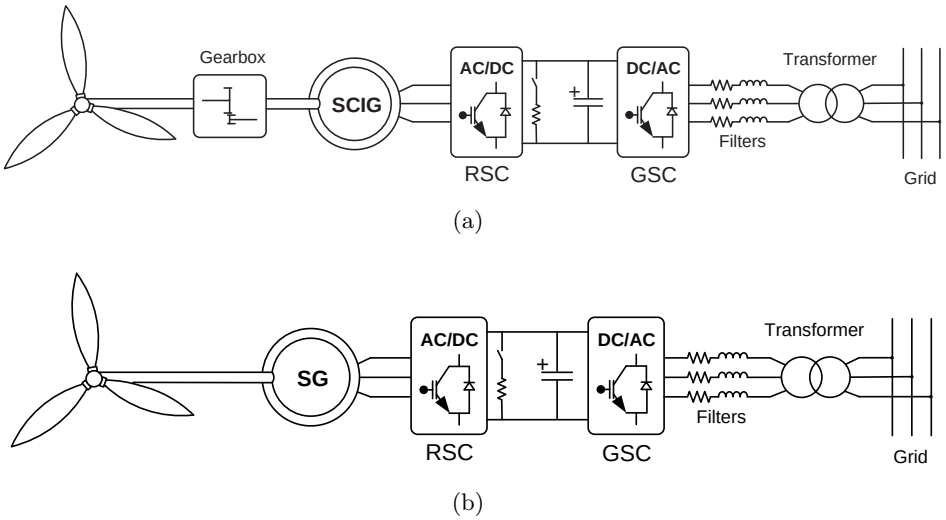

Figure 2.5: Variable speed wind turbine with full rate converter SCIG (a) and direct drive SG (b).

the converter. However, the main drawback refers to its high cost because of the full rate converter.

2.2.2 Submarine cables

In general terms, AC cables can be classified in single core and three core cables (Figure 2.6). The former refers to three single cables (one per phase) separated by a certain distance from each other. The latter consist of three insulated cores bundled together in trefoil configuration, made up of copper (usually) or aluminium (for cost and weight reduction but for small power ratings), all sharing a common over sheath and armouring. Three core cables have the advantage of presenting reduced power losses due to the cancellation of magnetic fields between three cores. In addition, these are considerably cheaper to install compared to single cables, since the cable is laid in only one instance and it does not require extra operations for laying fiber optical cable as it is possible to produce the cable with integrated communications. However, and despite sharing some components, the handling of three core cables is more difficult than installing three single core cables due to their greater weight [67]. Furthermore, other drawbacks of three core cable refer to the greater technical difficulty of making cable joints and the fact that a single failure occurred in a three core cable means to replace the damaged

cable with an entire new one instead of having to only substitute the single phase cable affected.

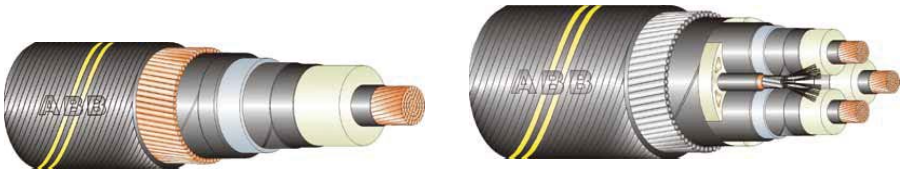

(a) (b)

Figure 2.6: (a) Single–core cable with lead sheath and wire armour. (b) Three–core cable with optic fibers, lead sheath and wire armour (courtesy of ABB).

Focusing only on the MVAC collection grid, the most common submarine cable technologies thus far are the extruded insulation cables. These cables are characterized by an insulation consisting of laminated ethylene propylene rubber (EPR) or cross–linked polyethylene (XLPE), unlike mass–impregnated (MI) cables whose insulation is based on impregnated paper tapes with a high viscosity compound. This allows to operate cables at high temperature (near 100 degrees) and to withstand high electrical stresses. Also, other sheets of lead sheath or aluminium are applied over each core for water isolation in case of using XLPE. This additional isolation is not needed in case of using EPR though [68]. Furthermore, other components such as additional layers based on polypropylene for corrosion protection and galvanized steel wire armour to increase tensile strength could be included for submarine applications.

2.2.3 Transformers

Power transformers are needed in the offshore wind power plants to step up the voltage output of the power conversion system of the wind turbines (i.e. the power electronic converters) for power transmission within the collection grid, as well as for the voltage step up for export cables to the onshore main grid. Those located inside each wind turbine (in the tower base or in the nacelle) step up the turbine output voltage from typically 690 V to 10–36 kV, whereas power transformers installed onto the offshore platform(s) increase the voltage usually from 10–36 kV to 110–150 kV. Thereby, power losses are reduced (as the currents become lower) and smaller cross–section cables are

required; with the consequent reduction of capital costs.

The design of power transformers for offshore applications does not differ much from those used in the electrical power system. Although, corrosion issues are specially addressed for protection in marine environments. Transformers are usually made up of copper windings, which are wrapped around laminated iron cores. They can be mainly classified in two types: liquid–filled and dry–type transformers. The difference between them is the electrical insulation medium used, i.e., paper/liquid and air/resin, respectively. Until a few years ago, dry–type transformers were installed in the vast majority of wind turbines because of their good fire behaviour and compact dimensions. However, the state of the art of liquid–filled transformers based on fire–retardant fluids such as silicone liquid or a biodegradable ester liquid (replacing the mineral oil used in the conventional liquid transformers), have recently been developed for modern turbines because their performance and reliability makes them particularly suited to offshore applications [69].

Similarly to induction generators (IG), power transformers require reactive power to support the magnetic field in their core. Moreover, it is worth noting that power transformers could provide voltage control services thanks to the inclusion of tap changers.

2.2.4 Protections and grounding

Electrical and mechanical protection elements are necessary to protect all the electrical components within the wind farm from any type of electrical fault. The most relevant protection devices (switchgears) are the circuit breakers, relays, fuses, meters and control switches. Those elements may need coordinated actions among them in order to ensure proper fault clearing, and both safe and correct equipment operation, for example, any element functioning correctly is disconnected by mistake [70].

The main purposes of the switchgears at the medium voltage side (offshore collector grid) are to protect both wind turbine equipment and wind farm array components, connect various wind turbines in string or radial and finally control the connection and disconnection of single wind turbines or strings. Circuit breakers that protect against faults in the transformer and in the cable to the next turbine can be remotely operated from the shore via Supervisory Control And Data Acquisition (SCADA) [71]. Also, manually operated equipment to isolate and earth the cables and transformer can be found.

In general, existing switchgear can be classified into two main types according to their insulation technology. The first type is based on air insulated

switchgear (AIS) which is the one used in conventional onshore substations, whilst the other uses gas–insulated switchgear (GIS) where the conductors and contacts are insulated by pressurized sulfur hexafluoride (SF_6) gas which is a superior dielectric gas [72]. The latter is the technology mainly used for offshore locations due to its compact structure and low maintenance needs in comparison with the former.

It is important to remark that the switchgear must be as small, light and reliable as possible due to the special conditions related to offshore installations; since, they must fit on limited space when located at the wind turbine towers, and tight limits on weight to be able to reduce offshore substations (Figure 2.7).

(a)

(b)

Figure 2.7: (a) Switchgear slim enough to fit through a tower door [73]. (b) Switchgear installed inside a wind turbine tower [74].

To guarantee safety of personnel and equipment in case of electrical failures, and to prevent fires, mechanical damage or malfunction resulting from lightning or static electricity, proper earthing (i.e. an intentional connection of the neutral point of the electrical power system to earth) and equipotential bonding is necessary [75]. As the platform will be exposed to lightning, especial precautions shall be made to prevent damage to the structures and the equipment on the platform. The lightning protection systems shall be designed in order to ensure that no major equipment is exposed to a direct lightning flash [75]. The main functions of the grounding system for lightning of the wind turbine are:

- to ensure safe step and touch voltages for people staying close to the wind turbine tower footing during possible lightning strikes and

- to ensure a low grounding resistance for the lightning current and create a reference potential to each equipment can be connected.

Equipotential bonding shall be made locally in close proximity to the parts which require bonding. Every bonding connection to earth shall be of corrosion resistant and secured against becoming loose due to vibration, which is especially important in offshore environments [75].

2.2.5 Offshore Platforms

Offshore platforms are a crucial component of the entire offshore grid's connection to shore. They can be divided into two types: collector platform and HVAC or HVDC platform. The former is an intermediate offshore platform located between the OWPP and offshore substation whose main tasks are to gather the MVAC inter–array cables from the wind turbines and to reduce electrical losses by increasing the voltage (from MV to HV) just before the transmission link to shore. The latter is usually located slightly away from the OWPP to facilitate others OWPPs connections and to transmit the combined power generated by all of them through a single HVAC or HVDC link.

Figure 2.8 shows the BorWin alpha HVDC platform that was installed in the German part of the North Sea in June 2009 [76]. As it can be seen, the platform consist of a foundation structure and a topside.

The most relevant foundation structures for offshore platforms (both collector and HVAC or HVDC platforms) can be a monopile (similar to the wind turbines), a hybrid or gravity–based (built up of a concrete caisson with a steel leg structure mounted on its top) or a jacket construction. The last of these has been widely used in the offshore oil and gas industry for many years and appears to be as a solid alternative for the construction of the future offshore platforms. It is made up of three or four main legs (depending on the seabed conditions and the platform weight) and supported by piles in each corner of the foundation structure. Moreover, it contains J–tubes to route the inter–array cables from the offshore collection grid onto the platforms. Aside from being required as a steel frame supporting the topside, the jacket structure is designed to bear against multiple constraints such as the impact of the waves, corrosion or the flow of the sea water streams and tides, among others.

Figure 2.8: BorWin Alpha HVDC offshore platform located in the German North Sea, around 130 km from the coast [77].

The platform topside is equipped with different devices to make a substation operational such as the VSC converter (only for HVDC transmission), transformers, switchgears, backup diesel generators, coolers for the ventilation, winch to hoist the subsea cables, pumps, fans, etc. Furthermore, it accommodates other required necessities as living quarters to host all the people on board, a crawler crane, a helipad, a boat landing, safety equipment and a meteorological mast, among others.

In order to design the appropriate platform topsides dimensions and weights, key factors as water depth and the size of the wind power plant are essential to be considered. Typically, platforms topsides can weight about 2.000 tonnes and have an area of 800 m^2 and a height of 25 m above sea level. In the case of a large wind power plant, more than one offshore platform may be required.

Due to the large size of the offshore platforms and the extreme difficulty of constructing the installation at sea, all platforms are assembled on land and then transported out to the sea. Regarding their location, platforms should be situated somewhere which can be easily accessible in the future and without damaging any inter–array or export cable.

2.2.6 Control Systems

The global control and management of an offshore wind power plant is done by the Supervisory Control And Data Acquisition (SCADA) system (Figure

2.9). The SCADA system is the responsible to provide real time visibility of the wind power plant operation by means of monitoring, and it has the ability to control the wind power plant both centrally or remotely. The latter is the usual choice for offshore locations [78].

(a)

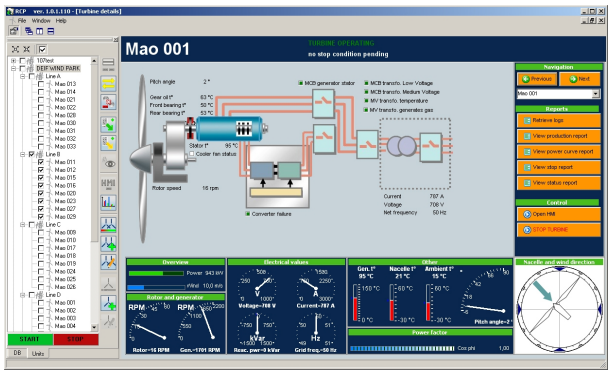

(b)

Figure 2.9: (a) Business Technology Consulting (BTC) Wind Farm Center: High performance SCADA control center of the offshore wind farm "BARD Offshore 1" [79]. (b) SCADA system for wind turbines from DEIF Wind Power Technology [80].

The SCADA introduces some advantages on the wind power plants including integration with wind turbine controls, detailed information for wind turbine and network diagnosis, reduce the maintenance needs which is really important offshore, and ensure the accomplishment of power generation requirements [81].

With the aim of wind power plant monitoring and control, the SCADA requires a communication network between the wind turbines and the HVDC converter, and the latter also with shore [71]. Such communications can be done through different technologies as Copper twister pair (RS485), Radio Telemetry or Fiber optic which is the most common for plant interconnections due to its speed and bandwidth.

It is worth remarking that not only wind turbine manufactures develop their own SCADA system, for example, WindAccess (Alstom Wind) [82], Wind Farm SCADA (REpower) [83], VestasOnline Compact II (Vestas) [81], but also other companies such as GH SCADA (Garrad Hassan) [84], among others.

2.3 AC collection grid topologies overview

Leaving aside the transmission system and focusing on the AC OWPP collection grid, there are mainly three different possible connection designs known as radial, ring and star [17, 65, 85–87].

2.3.1 Radial

In the radial collection system, the wind turbines included within the same feeder are installed in string configuration as shown in Figure 2.10. The maximum number of wind turbines that can be connected to one feeder is determined by the cable ampacity and the rated power of the generators. It is the most common, cheapest and simplest collection system but it presents some reliability issues, since if a failure occurs in the cable connecting the first turbine and the hub of a feeder, all the power generated by the downstream wind turbines in the string will be lost [65, 85–88].

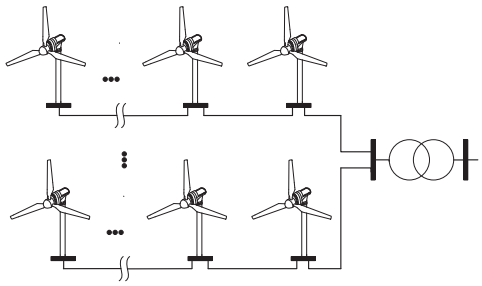

Figure 2.10: Radial collection configuration

2.3.2 Ring

The ring collection system (shown in Figure 2.11) can be understood as an improved version of the radial design in terms of reliability, but it becomes costly. There are different ring designs defined depending on how the ring is formed; they are known as single–sided, double–sided and multi–ring [86–88]. In all cases, redundant cables are added so that the power flow within a feeder have more options to be transmitted. Thus, a single–sided configuration (Figure 2.11(a)) consists in connecting a cable from the outermost turbine in the feeder to the collector hub whereas in the double–sided ring two feeders are connected together by means of a cable as it is shown in Figure 2.11(b). One drawback of this scheme is that some cables must be oversized to allow bidirectional power flow in case of a cable failure.

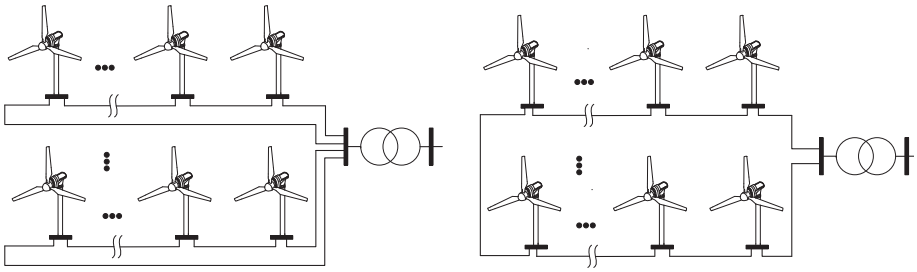

(a) (b)

Figure 2.11: Ring collection configuration. (a) Single–sided ring example. (b) Double-sided or multi-ring examples.

2.3.3 Star

The star collection system attempts to reduce the cable ratings of the cables which connect the wind turbines and the collector point. Such common connection point is usually located in the middle of all wind turbines disposition, as drawn in Figure 2.12.

The advantage of this topology is that the reliability of the system increases, since a cable failure causes the loss of only one machine. However, due to the longer cable lengths and lower voltage ratings of this configuration, cable losses and their costs are significantly higher than in other WPP designs [55, 65, 86–88].

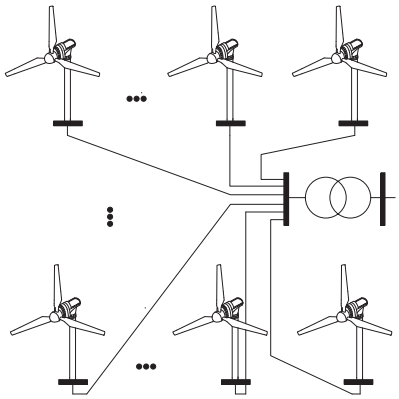

Figure 2.12: Star collection configuration

2.4 Electrical system design

The construction of an OWPP, as well as the O&M tasks performed throughout its lifetime (typically 20 years), entails some challenges and risks that should be taken into account in order to determine both its optimal location and the viability of the project itself. Thus, Front End Engineering and Design (FEED) studies needs to be performed in advance of contracting any offshore wind project. One task to be considered within these planning and development tasks refers to the electrical offshore wind power plant design.

In general, the design of the already existing offshore wind power plants is broadly similar to those installed onshore, i.e., both the collection grid and the transmission–link to the main electrical network by using AC technology. However, HVDC transmission systems arose in the last years, posing an alternative to the conventional AC offshore transmission systems. The decision on what kind of transmission–link is most suitable depends on several factors. Power losses in DC could be lower than in AC systems but the capital costs of the DC transmission systems are likely to be higher than AC equivalents due to the youth of the technology. Other aspects have to be considered though, as the need of installing reactive power compensators in AC systems, which also increases the capital costs of the system [89]. All these aspects leads to a clear trade–off analysis in which the length of the cables results decisive as it greatly affects the magnitude of the capital costs of the transmission facility.

Regardless of the type of transmission used (HVAC or HVDC), any wind farm whose capacity exceeds a certain minimum, requires an offshore substa-

tion platform. In the following, the electrical design of an offshore substation platform is presented for AC OWPP collection grids with both HVAC and HVDC transmission systems.

2.4.1 Offshore platform electrical design

With the aim of providing an insight on equipment arrangements and layout within an offshore platform, two electrical designs based on National Grid's references offshore design arrangements that act as a standard blocks [67], are introduced below as illustrative examples.

These designs are represented as a single line network and refer to a 900 MW AC OWPP with an HVAC transmission (AC900) and a 1000 MW AC OWPP with an HVDC transmission (HVDC1000).

AC collection grid with HVAC transmission

The reference arrangement AC900 consisting of common electrical equipment such as transformers, circuit breakers, busbars, earthing transformers and cables, is displayed in Figure 2.13. As it can be seen, it is composed of two 600 MVA offshore substation platforms to which the radial feeders from the wind turbine array are connected. Each substation contains two 320 MVA (220/36 kV) tertiary transformers with a star/delta/delta configuration and the primary winding solidly earthed. Two earthing transformers are installed on the secondary side to provide an earth on the delta winding of the transformer. The low voltage secondary side of the network has a number of busbars which can operate as one solid bus or as a sectionalized busbar in order to provide more redundancy to the system and, thus, improve its reliability. Additionally, two shunt reactors per platform are connected to the medium voltage busbar aiming to cater reactive power support. As this system is oversized because it has four 320 MVA transformers and a wind power plant capacity of 900 MW, a fault or a maintenance outage of one of the tertiary transformers would not result in a loss of the power generated by the wind farm. In reality the transformers are designed to operate at 70–90% of their rated value when wind speed is higher than its nominal value in order to optimize their lifetime.

The two offshore platforms have the possibility to be interconnected to form one 220 kV solid bus or to sectionalize or isolate one of them in case of a fault. The power generated by the offshore wind power plant is transmitted to shore through three 220 kV 3–core AC submarine cables. The transition

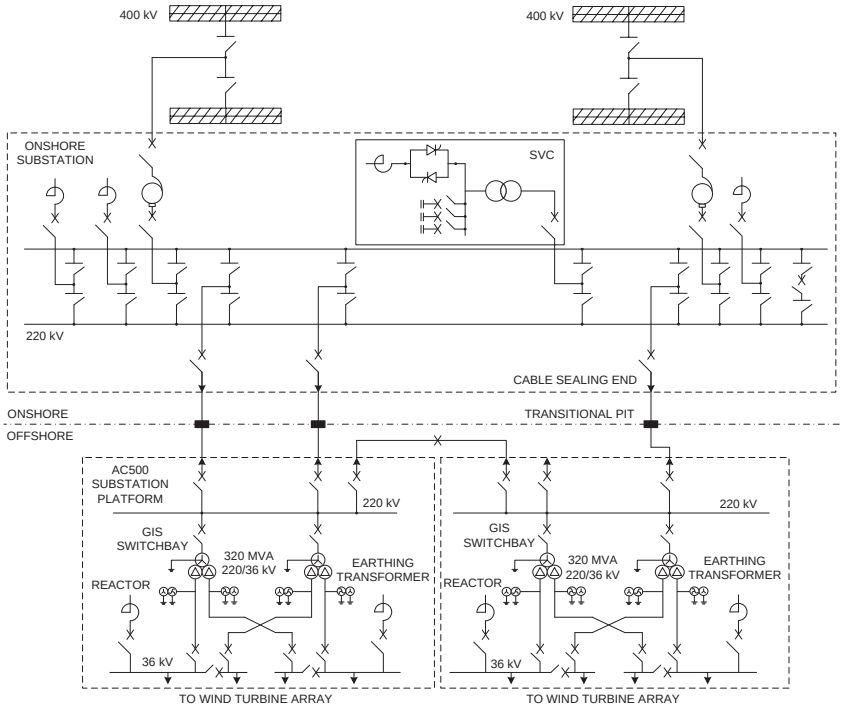

Figure 2.13: Single-line diagram based on the AC900 scheme proposal based on National Grid's reference offshore design arrangements [67].

joint pit is an intermediate point where the onshore network meets the offshore network.

Regarding the onshore side, two feeders are connected to the main 400 kV onshore network providing redundancy to the system to improve its secure operation. Each feeder is connected in turn to an autotransformer which steps down the voltage from 400 kV to 220 kV and is earthed on the primary star point. In order to provide voltage support, a SVC and three shunt reactors are required to be connected to the 220 kV busbar.

AC collection grid with HVDC transmission

To illustrate the electrical system design enclosed between the main onshore network and an offshore substation platform that has been built to operate an AC OWPP with an HVDC–link transmission system, the reference HVDC1000 reported in [67] is described. Figure 2.14 depicts the detailed single-line scheme.

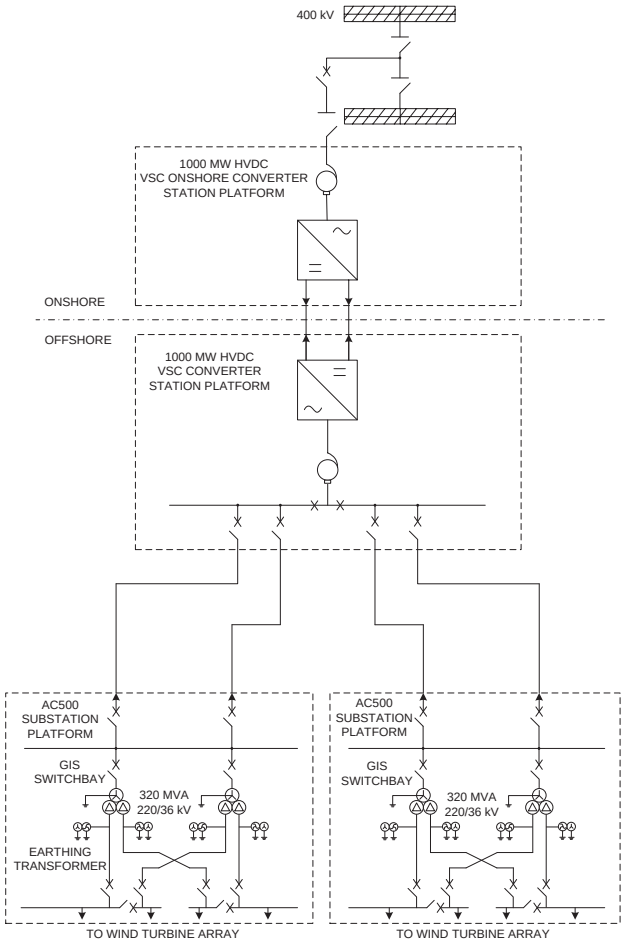

Figure 2.14: Single-line diagram based on the HVDC1000 scheme proposal based on National Grid's reference offshore design arrangements [67].

As it is shown in Figure 2.14, the HVDC1000 design consists of three offshore platforms (composed of one VSC converter and two 520 MVA substations), and one VSC onshore converter station platform. Thus, the radial feeders from the wind turbines array are directly connected to one of two 520 MVA AC intermediate collector platforms. The AC offshore platforms arrangements are similar to that presented above for the AC900 scheme, with the only exception that no shunt reactor is required. Therefore, two 320 MVA tertiary transformers are installed in each platform increasing re-

liability. Both platforms are directly connected to the solid bus of the VSC offshore platform via 3–core AC submarine cables, which voltage is rated at 220 kV. Likewise, the onshore and offshore VSC station platforms are interconnected by means of two ±300 kV submarine dipole cables. Finally, the HVDC VSC converts the ±300 kV DC voltage into 400 kV AC voltage for the main onshore grid. As in the previous case, the primary winding of the autotransformer is solidly earthed.

This type of design based on DC technology should result more economical than any AC scheme that involves large rated powers (over 1000 MW) and that is located further from the shore.

2.4.2 Inter–array cable selection design

When designing an offshore wind power plant project, one of the tasks that is performed prior to technical analysis is the cable selection process. This activity is carried out once all the wind turbine positions and locations of the offshore substations have been defined by optimizing the wind farm layout based on environmental, met station and sea bed surveys. It aims at determining the optimal number of parallel lines to install and selecting their optimal cable cross–sections to be used to interconnect the wind turbines, so that the capital expenditures of the cables and their installation costs are minimized provided that the proper operation of the system under full load is ensured. Figure 2.15 shows the flow chart of the methodology used in this work for the cable selection process.

As it can be seen, it consists of an initial step where the selection of the most economical available cables (i.e., minimum cross–sections) is performed ensuring not overcoming the maximum admissible loading under full load operation (STEP 1). After that, if any of the inter–array cables interconnecting wind turbines is overloaded (since none of the available cables in the database is capable of operating properly under full load conditions), STEP 2 is executed. Otherwise, the process ends. STEP 2 deals with the selection of the minimum number of parallel cables that are needed to work within the admissible conditions. This process is only carried out for those cables with the highest available cross–section that are overloaded. Finally, once all the currents of the cables are below its allowable limit, STEP 3 is performed. This step aims to reduce the cross–sections of those cables with two or more parallel cables in order to minimize the total cable costs of the offshore wind power plant.

With the aim of better understanding the aforementioned process, three application examples are shown. All of them present identical OWPP layout

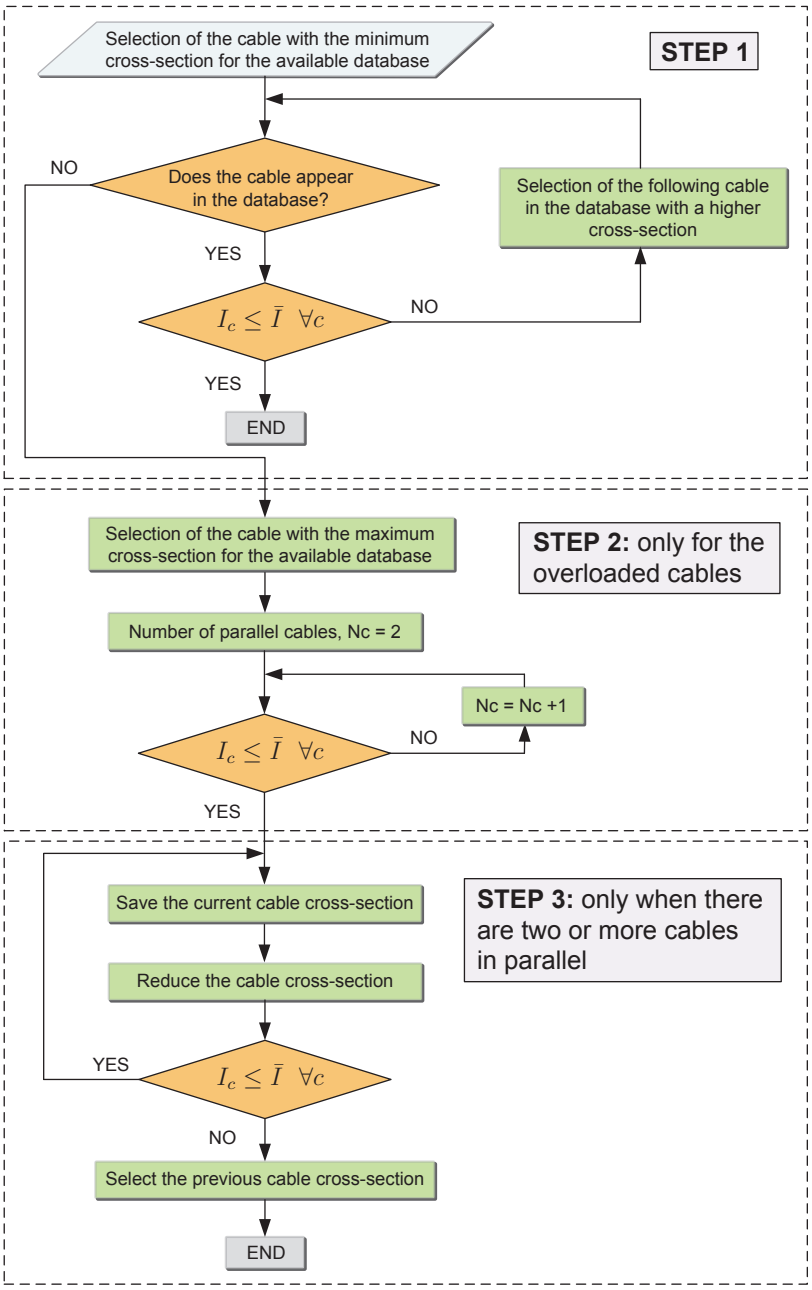

Figure 2.15: Flow chart of the cable selection process.

and differ in the power ratings of their wind turbines (2.5, 5 and 7.5 MW). The OWPP analyzed for the three cases consists of 80 wind turbines laid out in a rectangular matrix form of 10 columns and 8 rows. It is considered that the wind farm adopts a radial design. Likewise, the spacing between two nearby wind turbines is 7 rotor diameters (D) in both directions.

The electrical characteristics of the AC submarine 33 kV XLPE three–core cables database are shown in Table 2.3.

Table 2.3: Electrical characteristics of the AC submarine 33 kV XLPE Three–core cables database.

Section (mm^2)	**R** (Ω/km)	**L** (mH/km)	**C** (μF/km)	**Ampacity** (A)
95	0.2478	0.420	0.161	358
120	0.1967	0.401	0.176	406
150	0.1597	0.387	0.188	452
185	0.1281	0.374	0.203	507
240	0.0981	0.358	0.228	582
300	0.0790	0.344	0.244	649
400	0.0629	0.331	0.270	713
500	0.0505	0.315	0.300	790
630	0.0409	0.305	0.328	861

As it can be seen in Figure 2.16(a), when the rated power of each wind turbine is 2.5 MW, only two different cross–sections (95 mm^2 and 120 mm^2) are needed to ensure proper operation of the wind farm under full load conditions. Nevertheless, the number of cable cross–sections needed to minimize the costs associated with cables and their installation while avoiding overloading operation is increased if the rated power of the wind turbines amounts to 5 MW (Figure 2.16(b)). Both examples refer to STEP 1 of the cable selection process of Fig. 2.15, since there is no need for adding parallel lines with the available cable database. Conversely, STEP 2 and STEP 3 of the cable selection methodology are required for the third example shown in Figure 2.16(c), where the wind turbine rated power is 7.5 MW. Thus, the number of cables placed in the first three rows must be duplicated for guaranteeing the correct behavior of the system under full load operation. Thereby, these cables can be reduced in cross–section to optimize the total cable cost.

In order to demonstrate that, for the given cable database, it is always more economical to install a single cable (albeit the cable has the highest available cross–section, worst case) than installing two parallel lines with the smallest cable cross–sections (best case), Figure 2.17 is presented. As it is expected, the results indicate that as the cable length increases, the cost

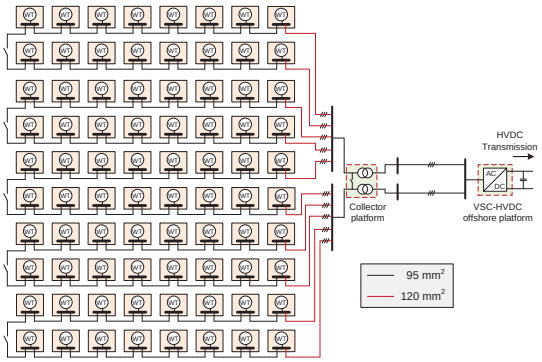

(a) Rated power of each wind turbine = 2.5 MW

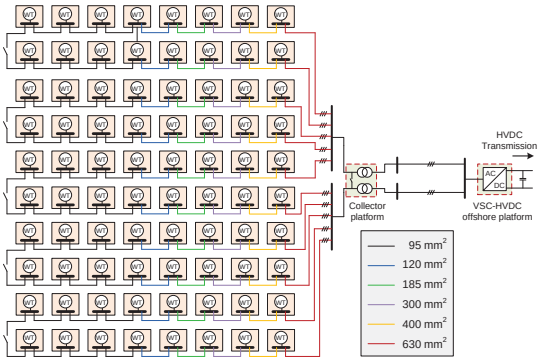

(b) Rated power of each wind turbine = 5 MW

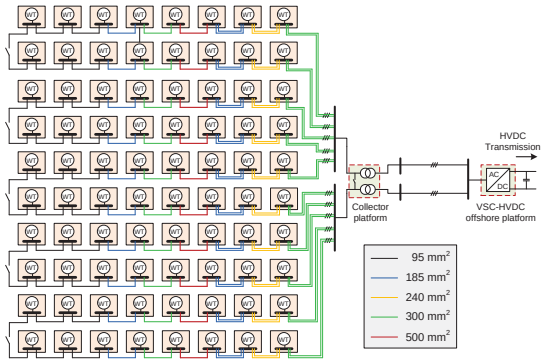

(c) Rated power of each wind turbine = 7.5 MW

Figure 2.16: Cable selection process applied to 3 OWPPs with 80 WTs and different power ratings (200 (a), 400 (b) and 600 MW (c)).

increment by installing two parallel cables is much greater. Therefore, it justifies carrying out STEP 2 of the cable selection process only if STEP 1 has not been successful.

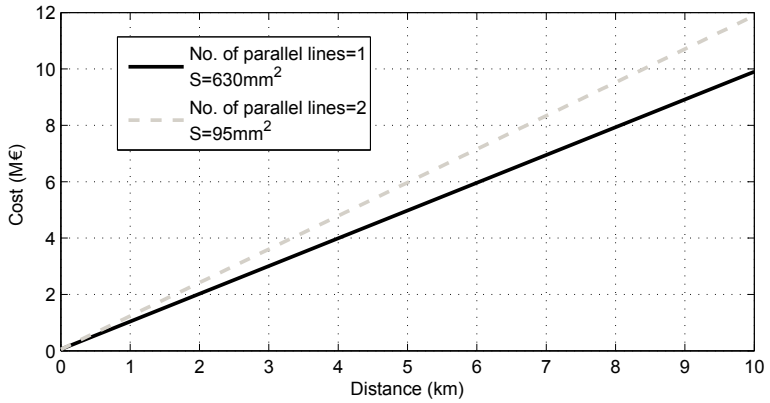

Figure 2.17: Demonstration that it is more economical to install a single 630 mm^2 cross–section cable than two parallel cables of 95 mm^2. These two cable cross–sections correspond to the widest and the thinnest cables available in the database, respectively.

It should be remarked that due to the currently limited suitable vessels for offshore wind power plant installations and the excessive cost that may lead requiring one of them for a long period of time, it may be more practical, depending on the cases, to simplify the results obtained in the cable selection process by reducing the number of cable cross–sections to two or three different ones, so that the required number of trips is minimized.

2.4.3 Energy yield assessment

Once the cable selection process is completed, the technical analysis of the offshore wind power plant is performed. It consists in estimating the total energy yield by the wind farm over its lifetime. This technical assessment may be more or less accurate depending on the degree of rigor required by the study being undertaken. For instance, in those studies aiming to get a rough idea of how much energy an offshore wind power plant can generate throughout its lifetime, a common assumption is based on computing the potential energy output generated by the OWPP (i.e., the hypothetical energy generated by the wind farm if it were continuously operating under full load conditions) and multiplying the resulting value by the capacity factor

of the OWPP. This capacity ratio accounts to be approximately 40% for the existing offshore wind power plants [90]. Another possible approach is to consider all wind turbines have the same wind speed and to calculate the energy produced by the wind farm using the average wind speed at the OWPP location during the time given by the available data. By contrast, other technical assessments estimate the energy generated by the OWPP by multiplying the electrical power produced by the wind turbines as a function of the wind speed and taking into account its probability of occurrence. Mathematically, this is expressed as

$$E^G = NT \int_{v_{min}}^{v_{max}} P^G(v) f(v)\, \mathrm{d}v \tag{2.1}$$

where N is the number of wind turbines comprising the wind farm, T is the period of time considered for the analysis, v_{min} and v_{max} are the minimum and maximum wind speeds considered for the case under study, $P^G(v)$ is the electrical power generated by a wind turbine as a function of the wind speed and $f(v)$ is the likelihood of occurrence of each wind speed (which is assumed to be given by the Weibull distribution function). Thus, $P^G(v)$ and $f(v)$ can be computed as follows

$$P^G(v) = \frac{1}{2}\rho A C_P(\lambda, \beta) v^3 \tag{2.2}$$

$$f(v) = \frac{k}{c}\left(\frac{v}{c}\right)^{k-1} e^{\left[-\left(\frac{v}{c}\right)^k\right]} \tag{2.3}$$

where ρ is the air density, A is the area swept by the turbine blades, C_P is the power coefficient which is a function of the tip–speed ratio λ and the pitch angle β, v is the wind speed and k and c are the dimensionless shape (k) and scale (c) parameters characteristics of the Weibull distribution function.

Figure 2.18 shows the Weibull distribution function (2.18(a)), the power generation curve (2.18(b)) and the energy yield by a wind turbine as a function of the wind speed (2.18(c)).

It is worth noting that, at high wind speeds (under full load operation), the total available power that can be extracted from the wind (dash gray line) is curtailed by the pitch control action with the aim of keeping the power output constant at rated power (solid black line) in order to avoid overloading. Therefore, the area enclosed by the solid black curve of Figure 2.18(c) corresponds to the total actual energy produced by a wind turbine during a certain period of time T.

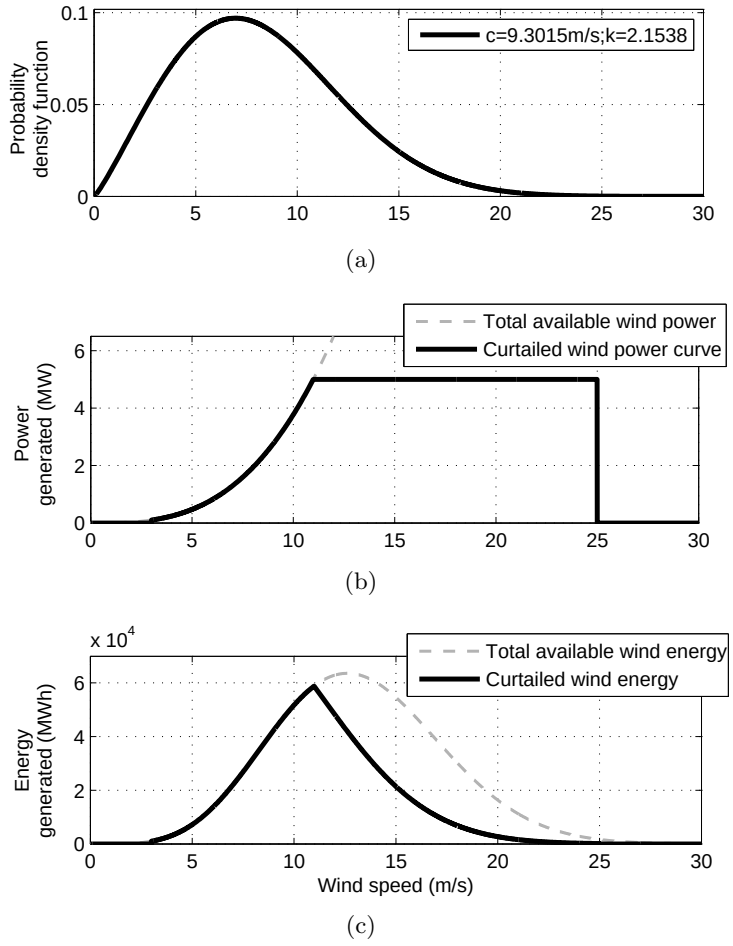

Figure 2.18: (a) Weibull distribution function (b) Power generation curve of a wind turbine (c) Energy yield function by a wind turbine during a certain period of time T.

Both studies previously mentioned estimate the total energy generated by the OWPP assuming an identical behavior for all wind turbines since all of them are considered to be subjected to the same wind regime. However, any wind power plant presents some wind speed variability among wind turbines caused by the wake effect given for each wind direction. Thus, (2.1) must be modified (if required) by including the wind direction distribution function, i.e., the wind rose distribution, and taking into account the wake effect among turbines. Thereby, the energy generated by a single wind turbine

and the WPP can be computed as

$$E^G_{wt-i} = T \int_{0^\circ}^{360^\circ} \int_{v_{min}}^{v_{max}} P^G_{wt-i}(v,d) f_1(v) f_2(d)\, \mathrm{d}v\, \mathrm{d}d \tag{2.4}$$

$$E^G_{WPP} = \sum_{i=1}^{N} E^G_{wt-i} \tag{2.5}$$

where $P^G_{wt-i}(v,d)$ is the power generated by each wind turbine i for a particular average wind speed (v) and a certain wind direction (d) and $f_1(v)$ and $f_2(d)$ are the probabilities of occurrence according to the Weibull and wind rose distribution functions, respectively.

In practice, in order to obtain the most accurate computation of the total energy that can be produced by an OWPP over a certain period of time, a large number of factors should be taking into consideration, such as, the aerodynamics of the wind turbines, the wind farm layout, the wind speed and wind direction distributions and the turbulence levels.

It is also worth noting that such total energy that can be generated by an OWPP over a certain period of time for a particular wind farm layout and specific wind conditions does not correspond to the actual energy delivered to the grid through the point of common coupling (PCC) during this time. To do so, the total energy losses produced in the OWPP and its availability should be considered in the technical analysis. These losses can be classified into two main groups: the steady state losses or power flow losses and the unavailability or maintenance losses.

Power flow losses refers to the electricity dissipated as heat within the OWPP as a result of the efficiency losses of its components (transformers, converters, cables, etc.). Theses are computed as

$$E^L_{pf} = T \int_{0^\circ}^{360^\circ} \int_{v_{min}}^{v_{max}} [P^G(v,d) - P^T(v,d)] \cdot f_1(v) f_2(d)\, \mathrm{d}v\, \mathrm{d}d \tag{2.6}$$

where $P^G(v,d)$ is the power generated by all wind turbines comprising the WPP and $P^T(v,d)$ is the net active power transferred to the grid at the Point of Common Coupling (PCC) obtained by means of power flow calculations.

Wind energy curtailed by unavailability or maintenance purposes are more complex to calculate than steady state losses, since they occur due to the unforeseen equipment failure (corrective or unexpected maintenance losses) or because of partial or total outages of the installation during a fixed time for preventive maintenance purposes (preventive or planned maintenance losses).

Figure 2.19 illustrates an example of the results obtained from a power flow simulation considering wind turbines operating at their rated power (2 MW). As it can be seen, the power flow calculation determines the voltage magnitude (u) and the voltage angle ($phiu$) of the nodes, as well as the active (P) and reactive (Q) power flow on branches. Furthermore, the figure displays other results such as the apparent power (S) and the current (I), loading ($loading$) and power losses (P_{loss})of each branch. According to the results, the net active power transferred to the grid at the PCC ($P^T(v,d)$) for this particular example (rated wind speed and 0°) is 149.67 MW.

Thus, the power flow energy losses (E^L_{pf}) can be calculated by simulating multiple power flows for different loading conditions taking into account the probabilities of occurrence of each wind speed and direction considered ($f_1(v)$ and $f_2(d)$). The wind conditions (Wind rose and Weibull distribution functions) used for the example are presented in Table 2.4 [91]. Twelve 30° wind direction sectors and a different set of Weibull parameters have been considered (mean wind speed, scale (c) and shape (k) parameters) for each direction.

Table 2.4: Wind conditions (Wind rose and Weibull distribution functions) at the OWPP location [91].

Wind direction	**Probability (%)**	**Mean wind speed (m/s)**	**Scale factor (c) (m/s)**	**Shape factor (k)**
N	8.2	7.34	11.15	1.27
NNW	4.5	6.39	9.04	0.55
WNW	3.7	6.89	10.02	0.53
W	3.9	7.59	10.98	1.26
WSW	9.5	9.13	10.95	1.71
SSW	13.5	8.72	10.93	1.62
S	12.7	7.93	11.22	1.73
SSE	12.3	8.34	10.90	1.69
ESE	10.1	8.41	10.82	1.70
E	6.4	8.36	10.61	1.48
ENE	6.5	8.01	10.55	1.97
NNE	8.7	8.08	10.86	2.14

Solving (2.5) and (2.6), the total energy generated and the power flow energy losses per year for the offshore wind power plant under study result 560.6 and 34.2 GWh/year, respectively. Therefore, the net energy transferred by the offshore wind power plant (without considering maintenance losses) can be obtained as

$$E^{NT}_{WPP} = E^{G}_{WPP} - E^{L}_{pf} = 560.6 - 34.2 = 524.4\ GWh/year \tag{2.7}$$

With regard to the unplanned maintenance losses, it can be calculated

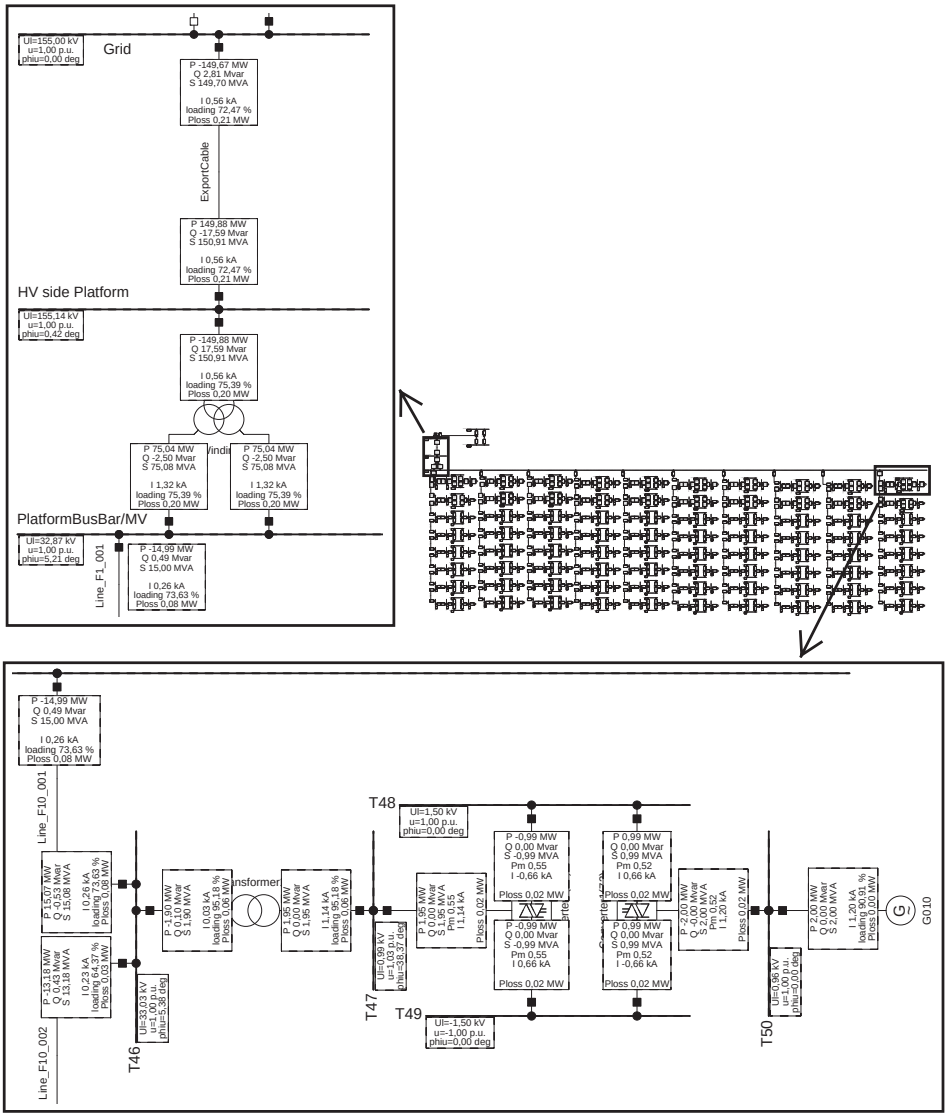

Figure 2.19: Power flow solution obtained using DIgSILENT Power Factory® software.

based on the reliability multi–state models explained in detail in [92], in which the Expected Energy Not Supplied (EENS) depends on the failure rate (λ) and the mean time to repair (MTTR) of all the components encompassed within the OWPP. This models considers that each component has

several states of service and has a probability of malfunction in each state per year. Concerning the preventive maintenance losses, they are planned to be performed during periods of low wind speeds where the energy yield is limited or nonexistent in order to maximize the availability of the offshore wind power plant. However, this is not always possible to be achieved due to the stochastic behavior of the wind, so as some downtimes may occur in periods of high winds. Hence, the actual net energy transferred to the grid by the OWPP can be computed as

$$E_{WPP}^{ANT} = \eta_{availability} \cdot E_{WPP}^{NT} \tag{2.8}$$

According to some experiences from Middelgrunden and Nysted OWPPs reported in [93,94], respectively, the average availability of the existing OWPPs can be assumed to be 95–96% (covering both wind turbine and collection grid availability).

Therefore, the total energy yield per year by the given offshore wind power plant considering an availability of 96% and taking into account the wind conditions presented in Table 2.4 accounts to be 503.5 GWh/year.

3

Optimal wind power plant operation by reducing the wake effect

3.1 Introduction

Wind turbines interact with the wind, capturing part of its kinetic energy and converting it into usable energy. Following directly on from the first principle of thermodynamics, this extraction of energy creates a wind energy deficit between the wind leaving the turbine (known as wake) and the wind arriving in front of the turbine. Thus, the wind speeds in the rear of the turbines are lower than the upstream wind speeds and, therefore, a reduction of power output is produced at downwind turbines. The turbine wake also causes high turbulence levels in downwind turbines, giving rise to additional mechanical stress, which may reduce their operating life.

For the time being, offshore wind power plants seek to maximise its power extraction by optimizing wind turbine operation individually and by designing its optimal layout that minimise the wake effect. Thus, wind turbines are typically spaced out by a certain distance resulting from a trade–off between maximizing the WPP energy capture by reducing the wake effects and minimizing the costs associated with the logistics and electrical interconnections between turbines.

Recent studies have shown that operating each wind turbine at its optimal individual point without considering the impact of the wake effect on the

other turbines does not maximise the power output of the whole wind power plant [95–101]. For this purpose, they suggest to increase the total WPP power generated and reduce structural loads by properly operating some wind turbines at non–optimum points, based on the fact that operating the upstream turbines at a lower rotational speed results in higher wind speeds for downstream wind turbines.

In this chapter, a comparative steady state analysis between these two different control strategy approaches is presented. For the sake of completeness, an introductory explanation of single turbine operation and a brief description of the wake model used in the methodology, is included. With the aim to better understanding the optimal wind power plant operation concept, first a very simple model consisting of three turbines aligned in a row is considered. Then, a more complex model based on a wind farm composed by 9 wind turbines and taking into account wind directions, is assessed.

3.2 Single turbine operation

The power P_{wti} generated by a single wind turbine can be expressed as

$$P_{wti} = C_P P_{wind} = \frac{1}{2} C_P \rho A v_w^3 \tag{3.1}$$

where P_{wind} is the air stream kinetic power, ρ is the air density, $A = \pi R^2$ is the swept area of the wind turbines blades of radius R, v_w is the average wind speed at hub height, and C_P is the power coefficient, which can be written as [21, 102]

$$C_P\left(\lambda, \theta_{pitch}\right) = c_1 \left(c_2 \frac{1}{\Lambda} - c_3 \theta_{pitch} - c_4 \theta_{pitch}^{c_5} - c_6 \right) e^{-c_7 \frac{1}{\Lambda}} \tag{3.2}$$

where θ_{pitch} is the pitch angle, and λ is the so–called tip speed ratio defined as

$$\lambda = \frac{\omega_t R}{v_w} \tag{3.3}$$

and

$$\frac{1}{\Lambda} = \frac{1}{\lambda + c_8 \theta_{pitch}} - \frac{c_9}{1 + \theta_{pitch}^3} \tag{3.4}$$

where $[c_1 \dots c_9]$ are characteristic constants for each wind turbine.

In order to know how much power can be extracted from the wind, it is usual to represent a curve of the generated power versus wind speed, called ideal power curve.

The ideal power curve for a typical pitch controlled wind turbine is shown in Figure 3.1. It can be observed that the range of operational wind speeds is delimited by the cut–in and cut–out wind speeds. The turbine remains stopped beyond these limits. Below cut–in wind speed, the system would not be profitable since the available wind energy is too low to compensate for the operation costs and losses. Above cut–out wind speed, the turbine is shut down to protect the wind turbine from damage.

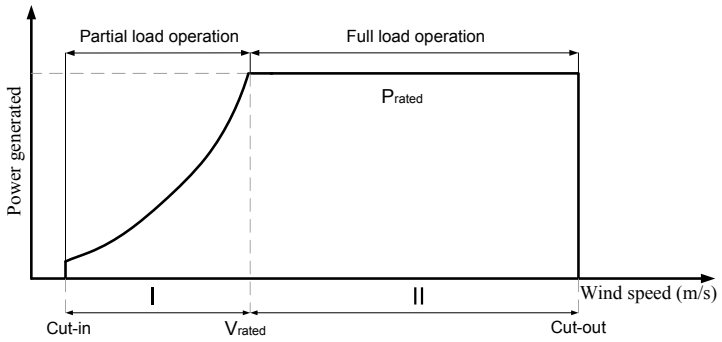

Figure 3.1: Ideal power curve of a typical wind turbine.

There are two different regions with distinctive generation objectives. On the one hand, the objective of the region I, which corresponds to wind speeds lower than the rated speed, is to extract all the available power from the wind. Thus, given a fixed rotor area A, a constant air density ρ and considering the wind speed v_w as an external and uncontrollable variable, the only way to maximise the power P_{wti} of (3.1) is by means of the power coefficient C_P. Besides, in order to maximise the power extracted by a wind turbine, θ_{pitch} is assumed to be zero, so that (3.2) only depends on the tip speed ratio parameter λ. On the other hand, at high wind speeds (region II), the pitch control is activated with the aim of keeping the power output constant at rated power (P_{rated}) in order to avoid overloading [103].

In Figure 3.2, a typical $C_P - \lambda$ curve is depicted. The $C_P - \lambda$ curve has a maximum value (C_P^{max}) which corresponds to the optimum operating point of the wind turbine (λ_{opt}), as long as the wind speed does not overcome the maximum threshold.

In a single wind turbine, the maximum C_P is obtained applying the following maximum power point tracking (MPPT) control strategy reported in [27]

$$T_{wti} = K\omega_t^2 \tag{3.5}$$

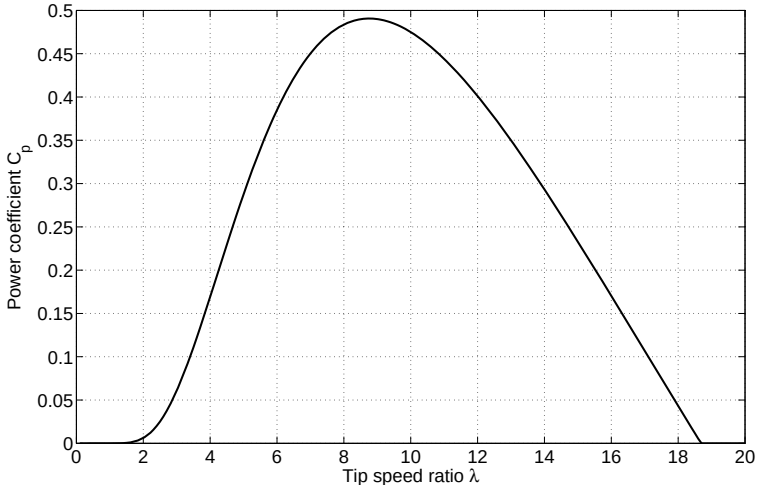

Figure 3.2: Typical $C_p - \lambda$ curve

where T_{wti} is the rotor mechanical torque, ω_t is the rotational wind turbine speed and K is a constant parameter that depends on the geometry of the turbine and is expressed as follows

$$K = \frac{1}{2} C_P^{max} \rho A \frac{R^3}{\lambda_{opt}^3} \tag{3.6}$$

with

$$C_P^{max} = C_P(\lambda_{opt}) = \left(\frac{c_1 c_2}{c_7} \right) e^{-\frac{c_6 c_7}{c_2} - 1} \tag{3.7}$$

and

$$\lambda_{opt} = \frac{c_2 c_7}{c_2 c_9 c_7 + c_6 c_7 + c_2} \tag{3.8}$$

3.3 Impact of wake effects on wind power generation

The wake effect is not only dependent on the incoming wind speed and its direction, but also on the design characteristics of the rotor blades, as well as the distance between the turbines. According to [104], wind turbines should be spaced at least 5 to 9 rotor diameters (D) away from each other in the prevailing wind direction and about 3 to 5 rotor diameters for winds coming perpendicularly, in order to reduce the effects of wakes. As stated in [105], the power losses due to wind turbine wakes that can be expected if

the wind turbines are separated between 4 and 8 rotor diameters from each other result to be in the range of 5 to 10% of the total power generated by the wind power plant.

As an illustrative example, Figure 3.3 shows the resulting wind speed decay obtained in [56] of 10 turbines aligned in one row, varying the distance among them from 5 to 9 rotor diameters.

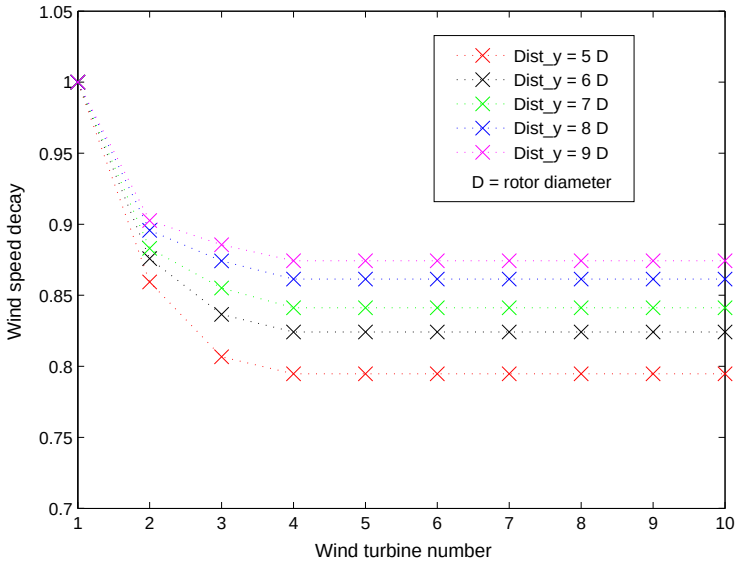

Figure 3.3: Wind speed decay of ten wind turbines aligned in one row varying the spacing between turbines from 5 to 9 rotor diameters (D).

As expected, it can be seen that when the distance between wind turbines increases, the wind speed decay is lower. Furthermore, the wind speed deficit among turbines is significantly higher for the first turbine immediately downstream of the most upstream turbine that is exposed to the undisturbed free stream conditions. A similar effect is experienced on the subsequent downstream turbines but the effect slowly decreases downstream.

Many comprehensive studies have been carried out regarding wind turbine wakes, and several models have been developed by researchers, such as Ainslie's model [106], Frandsen's model [107], Mosaic Tile model [108], Jensen's model [109] and CFD (Computational Fluid Dynamics) model [110]. The choice of the model depends on the desired prediction accuracy and on computational time. In [105], a comparison of different wake

models is presented, and it can be observed that the sophisticated models have a similar level of accuracy as simpler ones. One of the most widely used wake model, developed by Jensen [109], has been chosen for this study, as it provides adequate accuracy and reduced computational time. It is based on global momentum conservation in the wake downstream of the wind turbine and assumes that the wake downstream of the turbine expands linearly.

The comprehensive wake model implemented for the analysis, considering single, partial and multiple wakes within a wind farm, is detailed below. The study neglects the turbulent behavior caused by wakes as it does not directly affect the wind power generation output [104].

3.3.1 Single wake

According to Jensen's wake model [109], the following equation describes the downstream wind speed of a single turbine (Figure 3.4)

$$v_2 = v_1 \left[1 - \left(\frac{D}{D + 2kx} \right)^2 (1 - \sqrt{1 - C_T}) \right] \tag{3.9}$$

where v_2 is the wind speed at distance x from the turbine, D is the diameter of the turbine rotor, C_T is the thrust coefficient, v_1 is the free stream wind and k is the wake decay constant or opening angle which represents the effects of atmospheric stability. Jensen experimentally found the value of k to be 0.075 for onshore applications and 0.04 for offshore applications.

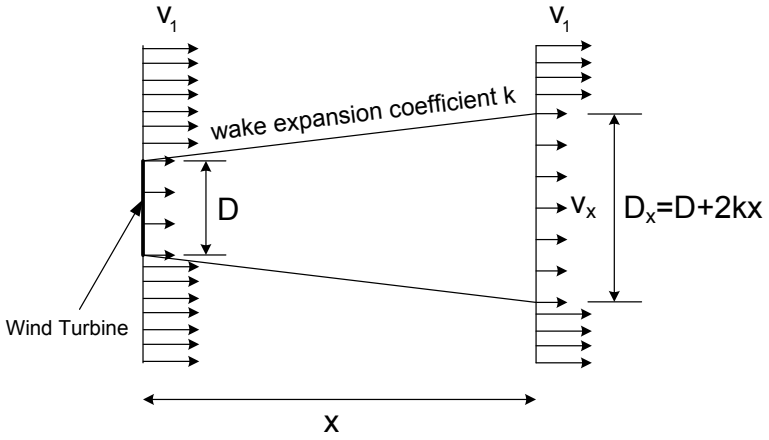

Figure 3.4: Schematic view of a single wake effect.

In general terms, the thrust coefficient C_T is wind turbine specific, being the result of blade geometry, the tip speed ratio λ and the applied control strategy of the wind turbine (stall or pitch control). This coefficient can be given by the manufacturer or can be calculated with adequate simulation software if the required simulation data is available.

3.3.2 Partial wakes

Partial shadowing is a phenomenon which occurs when one or more upwind wind turbines cast a "single" shadow on a downwind turbine. The wind speed entering into the turbine j affected by the k upwind WTs is then given by [104]

$$v_{Tj} = v_1 \left(1 - \sqrt{\sum_{k=1}^{N} \beta_{Tj,Tk} \left(1 - \frac{v_{ps,Tk}}{v_1} \right)^2} \right) \tag{3.10}$$

where v_{Tj} is the wind speed of the downwind turbine j, k is the upwind turbine, v_1 is the initial wind speed entering into the wind turbine k, $v_{ps,Tk}$ is the shadow of k falling on the j^{th} wind turbine and $\beta_{Tj,Tk}$ is the ratio (the weighting factor) of the shadow area by the wake to the total rotor area. This ratio can be calculated using the following expression [111]:

$$\beta_{Tj,Tk} = \frac{A_{shad}}{A_{wind}} \tag{3.11}$$

with

$$A_{wind} = \pi r_2^2 \tag{3.12}$$

and

$$\begin{aligned} A_{shad} \;=\; & \arccos\left(\frac{r_1^2 + d^2 - r_2^2}{2 \cdot r_1 \cdot d} \right) \cdot r_1^2 \\ & + \arccos\left(\frac{r_2^2 + d^2 - r_1^2}{2 \cdot r_2 \cdot d} \right) \cdot r_2^2 \\ & - \sin\left[\arccos\left(\frac{r_1^2 + d^2 - r_2^2}{2 \cdot r_1 \cdot d} \right) \right] \cdot r_1 \cdot d \end{aligned} \tag{3.13}$$

where the parameters r_1, r_2 and d are described in Figure 3.5.

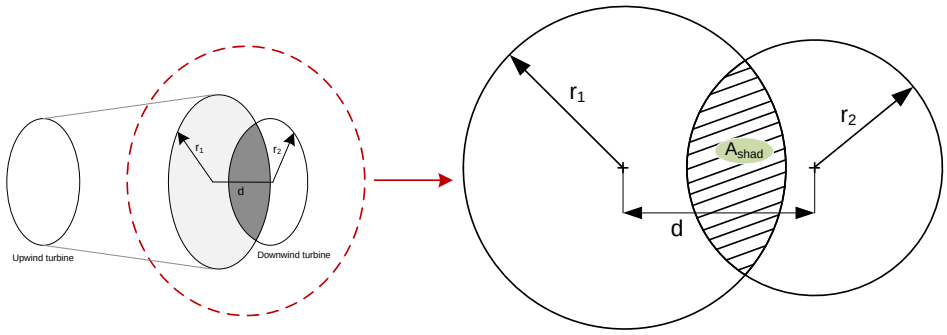

Figure 3.5: Shade area of a downstream wind turbine in partial wakes.

3.3.3 Multiple wakes

In a wind farm with a large number of wind turbines, it is quite possible that one turbine is affected by several wakes. Therefore, the multiple wake effect should be taken into account. This model assumes that the kinetic energy deficit of interacting wakes is equal to the sum of the energy deficits of the individual wakes. Thus, the velocity at the intersection of several wakes is [112]

$$1 - \frac{v_x}{v_1} = \sqrt{\sum_{i=1}^{N} \left(1 - \frac{v_i}{v_1}\right)^2} \tag{3.14}$$

where v_1 is the initial free stream velocity, N is the total number of upwind influencing turbines, v_i is the wind speed affected by the individual wake i and v_x is the wind speed such that all the wakes are taken into account.

3.4 Optimal wind power plant operation

As previously mentioned, this chapter aims to analyse the potential benefits of applying the optimal wind power plant operation concept (which takes into consideration the wake effect within the WPP) in comparison to the conventional control strategy based on maximizing the energy captured by the WPP by operating each turbine at its optimal individual point. Thus, the following analysis methodology has been developed and applied to two particular study cases to assess the performance of both control approaches.

3.4.1 Methodology description

A simple example is presented in order to facilitate the comprehension of the proposed methodology. The example aims to show that the total power generated by the WPP can be increased by properly operating some wind turbines at non–optimum points and, therefore allowing the downstream turbines to produce more power, rather than by using the conventional approach based on optimizing the operation of each wind turbine individually. As it can be seen in Figure 3.6, it consists of three wind turbines with a rated power of 5 MW and a rotor diameter of 126 m aligned in a row. The spacing between wind turbines is 7 rotor diameters (D).

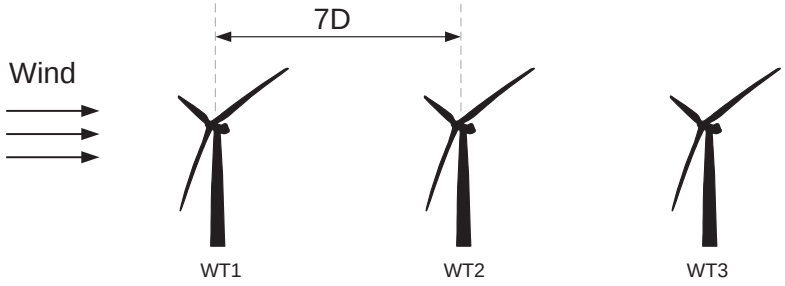

Figure 3.6: Schematic layout of the system under study consisting of three wind turbines aligned in a row.

The power coefficient (C_P) and thrust coefficient (C_T) curves used for the study are shown in Figure 3.7 [17, 97].

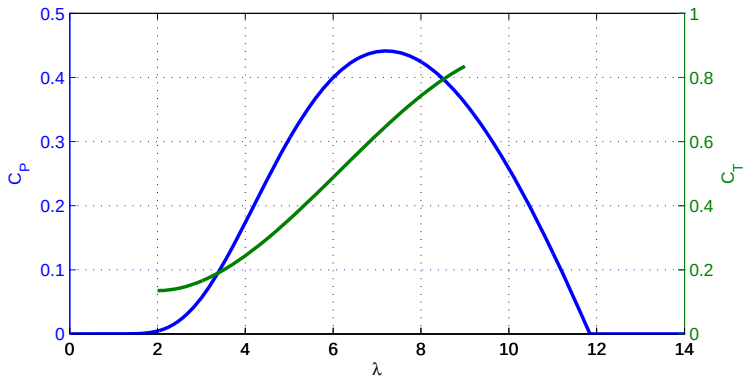

Figure 3.7: Power coefficient (C_P) and thrust coefficient (C_T) used for the study.

The procedure of obtaining the optimal operating points of each wind turbine that maximise the total WPP power generation is described as follows:

- **Step 1:** Firstly, the power generated by the upstream wind turbines is calculated for all their operating points (i.e., varying their tip speed ratios, λ_1, from 2 to 9). For this particular example, only the power produced by WT1 is computed since it is assumed that the wind comes just from the one direction indicated in Figure 3.8. Thereby, the power generated by WT1 can be expressed as

$$P_{WT1}(\lambda_1) = \frac{1}{2}\rho A C_P(\lambda_1) v_1^3 \qquad \forall\ \lambda_1, \lambda_2 \in [2, 9] \tag{3.15}$$

  where v_1 is the upwind speed and the power coefficient, C_P, is only dependent on the tip speed ratio, λ_1, since the pitch angle, θ_{pitch}, is set to zero.

  Figure 3.8 presents the results obtained by computing (3.15). As it is shown, the optimal tip speed ratio that maximises the power output of WT1 is $\lambda_1 = 7.22$, regardless of the λ_2 value.

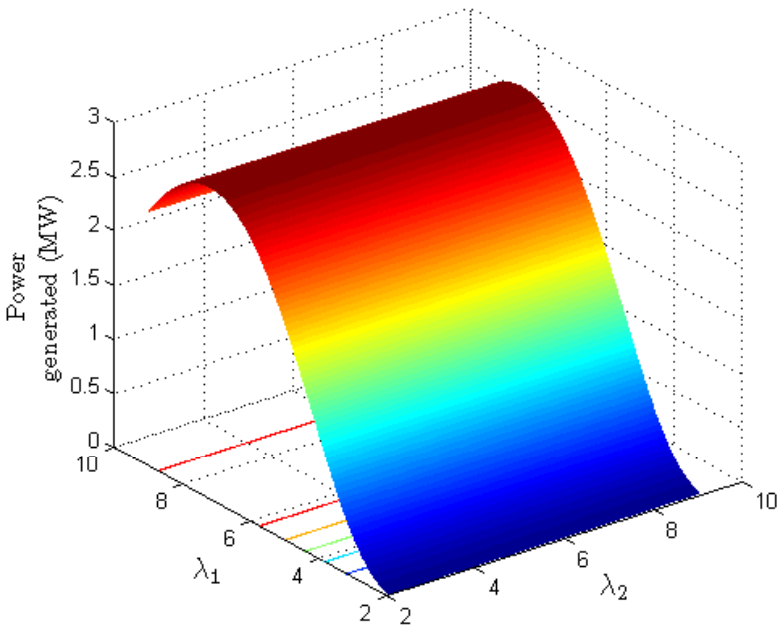

Figure 3.8: Power generated by the upwind turbine (WT1) as a function of λ_1 and λ_2. Upwind speed=9.5 m/s.

- **Step 2:** Secondly, the power produced by the first turbines affected by the wake effect (in this case WT2) is computed according to the following equation

$$P_{WT2}(\lambda_1, \lambda_2) = \frac{1}{2}\rho A C_P(\lambda_2) v_2^3(\lambda_1) \qquad \forall\ \lambda_1, \lambda_2 \in [2, 9] \qquad (3.16)$$

As it can be seen, it depends on two parameters: λ_1 and λ_2. The former has an influence on wind speed of WT2 (v_2) by modifying the $C_T(\lambda_1)$ value (using (B.1)), whilst the latter changes the power coefficient $C_P(\lambda_2)$ similarly to the previous case with WT1. Thus, the resulting surface $P_{WT2}(\lambda_1, \lambda_2)$ of computing (3.16) for all possible combinations of λ_1 and λ_2 parameters, is depicted in Figure 3.9.

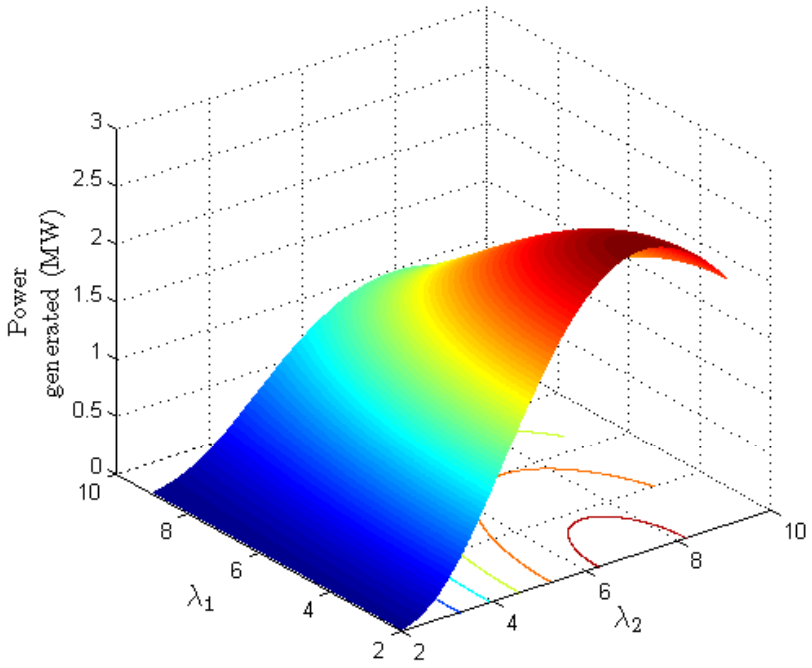

Figure 3.9: Power generated by WT2 as a function of λ_1 and λ_2. Upwind speed=9.5 m/s.

It should be noted that maximum power generation for WT2 is achieved when λ_1 is minimum and $\lambda_2 = 7.22$. This result is consistent with the fact that the lower the rotational speed of WT1 (lower λ_1), the smaller the impact of the wake effect on downstream wind turbines and, therefore, the greater the power produced by WT2.

- **Step 3:** Next, the power extracted by WT3 is calculated as

$$P_{WT3}(\lambda_1, \lambda_2) = \frac{1}{2}\rho A C_P^{max} v_3^3(\lambda_1, \lambda_2) \qquad \forall\ \lambda_1, \lambda_2 \in [2, 9] \quad (3.17)$$

In this case, the turbine operates at its optimum point (C_P^{max}) because no downstream wind turbine is located behind. Regarding its wind speed (v_3), it is computed by considering the multiple wakes described in (3.14). Figure 3.10 shows the power P_{WT3} obtained by sweeping λ_1 and λ_2 from 2 to 9.

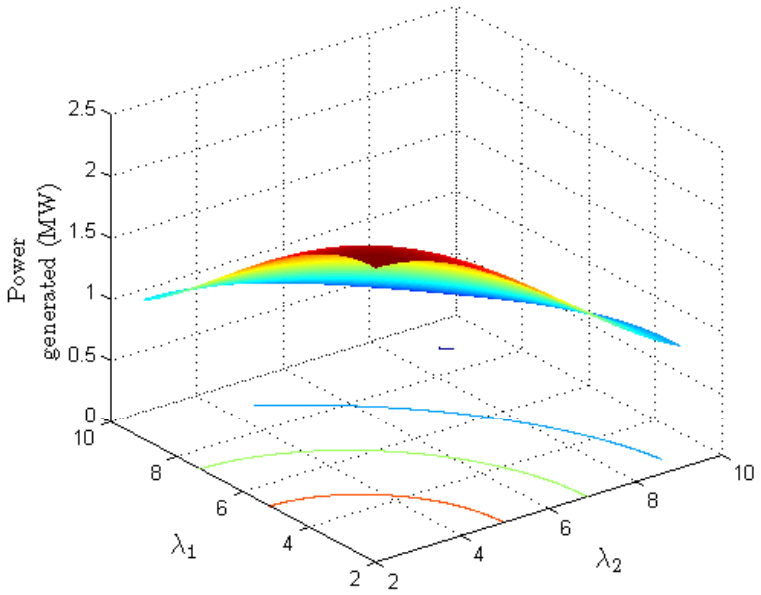

Figure 3.10: Power generated by WT3 as a function of λ_1 and λ_2. Upwind speed=9.5 m/s.

As expected, the maximum power that can be generated by WT3 occurs when the operating points of WT1 and WT2 are minimum.

- **Step 4:** Finally, the total power produced by the set of the three wind turbines ($P_{TOT} = P_{WT1} + P_{WT2} + P_{WT3}$) is presented in Figure 3.11.

As it can be seen, P_{TOT} reaches its maximum value for $\lambda_1 = 6.12$ and $\lambda_2 = 6.43$. It is worth noting that although the available data of tip speed ratio (λ) for the C_T curve are constrained within the range [2,9] (Figure 3.7), it does not pose a problem for the purpose of the study

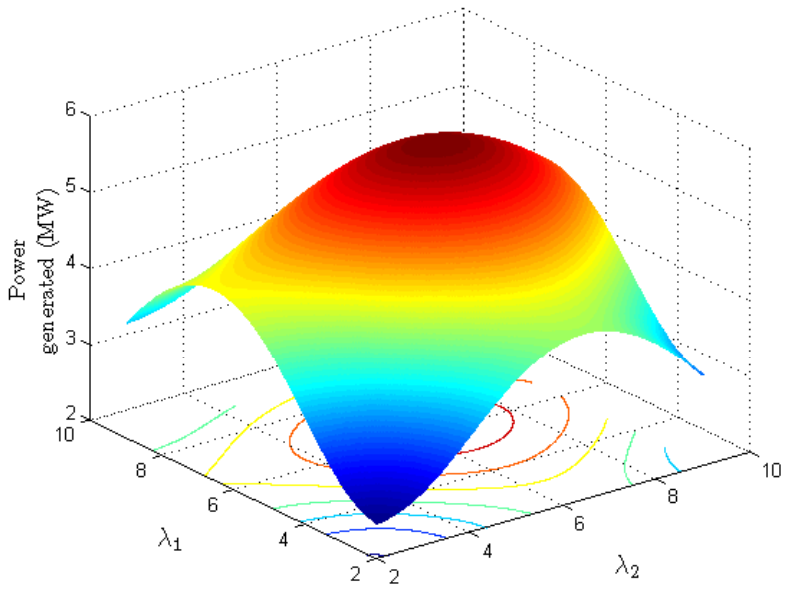

Figure 3.11: Total power generated by the set of three wind turbines (WT1, WT2 and WT3) as a function of λ_1 and λ_2. Upwind speed = 9.5 m/s.

since the optimal operation points obtained for each turbine are within these boundaries.

Given the new tip speed ratios for each wind turbine, their new nominal operating points can be obtained, as it is shown in Table 3.1.

Table 3.1: Nominal operating points of each wind turbine.

	λ^N	C_P^N	W_s^N (m/s)	ω^N (rad/s)
WT1	6.12	0.4075	11.7121	1.1377
WT2	6.43	0.4241	11.5574	1.1796
WT3	7.22	0.4412	11.4060	1.3072

In order to compare the operation of each wind turbine for the two aforementioned control strategies analysed, Figure 3.12 is presented. It shows the tip speed ratio (λ) of each wind turbine and power generated by each turbine as a function of the upwind speed. As it can be noted, WT2 and WT3 reach their rated power at higher wind speeds when the conventional WPP operation approach is applied because of the increased wake effect.

Moreover, whereas the three wind turbines operate at their optimum point (λ_{opt}) by considering the conventional control strategy, the proposed WPP control method forces WT2 and WT3 to operate at sub–optimum points. It is worth remarking that the abscissa for all the graphs of Figure 3.12 refers to the upwind speed. Therefore, it is reasonable that the wind speeds from which WT2 and WT3 operate at their rated values are slightly higher than their nominal values shown in Table 3.1.

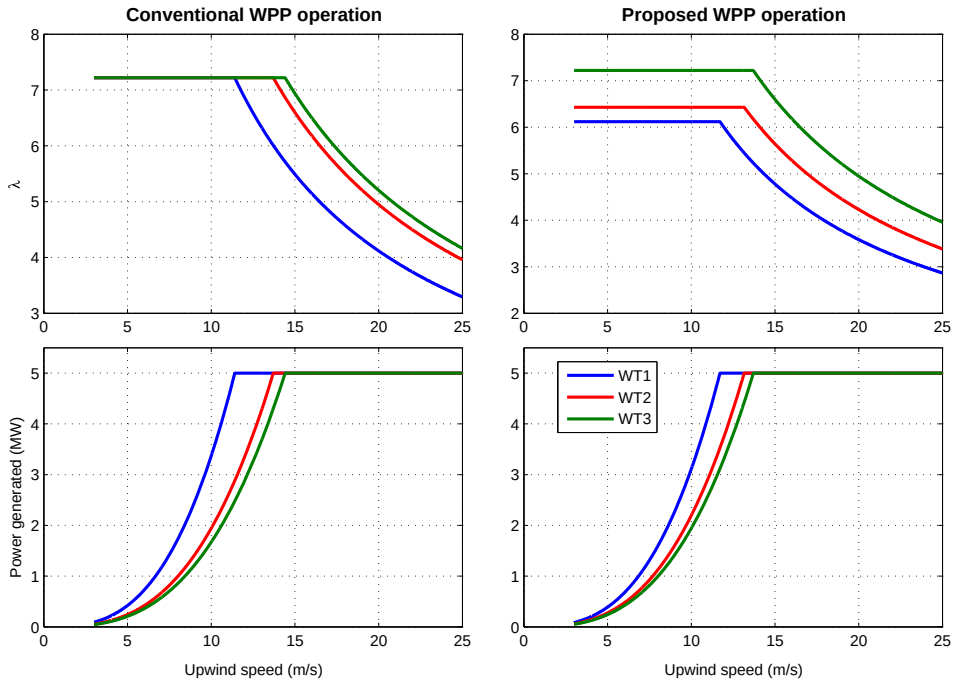

Figure 3.12: Tip speed ratio (λ) of each wind turbine (up) and power generated by each wind turbine (down) as a function of the upwind speed (considering wake effects) for both control strategies analysed.

To perform a technical assessment of both WPP control schemes (conventional and proposed WPP operation) the power generated and the energy yield per year by the set of three wind turbines (WT1, WT2 and WT3) as a function of the upwind speed is calculated and displayed in Figure 3.13. As it is shown, the effectiveness of operating the appropriate wind turbines at their non–optimum points to maximise the total energy capture by the WPP is demonstrated. Thus, the energy extracted per year by the set of three

wind turbines is 44.62 GWh/year for the optimal WPP operation case and 42.85 GWh/year by considering the conventional approach based on optimal WT operation. It represents an increase of 3.97% of the energy produced per year.

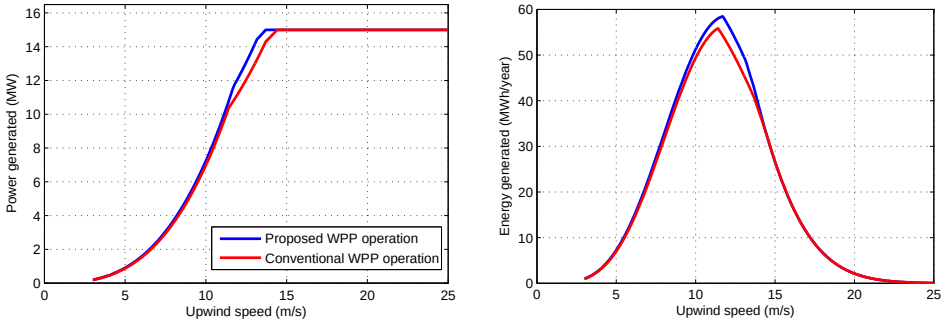

(a) (b)

Figure 3.13: Power produced (a) and energy yield (b) by the set of three wind turbines (WT1, WT2 and WT3) as a function of the upwind speed for both types of control systems.

It is important to note that the wind direction of the scenario assumed for this conceptual case study is always kept constant (best possible scenario for the proposed concept). However, in order to accurately quantify both WPP operation alternatives, this methodology is applied to a realistic case study, in which the wind direction is changing with the time.

3.4.2 Application case

The wind power plant layout of the system under study is shown in Figure 3.14. It consists of 9 wind turbines laid out in a rectangular matrix of 3 rows and 3 columns. The spacing between wind turbines is detailed in the figure. Each wind turbine has the same characteristics of the previous case, i.e., 5 MW of rated power and 126 m of rotor diameter.

Wind speed of each upstream turbine is randomly generated by means of a normal distribution function, $\mathcal{N}(\mu_i, \sigma_k^2)$, whose average value μ is estimated by using a Weibull distribution with the dimensionless shape (k) and scale (c) parameters obtained from [113, 114], and the standard deviation parameter σ is set to 0.5 m/s. It has been considered 12 incoming wind direction sectors of 30° each.

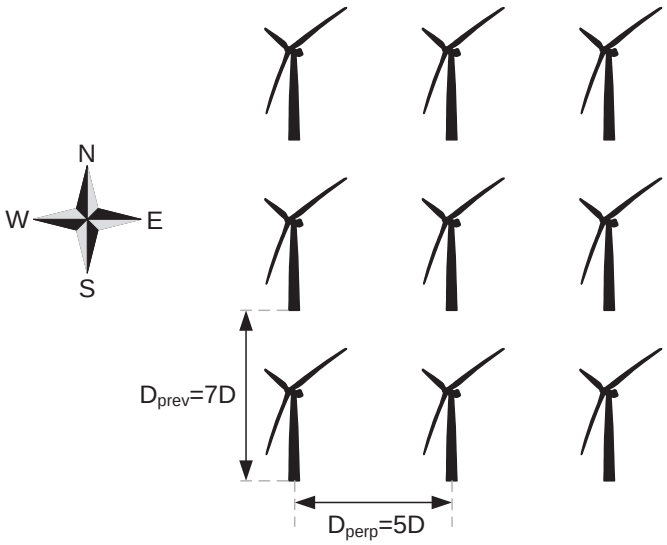

Figure 3.14: Schematic layout of the system under study consisting of 9 wind turbines laid out in a regular matrix of 3 rows and 3 columns.

Figure 3.15 displays the wake effect within the wind farm for each wind direction sector considered in the study. As it can be seen, the impact of wake effect on the wind turbines can be classified into three main groups:

- for wind direction sectors of 0°, 90°, 180° and 270°, six wind turbines are completely affected by wakes (three affected by single wakes and three by multiple wakes).
- for wind direction sectors of 30°, 150°, 210° and 330°, four wind turbines are partially affected by wakes (three affected by partial wakes and one by multiple wakes).
- for wind direction sectors of 60°, 120°, 240° and 300°, only two wind turbines are partially affected by wakes (both affected by partial wakes and none by multiple wakes).

Analogously to the previous case, the procedure of obtaining the optimal operating points of each wind turbine for each wind direction sector that maximise the total WPP power generation is carried out. Table 3.2 shows the obtained results. It should be noted that wind direction sectors of 0° and 180° are distinguished from 90° and 270° because of the spacing between wind turbines is different.

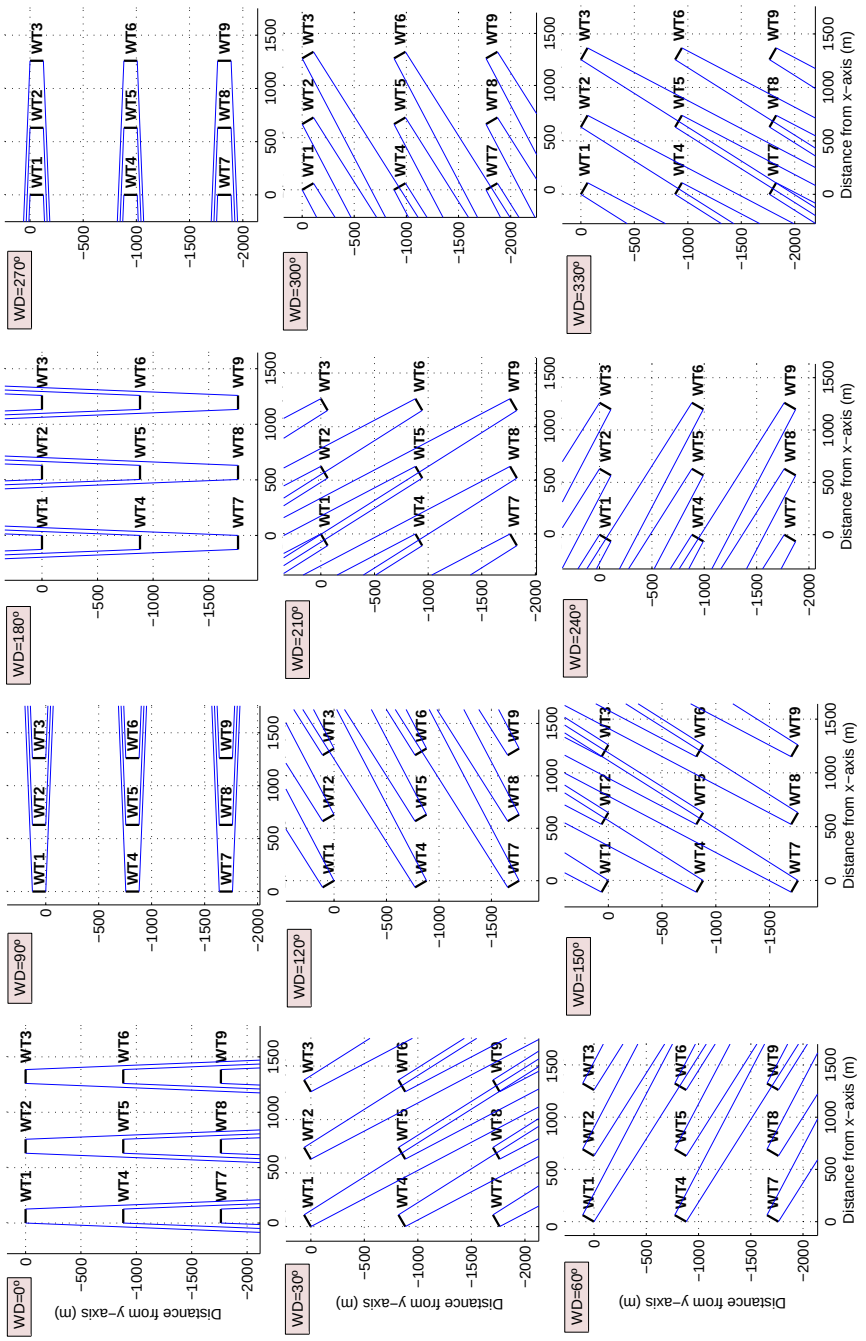

Figure 3.15: Wake effect within the wind farm for each wind direction sector considered in the study.

Table 3.2: Nominal operating points of all the wind turbines for any wind direction.

(a) Wind directions = 0° and 180°

	λ^N	C_P^N	W_s^N (m/s)	ω^N (rad/s)
Upwind turbines	6.12	0.4075	11.7121	1.1377
WTs affected by single wakes	6.43	0.4241	11.5574	1.1796
WTs affected by multiple wakes	7.22	0.4412	11.4060	1.3072

(b) Wind directions = 90° and 270°

	λ^N	C_P^N	W_s^N (m/s)	ω^N (rad/s)
Upwind turbines	6.01	0.4003	11.7820	1.1240
WTs affected by single wakes	6.30	0.4178	11.6150	1.1615
WTs affected by multiple wakes	7.22	0.4412	11.4060	1.3072

(c) Wind directions = 30°, 150°, 210° and 330°

	λ^N	C_P^N	W_s^N (m/s)	ω^N (rad/s)
Upwind turbines	6.62	0.4315	11.4910	1.2075
WTs affected by partial wakes	6.74	0.4351	11.4593	1.2260
WTs affected by multiple wakes	7.22	0.4412	11.4060	1.3072

(d) Wind directions = 60°, 120°, 240° and 300°

	λ^N	C_P^N	W_s^N (m/s)	ω^N (rad/s)
Upwind turbines	6.88	0.4382	11.4318	1.2484
WTs affected by partial wakes	7.22	0.4412	11.4060	1.3072
WTs affected by multiple wakes	–	–	–	–

Once the nominal operating points of all the wind turbines for any wind direction sector are known, the power generated by each wind turbine as a function of the upwind speed can be determined. As it is shown in Figure 3.16, the power curves of each turbine obtained for the incoming wind directions of 60°, 120°, 240° and 300° are more similar than for other wind directions, since the wake effect has a reduced impact on the turbines. However, those are more different for wind directions of 90° and 270° as a consequence of the greatest wake effect.

Next, similarly to the prior example, the power generated by the WPP for each wind direction sector considered, is calculated and presented in Figure 3.17. As discussed above, the major benefit of operating some wind turbines at their non–optimum points is given for wind directions of 90° and 270°, while the improved efficiency achieved for wind directions of 60°, 120°, 240° and 300° is very limited, as expected.

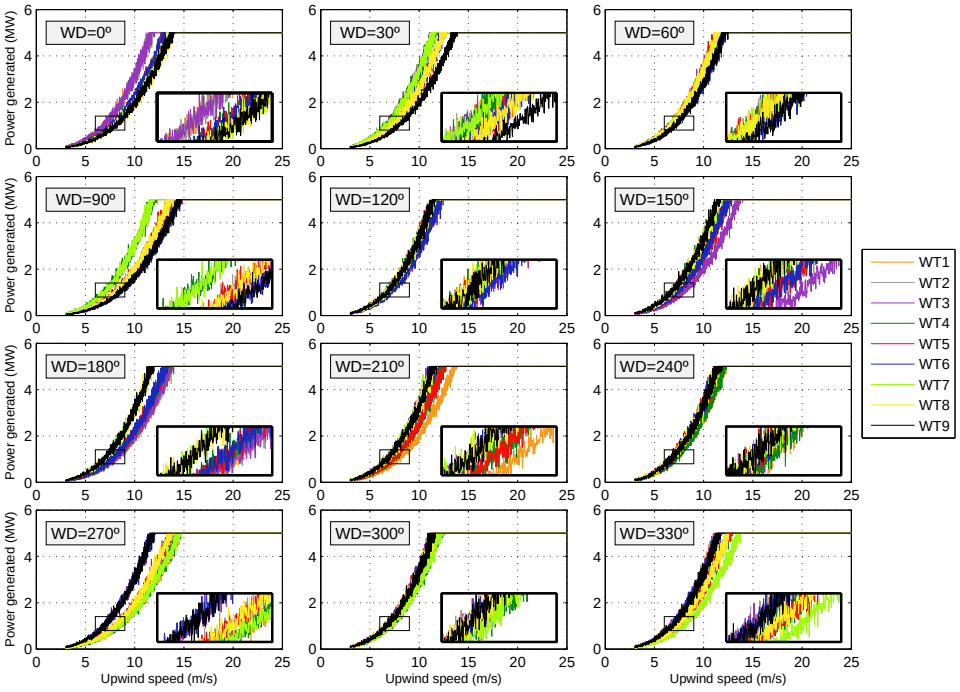

Figure 3.16: Power generated by each wind turbine, for each wind direction sector, as a function of the upwind turbine.

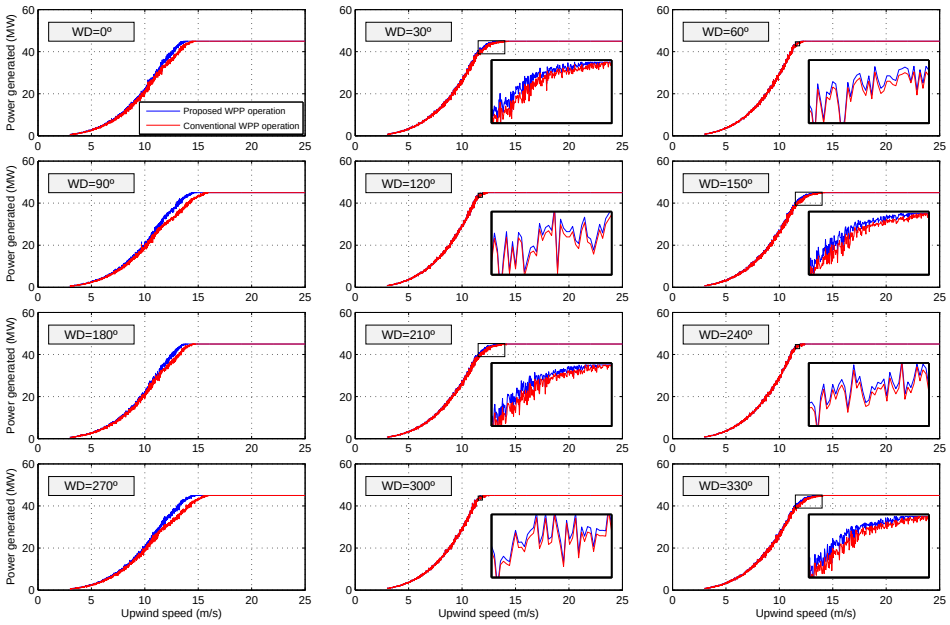

Figure 3.17: Power generated by the wind power plant (WPP), for each wind direction sector, as a function of the upwind turbine.

Finally, the energy yield per year by the WPP, for both control strategies considered, is computed. In order to evaluate the influence of the probability of occurrence of the wind directions on the energy captured, two different wind roses distribution functions are taking into account. The results are presented in Figure 3.18 and detailed in Table 3.3.

Table 3.3: Technical assessment of both WPP control strategies considering two different wind roses.

	Energy produced (GWh/year)		**Energy increment (%)**
	Scenario 1	**Scenario 2**	
Wind rose (a)	117.89	125.74	6.24
Wind rose (c) [91]	142.37	145.07	1.86

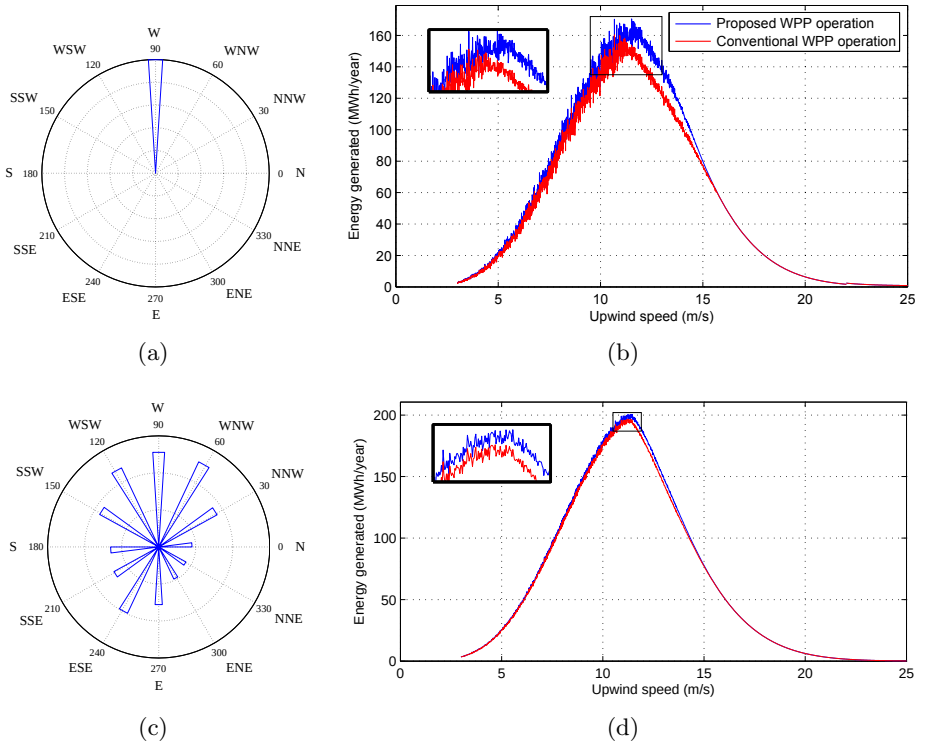

Figure 3.18: (a) and (c): Wind roses for the two cases under study. (b) and (d): Energy produced by the wind power plant (WPP) for both types of control systems and taking into account wind roses (a) and (c), respectively.

where scenario 1 refer to the proposed control strategy based on optimal WPP operation and scenario 2 corresponds to the conventional approach based on optimal WT operation. The wind rose of Figure 3.18(c) is obtained from [91] and reports the meteorological mast data from Horns Rev.

Hence, the cost associated with the annual energy increment achieved during a lifetime of the installation of 20 years accounts for 5.75 M€ for wind rose (a) and 1.98 M€ for wind rose (c) considering a price of energy of 46.84 €/MWh [115], a market interest of 4.5% [116] and an inflation rate of electricity prices of 2% [117].

3.5 Conclusions of the chapter

In this chapter, the potential benefit of operating some wind turbines at their non–optimum points in the attempt of reducing the wake effect within a wind power plant, such that its total power output is maximised, is analysed from the steady state point of view. A description of the current wind power plant control strategy based on an individual optimisation of each turbine, as well as, the impact of wake effects on wind power generation, is presented. The implemented methodology has been applied to two particular study cases to assess the performance of both control approaches. According to the results obtained for both application examples, the effectiveness of the proposed concept is demonstrated. Thus, an increase from 1.86% up to 6.24% in the annual energy captured by the wind power plant can be achieved (depending on the wind rose at the WPP location) by operating the upstream turbines slightly away from their optimum point and reducing the wake effect within the wind power plant.

4

Technical and economic assessment of offshore wind power plants based on variable frequency operation of wind turbine clusters with a single power converter

4.1 Introduction

Unlike offshore wind farms connected through HVAC transmission links where the collection grid frequency is synchronised with the electrical network frequency (50 or 60 Hz), offshore wind farms using voltage source converters for high voltage DC transmission (VSC–HVDC) allows variable frequency operation within the OWPP collection grid. This ability of HVDC transmission to electrically decouple the OWPP collection grid from the onshore power system leads to propose new offshore wind power plant designs in order to find a more cost–effective solution than the conventional OWPP topologies aforementioned in Chapter 2.

In this chapter, an alternative proposal for synchronous generator based wind power plants connected to the onshore grid via an HVDC transmis-

sion link is presented and analysed from the technical and economic point of view. It is based on removing the individual power converter of each wind turbine and connecting an entire AC collection grid (or a wind turbine cluster) to a Single Large Power Converter which operates at Variable Frequency (SLPC-VF). Thereby, an unique VSC-HVDC converter is in charge of controlling the whole offshore wind power plant (or the WT cluster) and all the wind turbines operate at the same electrical frequency, which is time variant. The main advantage of this novel concept lies in its capital cost savings and its expected maintenance cost reduction as fewer components are required. However, this novel approach entails the drawback of not achieving maximum power extraction efficiency of the WPP when the wind speed differs between WTs, since variable speed generator control cannot be individually provided to each turbine. Therefore, this proposed concept is specially worthwhile for HVDC interfaced offshore or remote OWPPs where the wind flow is assumed to be more uniform compared to onshore and maintenance issues have a greater relevance.

This proposed OWPP topology has been also investigated by some researchers during the recent years. Some of these studies are focused on the implementation and validation of different controls of this single VSC–HVDC converter [47–51], while others deals with the energy capture analysis of both OWPP topologies (conventional and proposed) without taking into account any cost assessment [52–54, 56]. In [50] and [55], costs are considered in order to analise both the technical and economic benefits of the proposed scheme compared to the conventional case. However, the former only computes the investment costs without taking into consideration the energy losses produced during the lifetime of the installation, and the latter calculates both capital expenditures and costs associated with energy losses, but it provides neither corrective nor preventive maintenance energy losses.

The technical and economic analysis carried out in this chapter considers both the capital expenditures (CAPEX) and the operational and maintenance (O&M) energy costs. With the aim to thoroughly assess the feasibility of the proposed OWPP topology compared to the conventional scheme for any OWPP layout under any wind condition, a detailed methodology is developed and applied to a case study. In order to obtain accurate results, a wake model considering single, partial and multiple wakes within a OWPP is considered. The implemented algorithm takes into account the steady state and maintenance (preventive and corrective) energy losses produced by the OWPP over the lifetime of the offshore wind project, as well as investment and operation and maintenance (O&M) costs, to provide a comprehensive technical and economic assessment of each WPP topology analysed. Due

to the uncertainty of certain parameters, a sensitivity analysis varying the cost and efficiency of the individual power converters of each wind turbine, as well as the main economic indicators, has been performed.

For the sake of simplicity, the chapter hereinafter only refers to the proposed topology by considering a single VSC–HVDC converter connected to the whole WPP (one unique cluster). However, it can be extrapolated to consider several wind turbine clusters, such that each turbine cluster is connected to its respective common power converter.

4.2 Wind power plant concepts analyzed

In this section, both the conventional and proposed offshore wind power plant topologies analysed are described. Figure 4.1 shows the electrical layout of both OWPP concepts considered.

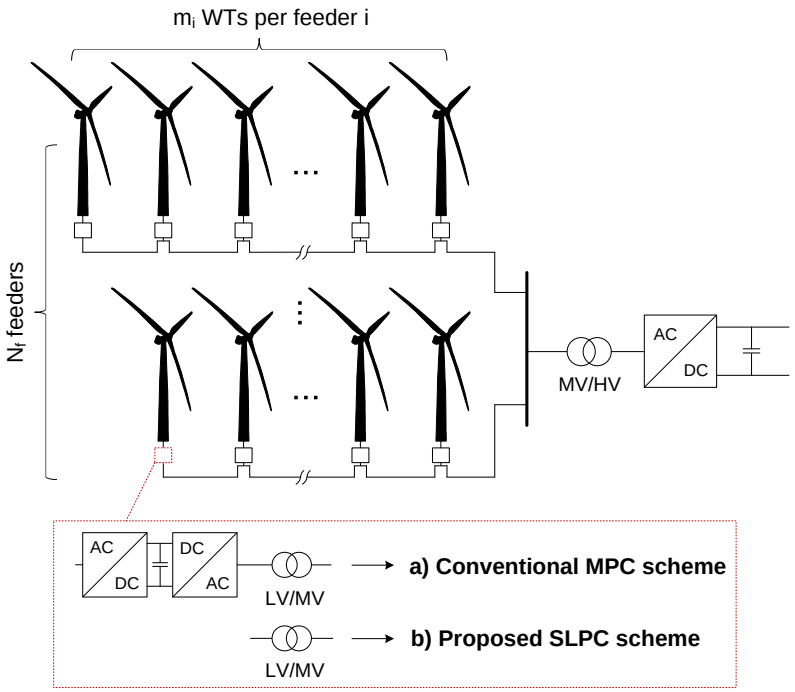

Figure 4.1: Example of an OWPP (or an unique wind turbine cluster) considering both the conventional MPC (a) and proposed SLPC (b) scheme.

- **Conventional or MPC concept:** This offshore wind power plant topology consists of a conventional AC collection grid with Multiple Power Converters (MPC), one per each wind turbine, connected to the main onshore grid by means of an HVDC transmission link. Thus, maximum power generation efficiency can be achieved regardless of the wind speed variability within the wind power plant because each full power converter allows independent speed control for each wind turbine. Likewise, the single VSC–HVDC converter operates at a standard frequency (50 or 60 Hz) within the collection grid.
- **Proposed or SLPC concept:** As it can be seen in Figure 4.1, this offshore wind power plant scheme is based on removing the individual full power converter of each turbine, so that the Single Large Power Converter (SLPC) provides active and reactive power control for all wind turbines. Thereby, capital cost savings can be obtained as fewer components are required. Nevertheless, the impossibility of independently controlling the speed of each wind turbine implies the fact of not being able to guarantee the maximum power extraction efficiency in opposition to the MPC concept.

  This single VSC–HVDC is intended to be operated at variable frequency (SLPC–VF) within the collection grid to maximise (as much as possible) the WPP energy captured for the chosen topology. However, this chapter also considers the possibility that such converter operates at a constant frequency (SLPC–CF) with the aim of evaluating the effectiveness of implementing an optimum electrical frequency calculation algorithm for variable frequency operation within the OWPP.

Hence, three different wind power plant concepts will be analyzed in this chapter: multiple power converters (MPC) and single large power converter operated with variable frequency (SLPC–VF) or constant frequency (SLPC–CF).

4.3 Methodology overview

The flow chart of the proposed methodology for technical and economic assessment of OWPPs is presented in Figure 4.2. It consists of six steps with its input data required by each one. As it can be seen, this six–steps approach is repeated as many times as OWPPs (index i) and wind conditions (index j) are being analysed. In addition, in order to evaluate the influence of wind speed variability in wind farms, another loop is considered (index k), varying the wind speed standard deviation of the upwind turbines.

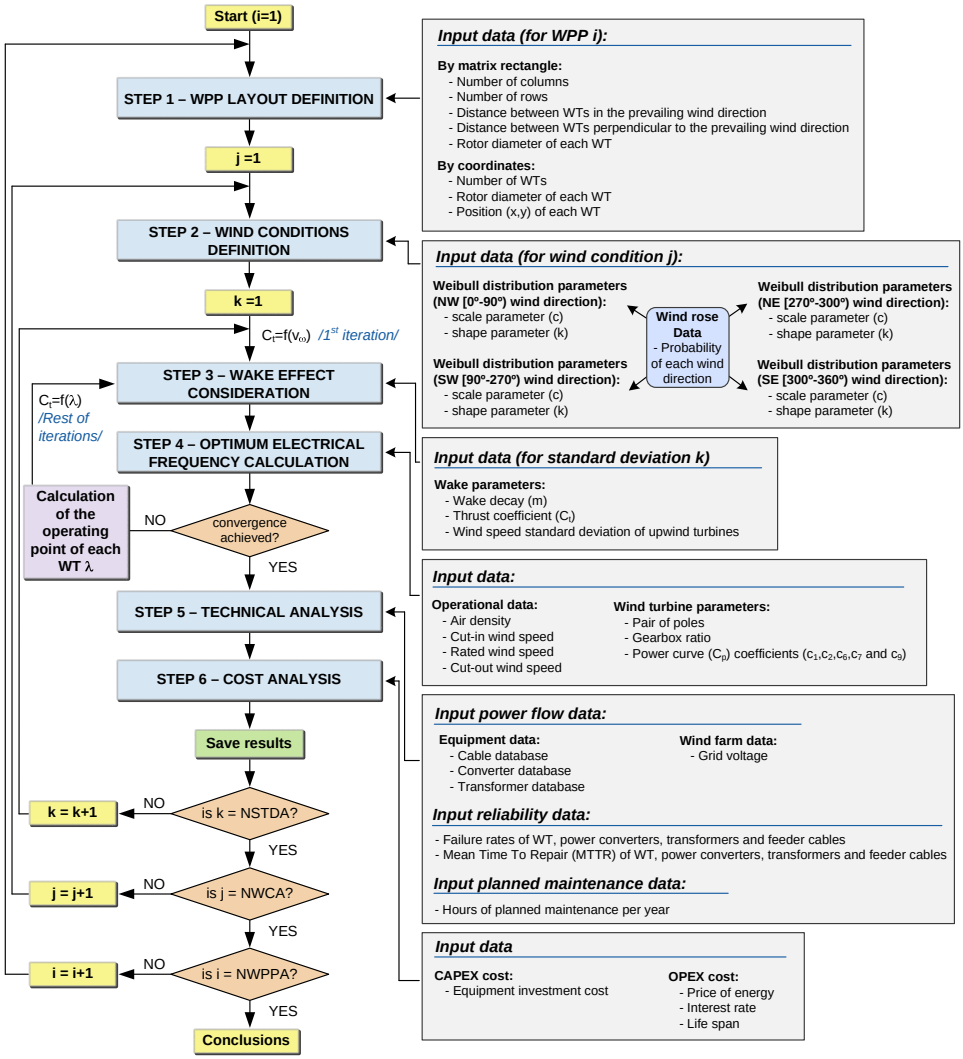

Figure 4.2: Flow diagram of the proposed methodology for technical and economic assessment of OWPPs.

The acronyms NWPPA, NWCA and NSTDA mean the number of WPPs analysed, the number of different wind conditions analysed and all the wind speed standard deviation of upwind turbines considered, respectively. It is worth mentioning that a new assessment tool (explained in detail in Appendix B) has been created to apply the following methodology.

4.3.1 Wind power plant layout definition (step 1)

The first step of the methodology is to define a specific wind farm layout in order to compare both WPP topologies (conventional and proposed) in a same scenario. Thus, a completely generic WPP layout is defined so that it can be determined not only by considering a matrix rectangle, but also by specifying the coordinates of each wind turbine (Figure 4.3). If the WPP layout is defined by a matrix rectangle, five parameters are required: the number of rows and columns of the WPP, the distance between nearby wind turbines in the prevailing wind direction, the crosswind spacing among wind turbines within a same row and the rotor diameter of each turbine. Otherwise, if the WPP layout is defined by coordinates, the input data required are the rotor diameter of each wind turbine and its position (x,y) in meters.

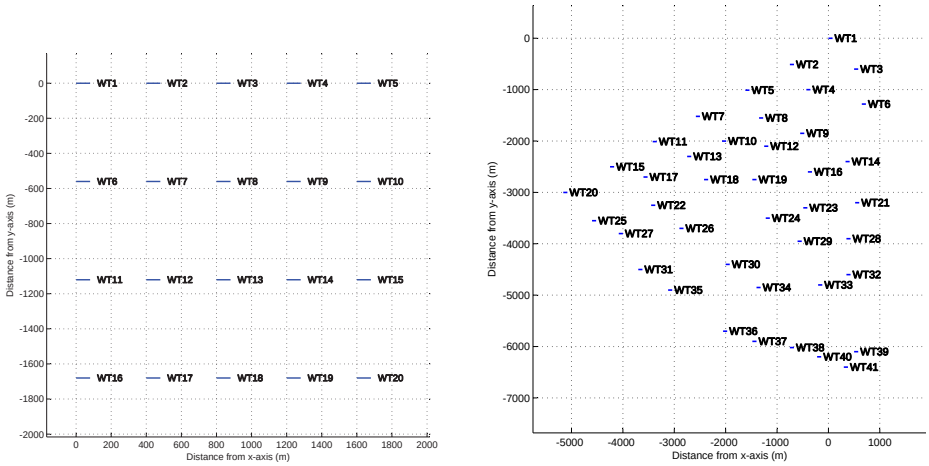

(a) (b)

Figure 4.3: Two examples of wind power plant layouts defined by matrix rectangle (a) or by coordinates (b).

4.3.2 Wind conditions definition (step 2)

In this step, wind conditions are established for the WPP–i previously defined. These wind conditions are characterised by specific wind speeds and wind directions. According to a wind rose distribution function, the likelihood that the wind blows in a certain direction at a given location, are

introduced. It is assumed that the wind strikes the blades of each turbine under the same wind direction. In order to estimate the wind speed distribution for a particular WPP–i, the Weibull probability density function is used. It is considered that the incoming wind speeds depends on its wind direction. Thereby, the number of different sets of Weibull parameters (dimensionless shape–k and scale–c) required depends on how many wind direction sectors are considered for the study.

4.3.3 Wake effect consideration (step 3)

Once the WPP–i layout and its wind conditions–j are known, the next step consists in computing the wind speed of each turbine within the WPP–i. This set of wind speeds is obtained for different scenarios varying the wind direction and the average wind speed of the WPP–i and by assigning to each case its probability of occurrence according to the wind rose and Weibull distribution functions defined in the previous step. The average wind speeds considered are delimited by the cut–in and the cut–out wind speed, 3 and 25 m/s, respectively. Hence, if, for example, 23 average wind speeds (3 to 25 m/s) and 12 wind directions (N, NNW, WNW, W,..., NNE) are taken into account, a total of 23 x 12 different sets of wind speeds are generated.

The wind speed calculation process is divided into two parts. First, given a certain incoming wind direction and an average wind speed for the entire WPP–i, the wind speeds of upstream turbines are randomly generated by means of a normal distribution function – $\mathcal{N}(\mu_{ij}, \sigma_k^2)$. Then, the wind speeds of downwind turbines are computed, taking into consideration the wake effect. The subscripts i and j of the mean value, μ_{ij}, indicate the average wind speed for a particular WPP–i and specific wind conditions-j. The subscript k of the standard deviation value, σ_k, means that the process is repeated NSTDA times with the aim to analyse the influence of wind speed variability in the upstream turbines. Regarding the downwind turbines, the widely used wake model developed by Jensen [109] has been chosen for this study, as it provides adequate accuracy and reduced computational time. It is based on global momentum conservation in the wake downstream of the wind turbine and assumes that the wake downstream of the turbine expands linearly. Detailed explanation about wake effect theory can be found in Section 3.3 of the previous chapter.

A comprehensive wake model considering single, partial and multiple wakes within a WPP has been implemented in order to obtain more accurate results. It enhances the model presented in [56] using a more real-

istic value of the thrust coefficient based on a tip–speed ratio dependence ($C_t = f(\lambda)$) rather than relying on the incoming wind speed ($C_t = f(v_w)$). In general terms, this coefficient is wind turbine specific, being the result of blade geometry, rotational speed of the rotor and the applied control strategy of the wind turbine (stall or pitch control). Due to the unavailability of tip–speed ratio value upon the start of the steady state calculation (it is not possible to compute the operating point of each wind turbine without knowing its corresponding wind speed (step 3) and the electrical frequency of the collection grid (step 4)), some iterations should be carried out to find the proper tip–speed ratio of each wind turbine. Therefore, the algorithm developed in step 3 makes a distinction between the first iteration and the others depending on the input data corresponding to the thrust coefficient C_t (Figure 4.2).

4.3.4 Optimum electrical frequency calculation (step 4)

In the fourth step, the optimum electrical frequency at which the VSC–HVDC converter should operate to maximise the power generated by the WPP, for a given set of wind speeds, is computed according to the following procedure. It should be noted that this step is only performed for the SLPC–VF concept.

First, the power P_{wti} generated by a single wind turbine expressed in (3.1) is calculated by approximating the power coefficient C_P defined in (3.2) to a polynomial of degree N_{pol} and coefficients a_j

$$C_P(\lambda, \theta_{pitch}) = \sum_{j=0}^{N_{pol}} a_j \lambda^j = \sum_{j=0}^{N_{pol}} a_j \frac{(\omega_t R)^j}{v_w^j} \tag{4.1}$$

where the pitch angle θ_{pitch} has been assumed to be zero since it will be zero, if the maximum power is to be extracted.

Thus,

$$P_{wti} = \frac{1}{2}\rho A v_{wi}^3 \sum_{j=0}^{N_{pol}} a_j \frac{(\omega_t R)^j}{v_{wi}^j} \tag{4.2}$$

For a synchronous generator, the wind turbine speed in steady state conditions can be written as

$$\omega_t = \frac{\omega_e}{pN_{gr}} \tag{4.3}$$

where p is the pole pairs number, N_{gr} is the gearbox ratio of the wind turbine and ω_e is the grid electrical angular speed within the AC collection grid.

Substituting (4.3) in (4.2) and rearranging, this can be simplified to

$$P_{wti} = \frac{1}{2}\rho A \sum_{j=0}^{N_{pol}} a_j \left(\frac{R}{PN_{gr}}\right)^j \omega_e^j v_{wi}^{3-j} \tag{4.4}$$

Therefore, the total power generated by a WPP composed of N_{wt} identical wind turbines can be written as

$$P^{GT} = \frac{1}{2}\rho A \sum_{i=1}^{N_{wt}} \sum_{j=0}^{N_{pol}} a_j \left(\frac{R}{pN_{gr}}\right)^j \omega_e^j v_{wi}^{3-j} \tag{4.5}$$

To determine the electrical angular speed ω_e that maximizes the total generated power, (4.5) is derived and equal to zero.

$$\frac{dP^{GT}}{d\omega_e} = \frac{1}{2}\rho A \sum_{i=1}^{N_{wt}} \sum_{j=1}^{N_{pol}} j a_j \left(\frac{R}{PN_{gr}}\right)^j \omega_e^{j-1} v_{wi}^{3-j} = 0 \tag{4.6}$$

which can also be expressed as

$$\sum_{j=1}^{N_{pol}} b_j \omega_e^{j-1} = 0 \tag{4.7}$$

where b_j is defined as

$$b_j = \frac{1}{2}\rho A j a_j \left(\frac{R}{PN_{gr}}\right)^j \sum_{i=1}^{N_{wt}} v_{wi}^{3-j} \tag{4.8}$$

Solving (4.7), $N_{pol} - 1$ solutions are found. Among these roots, only the real ones can be substituted in (4.5) in order to determine the optimal solution (ω_e^{opt}).

The number of optimum electrical frequencies obtained in this step will be the same as sets of wind speeds previously calculated in step 3 for a particular WPP–i, a certain wind condition–j and a specific wind speed standard deviation–k of the upwind turbines. It is important to remark that the resulting optimum electrical frequency ω_e^{opt} must be within an admissible range delimited by the saturation effects of the generators and transformers for low frequency and the field weakening effects for high frequency [118].

To illustrate the aforementioned concept, a simple example is included below. Figure 4.4 shows the optimum electrical frequency at which the

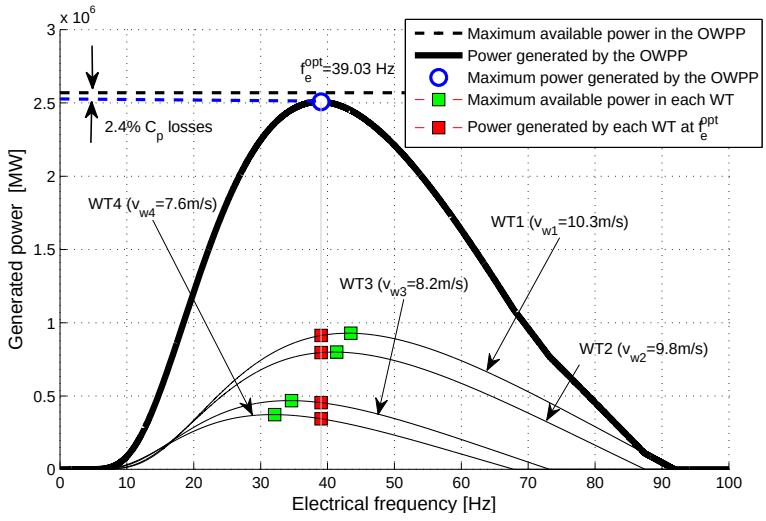

(a)

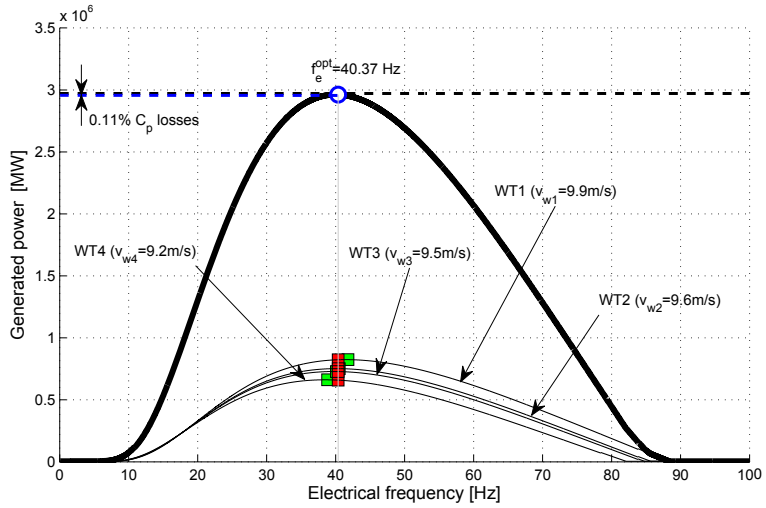

(b)

Figure 4.4: Generated power depending on the electrical frequency in a wind turbine cluster composed by four wind turbines with high (a) and low (b) wind speed variability among them.

VSC–HVDC power converter should operate to maximise the total power generated by a cluster composed of four wind turbines considering different wind speed variabilities among them.

As it is shown, the higher wind speed diversity cause larger deviations of the operating point of each turbine from its optimum and, therefore, the more energy is lost (know as C_P losses in [50, 56, 119]) by the wind turbine cluster compared to the maximum available power that can be produced with the conventional MPC approach.

4.3.5 Technical analysis (step 5)

According to the output data resulting from step 1 to 4, the technical analysis developed in step 5 of the methodology (Figure 4.2) to evaluate the feasibility of the proposed OWPP topology, is presented in this subsection. In order to provide an accurate assessment, different types of losses have been taken into consideration. As it can be seen from Figure 4.5, these losses can be classified into two main groups: the steady state losses (C_P losses and power flow losses) and the unavailability losses of the system due to the failure of a certain equipment (corrective maintenance losses) or the partial or total stop of the installation during a fixed time for preventive maintenance purposes (preventive maintenance losses).

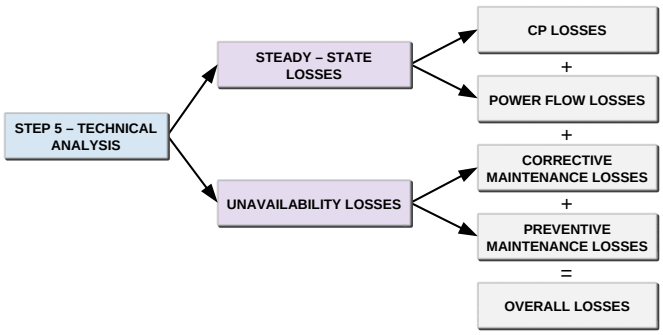

Figure 4.5: Classification of the different losses considered in step 5 (technical analysis).

As mentioned above in Section 4.2, the analysis compares between three different configurations: MPC, SLPC–VF and SLPC–CF (for the sake of brevity, hereinafter referred to as C1,C2 and C3).

It should be noted that this technical analysis is carried out as many times as offshore WPPs or clusters and wind conditions are analysed (NWPPA and NWCA), as well as for different wind speed standard deviation values among upstream turbines considered (NSTDA).

Steady state losses

Steady state losses refer to the energy lost over the lifetime of an OWPP as a result of the efficiency losses of its components (transformers, converters, cables, etc.) or due to the inherent limitations of the OWPPs topologies analysed (power flow losses and C_P losses, respectively).

C_P losses Energy efficiency losses (so–called "C_P losses") occur due to the nature of the proposed WPP concept based on a centralised control of a common power converter connected to a cluster of wind turbines. Unlike conventional WPP topology in which each dedicated power converter regulates the speed of each generator according to a MPPT approach [21,27,102,103,120], in the proposed WPP topology, the wind speed differences among turbines within a cluster bring about the inability to operate each generator at its optimum point (maximum power coefficient C_P^{max} – optimal tip speed ratio λ_{opt}).

The power output generated by a cluster of N_{wt} wind turbines for each concept can be expressed as

$$P^{GTC1} = \frac{1}{2}\rho A C_P^{max} \sum_{i=1}^{N_{wt}} v_{wi}^3 \tag{4.9}$$

$$P^{GTC2} = \frac{1}{2}\rho A \sum_{i=1}^{N_{wt}} \underbrace{C_{Pi}}_{f(\omega_e^{opt})}\ v_{wi}^3 \tag{4.10}$$

$$P^{GTC3} = \frac{1}{2}\rho A \sum_{i=1}^{N_{wt}} \underbrace{C_{Pi}}_{f(2\pi 50)}\ v_{wi}^3 \tag{4.11}$$

where the only difference between them is the power coefficient C_P value of each wind turbine. In the first case (C1 or MPC), all the wind turbines achieve the maximum power coefficient C_P^{max} optimizing their power generation. However, considering both SLPC-VF and SLPC-CF topologies (C2 and C3), each turbine operates at a different C_P value (lower than C_P^{max}) set by the optimal electrical frequency ω_e^{opt} for each scenario or a constant frequency of $2\pi 50$ rad/s, respectively. As an example, Figure 4.6 shows the operating point of 9 wind turbines for a given set of wind speeds and for each configuration.

In order to determine the "C_P losses" for each topology, the energy cap-

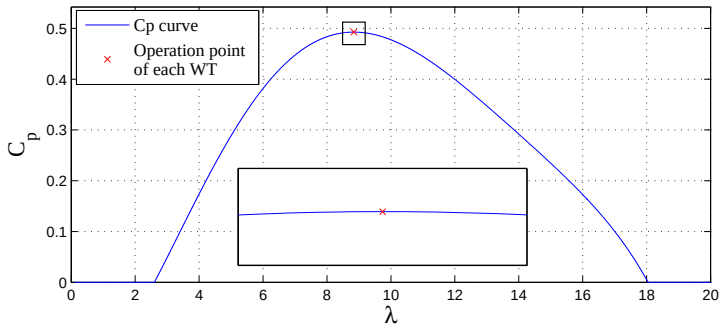

(a)

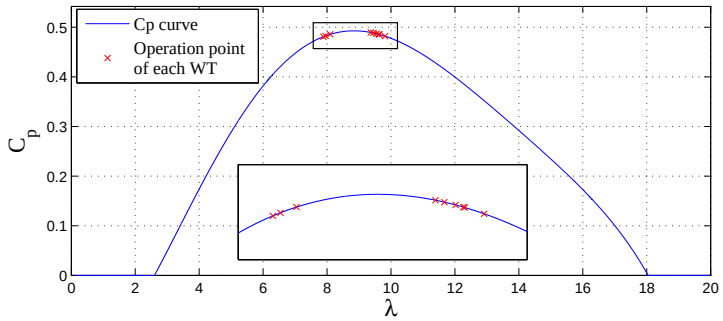

(b)

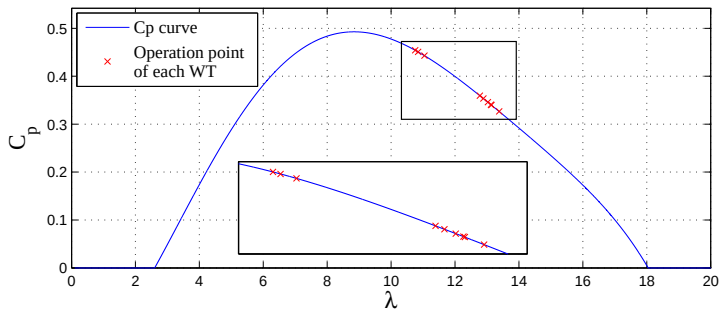

(c)

Figure 4.6: C_P–λ curve with the operating points of 9 wind turbines generating with different wind speeds for the three concepts analysed: a) MPC, b) SLPC-VF and c) SLPC-CF.

tured by a cluster over a period of time T is calculated as

$$E^{GT} = T \sum_{i=1}^{N_{aws}} \sum_{j=1}^{N_{wd}} P_{ij}^{GT} p_{wbij}\, p_{wrj} \tag{4.12}$$

where p_{wrj} and p_{wbij} are the probabilities of occurrence according to the wind rose and Weibull distribution functions, respectively, N_{wd} and N_{aws} are the number of wind directions and average wind speeds considered, and P_{ij}^{GT} is the power generated by a cluster for a particular average wind speed (i) and a certain wind direction (j).

Therefore, the resulted "C_P energy losses" for each topology are

$$E_{C_P\_L}^{C1} = 0 \tag{4.13}$$

$$E_{C_P\_L}^{C2} = E^{GTC2} - E^{GTC1} \tag{4.14}$$

$$E_{C_P\_L}^{C3} = E^{GTC3} - E^{GTC1} \tag{4.15}$$

Power flow losses As it is shown from (7.3), power flow losses are obtained by the difference between the total energy generated at the turbine connection and the total net energy delivered to the grid through the point of common coupling (PCC).

$$E_{PF\_L} = T \sum_{i=1}^{N_{aws}} \sum_{j=1}^{N_{wd}} (P_{ij}^{GT} - P_{ij}^{NT}) p_{wbij}\, p_{wrj} \tag{4.16}$$

Analogously to the previous case, this energy losses are calculated for several cases (varying the average wind speed and the wind direction) taking into account their probability of occurrence.

The net active power transferred to the grid for each scenario (P_{ij}^{NT}) is computed by means of a power flow calculation. Given a cable database and a voltage level within the WPP, an inter–array cable selection is made base on minimising their cross–sectional area ensuring a proper and continuous operation under full load without being damaged. Thereby, the total costs are minimised due to the lower copper sections needed.

Unavailability losses

As discussed above, the unavailability or maintenance losses are classified into two types depending on whether are unexpected or planned losses. The former, so–called corrective maintenance losses, are due to an unforeseen equipment failure and can be of crucial importance when the WPP is inaccessible by boat or helicopter because of harsh weather conditions (i.e., wind and significant wave height). The latter, known as preventive maintenance losses, refer to the expected energy losses during a fixed time along

the year due to partial or total outages in the WPP designed to prevent possible damage of its components. The period of time intended for repair and maintenance operations is chosen to maximise the availability of WPPs. Therefore, these type of losses are usually small as they are planned to be performed during periods of low wind speeds where the energy yield is limited or nonexistent.

According to some experiences from Middelgrunden and Nysted OWPPs reported in [93, 94], respectively, the average OWPP availability can be assumed to be 95–96% (covering both wind turbine and collection grid availability).

Corrective maintenance losses Reliability of WPPs, especially offshore, can be critical if the failure of its components occurs in a period of adverse weather where accessibility to the WPP may be limited or none. Likewise, the unavailability of appropriate vessels at a specific time can lead to long downtimes. For these reasons, corrective maintenance can be extensive and costly [121].

The unplanned maintenance losses or the so–called Expected Energy Not Supplied (EENS) are calculated based on the reliability multi–state models explained in [92]. This models considers that each component has several states of service and has a probability of malfunction in each state per year.

Table 4.1 shows the five basic components of a WPP considered in the study. For simplicity, it is assumed that all wind turbines, power converters, transformers and feeder cables in one cluster are of the same type, respectively. Switches performance have not been taken into account, since they are presumed to be in service all the time. The radial connection topology, adopted for most OWPPs designs, have been considered for the analysis.

Table 4.1: Reliability indices of the WPP components considered in the model.

Equipment	**Availability**	**Unavailability**
Wind Turbine	A_w	U_w
Power Converter	A_c	U_c
Feeder Cable	A_f	U_f
LV/MV Transformer	A_{tt}	U_{tt}
MV/HV Transformer	A_{tp}	U_{tp}

The availability (A) and unavailability (U) of each equipment is defined

as

$$A = \frac{1}{1 + \lambda \cdot MTTR} \tag{4.17}$$

$$U = 1 - A \tag{4.18}$$

where λ is the failure rate and MTTR is the mean time to repair the faults.

In general terms, the EENS (or corrective maintenance losses) of a system can be obtained by

$$EENS = E_{CM\_L} = T \sum_{i=1}^{N} P_{ci}\, p_{oi} \tag{4.19}$$

where p_{oi} is the probability of operation of each state–i, P_{ci} is the power constrained or not delivered in each state–i due to the equipment failures, N is the maximum number of states, and T is the period of time.

SLPC–VF and SLPC–CF topologies are equally evaluated in terms of EENS, since the only difference between them (i.e., the electrical frequency calculation method) is not taken into account within the reliability model of this paper. Therefore, EENS is calculated for the two following WPP concepts analysed: MPC and SLPC.

As it can be seen in Figure 4.1, a generic WPP consisting of N_f feeders with m_1, m_2,..., m_{N_f} machines per feeder is considered for the analysis of both WPP schemes. The availability of the wind turbine, the power converter and the LV/MV transformer (MPC case) and the availability of these components without the dedicated converter (SLPC case), can be combined as A_{wctt}=$A_w \cdot A_c \cdot A_{tt}$ and A_{wtt}=$A_w \cdot A_{tt}$, respectively. It can be done due to its series connection where an individual failure of a component affects the overall block.

Likewise, the combined availability of the converter platform and the MV/HV transformer can be represented by A_{ctp}=$A_c \cdot A_{tp}$ for both MPC and SLPC configurations. (4.20) and (4.21) show the formula used to calculated the EENS for both WPP topologies.

$$
\begin{aligned}
E_{CM\_L}^{C1} &= T\Bigg[\Bigg(\sum_{i=1}^{N}\sum_{j=1}^{S_i}\Bigg[(j-1)P_i^{fw} + \binom{S_i}{j-1}P_i^{fnw}\Bigg]\cdot\Psi^{C1} \\
&+ \sum_{i=1}^{N}(P_i^{fw}+P_i^{fnw})\Phi^{C1}\Bigg)\cdot A_{ctp}^{1}U_{ctp}^{0} \\
&+ P^{GT}A_{ctp}^{0}U_{ctp}^{1}\Bigg]
\end{aligned} \tag{4.20}
$$

$$
\begin{aligned}
E_{CM\_L}^{C2\&C3} &= T\Bigg[\Bigg(\sum_{i=1}^{N}\sum_{j=1}^{S_i}\Bigg[(j-1)P_i^{fw} + \binom{S_i}{j-1}P_i^{fnw}\Bigg]\cdot\Psi^{C2\&C3} \\
&+ \sum_{i=1}^{N}(P_i^{fw}+P_i^{fnw})\Phi^{C2\&C3}\Bigg)\cdot A_{ctp}^{1}U_{ctp}^{0} \\
&+ P^{GT}A_{ctp}^{0}U_{ctp}^{1}\Bigg]
\end{aligned} \tag{4.21}
$$

with

$$\Psi^{C1} = A_f^{|F_i^w|}U_F^{N_f-|F_i^w|}A_{wctt}^{S_i-(j-1)}U_{wctt}^{j-1} \tag{4.22}$$

$$\Psi^{C2\&C3} = A_f^{|F_i^w|}U_F^{N_f-|F_i^w|}A_{wtt}^{S_i-(j-1)}U_{wtt}^{j-1} \tag{4.23}$$

$$\Phi^{C1} = A_f^{|F_i^w|}U_f^{N_f-|F_i^w|}A_{wctt}^{0}U_{wctt}^{S_i} \tag{4.24}$$

$$\Phi^{C2\&C3} = A_f^{|F_i^w|}U_f^{N_f-|F_i^w|}A_{wtt}^{0}U_{wtt}^{S_i} \tag{4.25}$$

The variable P_i^{fw} means the sum of power generated by all the turbines connected to the $|F_i^w|$ number of feeders in service for each state–i. In the same manner, P_i^{fnw} is the total power extracted by all the turbines connected to the $N_f - |F_i^w|$ feeders that have failed for each state–i. $N(=2^{N_f})$ is the maximum number of states when the platform converter and the MV/HV transformer are working ($A_{ctp}^{1}U_{ctp}^{0}$). Otherwise, one more state must be taken into account in which the total power generated by the cluster (P^{GT}) is curtailed as a consequence of a platform converter or a MV/HV transformer failure ($A_{ctp}^{0}U_{ctp}^{1}$). Finally, S_i is the number of machines connected to the feeders that are in service for each state–i.

Mathematically, it can be written as

$$P_i^{fnw} = \sum_{k \in F_i^{nw}} \sum_{j=1}^{m_k} P_{kj}^{wt} \qquad \forall i \in [1, \ldots, N] \tag{4.28}$$

$$P_i^{fw} = \sum_{k \in F_i^{w}} \sum_{j=1}^{m_k} P_{kj}^{wt} \qquad \forall i \in [1, \ldots, N] \tag{4.29}$$

$$S_i = \sum_{k \in F_i^{w}} m_k \qquad \forall i \in [1, \ldots, N] \tag{4.30}$$

where $F = \{1, 2, \ldots, N_f\}$ is the set of feeders, F_i^w the subset of feeders in service, and F_i^{nw} the subsets of feeders that are not working properly depending on the state–i.

Although $E_{CM\_L}^{C2}$ and $E_{CM\_L}^{C3}$ are based on the same formula (4.21), it should be noticed that their values may not be the same as P_i^{fw} and P_i^{fnw} can differ between SLPC–VF and SLPC–CF.

Preventive maintenance losses In order to calculate the preventive or planned maintenance losses the only input datum required is the number of hours for planned maintenance purposes (h_{pm}) per a certain period of time T (typically a year). Thus, depending on whether h_{pm} is greater or less than the hours with non–profitable wind (i.e., wind speeds lower than cut–in speed, h_{lci}), the planned maintenance losses can be expressed as follows

$$E_{PM\_L} = \begin{cases} 0 & \text{if } h_{pm} \leq h_{lci} \\ \alpha E_{curtailed} & \text{if } h_{pm} > h_{lci} \end{cases} \tag{4.31}$$

where α is a correction factor which takes into account that even when weather conditions are favourable it might not be always possible to perform maintenance operations (e.g., during a period with harsh weather, there might be an instant of quietness, but too brief to fulfill the maintenance duties), and $E_{curtailed}$ is the minimum energy that would be lost in the hypothetical ideal case in which preventive maintenance is only carried out for the more suitable weather conditions. Thereby, the parameter α is greater than one ($\alpha > 1$) and $E_{curtailed}$ is given by

$$\begin{aligned} E_{curtailed} &= T\Bigg(\sum_{i=1}^{N_{sc}-1} \sum_{j=1}^{N_{wd}} p_{wbij}\, p_{wrj} P_{ij}^{GT} \\ &+ \sum_{j=1}^{N_{dc}-1} p_{wbN_{scj}}\, p_{wrj} P_{N_{scj}}^{GT} \\ &+ \beta_{N_{sc}N_{dc}}\, p_{wbN_{sc}N_{dc}}\, p_{wrN_{dc}} P_{N_{sc}N_{dc}}^{GT} \Bigg) \end{aligned} \tag{4.32}$$

where N_{sc} and N_{dc} are the number of average wind speeds and directions curtailed for preventive maintenance issues that fit the the following expression

$$\underline{H} < h_{pm} - h_{lci} \leq \overline{H} \tag{4.33}$$

with

$$\underline{H} = T \left(\sum_{\substack{1 \leq i < N_{sc} \\ N_{sc} > 1}} \sum_{j=1}^{N_{wd}} p_{wbij}\, p_{wrj} + \sum_{\substack{1 \leq j < N_{dc} \\ N_{dc} > 1}} p_{wbN_{scj}}\, p_{wrj} \right) \tag{4.34}$$

and

$$\overline{H} = T \left(\sum_{\substack{1 \leq i < N_{sc} \\ N_{sc} > 1}} \sum_{j=1}^{N_{wd}} p_{wbij}\, p_{wrj} + \sum_{j=1}^{N_{dc}} p_{wbN_{scj}}\, p_{wrj} \right) \tag{4.35}$$

and $\beta_{N_{sc}N_{dc}}$ is the ratio between the energy lost due to partial or total outages in the WPP and the energy that could be generated for a specific average wind speed and direction determined by N_{sc} and N_{dc}.

$$\beta_{N_{sc}N_{dc}} = \frac{(h_{pm} - h_{lci}) - \Lambda}{T p_{wbN_{sc}N_{dc}}\, p_{wrN_{dc}}} \cdot \underbrace{\frac{P_{N_{sc}N_{dc}}^{GT}}{P_{N_{sc}N_{dc}}^{GT}}}_{=1} \tag{4.36}$$

with

$$\Lambda = T \left(\sum_{i=1}^{N_{sc}-1} \sum_{j=1}^{N_{wd}} p_{wbij}\, p_{wrj} + \sum_{j=1}^{N_{dc-1}} p_{wbN_{scj}}\, p_{wrj} \right) \tag{4.37}$$

The planned maintenance losses for each WPP topology analysed (C1, C2 and C3) can be obtained by substituting P^{GT} of (4.32) for its corresponding value presented between (4.9) and (4.11).

Overall losses

Finally, the total losses considering all the different types (steady state and unavailability losses) are resulted as

$$E_{O\_L}^{Ci} = E_{C_P\_L}^{Ci} + E_{PF\_L}^{Ci} + E_{CM\_L}^{Ci} + E_{PM\_L}^{Ci} \tag{4.38}$$

for MPC, SLPC–VF and SLPC–CF WPP topologies (i=1, 2 and 3, respectively).

4.3.6 Cost analysis (step 6)

To evaluate the total cost of the three WPP topologies analysed (MPC, SLPC–VF and SLPC–CF), a comprehensive model considering both the initial investment costs and the operation and maintenance (O&M) costs has been developed.

Investment costs

The capital expenditures (CAPEX) have been obtained using the cost functions reported in [122, 123]. All the costs are resulted in k€.

Fully–equipped wind turbines

According to [122], the cost of a fully–equipped wind turbine including not only the turbine, but also the back–to–back converter (AC/DC and DC/AC) and the LV/MV transformer (MPC scheme), as well as the transport and installation can be expressed as

$$C_{wt\&inst}^{C1} = 1.1 \cdot \underbrace{(2.95 \cdot 10^3 \cdot \ln(P_{wt}) - 375.2)}_{C_{wt}} \tag{4.39}$$

where P_{wt} is the rated power (in MW) of a single wind generator and the coefficient 1.1 accounts for transport and installation additional costs.

Thereby, the wind turbine costs for the SLPC concept can be calculated as

$$C_{wt\&inst}^{C2\&C3} = 1.1 \cdot \left(1 - \frac{K_c}{100}\right) \cdot C_{wt} \tag{4.40}$$

where K_c is the contribution in percentage of the power converter to the overall wind turbine cost.

Collection system The cost of switchgears and MVAC submarine cables contained in the MV collection grid of an OWPP are given by the following expressions based on [122].

$$C_{sg} = 40.543 + 0.76V_n \tag{4.41}$$

$$C_{ca} = \alpha + \beta \exp\left(\frac{\gamma I_n}{10^5}\right) \cdot L \tag{4.42}$$

where V_n is the nominal voltage (in kV), I_n is the cable ampacity for a specific conductor section (in A), L is the cable length (in km) and the coefficients α, β and γ depend on the nominal voltage level. For submarine cables of 30–36 kV: α=52.08 k€/km, β=75.51 k€/km and γ=234.34 1/A.

The costs associated with cable transport and installation are assumed to be

$$C_{ca\&inst} = 365L \tag{4.43}$$

where it should be noted that this is an average value which strongly depends on the particular case study characterised by a certain seabed composition, water depth, etc.

Integration system Integration system encompasses those components located between the MV collection grid and the HVDC transmission link. As it can be seen from Figure 4.1, it consists of one or several (one per WT cluster) MV/HV transformers and AC/DC power converters depending on the WPP topology and an offshore substation platform. It is assumed that the number of offshore platforms is the same for both WPP topologies.

The costs of an offshore substation platform and an AC/DC power converter are calculated by means of the following expressions [122, 123]

$$C_{pl} = 2534 + 88.7N_{wt}P_{wt} \tag{4.44}$$

$$C_{c\_ACDC} = 200P_r \tag{4.45}$$

where N_{wt} is the number of wind turbines within the OWPP and P_r is the rated power of each AC/DC power converter (in MW).

The cost of a MV/HV transformer designed for use at 50 Hz is computed as [122]

$$C_{tr50} = 42.688A^{0.7513} \tag{4.46}$$

where A is the rated power of the transformer (in MVA).

In the case of the SLPC–VF WPP topology, this cost is adapted to its operating frequency according to [57] as follows

$$C_{tr\_fr} = \frac{0.325 f_r + 0.22 f_r + 0.164 \sqrt[3]{f_r^2}}{0.325 + 0.22 + 0.164} C_{tr50} \tag{4.47}$$

where f_r is the normalised frequency, calculated as a ratio between the standard frequency and the analysed frequency ($f_r = 50\ Hz/f$).

Investment cost model The investment cost model for both WPP topologies is formulated as

$$\begin{aligned} C_{inv}^{C1} &= N_{wt} C_{wt\&inst}^{C1} + N_{ca}(C_{ca} + C_{ca\&inst}) \\ &+ N_{sg} C_{sg} + C_{tr50} + C_{c\_ACDC} + C_{pl} \end{aligned} \tag{4.48}$$

$$\begin{aligned} C_{inv}^{C2\&C3} &= N_{wt} C_{wt\&inst}^{C2\&C3} + N_{ca}(C_{ca} + C_{ca\&inst}) \\ &+ N_{sg} C_{sg} + N_{cl}(C_{tr\_fr} + C_{c\_ACDC}) \\ &+ C_{pl} \end{aligned} \tag{4.49}$$

where N_{ca} is the number of cables within the WPP, N_{sg} is the number of switchgears and N_{cl} is the number of wind turbine clusters. Notice that $C_{tr\_fr} = C_{tr50}$ for the SLPC–CF scheme (C3) if the operating constant frequency is 50 Hz ($f_r = 1$).

The costs of each component have been updated to 2013 prices using the Consumer Price Index (CPI) of Spain.

Operation and Maintenance costs

The cost associated with the annual energy losses produced during the lifetime of the installation, taking into account not only the efficiency energy losses but also the energy losses due to maintenance or technical failures of the equipment, is calculated as

$$C_{O\&M} = \sum_{k=1}^{LS} \frac{E_{O\_L}^{Ci} P_e}{\left(1 + \frac{R_r}{100}\right)^k} \tag{4.50}$$

where LS is the life span of the OWPP, P_e is the price of energy, and R_r is the real interest rate which is defined as a function of the market interest rate R and the inflation rate of electricity prices R_i as follows

$$R_r = \frac{R - R_i}{1 + \frac{R_i}{100}} \tag{4.51}$$

4.4 Application case

In this section, the proposed methodology has been applied to a case study to determine the cost–effectiveness of the three WPP concepts analysed: MPC, SLPC–VF and SLPC–CF.

The OWPP examined consists of an unique cluster composed by 20 wind turbines with a rated power of 5 MW and a rotor diameter of 126 m. It is laid out in a regular matrix of 5 rows and 4 columns (or radials). The spacing between two nearby wind turbines is 7 rotor diameters (D) in both directions.

The wind conditions within the WPP are defined according to the wind rose and Weibull distribution functions depicted in Figure 4.7. For this case under study, four sets of the Weibull function parameters (c,k) are used for the four wind direction sectors considered. These scale and shape parameters and the wind rose data are obtained from [59] and [91], respectively.

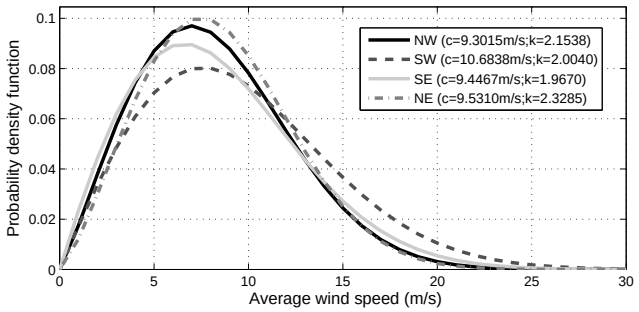

(a)

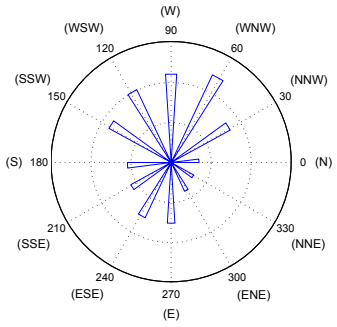

(b)

Figure 4.7: Wind conditions at the OWPP location characterised by a Weibull distribution function (a) [59] and a wind rose (b) [91].

Considering a wind speed standard deviation among the upwind turbines of 1 m/s (a realistic value according to [54]), the different wind speeds of each turbine (for all the scenarios analysed) are calculated based on the Jensen wake model. By way of illustrative example, Figure 4.8 shows the wake effect when the incoming wind direction is 30°.

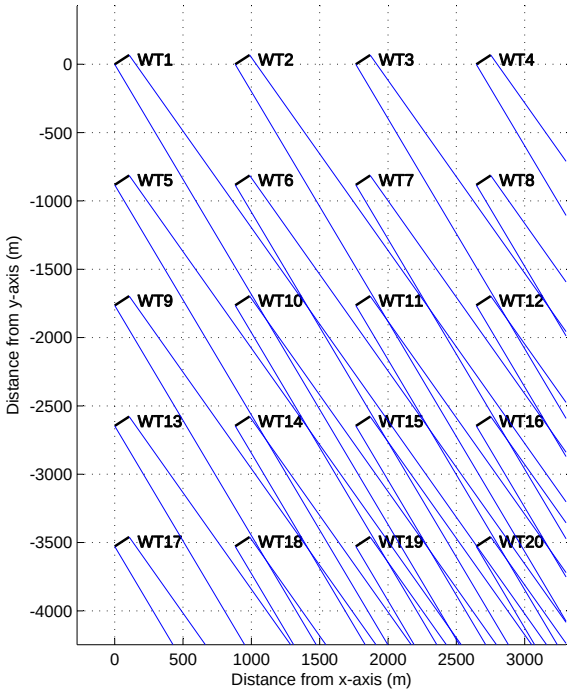

Figure 4.8: Wake effect within WPP under study when the incoming wind direction is 30°.

Once all the sets of wind speeds are determined, the optimum electrical frequency for each set is computed. In this case, the number of sets under study are 12 wind directions x 30 average wind speeds (although only those between cut–in and cut–out wind speeds are considered to calculate the frequency). In Figure 4.9, all the frequencies obtained are presented taking into account their likelihood of occurrence.

As expected, the most repeated frequency is around 50 Hz (19.1%), which is the nominal frequency designed to operate the turbine at full load. The gearbox ratio and the pair of poles of the generator used for the calculation are N_{gr}=105 and p=2, respectively. Likewise, Figure 4.10 depicts both the $C_P - \lambda$ curve and its polynomial approximation used for the optimum

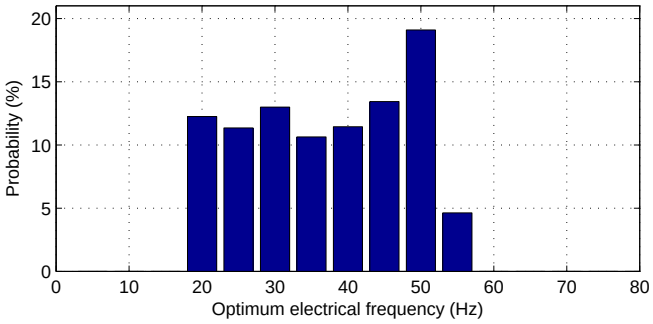

Figure 4.9: Bar diagram of the optimum electrical frequencies calculated depending on their probability of occurrence.

electrical frequency search procedure. As it can be seen, a good match is obtained within the operation range of these four wind turbines considered.

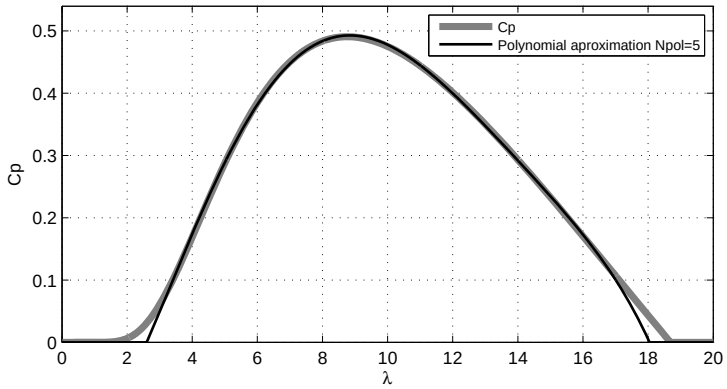

Figure 4.10: C_P curve and polynomial approximation. The obtained polynomial expression reads $-8.08 \times 10^{-6}\lambda^5 + 0.00042\lambda^4 - 0.0078\lambda^3 + 0.053\lambda^2 - 0.024\lambda - 0.176$

Table 4.2 contains the cable database required to perform the inter–array cable selection process. It shows the electrical characteristics of the AC three-core cables for several sections and a voltage level of 33 kV.

Due to the current uncertainty of the power converters efficiency values [124, 125], a sensitivity analysis is carried out to assess its influence on the power flow losses. Thus, the MPC case is evaluated considering three different back–to–back power converter efficiencies (AC/DC and DC/AC) of

Table 4.2: Electrical characteristics of the AC submarine XLPE cables database.

Section (mm^2)	R (Ω/km)	L (mH/km)	C (μF/km)	Ampacity (A)
95	0.2478	0.420	0.161	358
120	0.1967	0.401	0.176	406
150	0.1597	0.387	0.188	452
185	0.1281	0.374	0.203	507
240	0.0981	0.358	0.228	582
300	0.0790	0.344	0.244	649
400	0.0629	0.331	0.270	713
500	0.0505	0.315	0.300	790
630	0.0409	0.305	0.328	861

97%, 98% and 99%, respectively.

Table 4.3: Reliability data of a WPP components.

Equipment	**Failure rate (1/year) or (1/km·year)***	**Mean Time To Repair MTTR (h)**
Wind Turbine	1	144
Power Converter	0.27	120
Submarine Cable*	0.00021	144
LV/MV Transformer	0.007712	144
MV/HV Transformer	0.006	144

Regarding corrective maintenance losses due to reliability issues, [126] and [127] provides the failure rates and mean times to repair of the WPP equipments listed in Table 4.3.

Finally, a total of 1550 hours per year for preventive maintenance purposes have been considered (Figure 4.11(a)). Figures 4.11(b) and 4.11(c) show the power and energy generated (gray colors) and constrained (RGB colors) by the SLPC–VF WPP topology for each average wind speed and direction analysed. The colors red, blue and green represent, respectively, the three addends of (4.32).

Given all the input data required by step 5, the technical assessment for all the scenarios analysed can be performed. Table 4.4 presents the resulting breakdown of energy losses within the WPP for each case, as well as their percentage of total losses over the Total Energy Available (TEA) in the WPP or cluster per year. As it is shown, the best results in terms of lower overall losses are obtained for the MPC case considering a power converter efficiency of 99%. However, when compared to a lower efficiency case (power

converter efficiencies of 97% or 98%), the scenario with lower losses occurs for the SLPC–VF scheme.

In order to determine the most cost–effective WPP topology, a cost anal-

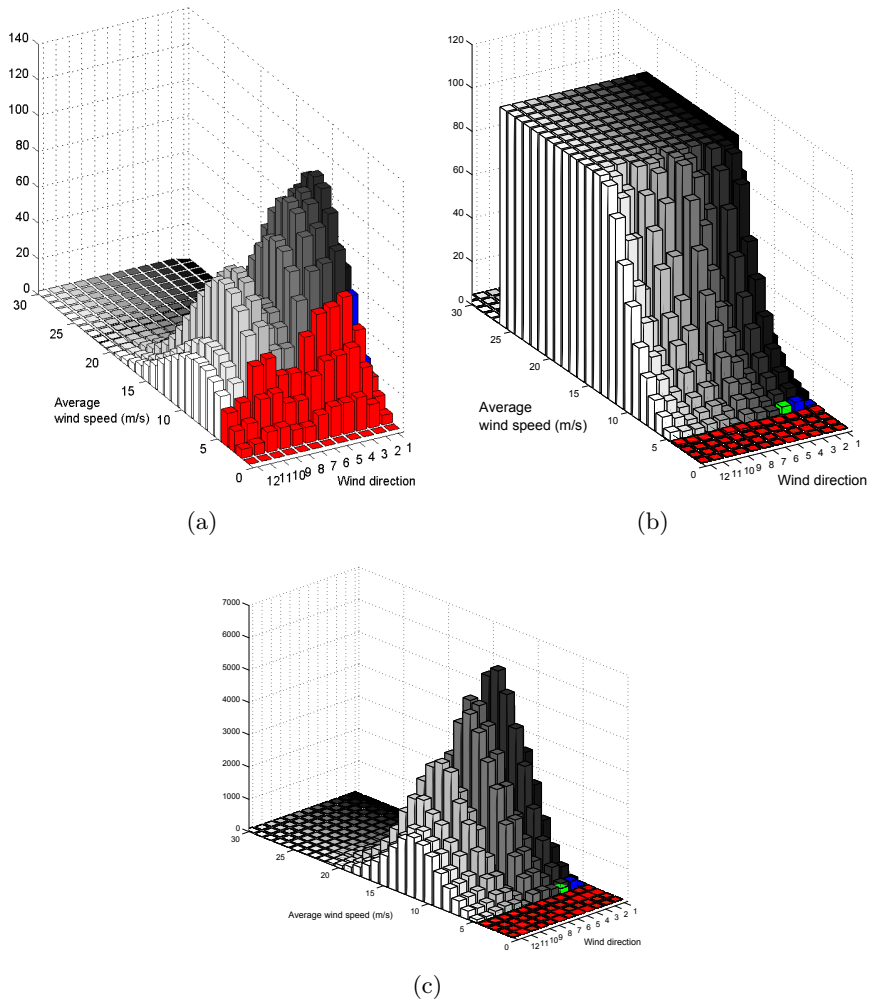

Figure 4.11: Number of hours per year (a), power (b) and energy (c) generated by the SLPC–VF WPP topology under study for each average wind speed and direction. The colors red, blue and green are related to the three addends of (4.32) and represent the 1550 hours per year considered for preventive maintenance purposes (a), as well as the power (b) and energy (c) constrained.

Table 4.4: Technical analysis results for the case study. Total Energy Available (TEA) in the WPP or cluster is 315.84 GWh/year.

Type of energy losses (GWh/year)	**MPC**			**SLPC–VF**	**SLPC–CF**
	$\mu_c = 97\%$	$\mu_c = 98\%$	$\mu_c = 99\%$		
C_P	0	0	0	5.1070	34.599
Power flow	12.525	9.3663	6.2079	2.9669	3.9839
Corrective maintenance	5.5763	5.5763	5.5763	4.6734	5.1634
Preventive maintenance	2.6627	2.6627	2.6627	2.5814	2.5814
Overall losses	20.764	17.605	14.447	15.329	46.328
$\frac{E_{O\_L}}{TEA}$ (%)	6.57	5.57	**4.57**	4.85	14.67

ysis needs to be considered. As previously mentioned, both the investment and the O&M costs have been estimated according to the cost functions detailed in Section 4.3.6.

The breakdown of the capital costs for the case study is presented in Table 4.5. Similarly to the technical assessment, a sensitivity analysis is performed for the SLPC–VF and SLPC–CF cases taking into account two different values for the parameter K_c. Thus, according to [50], the percentage in terms of cost of an individual converter over the total turbine cost (K_c) amounts to around 10% of the wind turbine capital cost, whereas in [90] it accounts to be 5%. As it can be seen from Table 4.5, a remarkable cost savings can be achieved by considering a K_c value of 10%. In addition, a cost benefit of 2 M€ for the SLPC–CF over the SLPC–VF scheme can be obtained because of the resulting increase in transformer weight (and therefore a cost penalty) for the SLPC–VF scheme to operate at frequencies below 50 Hz (Figure 4.9).

Table 4.5: Breakdown of the capital costs (in M€). Updated to 2013 prices using a Consumer Price Index of 2%.

WPP Components	**MPC**	**SLPC–VF**		**SLPC–CF**	
		$K_c = 5\%$	$K_c = 10\%$	$K_c = 5\%$	$K_c = 10\%$
$C_{wt\&inst}$	104.1279	99.3949	94.6618	99.3949	94.6618
C_{sg}	3.6937	3.6937	3.6937	3.6937	3.6937
C_{ca}	17.2484	17.2484	17.2484	17.2484	17.2484
$C_{ca\&inst}$	17.7789	17.7789	17.7789	17.7789	17.7789
C_{pl}	14.2643	14.2643	14.2643	14.2643	14.2643
C_{c_ACDC}	21.6486	21.6486	21.6486	21.6486	21.6486
C_{tr50} or C_{tr_fr}	1.5139	3.5544	3.5544	1.5139	1.5139
C_{inv}	180.2758	177.5832	172.8501	175.5427	**170.8096**

The O&M costs are based on a probabilistic computation due to the uncertainty of the economic data. In Table 4.6, the mean value and the standard deviation of the main economic indicators (explained above in Section 4.3.6) are shown.

Table 4.6: Main economic data used for the study.

	Mean Value (μ)	**Standard deviation (σ)**
Price of energy P_e (€/MWh)	46.84	2
Market interest rate R (%)	4.5	0.2
Inflation rate of electricity prices R_i (%)	2	0.1
Life span LS (years)	20	2

Figure 4.12 summarises the total WPP costs for all the cases considered. Notwithstanding not being the most economical option in terms of capital costs, SLPC–VF results to be the most cost–effective WPP alternative regardless of whether the parameter K_c is 5% or 10%.

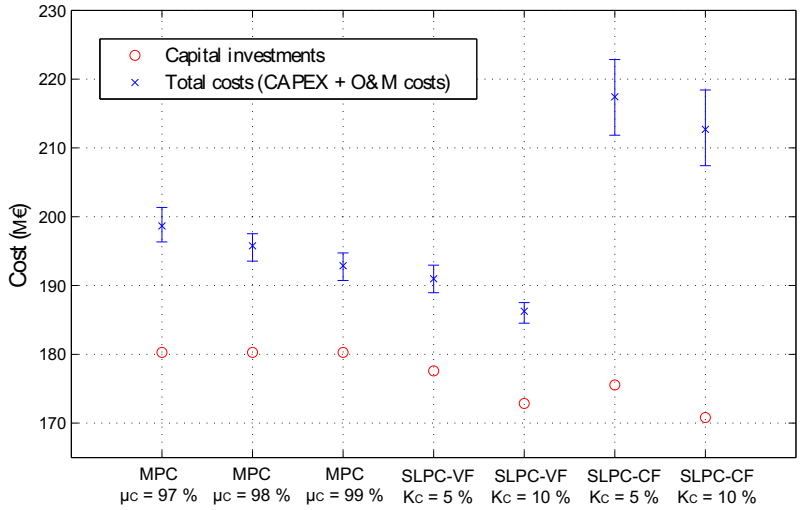

Figure 4.12: Total WPP costs (in M€) for all the cases analysed. Red circles indicate capital expenditures of each WPP topology.

In general terms, the potential cost saving with SLPC–VF WPP topology versus the conventional MPC concept is expected to be between 1-6% (taking into account exclusively the mean values of each case). Only in the case of considering a back–to–back power converter efficiency of 99% and that the cost of the converters represents 5% of the total turbine cost, the total costs

of both MPC and SLPC–VF WPP topologies are comparable. On the other hand, SLPC–CF is not economically beneficial because of the high cost that represent the C_P losses.

4.5 Further discussion about the SLPC–VF concept

With the aim to analyse the influence of some factors, such as the wind speed variability within the WPP, the wind power plant size and the wind direction, on the feasibility of the proposed SLPC–VF concept, further discussion is included in this section. The following assessments are performed only from the power extraction efficiency point of view.

4.5.1 Influence of wind speed variability and wind farm size on power generation efficiency analysis

Two parameters, such as the wind speed variability and the number of wind turbines connected to a single large power converter (SLPC), appear to be crucial to analyse the proposed topology. On one hand, wind speed variability in wind farms is difficult to analyse in a general way, since it heavily depends on multiple factors, such as the wind turbine distribution in wind power plants, the WPP location (onshore or offshore), the incoming wind directions, etc. However, it is possible to perform a statistical analysis in order to evaluate the effect of wind variation in terms of maximum available power, by considering the use of a single converter for the entire wind power plant or individual power converters for each wind turbine. On the other hand, the higher the number of generators connected to a common power converter, the worse the power extraction efficiency will be if different wind speeds among WTs are considered.

Hence, in order to analyse how the standard deviation and the number of wind turbines within a group affect the power extraction efficiency of the system, a range of simulations has been performed according to the methodology explained in Section 4.3.

A total of 10 OWPPs (NWPPA=10) composed of 2, 4, 6, 8, 10, 20, 40, 60, 80 and 100 wind turbines has been analysed. Obviously, it should be noted that offshore wind farms comprising few WTs such as 2, 4 or 6 are not an economically feasible option since the power output is too low. However, here they are not considered as wind farms, but as a cluster of machines connected to a single converter. The wind rose and Weibull distribution functions shown in Figure 4.7 has been used to define the wind conditions within all the OWPP considered for the study (NWCA=1). Likewise, the

number of standard deviations considered to assess the influence of wind speed variability within the OWPP on the power generation efficiency is set to 10 (NSTDA=10); varying its value from σ=0.5 to 5 m/s. Figure 4.13 depicts the obtained results. The ratio α_{opt} indicates the power extraction efficiency of the entire wind power plant and it is computed as

$$\alpha_{opt} = \frac{P_{SLPC-VF}}{P_{MPC}} \tag{4.52}$$

where $P_{SLPC-VF}$ and P_{MPC} are the power generated by the WPP by considering the proposed SLPC–VF and the conventional MPC concept, respectively.

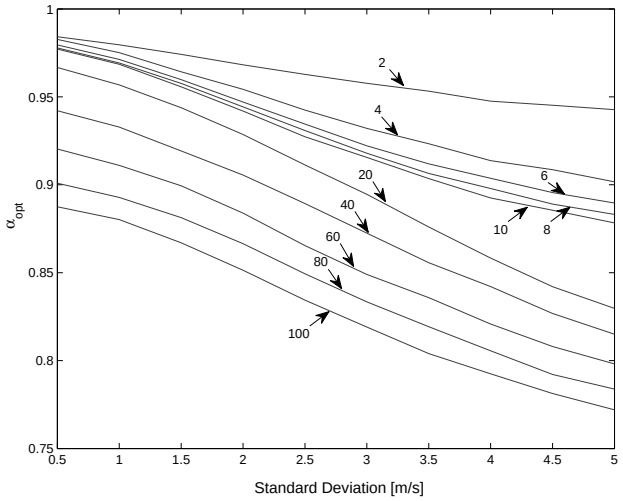

Figure 4.13: Dependence of the ratio α_{opt} on both the size of the wind farm and the wind speed variability within the wind farm.

Firstly, it can be noted that losses increase as expected, as the number of machines in the group as well as the wind speed variability among turbines increase. Compared with the MPC concept, the SLPC–VF scheme achieves between 98.42 and 87.83% of the maximum available power, if a wind power plant or a cluster composed of 10 machines or less are considered. Moreover, for low standard deviations (similar wind speeds throughout the wind power plant) and 10 WTs or less, the performance of the SLPC–VF is excellent (from 97.71 to 98.42%). However, if the standard deviation increases, the differences between the efficiency ratio α_{opt} become higher. Thus, if a 5 m/s standard deviation is considered, the C_P losses of the SLPC–VF scheme differ between 5.73% (2 WTs) and 12.17% (10 WTs).

In the case of large wind power plants, the dependence of the standard deviation on α_{opt} is maintained independently from the number of turbines within the wind farm. As it can be seen from Figure 4.13, for low standard deviations (0.5 m/s), the results obtained are quite satisfactory since α_{opt} is equal to 0.9667 for a wind power plant with 20 turbines and 0.8875 if the WPP is composed of 100 wind turbines. Similarly, when standard deviation increases, the performance of the single power converter topology decreases. However, the performance of a wind power plant with 100 turbines connected to a single power converter maintains α_{opt} above 0.85 (15% of C_P losses) until the standard deviation is larger than 2 m/s, which is larger than typical values of less than 1 m/s [128].

As it can be seen previously in Figure 4.13, higher number of machines connected to a common power converter implies worse performance of the system in terms of power extraction efficiency. Therefore, it will be required to analyse at what point the C_P losses are so high that a single power converter connected to all the WTs is no longer cost effective and different clusters of machines connected to a common power converter within a wind farm becomes a better option.

Thus, a wind power plant consisting of 40 wind turbines with three different power converter layouts according to their connection between them and the wind turbines has been analysed (Figures 4.14 and 4.15). In Figure 4.14(a) the whole OWPP is connected to a single large power converter. In Figure 4.14(b) a dedicated power converter is connected to the first row of wind turbines whereas a second one is connected to the next couple of rows and a third power converter connects the remainder turbines. Finally, in Figure 4.14(c), five power converters are used to connect the entire wind power plant. In blue, a single power converter is connected to the first row of wind turbines. Wind turbines 6, 11, 16, 21, 26 and 31 (in green) and 10, 15, 20, 25 and 30 (in red) forms two more clusters of wind turbines connected to a single power converter, respectively. The fourth group consists of wind turbines located on the last row of the wind farm whereas the fifth one connects the remainder WTs to another power converter. As it is shown in Figure 4.15, the power generation efficiency is evaluated for different standard deviations from 0.5 to 5 m/s (NSTDA=10) and compared between the three different WPP layouts depicted in Figure 4.14. As expected, the greater the number of clusters and power converters, the better the efficiency of the system will be. Hence, for low standard deviations (0.5 m/s), α_{opt} is 0.9428 for case (a), 0.9497 for the WF layout (b) and 0.9537 for the case (c), when five power converters are connected to all the wind turbines distributed into five different clusters. Similarly, the resulting C_P losses for high standard

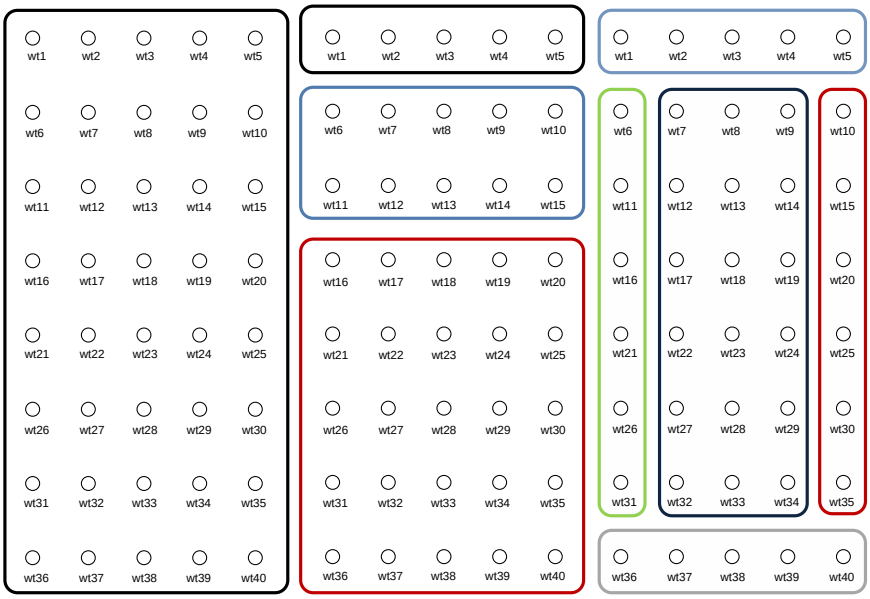

Figure 4.14: Three different WPP layouts consisting of 1 unique WPP cluster (a), 3 WT clusters (b) and 5 WT clusters (c).

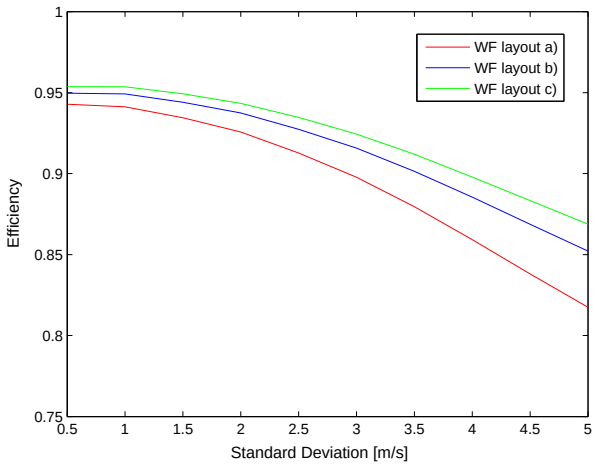

Figure 4.15: Comparison of power generation efficiency between the three different WPP layouts shown in Figure 4.14.

deviations (5 m/s) are 18.25%, 14.78% and 13.12%, for cases a, b and c, respectively.

4.5.2 Influence of wind direction on power generation efficiency analysis

Considering wind direction when analyzing wake effects is very important, as different wind directions cause different types of wake effects. Consequently, wind directions differently affect the variability of the wind turbines, which is a crucial parameter to determine the efficiency of the proposed topology, as previously shown in Section 4.5.1.

Thus, the four wind roses shown in Figure 4.16 have been applied to a particular case of study and the resulting power generation efficiency ratio for the SLPC–VF scheme (α_{opt}) has been compared and it is depicted in Figure 4.17.

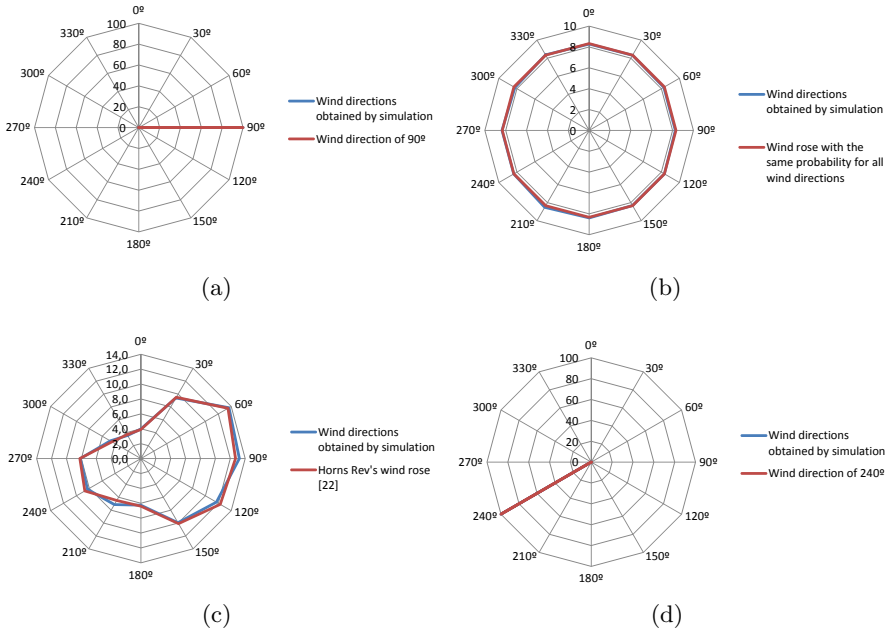

Figure 4.16: Comparison between different wind roses and 10000 data of wind directions randomly generated (N_{rvg}=10000). (a) The wind direction is set to 90°. (b) Wind rose with the same probability for all wind directions. (c) Wind rose for Horns Rev wind farm [91]. (d) The wind direction is set to 240°.

In the first scenario, the wind direction is considered constant and equal to 90° (Figure 4.16(a)). In the second scenario, the probability of generating one wind direction or another one, is the same and, therefore, all wind directions are the prevailing one (Figure 4.16(b)). The third scenario consists of using the wind rose for Horns Rev previously mentioned in Section 4.7 (Figure 4.16(c)). Finally, in the fourth case, the wind direction is constantly set to 240° (Figure 4.16(d)). In all cases, a wind farm with 30 wind turbines (5 columns and 6 rows) has been considered. The distance between two nearby wind turbines in the prevailing wind direction is 9 rotor diameters, whereas for perpendicularly coming winds it is 3 D. The prevailing wind direction is set to 0°.

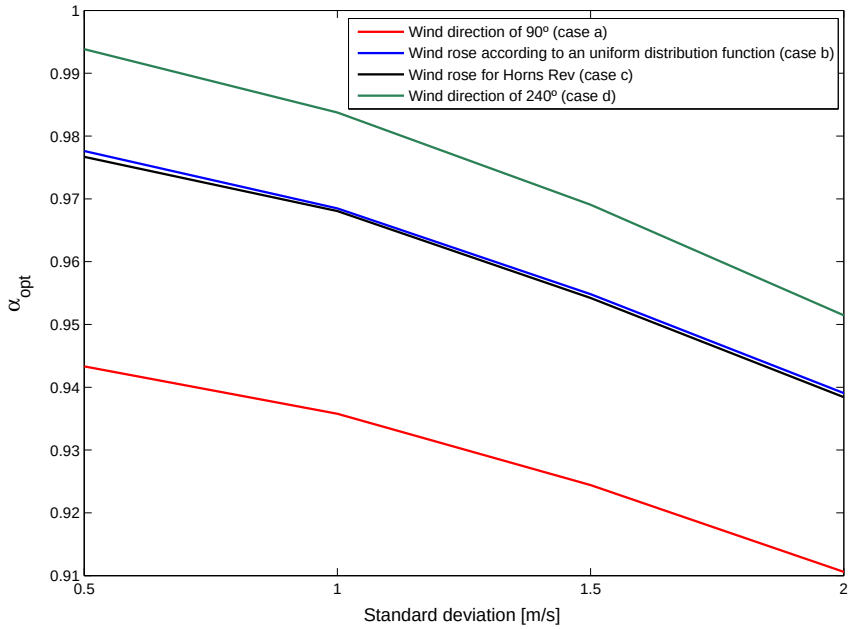

Figure 4.17: Ratio α_{opt} comparison for the four wind roses analysed and different standard deviations of wind speeds from 0.5 to 2 m/s ($N_{std} = 4$). The wind farm considered is composed of 30 wind turbines (5 columns and 6 rows).

As it can be seen from Figure 4.17, there is a significant difference between the first scenario (wind directions fixed to 90°), the second and third scenarios (all wind directions are taken into account) and the fourth (wind direction set to 240°). These results are consistent with the fact that the

higher distances between the upstream and the downwind turbines, the better the performance is. Moreover, the results show a very similar behavior when a wind rose with a uniform distribution function or a real wind rose is taken into account. Accordingly, for low standard deviations (0.5 m/s), the efficiency ratio α_{opt} is 0.9433 when the wind direction is 90° (case a), 0.9776 and 0.9767 for cases b and c, respectively, and 0.9938 if a constant wind direction of 240° (case d) is considered.

Therefore, wind direction should be taken into consideration as it can affect significantly the power extraction efficiency of the proposed SLPC–VF concept.

4.6 Conclusions of the chapter

This chapter analyses the suitability of two hypothetical WPP topologies in which individual converters are not required for each turbine but a single large power converter (SLPC) is connected to a wind turbine cluster (or to an entire WPP) operating at variable (SLPC–VF) or constant (SLPC–CF) frequency. These proposed schemes are specially appropriated for offshore wind power plants with an HVDC transmission link to shore.

By means of the presented methodology, a comprehensive technical and economic assessment has been applied to a case study in order to determine the cost–effectiveness of each concept. Due to the uncertainty of some parameters, a sensitivity analysis varying the cost and efficiency of the individual power converters of each wind turbine, as well as the main economic indicators, has been carried out.

According to the results obtained, SLPC–VF is presented as an appealing WPP alternative, since a total cost saving of up to 6% compared to the conventional MPC WPP topology can be achieved. Thus, although the optimal operation point of each turbine can not be assured due to the inherent configuration of the proposed scheme, the absence of dedicated power converters for each turbine brings a reduction in capital costs, as well as, in maintenance and power flow losses, so that economic benefit can be realized.

Likewise, the performed study has demonstrated the effectiveness of using the optimum electrical frequency calculation algorithm for variable frequency operation, as can be seen by comparing the total WPP cost resulted for SLPC–VF or SLPC–CF schemes.

With regard to the further discussion carried out in this chapter, it is concluded that factors such as the wind speed variability within the wind power plant, wind direction and the WPP size may significantly affect the power

generation efficiency of the system. However, if typical differences of wind speeds between turbines are considered (σ=1 m/s), SLPC–VF concept becomes a feasible option, in terms of power efficiency analysis, achieving more than 97.7% of the total available power obtained with the MPC concept. In addition, it has been clearly observed the energy efficiency improvement that can be realized by grouping some wind turbines and connecting each cluster to its respective single power converter. However, an increasing number of wind turbine clusters implies an increment of the OWPP cost due to the larger number of power converters needed (although these will be lower rated) and the additional offshore collector platform may be required to install. Thus, a trade–off between improving power generation efficiency of the WPP and reducing its capital cost should be accomplished to determine the optimal number of power converters and offshore collector platforms that minimize the total offshore wind power plant cost. Such analysis, as well as the assessment of optimal cable routing for the AC wind turbine array, will be addressed in the following Chapter 5.

5

Hybrid AC–DC offshore wind power plant topology: optimal design

5.1 Introduction

As discussed in the previous chapter, the proposed SLPC–VF concept for offshore wind power plants entails the drawback of not ensuring the optimum operational point of each wind turbine due to its inherent configuration in which the whole OWPP is controlled simultaneously by a common power converter regardless of the wind speed variability among them.

This limitation can be significant for large OWPPs projects, since the wind speed differences between turbines are tend to be higher as the wind farm size increases. For example, considering a hypothetical 500 MW OWPP with large distances between turbines (because of the wake effect), it may be more cost–effective to install several offshore collector platforms instead of a single platform and to group the wind turbines into a various clusters, such that each cluster consists of a power converter connected to a set of turbines with similar wind speeds.

Thus, an electrical design optimisation for large OWPPs is key to minimise their total cost [85, 129]. In this chapter, a hybrid AC–DC OWPP concept is presented and its design is optimised. This hybrid scheme is based on the SLPC–VF topology described in Chapter 4 but with the difference that the wind turbines are connected in clusters to their corresponding AC/DC

power converter located in an offshore collector platform via AC submarine inter–array cables, and an internal DC collector network export the power generated by the different clusters to the main DC/DC converter installed on the VSC–HVDC offshore platform.

The main objective of this work is to find the optimal design that minimises the total cost within a hybrid AC–DC OWPP collection grid. To this end, an optimisation model has been developed in order to determine the optimal number of power converters and offshore platforms needed, as well as their locations. The cable route connecting the wind turbines between each other is also optimised. The model has been formulated as a MINLP problem. The clustering design takes into account not only the capital costs of each component but also the costs associated to the inherent losses (known as C^P losses in [50, 56]) of this topology.

5.2 Hybrid AC–DC OWPP concept

The hybrid AC–DC OWPP concept presented in this section is based on the SLPC–VF scheme previously explained in Chapter 4 in which dedicated power converters are avoided with the aim of reducing the total OWPP cost. However, unlike the previous case, the hybrid AC–DC OWPP topology consists of wind turbine clusters connected through AC inter–array cables to AC/DC power converters located at the intermediate collector platforms, which are in turn connected to the VSC–HVDC offshore platform by means of DC export cables. Figure 5.1 shows an example of a hybrid AC–DC OWPP consisting of three wind turbine clusters operated by three AC/DC power converters located on two offshore collector platforms.

As it can be seen, each AC/DC power converter controls its wind turbine cluster and operates at the optimum electrical frequency that maximises its power generation for the chosen topology. It should be noted that the maximum available power can only be achieved by considering individual power converters for each turbine.

As stated in the previous chapter, wind speed variability within the wind power plant is an important factor to take into account in order to decide the effectiveness of the SLPC–VF topology. Thereby, the higher wind speed diversity cause larger deviations of the operating point of each turbine from its optimum and, therefore, the greater are the C^P losses produced in the wind turbine cluster. Thus, this hybrid AC–DC WPP topology is planned for future OWPPs with HVDC links where the wind speeds are supposed to be more uniform among turbines compared to onshore.

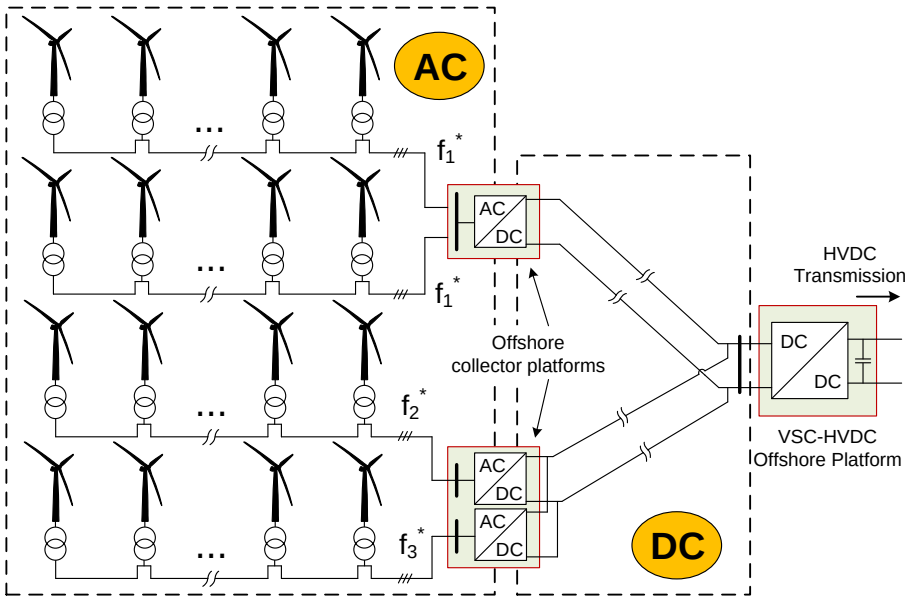

Figure 5.1: Example of a hybrid AC–DC OWPP consisting of three wind turbine clusters.

5.3 Problem statement

Figure 5.2 shows the layout of an OWPP collection grid connected to the onshore electrical network by means of an HVDC link. As it can be seen, it consists of 24 wind turbines, 28 possible AC/DC power converters and 7 possible locations for offshore collector platforms. It is worth remarking that the dedicated power converters of each wind turbine have been removed for the case under study, so that the turbines are directly connected to the AC/DC converters placed at the offshore collector platforms. Thereby, the OWPP is divided into several clusters composed by a group of turbines connected to AC/DC power converters (one converter per cluster) operating at variable frequency.

The starting point for the optimisation is that all the preliminary studies conducted during the development and consenting process (covering those aspects that are required to determine the optimal location of each wind turbine and the offshore VSC–HVDC platform [59]), such as environmental and sea bed surveys, meteorological and oceanographic analysis, etc., have already been performed.

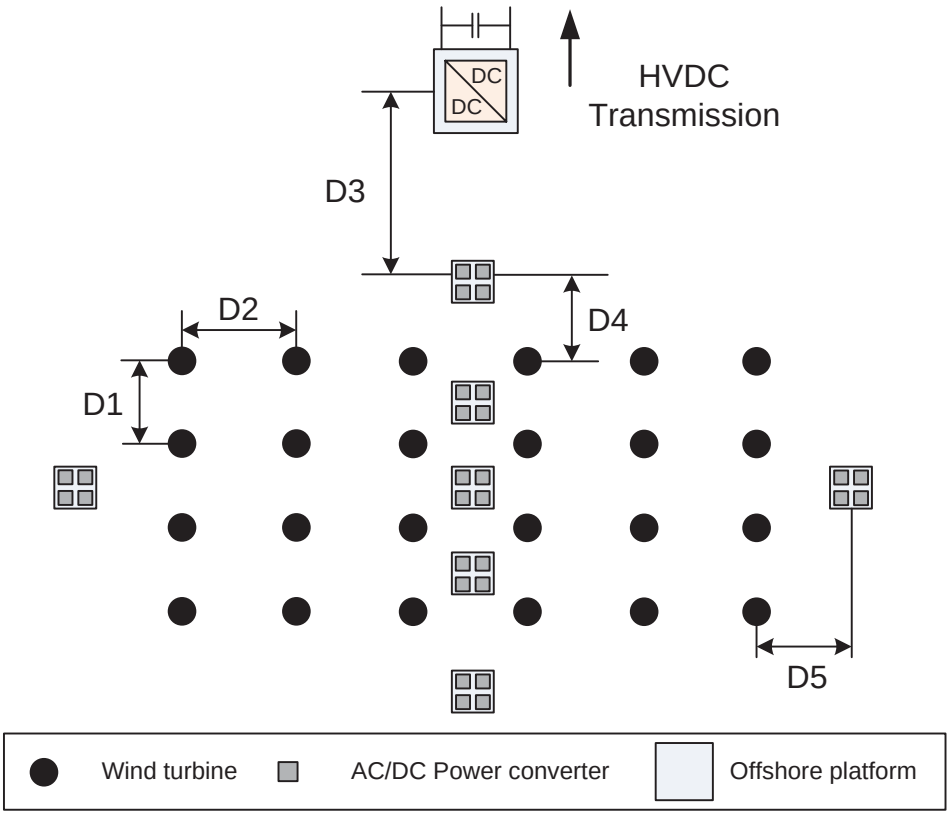

Figure 5.2: Example of a schematic OWPP collection grid composed of 24 wind turbines, 28 AC/DC power converters candidates and 7 possible intermediate offshore collector platforms.

On this basis, the model contemplates several possible locations for both collector platforms and AC/DC converters. It is considered that each offshore collector platform can accommodate at most four AC/DC converters and a platform is only installed if a converter is assigned to it. Regarding the cable route, the model optimises the interconnections between wind turbines, as well as the connections between turbines and converters in order to minimise the lengths of the installed cables. The problem employs one type of AC inter–array cable to connect each wind turbine either to another turbine or to a power converter, and one type of DC export cable for the connection between the AC/DC converters situated at the collector platforms and the DC/DC converter of the HVDC offshore substation.

5.4 Mathematical model

In this section, the mathematical programming problem for minimizing the total cost of an offshore collection grid based on the proposed hybrid AC–DC OWPP concept described previously, is presented. This minimization process implies a trade–off between cutting down the investment costs (by decreasing the number of converters and collector platforms) and attempting to reduce the energy losses caused by the considered OWPP topology (by increasing the number of clusters, so that the wind turbines can operate closer to their optimum point).

5.4.1 Technical constraints

In the following, the technical of the constraints optimisation problem are detailed. All the notation (sets, parameters and variables) used throughout this chapter can be found in Appendix C.

First, each wind turbine i must be controlled by one AC/DC power converter k, so that

$$\sum_{k \in \mathcal{K}} y_{i,k} = 1 \quad \forall i \in \mathcal{I} \tag{5.1}$$

where

- $y_{i,k} = 1$ if the wind turbine $i \in \mathcal{I}$ is controlled by the converter $k \in \mathcal{K}$
- $y_{i,k} = 0$ otherwise

Likewise, only if the turbine i is controlled by the converter k, this turbine can be connected to it through a single cable c, so that

$$\sum_{c \in \mathcal{C}} x_{i,k,c} \leq y_{i,k} \quad \forall i \in \mathcal{I},\ k \in \mathcal{K} \tag{5.2}$$

where

- $x_{i,k,c} = 1$ if the wind turbine $i \in \mathcal{I}$ is connected to the converter $k \in \mathcal{K}$ by means of the cable $c \in \mathcal{C}$
- $x_{i,k,c} = 0$ otherwise

The following set of constraints refers to the fact that two wind turbines i, j can be connected to one another at most through a single inter–array cable c:

$$\sum_{c\in\mathcal{C}} u_{i,j,k,c} \leq 1 \quad \forall i,j \in \mathcal{I},\ k \in \mathcal{K} \tag{5.3}$$

where

- $u_{i,j,k,c} = 1$ if the wind turbines $i, j \in \mathcal{I}$, controlled by the converter $k \in \mathcal{K}$, are connected through the cable $c \in \mathcal{C}$
- $u_{i,j,k,c} = 0$ otherwise

These inter–array cables have an upper limit on the number of wind turbines that can be connected into it, due to their capacities cannot be exceeded. Hence, to not overload the cables, the following set of equations must be fulfilled:

$$\sum_{i,j\in\mathcal{I}} u_{i,j,k,c} \leq \overline{N}_c - 1 \quad \forall k \in \mathcal{K},\ c \in \mathcal{C} \tag{5.4}$$

It is assumed as a hypothesis that each wind turbine i must be at least connected to another turbine j or to an AC/DC power converter k, so as not to be isolated. Similarly, each of the turbines can have at most one ingoing and one outgoing cable in order to facilitate the installation tasks carried out by the appropriate vessels. This hypothesis is represented through the following set of constraints:

$$1 \leq \sum_{\substack{k\in\mathcal{K}\\ c\in\mathcal{C}}} \left(x_{i,k,c} + \sum_{j\in\mathcal{I}:j>i} u_{i,j,k,c} + \sum_{j\in\mathcal{I}:j<i} u_{i,j,k,c} \right) \leq 2 \quad \forall i \in \mathcal{I} \tag{5.5}$$

Furthermore, only if there are two wind turbines i, j controlled by the same power converter k, these turbines can be interconnected to each other by means of one cable c. Therefore,

$$2\sum_{c\in\mathcal{C}} u_{i,j,k,c} \leq y_{i,k} + y_{j,k} \quad \forall i,j \in \mathcal{I},\ k \in \mathcal{K} \tag{5.6}$$

If two wind turbines i, j are connected through a cable c, any other component (other turbine i' or a converter k) connected to them must be connected via the same cable c, so that

$$\sum_{\substack{k\in\mathcal{K}\\ c'\in\mathcal{C}:c'\neq c}} \left(x_{i,k,c'} + x_{j,k,c'} + \sum_{i'\in\mathcal{I}:i'>j} u_{j,i',k,c'} + \sum_{i'\in\mathcal{I}:i'<j} u_{i',j,k,c'} + \sum_{i'\in\mathcal{I}:i'>i} u_{i,i',k,c'} + \right.$$

$$\left. + \sum_{i'\in\mathcal{I}:i'<i} u_{i',i,k,c'} \right) \leq 4\left(1 - \sum_{k\in\mathcal{K}} u_{i,j,k,c}\right) \quad \forall i,j \in \mathcal{I},\ c \in \mathcal{C} \tag{5.7}$$

The number of inter–array cables connected to one converter k is determined by both the amount of turbines controlled by it and the number of interconnections between them through

$$\sum_{\substack{i\in\mathcal{I}\\c\in\mathcal{C}}} x_{i,k,c} = \sum_{i\in\mathcal{I}}\left(y_{i,k} - \sum_{\substack{j\in\mathcal{I}\\c\in\mathcal{C}}} u_{i,j,k,c}\right) \quad \forall k \in \mathcal{K} \tag{5.8}$$

Moreover, as ring configuration is not considered in this study, the number of outermost wind turbines per string must match the total number of cables installed within the OWPP, therefore

$$\sum_{i\in\mathcal{I}}\left[2 - \sum_{\substack{k\in\mathcal{K}\\c\in\mathcal{C}}}\left(\sum_{j\in\mathcal{I}:j>i} u_{i,j,k,c} - \sum_{j\in\mathcal{I}:j<i} u_{j,i,k,c} - x_{i,k,c}\right)\right] = \sum_{\substack{i\in\mathcal{I}\\k\in\mathcal{K}\\c\in\mathcal{C}}} x_{i,k,c} \tag{5.9}$$

An inter–array cable c is assigned to a specific AC/DC power converter k in case there is one wind turbine connected to such converter by means of this inter–array cable. Then,

$$z_{k,c} = \sum_{i\in\mathcal{I}} x_{i,k,c} \quad \forall k \in \mathcal{K},\ c \in \mathcal{C} \tag{5.10}$$

where

- $z_{k,c} = 1$ if the cable $c \in \mathcal{C}$ is connected to the converter $k \in \mathcal{K}$
- $z_{k,c} = 0$ otherwise

In addition, there is no possible connection between two wind turbines i, j, controlled by a converter k through an inter–array cable c, if such cable is not connected to this converter, which means

$$u_{i,j,k,c} \leq z_{k,c} \quad \forall i, j \in \mathcal{I},\ k \in \mathcal{K},\ c \in \mathcal{C} \tag{5.11}$$

The AC/DC power converter k is out of service if it is not controlling any wind turbine i

$$q_k \leq \sum_{i\in\mathcal{I}} y_{i,k} \quad \forall k \in \mathcal{K} \tag{5.12}$$

where

- $q_k = 1$ if the AC/DC power converter $k \in \mathcal{K}$ is in service
- $q_k = 0$ otherwise

Additionally, the maximum number of wind turbines that can be connected to an AC/DC power converter k that is in service shall not exceed the total number of turbines of the OWPP analysed (N)

$$\sum_{i \in \mathcal{I}} y_{i,k} \leq N q_k \quad \forall k \in \mathcal{K} \tag{5.13}$$

Finally, one converter k will be in service only if the offshore collector platform s that houses it ($A_{s,k} = 1$) is installed, then

$$q_k \leq h_s \quad \forall s, k : A_{s,k} = 1 \tag{5.14}$$

where

- $h_s = 1$ if the offshore collector platform $s \in \mathcal{S}$ is installed
- $h_s = 0$ otherwise

With regard to the frequency at which an AC/DC power converter k can operate, it has an upper bound due to the maximum mechanical speed that the wind turbines can allow. When this frequency is reached, the electrical frequency will be kept constant, and the wind turbines will locally limit their injected power adjusting the pitch angle. Likewise, the frequency of each power converter must be a positive number since the OWPP collection grid considered in this chapter is in AC. These bounds are formulated as

$$\underline{f} q_k \leq f_k \leq \overline{f} q_k \quad \forall k \in \mathcal{K} \tag{5.15}$$

5.4.2 Objective function

The objective function represents the total cost of a hybrid AC–DC OWPP considering both the capital expenditures (CAPEX) of all the components involved in the system as well as the cost associated to the energy losses within the OWPP collection grid. It is formulated as

$$F(h,u,x,y) = (C^I + C^C)\left[\sum_{i,j}\left(D^{TT}_{i,j}\sum_{k,c} u_{i,j,k,c}\right) + \sum_{i,k,c} D^{TC}_{i,k} x_{i,k,c}\right] \tag{5.16}$$

$$+(C^X + C^C)\sum_{s} D^{PP}_{s} h_s \tag{5.17}$$

$$+C^K P^N \sum_{i,k} y_{i,k} + C^S \sum_{s} h_s \tag{5.18}$$

$$+C^E L \sum_{i,k} y_{i,k}(\overline{P}_i - P_{i,k}) \tag{5.19}$$

where

(5.16) corresponds to the capital cost of submarine AC inter–array cables. C^I refers to the cost per km, while C^C is the cost associated with their transport and installation. These constants have been obtained using the following cost functions reported in [122] and previously presented in Section 4.3.6 of Chapter 4.

$$C^I = \alpha + \beta e^{\left(\frac{\gamma I^I}{10^5}\right)} \cdot 10^{-3} \tag{5.20}$$

$$C^C = 0.365 \tag{5.21}$$

where I^I is the AC inter–array cable ampacity (in A) for a specific conductor section and the coefficients α, β and γ depend on the nominal voltage level.

(5.17) denotes the cost of the DC export cables and their installation. The DC cable costs (per km) can be computed by [123]

$$C^X = \psi + \sigma 2 V^N I^E \tag{5.22}$$

where V^N and I^E are the cable ratings (in V and A respectively) and the constants ψ and σ depend on voltage rating of the DC cable.

(5.18) represents the variable component of cost related to the AC/DC power converters in service, as well as the installed collector platforms. C^K and C^S refer to the cost of the power converter per MW and the cost of installing additional platforms, respectively.

(5.19) accounts for the cost associated with the C^P energy losses produced by the inherent configuration of the system under study. These losses are calculated as the difference between the maximum available power of each wind turbine $i \in \mathcal{I}$, $\overline{P}_i$, and the power generated by a certain wind turbine $i \in \mathcal{I}$ controlled by a converter $k \in \mathcal{K}$, $P_{i,k}$. Both variables are computed as

$$\overline{P}_i = \frac{1}{2}\rho A \overline{C}^P w_i^3 \tag{5.23}$$

$$P_{i,k} = \frac{1}{2}\rho A C_{i,k}^P w_i^3 \tag{5.24}$$

where ρ is the air density, $A = \pi R^2$ is the surface covered by the rotor blades of radius R, w_i is the average wind speed of each turbine over the lifetime of the OWPP, and $\overline{C}^P$ and $C_{i,k}^P$ are the maximum

available and the actual value of the power coefficient, respectively. This power coefficient denotes the efficiency of a wind turbine defined as the ratio of actual power transferred to the rotor to the theoretical power available in the wind. It is usually expressed as an exponential function. However, in this chapter, it has been approximated by a quadratic polynomial for λ between 4 and 10 with an accuracy of 99.96%. Besides many factors such as the rotor blades profile, the pitch angle, etc., the $C^P_{i,k}$ coefficient is highly dependent on the tip speed ratio, $\lambda_{i,k}$, defined as the relative velocity between the rotor tip and the wind. Thus,

$$\lambda_{i,k} = \frac{\omega^T_k R}{w_i} = \frac{2\pi f_k R}{pgw_i} \tag{5.25}$$

where ω^T_k is the rotor rotational speed, p is the pair of poles of each generator, g is the gearbox ratio and f_k is the electrical frequency of the converter $k \in \mathcal{K}$.

Hence, for the conventional OWPP topology in which the rotational speed of each turbine is controlled by a full power converter, this electrical frequency is optimised for each turbine as a function of its wind speed, so that the entire OWPP can operate at the optimum tip speed ratio that maximises the power coefficient, $\overline{C}^P$, and therefore, its power generated. However, for the hybrid AC–DC OWPP concept, each power converter optimises its electrical frequency, f_k, for a given set of wind speeds. Thereby, each wind turbine within a cluster operates at a different tip speed ratio (and distinct power coefficient, $C^P_{i,k}$) because the wind speeds among them, w_i, are different whereas the electrical frequency, f_k, is the same.

This cubic objective function, (5.16)-(5.19), together with the set of linear constraints, (5.1)-(5.15), defines a mixed integer non–linear programming (MINLP) which is minimised to obtain the optimal design for the proposed hybrid AC–DC OWPP.

5.5 Tests and results

5.5.1 Mathematical model results

The model has been implemented in GAMS [130] and solved with DICOPT. Table 5.1 contains the dimensions of the problem.

Table 5.1: Model statistics obtained with GAMS.

No. variables	No. binary variables	No. constraints	Execution Time
52.563	52.535	83.641	13h5min

The mathematical model has been applied to the hybrid AC–DC OWPP displayed in Figure 5.2, consisting of 24 wind turbines (6 columns and 4 rows) of 5 MW each (P^N), 28 AC/DC power converters candidates and 7 possible intermediate offshore collector platforms. The optimal design obtained that minimises the total OWPP's cost for the hybrid topology, is shown in Figure 5.3.

As it can be seen, the resulting layout is a feasible solution, since it satisfies all the model constraints previously mentioned. It consists of 2 AC/DC power converters installed on their respective offshore collector platforms. The spacing between two nearby wind turbines (D1 and D2) is 7 rotor diameters (D) in both directions, whilst the distance between the HVDC offshore platform and the nearest collector platform to it (D3) is 10 km. The distance D4 is 1 km and D5 is equal to 0 since there is no platform installed on the East side of the wind farm (it is considered that the OWPP is oriented North–South). The numbers in parenthesis indicate the average wind speed of each turbine (in m/s). The operational points of each wind turbine related to their $C^P_{i,k}$–$\lambda_{i,k}$ curve are depicted in Figure 5.4. As it is shown, all $\lambda_{i,k}$ values are within the admissible limits and, therefore, the polynomial approximation of the C^P curve used in the model is valid.

Table 5.2 shows the breakdown of the cost for the resulting optimal hybrid AC–DC OWPP design.

Table 5.2: Breakdown of the costs for the optimal hybrid AC–DC OWPP design.

	Cost (M€)
Cost of AC inter–array cables	7.8
Cost of DC export cables	6.5
Cost of AC/DC power converters	14.3
Cost of collector platforms	17.0
Cost of energy losses	3.3
Total cost	**48.9**

The inter–array cable that has been used is a 33 kV AC submarine cable with a cross section of 240 mm^2 and an ampacity (I^I) of 582 A. The coefficients α, β and γ for submarine cables of 30–36 kV are: α=0.05208 M€/km, β=0.07551 M€/km and γ=234.34 1/A. Regarding the DC export cables, a

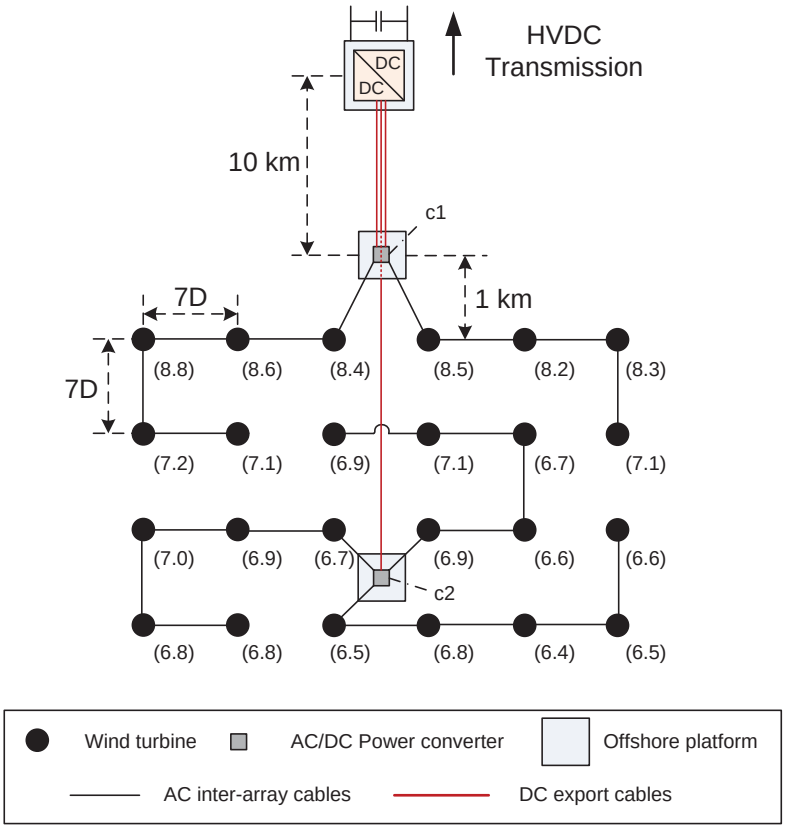

Figure 5.3: Optimal design obtained for the hybrid AC–DC OWPP topology consisting of 24 wind turbines, 2 AC/DC power converters and 2 offshore collector platforms. The number in parenthesis indicate the average wind speed (m/s) of each turbine.

XLPE cable with a cross section of 630 mm^2, an ampacity (I^E) of 835 A and a voltage rating (V^N) of ±80 kV has been selected. The constants ψ and σ are -0.012 M€/km and $1.97{\cdot}10^{-9}$ M€/(km·VA) according to [123].

The total cost of the power converters and collector platforms is obtained as a result of adding a fixed cost to equation 5.18 of the objective function. This constant term only depends on the rated power of the OWPP analysed ($P^N N$) and it is independent on the decision variables. The C^K and C^S constants used are 0.072 M€/MW [131] and 2.534 M€ [122], respectively.

The optimum frequencies for power converters c1 and c2 that minimise the C^P energy losses for the given wind speed sets and the chosen hybrid

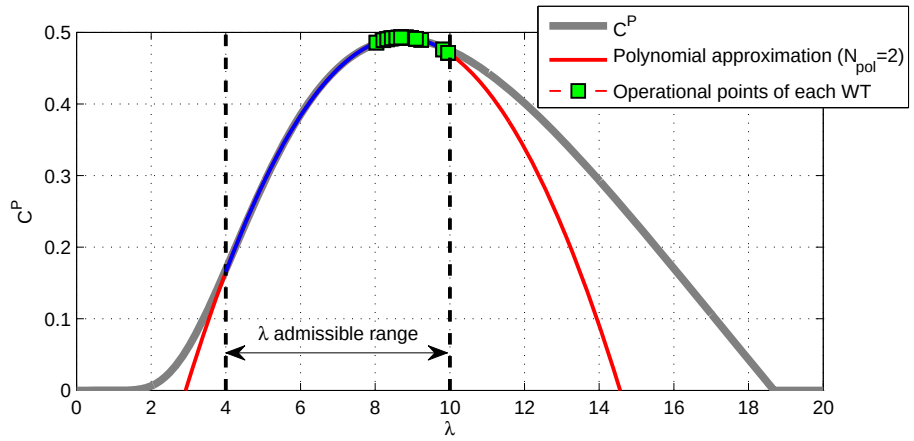

Figure 5.4: $C^P_{i,k}$–$\lambda_{i,k}$ curve and the polynomial approximation with all the operating points of each wind turbine $i \in \mathcal{I}$ which is controlled by the power converter $k \in \mathcal{K}$.

topology are 37.498 and 31.356 Hz, respectively. Comparing to an OWPP in which a single power converter is in charge of controlling the whole wind farm (and therefore, there is no individual converters in each turbine), the optimal hybrid AC–DC design is able to reduce the C^P energy losses over the lifetime of such OWPP by 109 GWh, which means a cost saving of up to 5.11 M€ (considering a lifetime (L) of 25 years and a cost of energy (C^E) of 46.84 €/MWh).

5.5.2 Application of the hybrid AC–DC OWPP topology

The model described is a non–linear mixed–integer problem with a great amount of binary variables, as it is shown in Table 5.1. For this reason, the dimension of the OWPP has been reduced in the mathematical model tests due to the computational limitations.

As mentioned in Chapter 4, the SLPC–VF topology becomes less cost–effective as the OWPP is growing in size and rated power, since the C^P energy losses that occur due to their inherent configuration, can be significant. Thus, the hybrid AC–DC OWPP concept proposed in this chapter will be profitable for such large OWPPs because the cost savings of reducing both the energy losses within the wind farm throughout its lifetime and the total length of the inter–array cables will more than likely be greater than the incremental cost of installing additional power converters and offshore

collector platforms.

To demonstrate that the proposed design of a hybrid OWPP can be more economical than an OWPP based on both the conventional scheme and the SLPC–VF topology, a comparative cost analysis is carried out. A feasible solution that satisfies all the constraints of the model has been chosen as an example of case study for the hybrid AC–DC OWPP topology. Thereby, if such feasible solution is found to be more economical than the other topologies, its optimal design will be as well.

Figure 5.5 shows the three topologies analysed (conventional, SLPC–VF and hybrid) for an OWPP consisting of 80 wind turbines with a rated power of 5 MW and a rotor diameter (D) of 126 m. It is assumed that the OWPP is far enough from the shore so that the DC interconnection is techno–economically feasible. It is laid out in a regular matrix of 10 columns and 8 rows. The spacing between two nearby wind turbines is 9 D in the prevailing wind direction and 7 D in its perpendicular direction, whilst the distance between the HVDC offshore platform and the nearest collector platform to it is 10 km.

Concerning the hybrid topology (case (c)), it consists of two collector platforms and three AC/DC power converters installed on it (c1, c2 and c3). Therefore, the wind turbines are arranged into three clusters which operate at different frequencies set by their respective converters. It is worth noting that both the SLPC–VF and the hybrid topologies (cases (b) and (c)) do not have individual power converters in each wind turbine. The obtained results are presented in Table 5.3.

Table 5.3: Breakdown of the costs for the three OWPP topologies analysed. All the prices are expressed in M€and updated to 2013 prices using a Consumer Price Index of 2%.

	Conventional (Figure 5a)	**SLPC–VF (Figure 5b)**	**Hybrid AC–DC (Figure 5c)**
Cost of inter–array cables	70.1	70.1	53.7
Cost of export cables	16.2	16.2	15.9
Cost of power converters	41.6	20.7	46.5
Cost of collector platforms	86.4	86.4	91.8
Cost of energy losses	16.6	31.5	14.3
Total cost	**230.9**	**224.9**	**222.2**

As it is observed, the hybrid AC–DC OWPP topology (c) is the most economical option, obtaining a cost benefit of 2.7 M€ and 8.7 M€ over the SLPC–VF (b) and conventional schemes (a), respectively. Hence, a total cost saving of up to 3.76% compared to the conventional OWPP topology can be achieved.

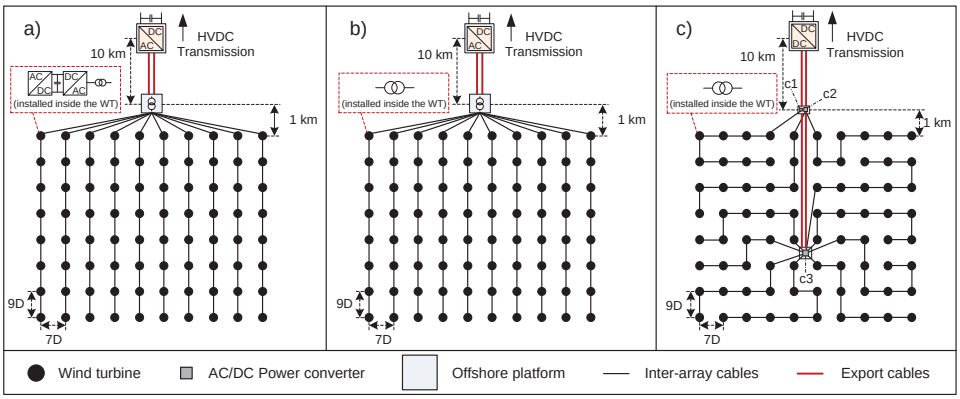

Figure 5.5: Three topologies analysed for an OWPP consisting of 80 wind turbines of 5 MW each: (a) Conventional scheme, (b) SLPC–VF scheme and (c) Hybrid AC–DC OWPP concept.

In general terms, the cost savings of reducing both the total inter–array cable length as well as the energy losses, coupled with the fact of not requiring dedicated power converters in each wind turbine, compensate the extra costs of installing additional offshore collector platforms and AC/DC power converters. With regard to the cost of the export cables, it remains practically unaltered for the three concepts, because even though the export cable length for the hybrid OWPP case (c) increases by 6.1 km compared to the other two OWPP topologies, its capital and installation cost is slightly lower. The cost of the power converters placed in each wind turbine has been considered to be 5% of the total turbine capital cost, according to [90].

In order to perform a more accurate comparison, the cost of energy losses has taken into account both the energy lost over the lifetime of an OWPP as a result of the efficiency losses of its components (transformers, converters, cables, etc.) and due to the inherent limitations of the OWPPs topologies analysed (transmission losses and C^P losses, respectively).

The optimum frequency at which the single large power converter of case (b) should operate to maximise the OWPP power generation for the given set of wind speeds is 39.34 Hz. Likewise, the optimum frequencies for power converters c1, c2 and c3 of the hybrid topology are 44.85, 41.37 and 37.69 Hz, respectively. It should be remarked that all these frequencies as well as the power generated by each wind turbine have been computed for a specific set of wind speeds that represents the average wind speed of each turbine over its lifetime.

5.6 Conclusions of the chapter

This chapter presents a novel hybrid AC–DC offshore wind power plant topology and an optimisation of its design in order to minimise its total cost. This proposed concept is planned for large OWPPs with an HVDC transmission link and where the single offshore HVDC platform is located slightly away from the wind turbine array to facilitate others OWPPs connections. It is based on installing one or multiple AC/DC power converters and intermediate offshore collector platforms between the HVDC platform and the OWPP, so that the inter–array AC voltage is step–up and the power is transmitted by the DC export cables. Likewise, the individual power converters of each turbine are removed and each of the aforementioned AC/DC converters controls a wind turbine cluster operating at variable frequency which is optimised for a given set of wind speeds.

The optimal design for an offshore wind power plant based on the hybrid AC–DC topology is formulated as a MINLP problem. The optimisation model has been developed in order to determine the optimal number of AC/DC power converters and offshore collector platforms needed, as well as their locations. Furthermore, the cable route connecting the wind turbines between each other is optimised. The results obtained demonstrate the good performance of the optimisation model and suggest the hybrid AC–DC topology as an appealing OWPP alternative, since a total cost saving of up to 3.76% compared to a conventional OWPP topology can be achieved.

6

Control of DFIG–based offshore wind power plant connected to a single VSC–HVDC operated at variable frequency

6.1 Introduction

As it can be noted in Chapter 4, the capability of HVDC technology to operate at variable frequency within an AC collection grid can bring cost savings by removing the individual power converters installed in each wind turbine driven by a synchronous generator. Similarly, this chapter investigates the feasibility of another novel concept for offshore wind power plants in the attempt of cutting down on LCOE. It consists of a DFIG–based OWPP with reduced size power electronic converters connected to a single large VSC–HVDC converter which operates at variable frequency within the AC collection grid. Thus, the common VSC–HVDC converter provides variable speed control to the whole wind power plant (or the wind turbine cluster) while the reduced size power converters inside each DFIG wind turbine are in charge of attenuating the mechanical loads and of partially or totally compensating the wind speed difference among turbines due to the wake effect. Consequently, improved reliability, increased efficiency due to the

lower losses and a cost reduction are expected to be achieved, whereas wind energy captured may be reduced owing to the narrower speed range that can be regulated by a smaller power converter [118, 132].

This chapter aims to evaluate the influence of the power converter rated slip and wind speed variability within the WPP on energy yield efficiency, as well as, to develop a coordinated control between the VSC–HVDC converter and the individual back–to–back power converters of each DFIG–based wind turbine in order to provide control capability for the wind power plant at a reduced cost. Both central wind power plant control level and each local wind turbine control level are presented and the performance of the system is validated by means of simulations using MATLAB/Simulink®.

6.2 Description of the proposed concept

Figure 6.1 shows the proposed wind power plant concept assessed in this chapter. As it can be seen, this wind power plant proposal combines DFIG

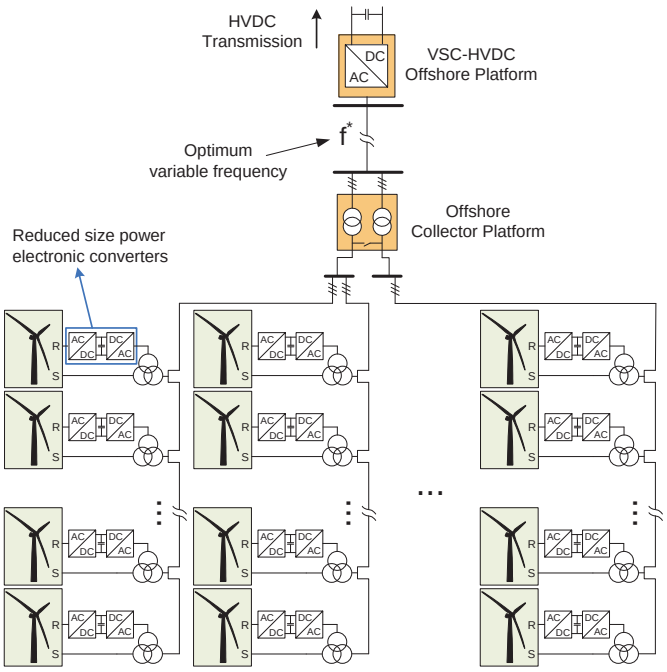

Figure 6.1: Proposal AC variable frequency OWPP with DFIG wind turbines.

wind turbines with reduced size power converters (approximately 5–10% instead of 25–35% of the rated power) and a single VSC–HVDC converter which dynamically changes the collection grid frequency (f*) as a function of the wind speeds of each turbine. This significant reduction of the power converter size is expected to be achieved as a consequence of the variable speed control provided by the common VSC to all the wind turbines. Analogously to the SLPC–VF concept presented in Chapter 4, this novel concept requires an HVDC transmission link to decouple the WPP collection grid from the electrical network and it is especially worthwhile for offshore wind power plants where the wind speed variability among turbines is assumed to be lower than in onshore. Likewise, this WPP configuration can be applied to either an entire wind power plant or to a wind turbine cluster, as for example, in Figure 6.2.

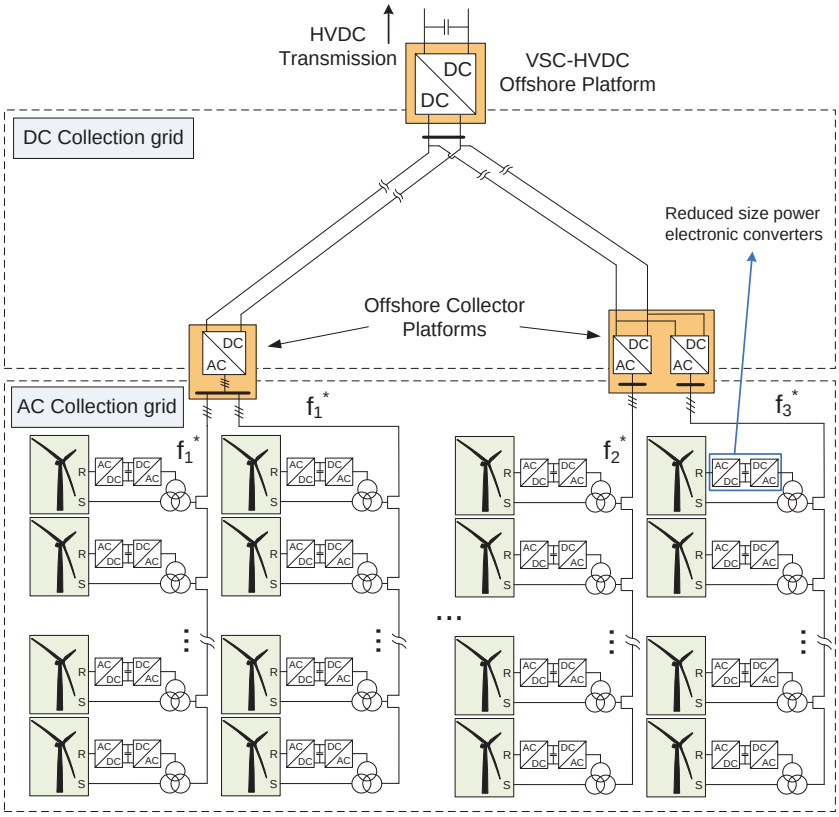

Figure 6.2: Proposal AC variable frequency hybrid OWPP with clusters of DFIG wind turbines.

In this case, the novel concept is applied to three clusters, each of which consists of a VSC that optimises its electrical frequency (f_1^*, f_2^* and f_3^*) to maximise its power generation. As it is shown, these AC/DC power converters are installed into two offshore collector platforms and they are connected to the main VSC–HVDC converter through MVDC export cables, establishing a DC collection grid. Thereby, an hybrid AC/DC OWPP topology, similarly to the OWPP scheme presented in Chapter 5, is obtained.

Unlike the SLPC–VF concept explained in Chapter 4, where all synchronous generators must rotate at the same speed regulated by the common VSC–HVDC converter, this WPP design allows each DFIG–based wind turbine to rotate at a different speed within a certain range defined by the size of the partial rating power converter. Thus, depending on the wind speed variability among the wind turbines and the power converter capacity, it is possible to ensure that each wind turbine operates at its optimum point. As an illustrative example, Figure 6.3 shows the range of speeds at which all wind turbines can rotate to guarantee its maximum power extraction for a given optimum electrical frequency set by the VSC (f^*=49.3 Hz) and depending on whether the fraction of total power generated by the generator is 30%, 5% or 0% (without converter).

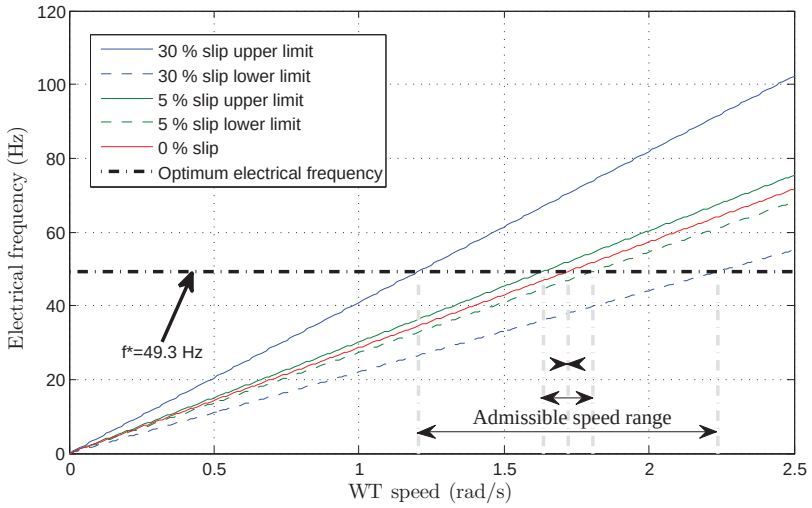

Figure 6.3: Illustrative example to explain the operation of the proposed WPP concept.

To determine the optimum size of the individual power converters, various criteria such as their capital costs, increased energy capture [133], mechanical

load reduction [134–136] and Fault Ride Through (FRT) capability [32, 33, 137–140] should be taken into consideration. This chapter focuses its study on the energy capture analysis by evaluating in detail the impact of the operating slip admissible range on the aerodynamic losses (or C_P losses) produced by each wind turbine.

6.3 Principle of operation of Doubly Fed Induction Generators (DFIGs)

As mentioned in Chapter 2, Doubly Fed Induction Generators (DFIGs) correspond to a Wound Rotor Induction Generator (WRIG) with a partial scale frequency converter. Because the stator windings are directly connected to the grid, the stator currents create a rotating magnetic field in the air gap which rotates at the synchronous angular frequency, ω_s. The principle of operation of DFIG is based on the Faraday's law, since the stator currents are induced in the rotor windings due to it sees a variation of magnetic flux to spin at a different speed from that of the rotational magnetic field. This relative speed difference between the stator magnetic field and the rotor is defined at the slip parameter, s, as

$$s = \frac{\omega_s - \omega_m}{\omega_s} \tag{6.1}$$

where ω_m is the rotor mechanical speed and $\omega_s = \omega_e/p$, being ω_e the angular electrical frequency of the grid and p the pair of poles of the machine. One advantage of DFIG machines is that the rotor power can flow bidirectionally in both directions due to the power electronics placed inside the back–to–back power converter. Depending on the sign of the slip, DFIG operates in a super–synchronous or sub–synchronous mode. Thereby, if $\omega_m > \omega_s$ $(s < 0)$ the machine operates in super–synchronous mode by delivering power to the grid from both the stator and rotor side, whilst if $\omega_m < \omega_s$ $(s > 0)$, the machine also acts as a generator transferring energy to the grid by the stator and absorbing energy from the grid through the rotor. In case that the rotor electrical speed matches the synchronous speed, $\omega_m = \omega_s$ $(s = 0)$, no currents would then be induced in its windings, since it would not observe any change in magnetic fluxes, and, consequently, the machine neither would generate nor would consume any power.

The total power generated by a DFIG–based wind turbine, P_{wt} is the sum of the power flowing from the stator, P_s, and the power flowing out of the rotor, P_r.

$$P_{wt} = P_s + P_r \tag{6.2}$$

These two active powers (P_s and P_r) are related to each other by means of the slip according to the following expression

$$P_r = -sP_s \tag{6.3}$$

so that only a small fraction of the power delivered to the grid via stator is flowing through the rotor. Hence, the power sharing between stator and rotor circuit can be expressed as follows

$$P_s = \frac{1}{1-s}P_{wt} = \frac{\omega_s}{\omega_m}P_{wt} \tag{6.4}$$

$$P_r = \frac{-s}{1-s}P_{wt} = \frac{\omega_m - \omega_s}{\omega_m}P_{wt} \tag{6.5}$$

Thus, given a fixed synchronous speed, the slip of the machine, as well as, the power generated delivered to the grid via stator and rotor can be controlled by regulating the mechanical rotor speed. However, if a variable frequency (ω_s or ω_e) is considered, this power sharing and the slip can be modified not only by changing the angular rotor speed, but also by dynamically varying the electrical frequency of the grid.

6.4 Influence of power converter size and wind speed variability on power generation efficiency

The maximum wind turbine speed range (or slip) that the power converter can regulate is related to the maximum power that can flow (in both directions) through the rotor circuit. This boundary is determined by the voltage upper limit that the power electronics placed inside the converter can withstand, which sets the power converter size. Thereby, the bigger the power converter, the more power can be generated by the generator, but at a higher cost.

In this section, the impact of the power converter rated slip on power generation efficiency is analysed. Besides, due to the inherent behaviour of the proposed OWPP concept, in which the electrical frequency within the collection grid is set by the common VSC–HVDC converter according to the individual wind speed of each turbine, the influence of wind speed variability within the OWPP on power extraction efficiency is also investigated.

To this aim, a wind power plant consisting of 12 wind turbines laid out in a rectangular matrix form of 3 columns and 4 rows is used as a case of study (Figure 6.4). Rated power of each wind turbine is 5 MW and its rotor diameter is 126 m. The spacing between two nearby wind turbines is 7 rotor

diameters (D) in the prevailing wind direction and 6 D in its perpendicular wind direction. Regarding the wind conditions within the OWPP, these are defined according to the wind rose presented in Figure 4.7(b) of Chapter 4, and the twelve Weibull distribution functions depicted in Figure 6.5 (one per each wind direction sector considered in the study). The sets of scale and shape parameters are randomly obtained basing on data reported in [91].

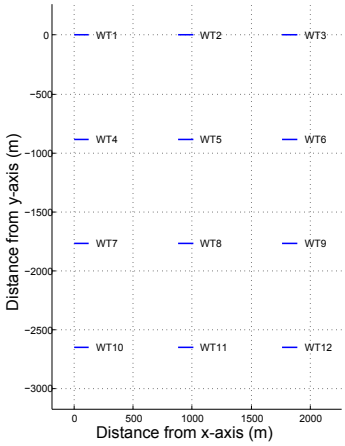

Figure 6.4: Wind power plant layout under study consisting of 12 wind turbines laid out in a regular matrix of 4 rows and 3 columns.

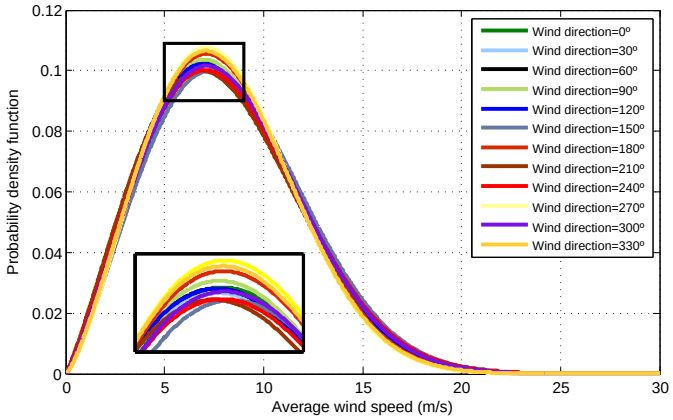

Figure 6.5: Weibull distribution function at the OWPP location under study for each wind direction sector considered.

Based on this scenario, the wind speed of each wind turbine, for all the cases analysed (30 different average wind speeds × 12 wind directions), is calculated taking into account the wake effect within the OWPP. This procedure, as well as the WPP layout and wind conditions definitions, are carried out by using the tool presented in Appendix B (referring to steps 1, 2 and 3 of the methodology explained in Chapter 4).

Once all the wind speeds are computed, the optimum electrical frequency at which the VSC–HVDC converter must operate to maximise the total power generated by the OWPP, should be calculated similarly to the approach carried out in step 4 of the methodology presented in Chapter 4. However, in this case it is not possible to perform the optimum electrical frequency algorithm as explained in Subsection 4.3.4 due to the total power generated by the OWPP depends not only on the electrical frequency of the collection grid, f_e, but also on the slip, s, of each wind turbine. These mathematical relations are shown below in (6.6) and (6.7).

$$\omega_t = \frac{2\pi f_e(1-s)}{pN_{gr}} \tag{6.6}$$

$$\begin{array}{cccc} eq.\ (3.1) & eq.\ (3.2) & eq.\ (5.25) & eq.\ (6.6) \\ \downarrow & \downarrow & \downarrow & \downarrow \\ \underbrace{P_{wt} = f(C_P, v_w) \ \rightarrow \ C_P = f(\lambda, \theta_{pitch}) \ \rightarrow \ \lambda = f(\omega_t, v_w) \ \rightarrow \ \omega_t = f(f_e, s)}_{P_{wt}=f(v_w,\theta_{pitch},f_e,s)} & & & \end{array} \tag{6.7}$$

where ω_t is the wind turbine low speed shaft and N_{gr} is the gearbox ratio. Therefore, the power generated by the OWPP, P^G, can be computed as

$$P^G = \frac{1}{2}\rho A \sum_{i=1}^{N_{wt}} \sum_{j=0}^{N_{pol}} a_j \left(\frac{2\pi f_e R}{pN_{gr}}\right)^j (1-s_i)^j v_{wi}^{3-j} \tag{6.8}$$

where θ_{pitch} is set to zero in order to maximise the total power generated and the power coefficient C_P is approximated to a polynomial of degree N_{pol} and coefficients a_j as in the previous chapters. Thus, the optimum electrical frequency, f_e^{opt}, is obtained for each set of wind speeds according to the following methodology. To better understand it, two application examples are shown in Figure 6.6.

1. Given a set of wind speeds, the optimum mechanical speeds at which each wind turbine must rotate to maximise its power output, ω_t^{opt}, are

computed. These optimum WT rotational speeds corresponds to the vertical gray lines of Figure 6.6.

2. The admissible operational region for all wind turbines is delimited by the size of the converter (lower and upper slip limits) and the minimum and maximum allowed electrical frequencies within the collection grid (due to the saturation effects of the generators and transformers and field weakening issues, respectively). This region is displayed in blue in Figure 6.6 for a particular power converter size of ± 5% slip.

3. The upper and lower frequency limits are defined according to the maximum and minimum values of the optimum wind turbines rotational speeds previously computed and the maximum slip (s_{max}) of the converter. These limits refer to the two horizontal dashed gray lines of Figure 6.6. At this point, two possible scenarios can occur: (i) there is a certain frequency range (for a given power converter size), in which all wind turbines operate at its optimum point, such that the total power generated is maximised (Figure 6.6(a)). (ii) according to the given slip limits of the converter and the optimum WT speeds of each wind turbine, there is no frequency that maximises the power generated by the whole wind power plant (Figure 6.6(b)). These two situations can be graphically identified by looking at the intersection points between upper and lower slip limits of the converter and minimum and maximum values of the optimum WT speeds. Thus, scenario (i) is when these intersection points correspond to P1 and P4, whereas scenario (ii) comes about for P2 and P3 intersection points. As it can be seen in Figures 6.6(a) and 6.6(b), these points from P1 to P4 determine the optimum and recommendable operational regions, respectively (green surface), at which the proposed WPP concept must operate to maximise (as much as possible) its power generation.

4. In this last step, the optimum electrical frequency, f_e^{opt}, is calculated for all wind speed sets considered. In case of scenario (i), all the frequency range covered by the optimum operational region are possible to be selected. Thereby, its mean value is chosen as the optimum electrical frequency. With regard to scenario (ii), the more suitable electrical frequency is obtained by undergoing a sweep of N_{freq} electrical frequencies and calculating for each of them the active power generated by the offshore wind power plant taking into account the technical constraints of reducing the power converter size. As a result of the analysis, the frequency that maximises the total power output

by the OWPP is chosen. These resulting electrical frequencies refer to the solid violet line of Figures 6.6(a) and 6.6(b), respectively.

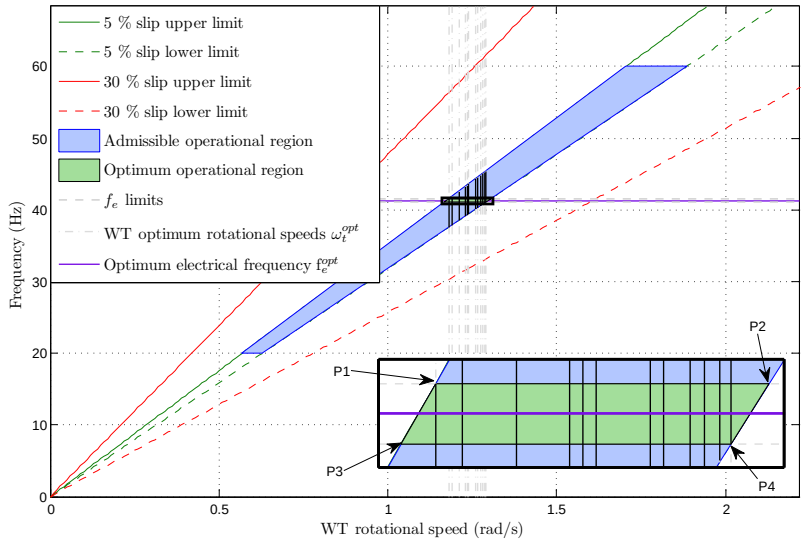

(a)

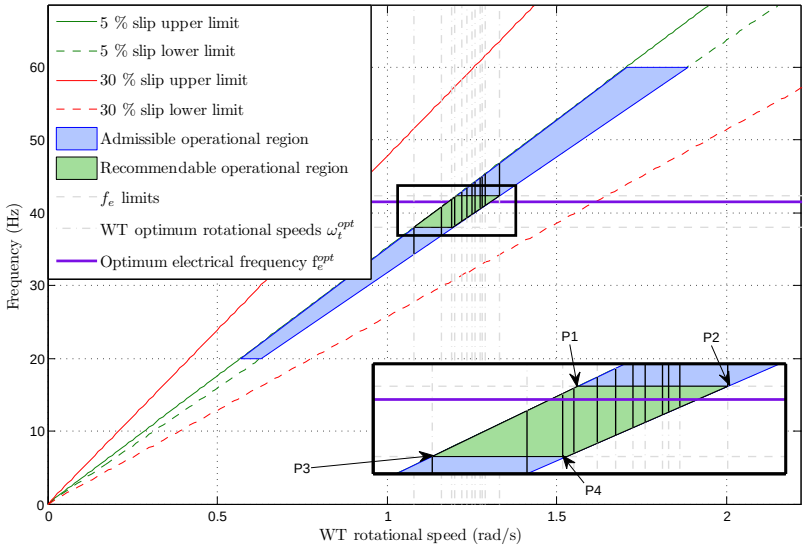

(b)

Figure 6.6: Two examples of applying the optimum electrical frequency search algorithm for two different sets of wind speeds.

Finally, once the optimum electrical frequency is selected and the total power generated is calculated, the energy captured by the OWPP throughout its lifetime, E^G, is obtained. Analogously to the previous chapters, this energy losses are calculated for all the cases analysed (varying the average wind speed and the wind direction) by taking into account their probability of occurrence (p_{wbij} and p_{wrj}).

$$E^G = T \sum_{i=1}^{N_{aws}} \sum_{j=1}^{N_{wd}} P_{ij}^G \, p_{wbij} \, p_{wrj} \tag{6.9}$$

where T is the lifetime of the offshore installation and N_{aws} and N_{wd} are the number of average wind speeds and wind direction considered, i. e., N_{aws}=30 and N_{wd} = 12. It should be mentioning that although the average wind speed range considered is from 1 m/s to 30 m/s, only those values greater than the cut–in speed and lower than the cut–out speed are taken into account to compute the total energy yield.

In order to evaluate the influence of the power converter rated slip and the wind speed variability within the offshore wind power plant on its energy capture efficiency, the aforementioned methodology has been applied to the case study considering different wind speed standard deviations among the upwind turbines (from 0 to 3 m/s) and different rated slips (0, 5, 15, 30 and 100%). The results are presented in Figure 6.7.

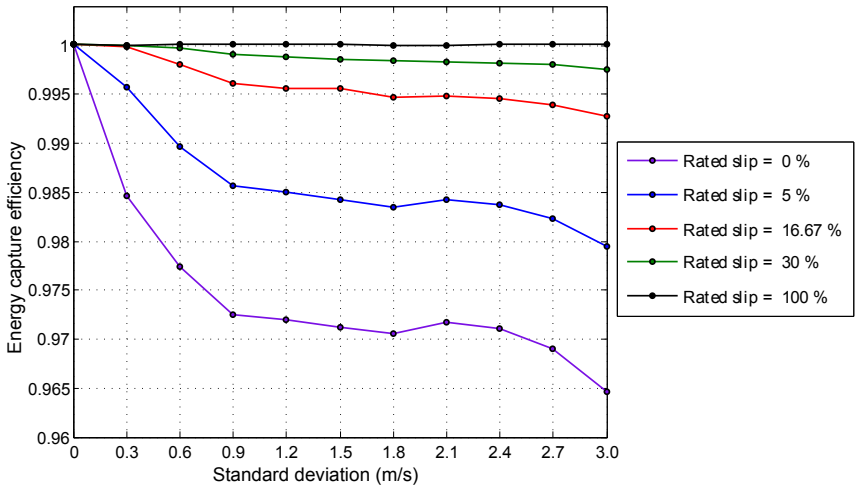

Figure 6.7: Energy capture efficiency as a function of different wind speed variability within the OWPP and different power converter sizes.

As it can be seen, the energy capture efficiency for a power converter rated slip greater than 16.67% is very high even for large wind speed variability within the wind power plant. For instance, the energy efficiency of a DFIG–based WPP with a power converter rated slip of 16.67% and 30% is 99.27% and 99.75%, respectively, for a standard deviation among the upstream wind turbines of 3 m/s. Likewise, it is also noteworthy the better performance of the proposed WPP concept with a reduced power converter rated at 5% of slip compared to the case of generators without any power converter (similar to the SLPC–VF concept described in Chapter 4). This energy efficiency improvement is especially significant when wind speeds are very uniform. For example, considering low standard deviations of 0.3 m/s and 0.6 m/s, it improves from 98.45% and 97.74% to 99.57% and 98.96%, respectively.

6.5 Comparative energy capture analysis between a power converter rated slip of 5% and 16.67%

In this section, two different cases corresponding to a DFIG–based OWPP connected to a single VSC–HVDC converter with the power converters of each wind turbine sized at 5% and 16.67% of rated slip, are chosen to be studied in detail. Thus, a comparative energy capture analysis is carried out between them from both the static and dynamic point of view.

In the following, the implemented control system based on a hierarchical structure with both a central control level (VSC–HVDC control system) and a local control level (DFIG wind turbines control system), is presented. This coordinated control is similar to previous DFIG–based WPP control schemes published in [141–143], but with the peculiarities that in this case there is a central VSC–HVDC large converter that dynamically change the collection grid electrical frequency to maximise the total power generation, as well as, the partial scale power converters of each DFIG wind turbine are reduced, and, therefore, its power control capacity is curtailed as well.

6.5.1 Overall control system

Figure 6.8 displays the offshore wind power plant configuration used as a case study. Due to computational reasons, it is only consisting of three pitch–controlled variable–speed 1.5 MW DFIG–based wind turbines connected to a single VSC–HVDC converter, which operates at a constant V/Hz operation. Thereby, the central converter changes the voltage with the frequency to maintain the flux constant. The output voltage of each wind turbine is

stepped–up from 690 V to 33 kV by a LV/MV transformer. All the parameters related to this system are detailed in Appendix D.

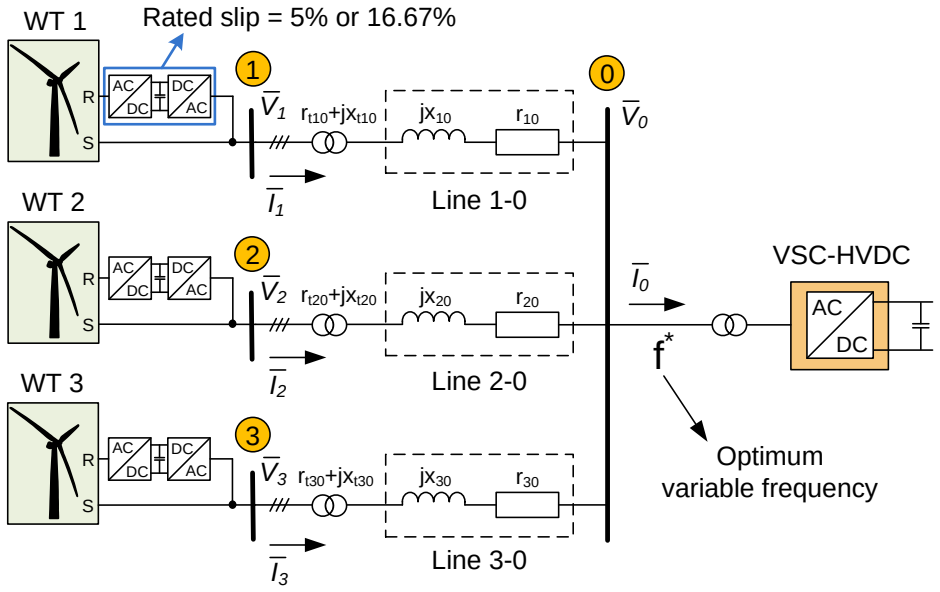

Figure 6.8: Electrical network topology used for the case of study.

The overall system is modelled using a RMS approach. The model is composed by four main blocks: the VSC–HVDC central control system, the wind speed model, the local control of each wind turbine and the collection grid model. The central control system sets the optimum electrical collection grid frequency according to the wind speeds of each wind turbine, and changes the voltage magnitude at the busbar zero. The wind speed model adopted is explained in detail in [144] and considers mean wind speed component, turbulence as well as rotating sampling effect. The collection grid is represented by the admittance matrix Y and the VSC–HVDC converter (normally based on Modular Multilevel Cascaded Converter, MMCC, technology [19, 44, 145–147]) is modeled as a controllable voltage source. In the following, the two control levels are described in more details.

6.5.2 Wind turbine level

DFIG Model The DFIG dq equivalent circuit, shown in Figure 6.9, is obtained from the following machine voltage equations [148]:

$$\begin{aligned} v_{sd} &= R_s i_{sd} - \omega_d \lambda_{sq} + L_{ls}\tfrac{d}{dt} i_{sd} + L_m \tfrac{d}{dt}(i_{sd} + i_{rd}) \\ v_{sq} &= R_s i_{sq} + \omega_d \lambda_{sd} + L_{ls}\tfrac{d}{dt} i_{sq} + L_m \tfrac{d}{dt}(i_{sq} + i_{rq}) \end{aligned} \tag{6.10}$$

$$\begin{aligned} v_{rd} &= R_r i_{rd} - \omega_{dA} \lambda_{rq} + L_{lr}\tfrac{d}{dt} i_{rd} + L_m \tfrac{d}{dt}(i_{sd} + i_{rd}) \\ v_{rq} &= R_r i_{rq} + \omega_{dA} \lambda_{rd} + L_{lr}\tfrac{d}{dt} i_{rq} + L_m \tfrac{d}{dt}(i_{sq} + i_{rq}) \end{aligned} \tag{6.11}$$

where L_{ls} and L_{lr} are the stator and rotor leakage inductances, L_m is the mutual inductance between stator and rotor windings, R_s and R_r are the stator and rotor resistance and ω_d and ω_{dA} are the dq–axis relative rotational speed with respect to the stator and rotor, respectively. In this chapter, a dq reference frame rotating at synchronous speed, ω_s, is used and, therefore, $\omega_d = \omega_s$ and $\omega_{dA} = \omega_s - \omega_m = \omega_{slip}$, being ω_s the electrical angular speed at the stator of the machine.

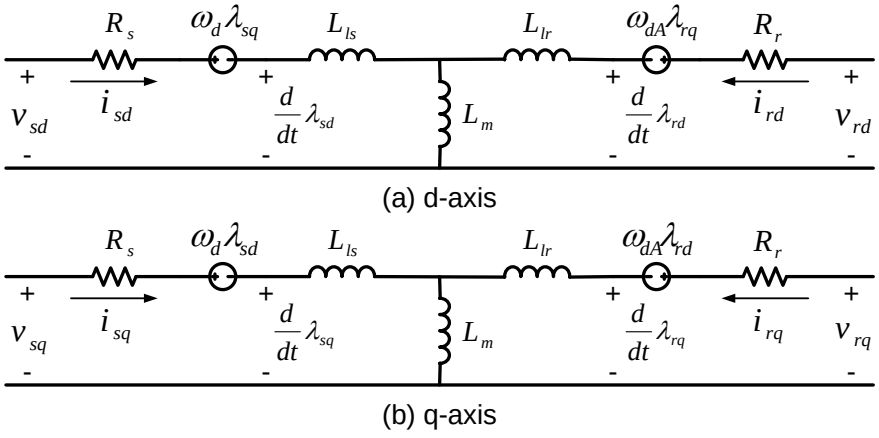

Figure 6.9: DFIG dq-axis equivalent circuit.

The electromagnetic torque and the stator reactive power, which are the variables to be controlled by the rotor side converter, can be expressed as [148]:

$$\Gamma_m = \frac{3}{2} p L_m (i_{sq} i_{rd} - i_{sd} i_{rq}) \tag{6.12}$$

$$Q_s = \frac{3}{2}(v_{sq}i_{sd} - v_{sd}i_{sq}) \tag{6.13}$$

Converter Model The converter model consists of an IGBT voltage source back–to–back power converter used as an interface between the AC grid and the rotor windings. As it can be seen in Figure 6.10, it consists of two independent converters connected to a common DC–bus. In order to consider that the applied voltages by the converter fit in with the voltages set points ($v^*_{rsc} \approx v_{rsc}$ and $v^*_{gsc} \approx v_{gsc}$), it is assumed that the switching frequency of the SVPWM is high (usually over 1 kHz) and the high–frequency components of the voltage signals generated by the inverters are filtered by the low pass nature of the machine and the grid–side circuit [27]. In addition, the electronic switching are considered to be ideal and without losses.

The DC–bus voltage, E, is calculated from an active power balance in the back–to–back converter (Figure 6.10). Thus, in the case that the dc–chopper is switch on, the equation is described as

$$P_{gsc} - P_{rsc} = P_{DC} + P_{Chopper} \tag{6.14}$$

being

$$\begin{aligned} P_{gsc} &= \tfrac{3}{2}(v_{gscd}i_{ld} + v_{gscq}i_{lq}) \\ P_{rsc} &= \tfrac{3}{2}(v_{rscd}i_{rd} + v_{rscq}i_{rq}) \\ P_{DC} &= \tfrac{1}{2}C\tfrac{d}{dt}E^2 \\ P_{chopper} &= \tfrac{E^2}{R_{chopper}} \end{aligned} \tag{6.15}$$

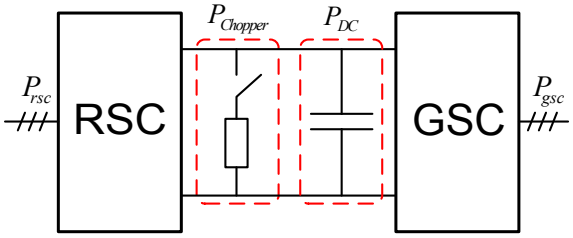

Figure 6.10: Active power balance in the back-to-back converter.

The voltage equation of the grid side electrical circuit, given by the space vector form, can be written as

$$\vec{v}_z^a - \vec{v}_{gsc}^a = r_{gsc}\vec{i}_l^a + L_{gsc}\frac{d}{dt}\vec{i}_l^a \tag{6.16}$$

where $\vec{v}_z^a$ and $\vec{v}_{gsc}^a$ are the voltage space vectors of the grid and the AC side of the converter, respectively, $\vec{i}_l^a$ is the current space vector and r_{gsc} and L_{gsc} are the resistance and the inductance of the circuit. The superscript "a" indicates that the space vectors are expressed as complex numbers with the stator a–axis chosen as the reference axis with an angle of 0°.

Pitch System Model As it is shown in Figure 6.11, the pitch system model is divided into two blocks: the pitch controller and the pitch angle actuator. The former determines the pitch angle reference, β_{ref}, from the difference between the measured and the desired rotor speed and is explained below in subsection 6.5.2. The latter consists of an actuator that rotates all the blades to a certain pitch angle, β, equal to the desired one.

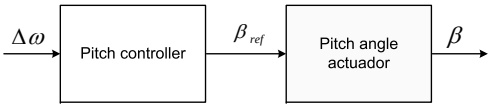

Figure 6.11: Basic configuration of the pitch system model.

The pitch actuator is a nonlinear servo that can be modeled in closed loop as a first–order dynamic system with saturation in the amplitude and derivative of the output signal [103]. Figure 6.12 shows a block diagram of the first-order actuator model. The dynamic behaviour of the pitch actuator operating in its linear region is described by the following differential equation

$$\dot{\beta} = -\frac{1}{\tau_{pitch}}\beta + \frac{1}{\tau_{pitch}}\beta_{ref} \tag{6.17}$$

where τ_{pitch} is the time constant. Typically, β ranges from -2° to 30° and varies at a maximum rate of $\pm 10°/s$ [103].

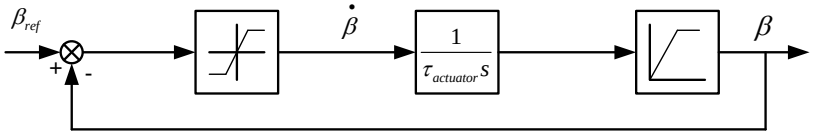

Figure 6.12: Model of the pitch angle actuator.

Control Scheme

As it is explained in Chapter 3, the main control objectives of WECS depends on its load operation mode. In partial load region, which corresponds to wind speeds lower than the rated speed, the aim is to maximize the energy capture from the wind. Otherwise, at hight wind speeds (full load operation mode), the control goal is to limit the generated power below its rated value to avoid overloading.

To achieve these objectives, the control system is divided into two levels (Figure 6.13): a high–level control or speed control and a low level control or electrical control. The former gives the proper torque, Γ_m^*, square dc voltage, $(E^2)^*$, and reactive powers, Q_s^* and Q_z^*, set points to the converter as function of the wind speed, the low speed shaft angular velocity and the grid voltage. The latter, regulates the incoming reference signals computing the appropriates voltage set points to the back–to–back power converter.

Apart from this control system, if the machine is operating in the full load region, pitch control is activated in order to keep the extracting power at its nominal value.

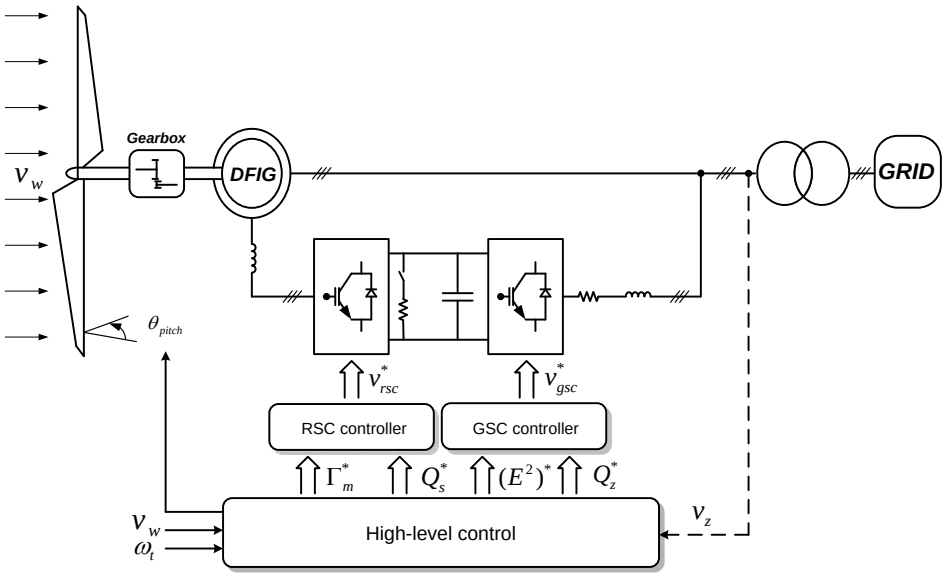

Figure 6.13: Wind turbine control level.

Speed Control

Depending on the region where the wind turbine is operating, two different control strategies are used. In the partial load region, the main goal is to extract all the available power from the wind. In this chapter, a MPPT strategy with only a rotation speed sensor required, is used. The advantage of this method is to avoid the measurement of the wind speed and, consequently, its stochastic nature.

According to [27], the maximum C_P and, therefore, the maximum power generation for a single wind turbine, is guaranteed to match the generator electrical torque with $K_{C_{P\_opt}}\omega_t^2$.

where $K_{C_{P\_opt}}$ is a constant parameter that depends on the geometry of the turbine and is expressed as follows

$$K_{C_{P\_opt}} = \frac{1}{2}\left(\frac{c_1 c_2}{c_7}\right) e^{-\frac{c_6 c_7}{c_2}-1} \rho A \frac{R^3}{(\frac{c_2 c_7}{c_2 c_9 c_7 + c_6 c_7 + c_2})^3} \tag{6.18}$$

The control strategy changes in the full load region. In this case, the torque reference signal (Γ_m^*) is fixed whereas the pitch control is activated to limit the captured power to its nominal value.

Figure 6.14 illustrates the basic variable–speed variable–pitch control strategy on the torque–rotational speed plane. Below rated wind speed of 10.1 m/s, at partial load mode, the turbine is operated along the C_P^{max} locus between the points A and B. Above rated wind speed, at full load operation, the pitch angle is controlled in order to keep the turbine operating at point B.

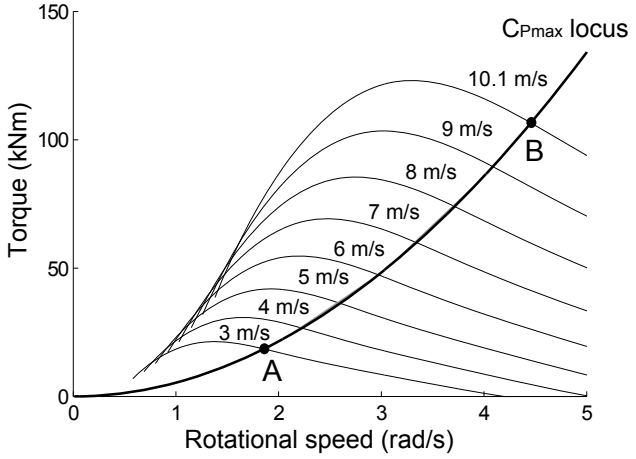

Figure 6.14: Basic variable–speed variable–pitch control strategy.

Pitch Control

The pitch controller is sketched in Figure 6.15. It consists in regulating the rotational wind turbine speed by means of a Gain Scheduling function block (GAINS) and a PI–controller, resulting a pitch angle reference (β_{ref}) to the pitch actuator. Gain Scheduling is a technique commonly used in the control of nonlinear systems [103,149]. In the case of Figure 6.15, the gain scheduled controller is implemented as a PI control and a gain depending on the pitch angle [103].

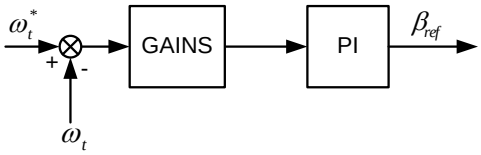

Figure 6.15: Pitch controller design.

Electrical Control

The electrical control or low level control is divided into two subsystems: the rotor side converter (RSC) control and the grid side converter (GSC) control. Both inner control loops are assumed to be ideal since the WT electric system time responses are much faster than the outer speed control loop or high level control [27]. Thus, it is possible to dissociate both control loops and to define a cascade control structure where the inner control loop concerns the back–to–back power converter and the outer control loop concerns the speed control. Additionally to the the RSC and GSC controls, a dc–chopper is implemented in order to dissipate the excess of energy that cannot be evacuated to the grid during a fault. The control system also includes the voltage and currents limitations according to the capacity of the generator and the rating of the converters.

Rotor Side Converter Control The RSC objective control is to regulate both the generator torque and the stator reactive power. To this aim, a vector control approach is deployed. A synchronously rotating dq–axis frame with the q–axis oriented along the stator flux vector position is chosen ($\lambda_{sd} = 0$). This enables a decoupled control of the torque and the stator reactive power, which can be expressed as a function of the direct and quadrature components of the rotor current references, respectively, as follows [32]

$$i_{rd}^{*} = \frac{2L_s\Gamma_m^{*}}{3pL_m\lambda_{sq}} \tag{6.19}$$

$$i_{rq}^{*} \approx \frac{\lambda_{sq} + \frac{2Q_s^{*}L_s}{3v_{sd}}}{L_m} \tag{6.20}$$

The rotor current control is implemented by the following state linearization feedback [32]:

$$\begin{aligned} v_{rscd} &= \hat{v}_{rscd} - \omega_{dA}\lambda_{rq} \\ v_{rscq} &= \hat{v}_{rscq} + \omega_{dA}\lambda_{rd} \end{aligned} \tag{6.21}$$

where the $\hat{v}_{rscd}$ and $\hat{v}_{rscq}$ are the output voltages of the dq–axis rotor currents controller. Thus, replacing (6.21) in (6.11) and neglecting the stator current transients, the following decoupled system is obtained

$$i_r^{dq}(s) = \underbrace{\begin{bmatrix} \frac{1}{R_r+L_rs} & 0 \\ 0 & \frac{1}{R_r+L_rs} \end{bmatrix}}_{G(s)} \hat{v}_{rsc}^{dq}(s) \tag{6.22}$$

The PI controllers are designed according to the Direct Synthesis methodology detailed in [150], with the desired close loop transfer function, M(s), and the plant, G(s), as

$$\begin{aligned} M(s) &= \frac{i_{rd}(s)}{i_{rd}^{*}(s)} = \frac{i_{rq}(s)}{i_{rq}^{*}(s)} = \frac{1}{\delta s+1} \\ G(s) &= \frac{K}{\tau s+1} = \frac{\frac{1}{R_r}}{s\frac{L_r}{R_r}+1} \end{aligned} \tag{6.23}$$

being

$$K_p = \frac{\tau}{K\delta} = \frac{L_r}{\delta} \quad y \quad K_i = \frac{1}{K\delta} = \frac{R_r}{\delta} \tag{6.24}$$

To sum up, the generator torque control loop and the stator reactive power control loop are shown in Figures 6.16 and 6.17, respectively. As it can be noted, the references voltages that the RSC must apply are limited according to the rated slip chosen for the partial scale frequency converter. This relation between rated slip and maximum rotor voltage allowed is depicted in Figure 6.18. Accordingly, the maximum rotor voltage for a power converter sized at 5% of its rated power (case A) is 29.792 V, whereas for a rated slip of 16.67% (case B) it corresponds to 99.326 V.

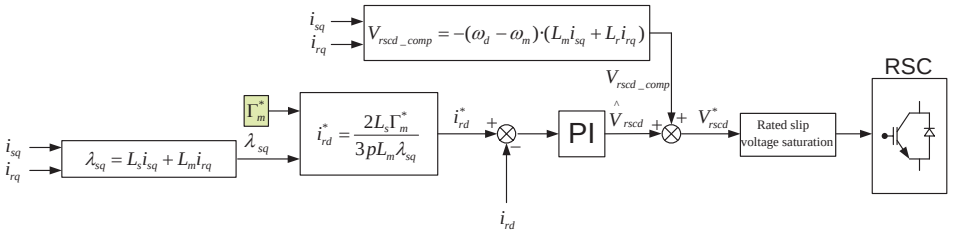

Figure 6.16: Block diagram of the generator torque control loop.

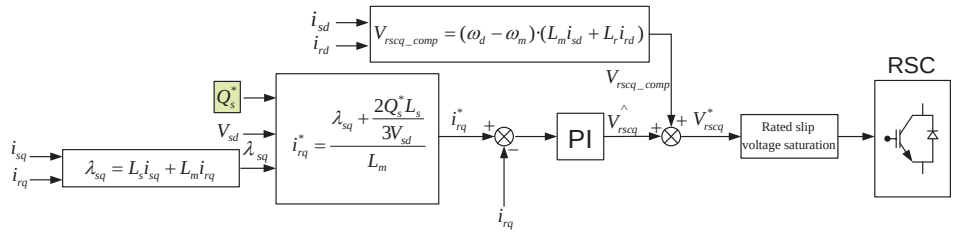

Figure 6.17: Block diagram of the stator reactive power control loop.

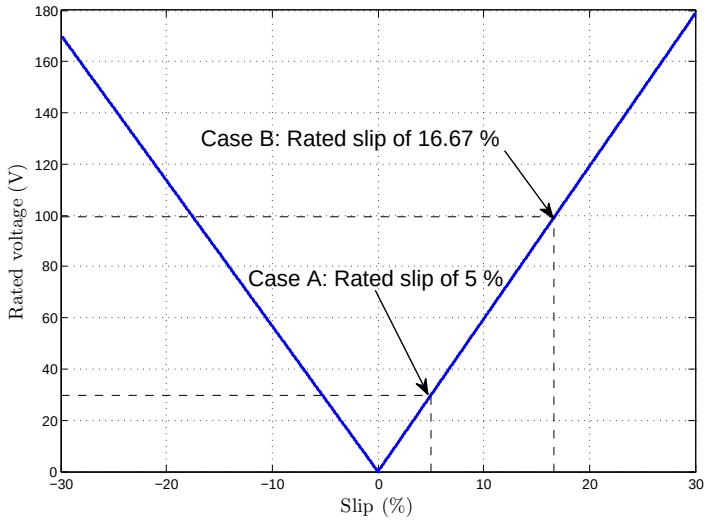

Figure 6.18: Rated slip - rotor voltage saturation.

Grid Side Converter Control The objectives of the GSC are to keep the DC–link voltage constant and to control the grid side reactive power, by means of regulating the dq–axis currents (i_l^{dq}) and applying the proper volt-

ages to the grid side. Using a vector control approach, with a synchronously rotating dq–axis frame and aligning the d–axis of the reference frame along the stator voltage vector position ($v_{sq} = v_{zd} = 0$), enables a decoupled control between the DC–voltage and the reactive power.

In the case of the reactive power control loop, the current reference is directly computed as

$$i_{lq}^{*} = -\frac{2Q_z^{*}}{3v_{zd}} \tag{6.25}$$

However, the calculation of the d–axis grid side current reference (i_{ld}^{*}) becomes more complex and some assumptions need to be considered. A cascade control structure is implemented, where the outer control loop is responsible for regulating the square dc voltage and the inner control loop consist in controlling the grid side currents (Figure 6.19). It is considered that the current response is much faster than the dynamics of the outer loop due to the slow response of the capacitors. Furthermore, the dc–chopper is not considered in the control design.

As in the RSC case, PI parameters are tuning according to the Direct Synthesis methodology, with M(s) equals to a first order transfer function and

$$G(s) = \frac{E^2}{P_{DC}^{*}} = \frac{2}{c \cdot s} \tag{6.26}$$

Thus, as can be seen in (6.27), a proportional controller (P) is only needed for tuning the controller R(s)

$$R(s) = \frac{M(s)}{G(s)(1 - M(s))} = \frac{\frac{1}{\delta s+1}}{\frac{K}{s}(1 - \frac{1}{\delta s+1})} = \frac{1}{K\delta} \tag{6.27}$$

being

$$K_p = \frac{1}{K\delta} = \frac{C}{2\delta} \tag{6.28}$$

Aligning the d–axis of the reference frame along the stator voltage position, the d–axis grid side current reference (i_{ld}^{*}) can be written as

$$i_{ld}^{*} = \frac{2P_{gsc}^{*}}{3v_{zd}} \tag{6.29}$$

A similar analysis for the control of the dq–axis rotor currents can likewise be done for the control of the dq–axis grid side currents. Therefore, the following state feedback is used to linearize the current dynamics.

$$\begin{aligned} v_{gscd} &= -\hat{v}_{gscd} + v_{zd} + \omega_d L_{gsc} i_{lq} \\ v_{gscq} &= -\hat{v}_{gscq} - \omega_d L_{gsc} i_{ld} \end{aligned} \tag{6.30}$$

where the $\hat{v}_{gscd}$ and $\hat{v}_{gscq}$ are the output voltages of the dq–axis grid side currents controller. The decoupling leads to

$$i_l^{dq}(s) = \underbrace{\begin{bmatrix} \frac{1}{r_{gsc}+L_{gsc}s} & 0 \\ 0 & \frac{1}{r_{gsc}+L_{gsc}s} \end{bmatrix}}_{G(s)} \hat{v}_{gsc}^{dq}(s) \tag{6.31}$$

Finally, using the Direct Synthesis methodology, the resulting PI parameters are computed as

$$K_p = \frac{\tau}{K\delta} = \frac{L_{gsc}}{\delta} \quad y \quad K_i = \frac{1}{K\delta} = \frac{r_{gsc}}{\delta} \tag{6.32}$$

Analogously to the RSC case, both the square DC voltage and the grid side reactive power control loops are shown in Figures 6.19 and 6.20, respectively.

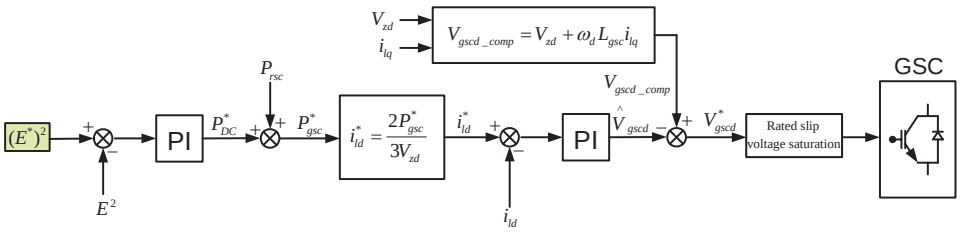

Figure 6.19: Block diagram of the square dc voltage control loop.

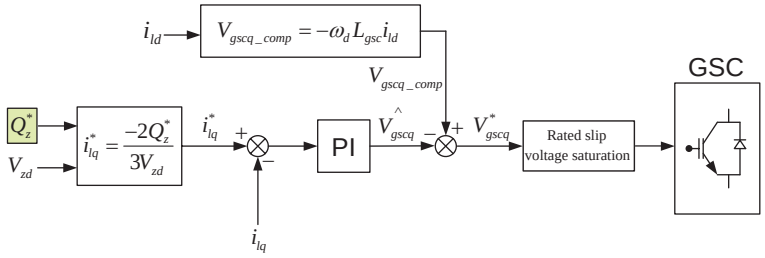

Figure 6.20: Block diagram of the grid side reactive power control loop.

6.5.3 VSC–HVDC control system

As previously stated, the VSC–HVDC control system is in charge of controlling its output voltage and the frequency of the collection grid to keep

the flux constant. This V/Hz control method has been widely used both in academia and industry due to its easy implementation and good performance [47, 50, 132, 151]. The electrical frequency is dynamically changed by the single converter according to the optimum electrical frequency search algorithm explained in detail in Section 6.4. This frequency is optimised (f_e^{opt}) based on the wind speed measurements of each wind turbine. In order to maintain the transformer and generator fluxes constant for different electrical frequencies, the output voltage set by the VSC–HVDC power converter located at the offshore platform (V_{VSC}) is given by the following expression:

$$V_{VSC} = K f_e^{opt} \tag{6.33}$$

where K is calculated as

$$K = \frac{V_{VSC-rated}}{f_{rated}} \tag{6.34}$$

where $V_{VSC-rated}$ is the rated voltage of the VSC–HVDC converter and f_{rated} is the rated frequency of the grid. Thus,

$$K = \frac{33000}{50} = 660 \tag{6.35}$$

6.5.4 Simulation results

In this section, two dynamic simulations are carried out by using MATLAB/ Simulink®. First, a wind speed step change is performed to understand the effect of reducing the power converter rated slip on the overall performance of the system. Then, a realistic wind speed scenario is tested to validate the implemented control scheme, as well as, to perform a comparative energy capture analysis between the two power converter sizes considered for the system under study, i.e., 5% and 16.67% of rated slip.

Simulation 1: wind speed step change

Figure 6.21 shows the wind speed profile of each wind turbine used for the former simulation. As is can be seen, a wind speed step change occurs at 10 seconds, so that the wind speeds of WT1, WT2 and WT3 before then are 7.5, 7.7 and 7.2 m/s, respectively, while after this time, these wind speeds change to 8.4, 7.9 and 6.6 m/s.

These wind speed values are intentionally chosen to analyse the influence of wind speed variability on the power generation efficiency of the system. Figures 6.22 and 6.23 show the steady state operational points of the three wind turbines for the two wind speed situations considered (before and after

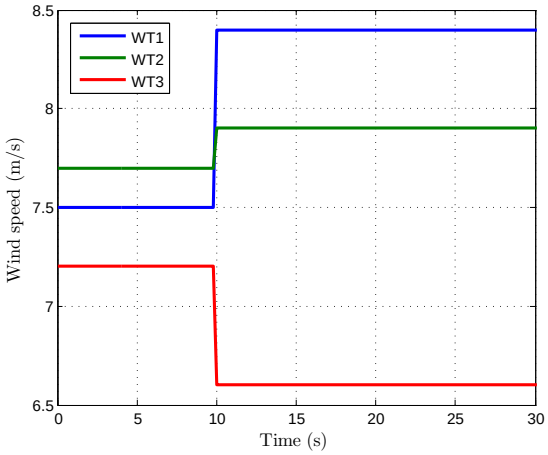

Figure 6.21: Wind speed profile of each WT considered in simulation 1.

10 seconds) and for the two power converter slip ratings analysed, 5% and 16.67%, respectively. The vertical gray lines correspond to the optimum rotational speeds of each turbine according to their wind speeds. The horizontal dash black lines represent the resulting optimum electrical frequencies, f_e^{opt}, that must be set by the VSC–HVDC converter to maximise the total OWPP power generation for each case. Thus, it is observed that when all wind speed are similar (a), both power converters are capable enough to carry out the MPPT approach within their limits, so that, in both cases the OWPP energy capture is maximised. However, if the wind speed variability among turbines increases (b), the small power converter sized at 5% of rated slip is not sufficient to cover this wind speed diversity range (only WT2 is optimised), whereas a higher power converter (rated slip = 16.67%) can bring each wind turbine speed at its optimum point (C_P^{max}).

To validate the simulation results obtained with the performed static analysis, Figures from 6.24 to 6.29 are presented. Figure 6.24 shows the electrical frequency imposed by the VSC–HVDC power converter for both cases considered. As it can be seen, they match their reference values, which has been computed previously in the static analysis. It is noteworthy that, for the cases where no wind turbine is limited (i.e., case (a) for power converter of 5% and cases (a) and (b) for power converter of 16.67%), not only these frequency references, but also any frequency within the range delimited by the green surface of Figures 6.22 and 6.23 can maximise the total power output for these particular wind speeds. Likewise, Figure 6.25 depicts the wind turbines rotational speeds for both cases studied (5% (a) and 16.67% (b)).

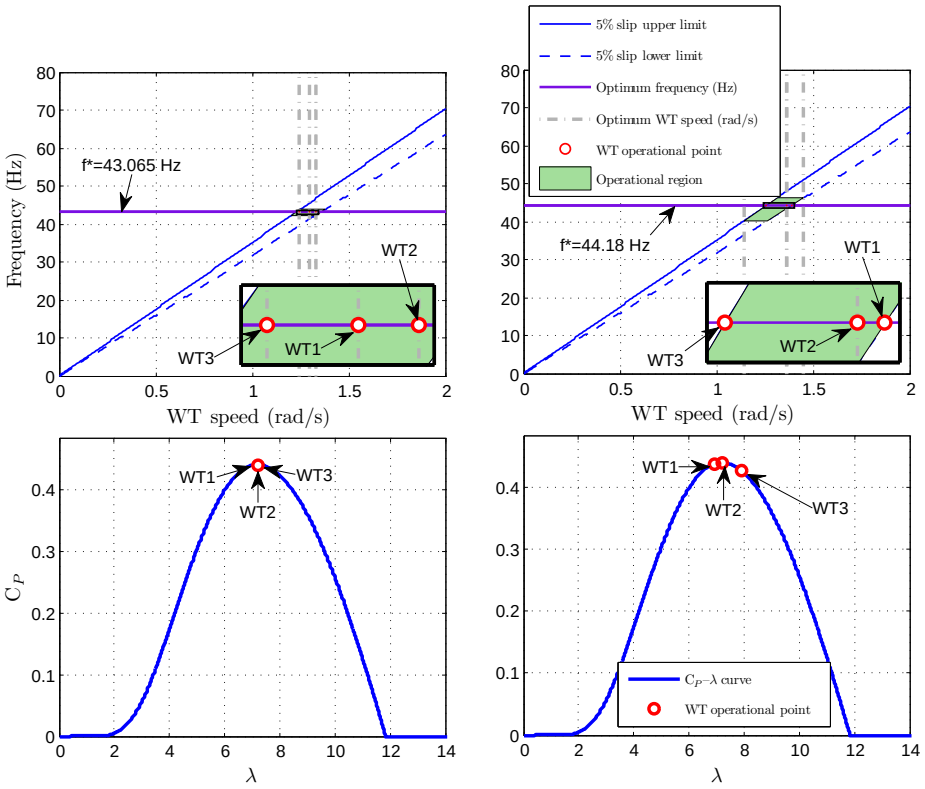

(a) Before 10 seconds (b) After 10 seconds

Figure 6.22: Operational points of WT1, WT2 and WT3 for the two wind speeds situations considered, (a) and (b), when the power converted is sized at 5% of rated slip.

The solid lines indicate the simulated values while the dash lines are the optimum WT speeds previously computed in the steady state analysis. As it is shown in Figure 6.25(a), only WT2 can reach its optimum speed when the wind speed differences between wind turbines increase, as expected. With regard to WT1 and WT3, they cannot reach their optimum speed due to the physical limitations of the power converter and because the collection grid frequency rises from 43.065 Hz to 44.18 Hz (which benefits the high wind speeds). On the other hand, in Figure 6.25(b), all wind turbines reach their optimum speeds, since none of them are limited. These limits can be clearly observed in Figure 6.26, where the rotor voltages of the three wind turbines, for both cases, are plotted. Regarding the case of considering a

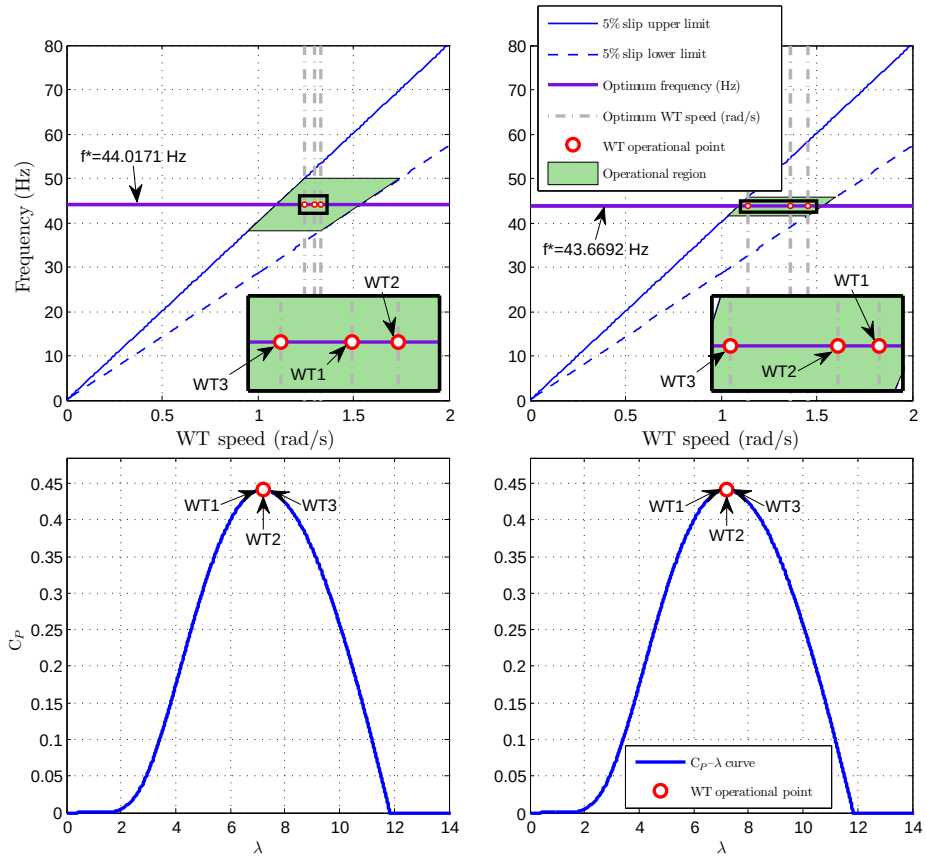

(a) Before 10 seconds (b) After 10 seconds

Figure 6.23: Operational points of WT1, WT2 and WT3 for the two wind speeds situations considered, (a) and (b), when the power converted is sized at 16.67% of rated slip.

smaller converter of 5% of rated slip (Figure 6.26(a)), both WT1 and WT3 are limited at its maximum admissible voltage for this rated slip. This value is obtained from the rated slip–rotor voltage saturation curve depicted in Figure 6.18 and corresponds to 29.792 V. Nevertheless, when considering a higher power capacity of the converter (rated slip = 16.67%), the desired rotor voltages related to WT1 and WT3 (48.275 V and 72.291 V, respectively) can be achieved, since their voltage limit for this rated slip is 99.326 V. Concerning to WT2, the rotor voltage required (14.684 V) is always lower than its upper limit, regardless the rated slip of the power converter.

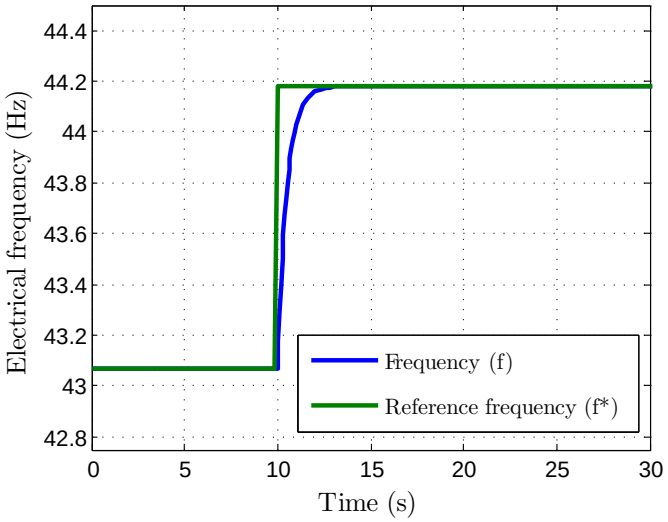

(a)

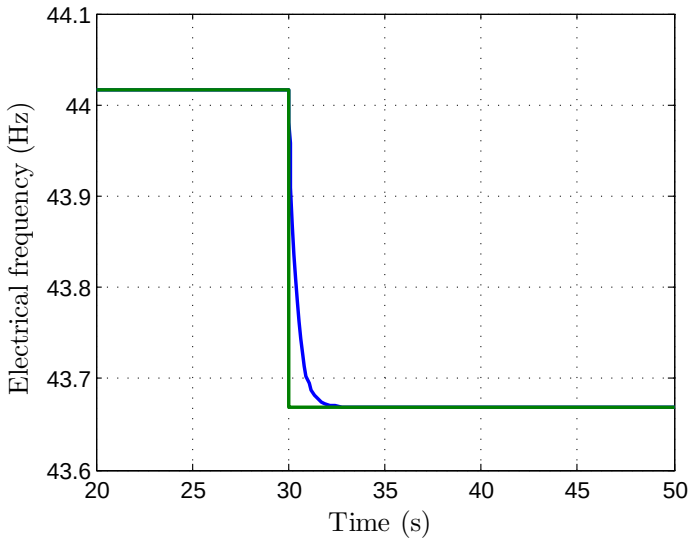

(b)

Figure 6.24: Electrical frequency set by the VSC–HVDC converter when the individual power converters of each DFIG–based wind turbine are at 5% (a) or 16.67% (b) of rated slip.

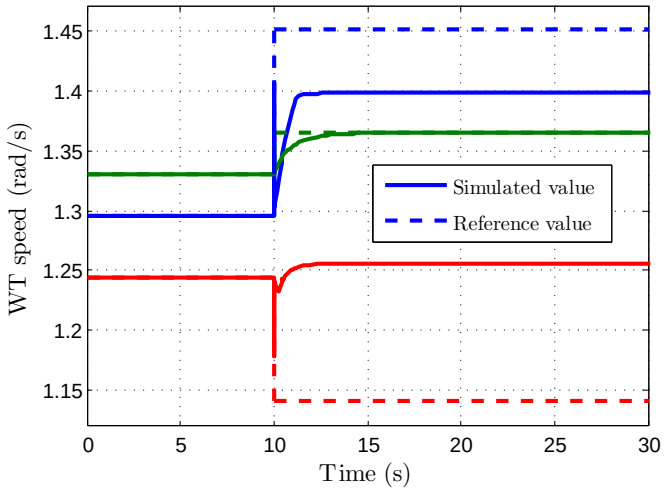

(a)

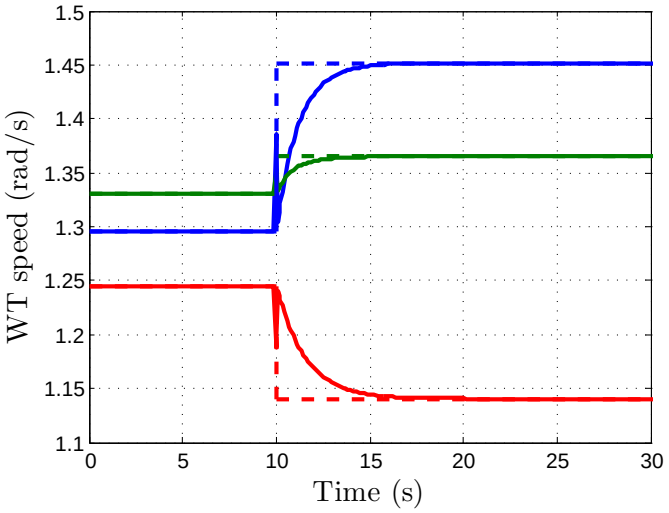

(b)

Figure 6.25: Rotational wind turbine speeds (low shaft) when the individual power converters of each DFIG–based wind turbine are at 5% (a) or 16.67% (b) of rated slip.

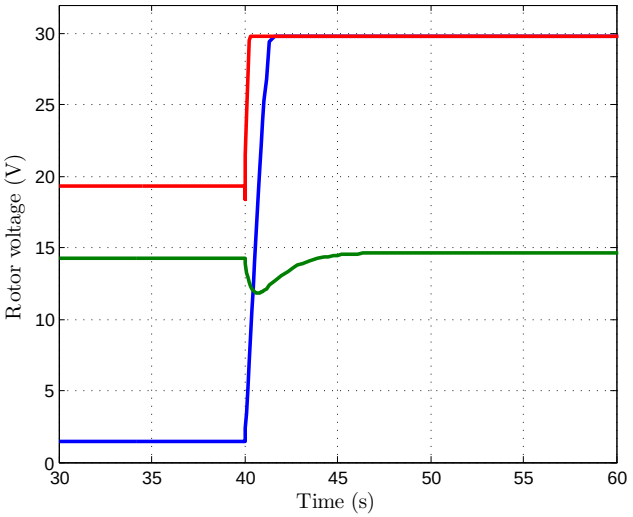

(a)

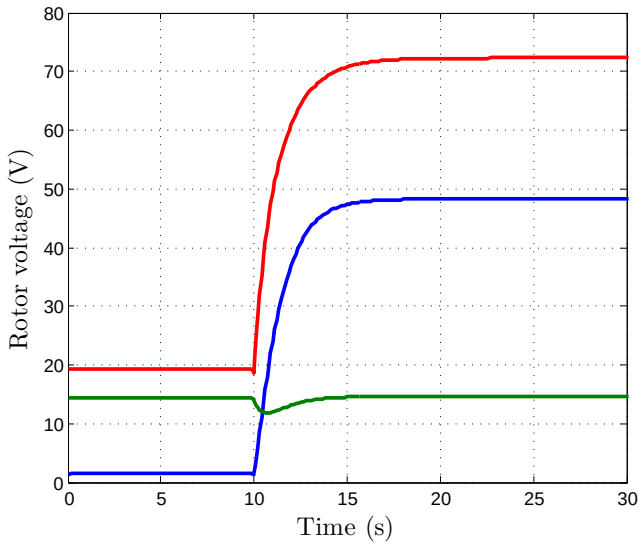

(b)

Figure 6.26: Rotor voltage module of each generator when the individual power converters of each DFIG–based wind turbine are at 5% (a) or 16.67% (b) of rated slip.

The last three figures corresponding to simulation 1 refer to active power (generator P_g, stator P_s and rotor P_r), slip and power coefficient C_P of each wind turbine. These variables are sketched in Figure 6.27, 6.28 and 6.29, respectively. Table 6.1 presents the active power generated by each wind turbine before and after 10 seconds for each power converter size considered. The power coefficient, C_P, value is given as well. As it can be noted, before 10 seconds both OWPP configurations work properly within their limits. Thus, each turbine generates its maximum available wind power, operates at C_P^{max} and presents a slip within the admissible range of $\pm 5\%$ and $\pm 16.67\%$. However, after 10 seconds, the wind speeds become less uniform between them and the performance of WT1 and WT3 decrease (when the rated slip of the converter is 5%). Thereby, their steady state C_P values are reduced from its maximum point and their slips are limited at its rated value. Moreover, it is worth noting the bidirectional behaviour of the converter according to its slip value. For example, WT1 and WT2 have a negative slip and, therefore, they generated power through the rotor and the stator. However, the positive slip of WT3 means that the rotor is consuming power from the grid, and consequently, it has a negative value.

Table 6.1: Comparative analysis between the performance of both power converter rated slips (case 1 = 5% and case 2 = 16.67%).

(a) Before 10 seconds

	Wind speed (m/s)	C_P^1	C_P^2	**Active power^1 (kW)**	**Active power^2 (kW)**
WT1	7.5	0.4412	0.4412	622.80	622.80
WT2	7.7	0.4412	0.4412	673.96	673.96
WT3	7.2	0.4412	0.4412	551.01	551.01
TOTAL	-	-	-	1847.80	1847.80

(b) After 10 seconds

	Wind speed (m/s)	C_P^1	C_P^2	**Active power^1 (kW)**	**Active power^2 (kW)**
WT1	8.4	0.4392	0.4412	871.02	874.99
WT2	7.9	0.4412	0.4412	727.85	727.85
WT3	6.6	0.4271	0.4412	410.86	424.42
TOTAL	-	-	-	2009.70	2027.26

The results indicate an excellence performance (power efficiency of 99.13%) of the proposed concept by installing smaller power converters inside each DFIG wind turbine. However, it is important remarking that this simulation is based on a wind speed step change, so that a more realistic situation

considering real time series data is required in order to properly assess both performances in terms of energy capture.

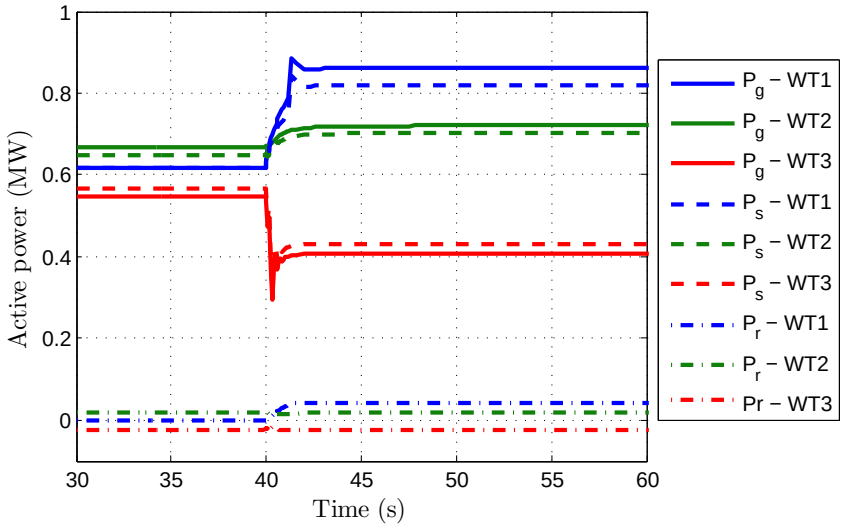

(a)

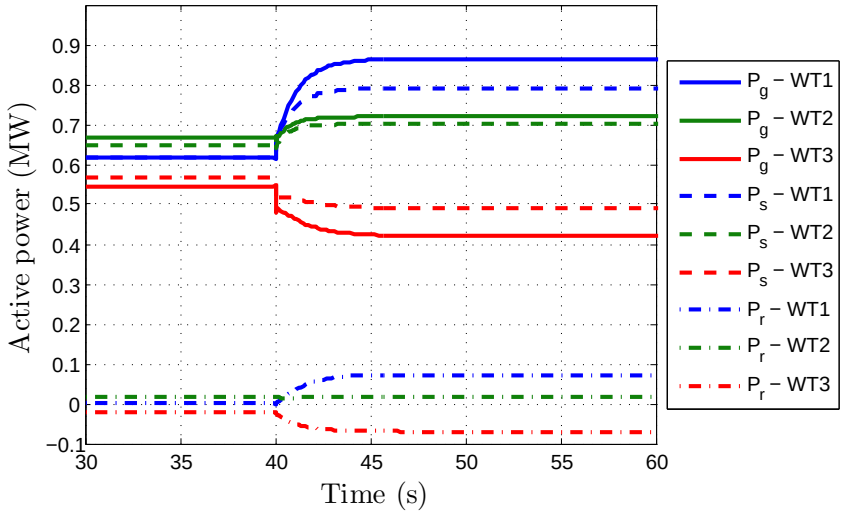

(b)

Figure 6.27: Generator, stator and rotor active power (P_g, P_s and P_r) when the individual power converters of each DFIG–based wind turbine are at 5% (a) or 16.67% (b) of rated slip.

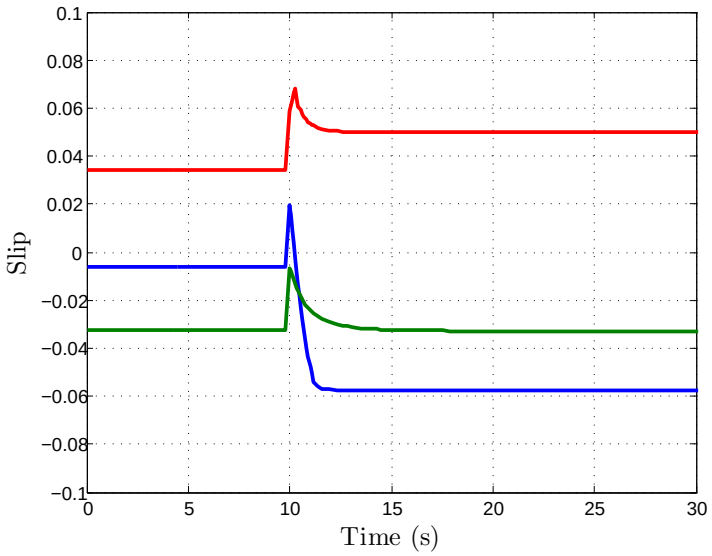

(a)

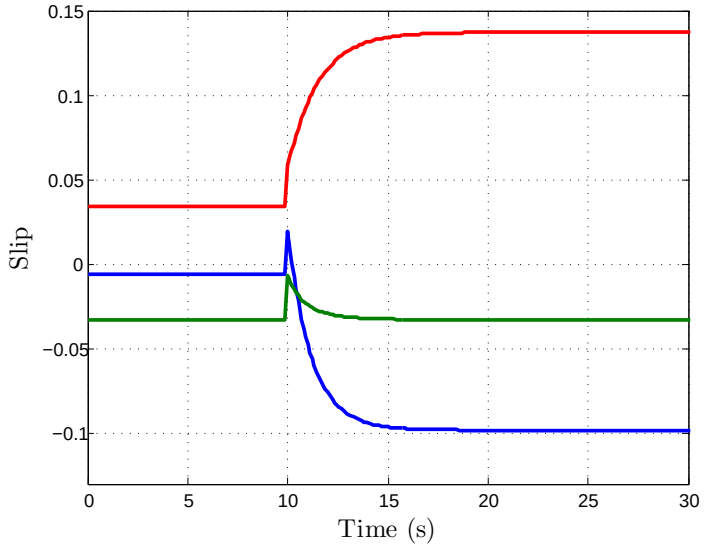

(b)

Figure 6.28: Slip of each wind turbine when the individual power converters of each DFIG–based wind turbine are at 5% (a) or 16.67% (b) of rated slip.

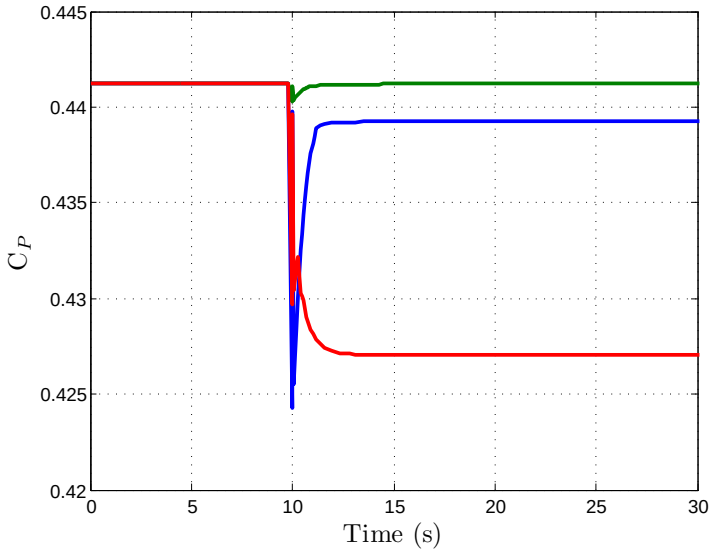

(a)

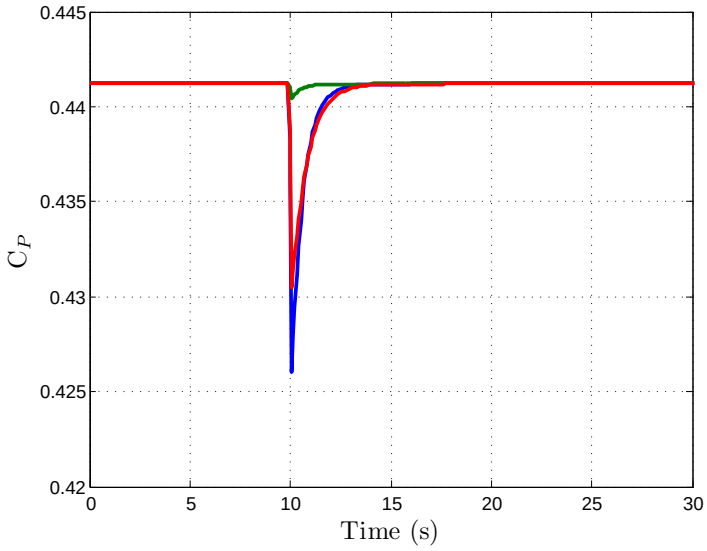

(b)

Figure 6.29: C_P power coefficient of each wind turbine when the individual power converters of each DFIG–based wind turbine are at 5% (a) or 16.67% (b) of rated slip.

Simulation 2: Performance of the system with measured wind data

The second simulation case has as goal to illustrate the overall system performance with measured wind speeds, as well as, to carry out a comparative energy capture analysis between the two WPP configurations analysed. Since it is not straightforward to graphically observe any difference between the two cases considered, the simulation results presented below are only referring to the case of a DFIG–based OWPP with reduced converters at 5% of rated slip. Nevertheless, both cases are simulated in order to draw conclusions about their energy capture effectiveness.

In this simulation, the three wind turbines are driven by different turbulent winds, with a time–variant mean speed value obtained from [152] and 5% turbulence intensity. The wind speed profile of each wind turbine is shown in Figure 6.30.

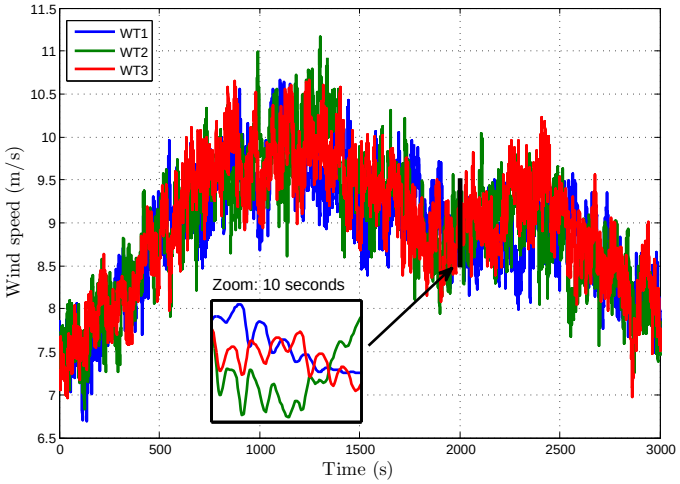

Figure 6.30: Wind speed data used for the study considering a time–variant mean value collected from [152] and a turbulence intensity of 5%.

Figure 6.31 illustrates both the reference frequency that outputs from the central WPP controller and the actual frequency which is set by the VSC–HVDC converter. To smooth the effect of operating the collection grid at a variable frequency, this reference signal is filtered.

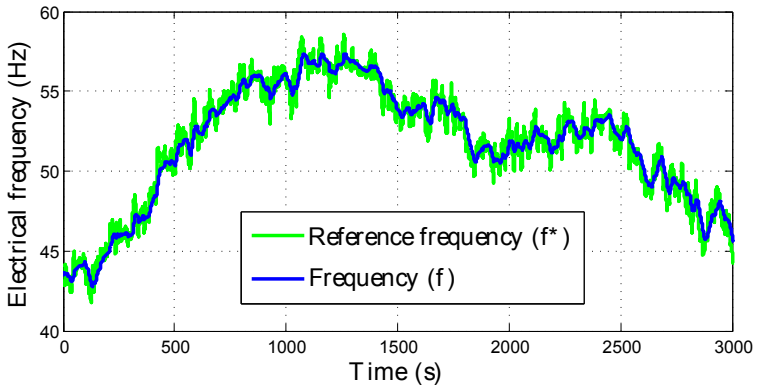

Figure 6.31: Electrical frequency set by the VSC–HVDC converter.

Similarly to simulation 1, active power of the generator, stator and rotor, WT speeds, slip of each machine, voltage rotor and C_P coefficient resulted from the simulation are displayed from Figure 6.32 to 6.37. Additionally, the control pitch action is included, since the wind speed data exceed at some points their rated value of 10.1 m/s.

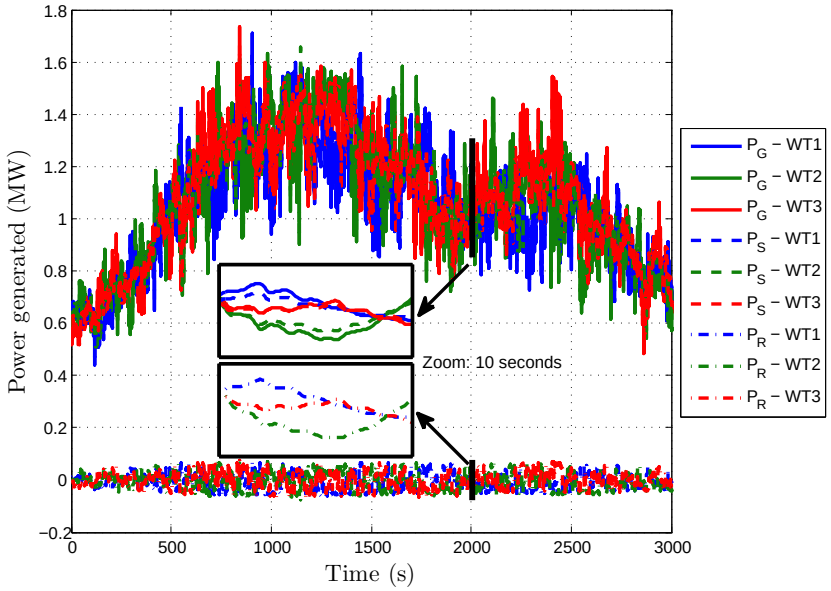

Figure 6.32: Active power of the generator (P_g), stator (P_s) and rotor (P_r) of each wind turbine.

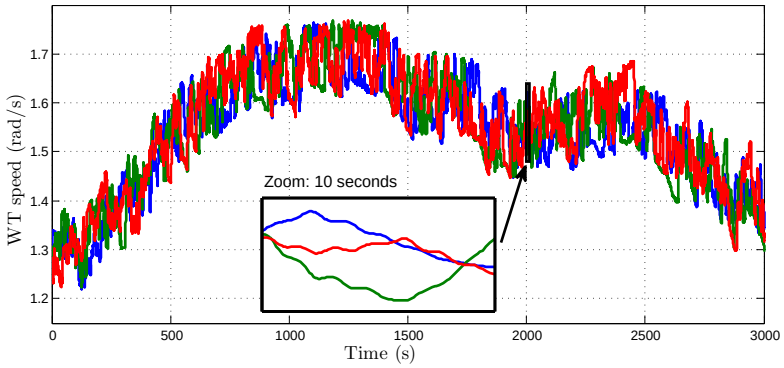

Figure 6.33: Wind turbine speed (low shaft).

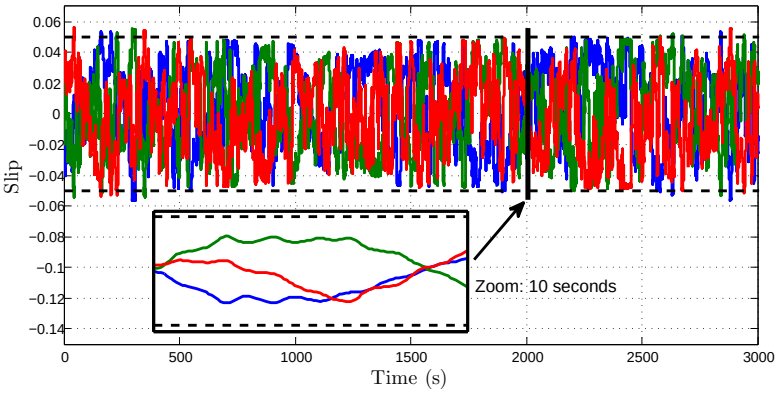

Figure 6.34: Slip of each wind turbine.

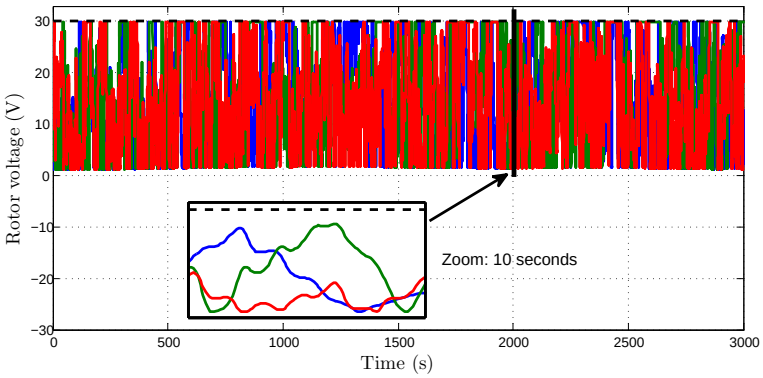

Figure 6.35: Rotor voltage of each wind turbine.

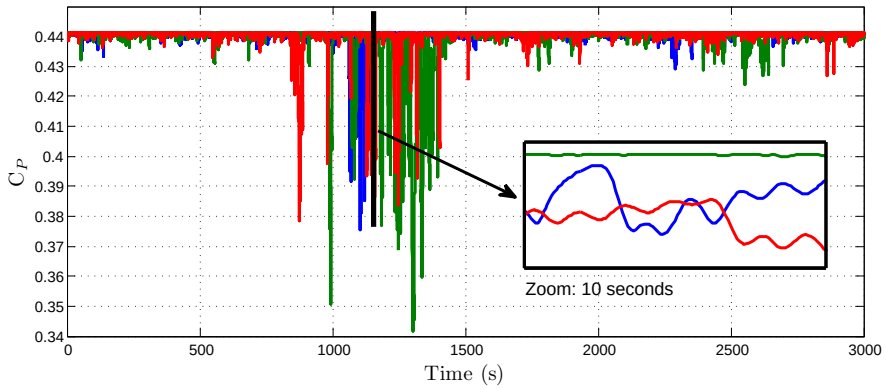

Figure 6.36: Power coefficient C_P of each wind turbine.

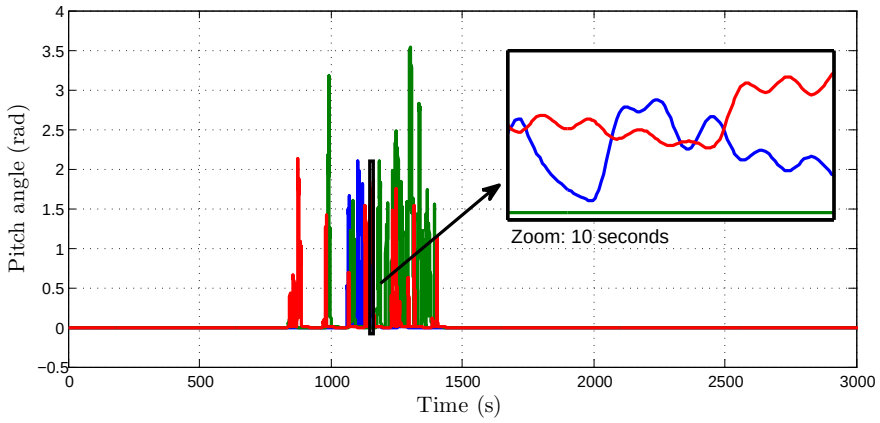

Figure 6.37: Pitch control action of each wind turbine.

The simulation results show a good performance of the control system operating in normal wind conditions. However, these figures do not reveal how much energy is curtailed by reducing the power converter at 5% of rated slip. Figure 6.38 presents both the available and actual power generated by the WT3. As it can be seen, actual power can achieve its total available power for certain wind speed conditions, whereas in other cases, it is slightly lower.

To quantify the performance of both OWPP configurations considering two different power converter sizes (5% and 16.67%), the total energy generated by the three wind turbines throughout the simulation is computed. The results are shown in Table 6.2.

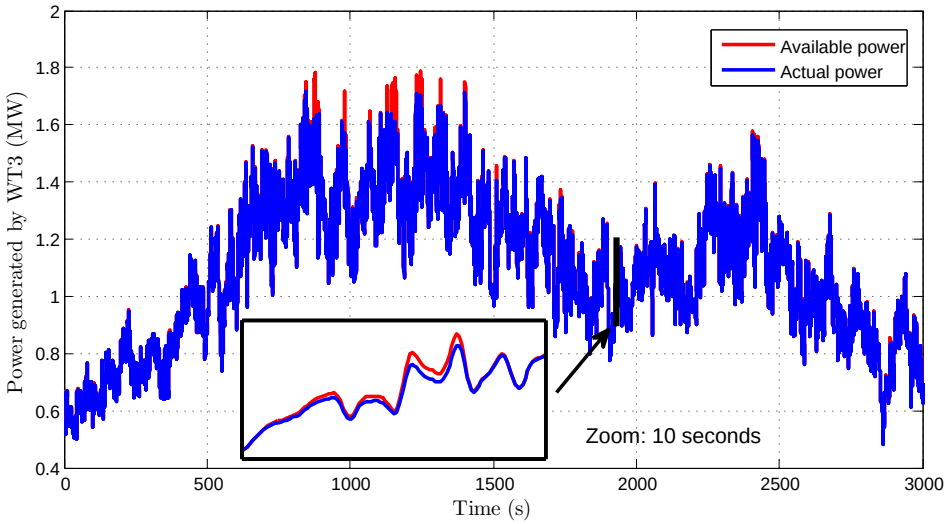

Figure 6.38: Available (a) and actual (b) active power generated by WT3.

Table 6.2: Comparative analysis between the performance of both power converter rated slips.

Rated slip (%)	**Energy (MWh)**			**Total energy (MWh)**
	WT1	**WT2**	**WT3**	
5	0.9698	0.9870	1.0015	2.9583
16.67	0.9722	0.9967	1.0087	2.9776

According to this results, the energy capture efficiency of the proposed OWPP concept based on reducing the power converters of each DFIG to a 5% of rated slip is very significant, accounting for 99.35% of the power generated by a greater power converter of 16.67% rated slip.

6.6 Conclusions of the chapter

This chapter proposes an offshore wind power plant configuration arisen thanks to the use of HVDC technology and its ability to allow variable frequency operation within the collection grid. This novel WPP configuration consists of a DFIG–based OWPP with reduced size power electronic converters connected to a single large VSC–HVDC converter which operates at variable frequency within the AC collection grid. Thus, the common VSC–HVDC converter provides variable speed control to the entire wind power

plant whilst the reduced size power converters installed inside each DFIG wind turbine aims to attenuate the mechanical loads and and to compensate (partially or totally) the wind speed difference among turbines due to the wake effect.

The impact of different power converter sizes and wind speed variability within the wind power plant on power generation efficiency is assessed. A coordinated control between the VSC–HVDC converter and the individual back–to–back power converters of each DFIG–based wind turbine is implemented and validated by means of simulations using MATLAB/Simulink®. Furthermore, a comparative energy capture analysis is carried out, from the static and dynamic point of view, between two different operating slip ranges of ±5% or ±16.67%.

The results show a good performance of the system in terms of energy capture efficiency. For example, a power converter with a rated slip of 5% achieves an energy capture efficiency higher than 99.27% for wind speed standard deviations equal or lower than 3 m/s. Therefore, it can be concluded that the proposed concept, based on DFIG wind turbines and variable frequency operation within the collection grid, could potentially reduce the power converter size, which would imply cost savings. However, since the size of the power converter is not only determined by the maximum slip range allowed, but also by grid integration requirements (e.g., fault ride through capability), this statement must be further analysed in more detail.

7

Analysis of DC collection grid for offshore wind power plants

7.1 Introduction

Thus far, this thesis has dealt with the analysis of offshore wind power plants with an AC collection grid and an HVDC transmission link to shore. In this chapter, the feasibility of an entire DC OWPP, considering both an HVDC transmission and a DC collection grid, is assessed from the technical and economic point of view.

As stated in Chapter 1, several studies agree that there is a break–even point in the range of 55–70 km where HVDC transmission becomes a preferred option in comparison to HVAC, due to its many advantages such as lower cable losses, enhanced power system stability and no reactive power compensation requirements [16, 89]. Adding these advantages to the recent development of DC technologies for HVDC transmission links enables the possibility to consider an OWPP concept in which both transmission and collection grid are in DC.

Although there are no existing wind power plants with DC collection grid installed or planned, the concept of DC OWPP is being analysed from technical and economic perspectives taking into consideration both shunt [55, 153–155] and series [58, 153] configurations. Due to the fact that DC technologies for collection networks are not standard and still under development, there are some uncertainties to consider and challenges to overcome. Therefore, the development of several critical DC components, such

as DC circuit breakers (DC–CB) [156–159] or DC/DC converters [160, 161] is crucial.

This chapter is divided into two parts: First, an overview of the main topologies of DC collection grids for offshore wind power plants reported in the literature is presented. Then, the second part of the chapter deals with the technical and economic assessment of four proposed DC offshore collection grids, aiming to determine their cost–effectiveness when compared to conventional AC OWPPs. Because of the uncertainty of DC technology, a sensitivity analysis is carried out taking into consideration various parameters which may affect technical and economic feasibility of DC OWPPs, for example, DC equipment efficiencies, DC component cost, OWPP rated power, export cable length, etc. The proposed analysis methodology is implemented in DIgSILENT Power Factory®, using the DIgSILENT Programming Language (DPL).

7.2 DC collection grid topologies overview

As it occurs in the conventional AC collection grid with the radial, ring and star connection design, DC offshore collection grids can be mainly classified into three different designs concerning how the wind turbines are connected among them: shunt, series or hybrid.

7.2.1 Shunt topology

In the shunt topology, the output voltage of each wind turbine is maintained constant, while the current flowing through the inter–array cables depends on the number of turbines connected on it. Thus, the power delivered by each feeder can be expressed as

$$P_{feeder} = V \sum_{j=1}^{N} I_{wt-j} \tag{7.1}$$

where N is the number of wind turbines connected to one feeder. It is worth remarking that this topology is the most similar to the conventional AC case; therefore, it is the logical first step for DC OWPPs.

There are many possible OWPP alternatives based on shunt topology. Following, the four most common proposals are briefly described.

DC OWPP configuration 1 (DC1)

In Figure 7.1, the scheme of DC1 configuration is presented. In this case, each wind turbine feeder is directly connected with the main HVDC substation, where a DC/DC converter is included to step–up the voltage and to deliver the power to the onshore network via an HVDC transmission link.

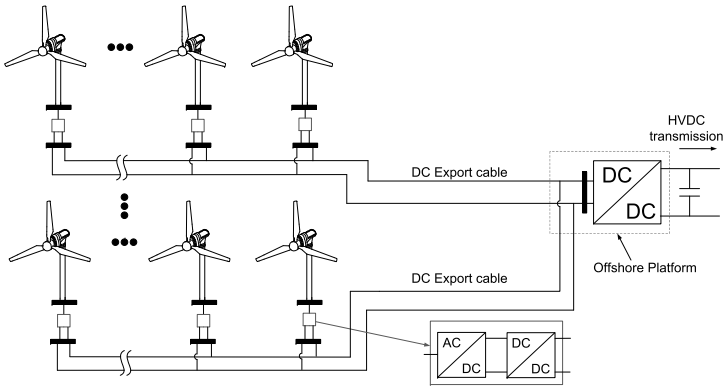

Figure 7.1: Scheme of the DC OWPP configuration 1 proposal (DC1).

The main benefit of this configuration is the avoidance of using an intermediate collector platform which implies savings in capital costs. Nonetheless, the considerable distance between the OWPP feeders and the main platform leads to the requirement of both larger number and an increased cross–section of inter–array cables in order to avoid large power losses.

DC OWPP configuration 2 (DC2)

This configuration design, shown in Figure 7.2, considers an offshore grid in which all wind turbine strings are connected to a common offshore collection point. The present scheme differs from DC1 in the connection to the main offshore platform, since such collector grid includes an intermediate offshore platform gathering the inter–array cables from the feeders. Export cables with higher cross–section are used to interconnect the intermediate platform with the main offshore substation, where, as in the previous case, a DC/DC converter is installed.

As in DC1 configuration, one of the main advantages of this scheme design is that it is not required to allocate any DC/DC converter into the offshore collector platform. This fact saves both investment costs and energy losses costs related to power converter. Moreover, it enables the installation of a

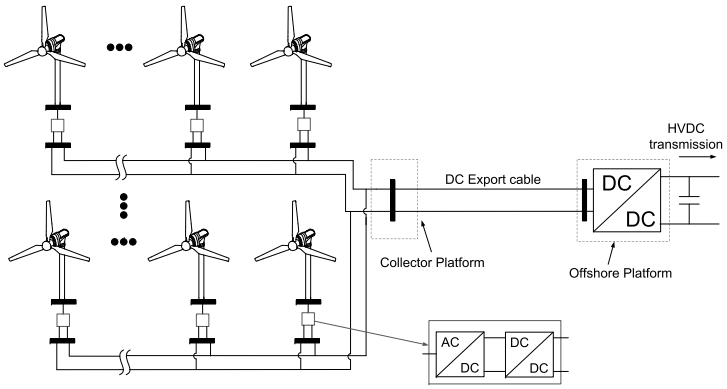

Figure 7.2: Scheme of the DC OWPP configuration 2 proposal (DC2).

smaller intermediate offshore platform in comparison with a conventional AC offshore platform with step–up transformer. On the other hand, one of the most relevant disadvantages may be the large amount of power dissipated in the export cable depending on the OWPP voltage level.

DC OWPP configuration 3 (DC3)

The scheme diagram of DC OWPP configuration 3 proposal is presented in Figure 7.3. Within this configuration, there are two step–up DC/DC converters. The first one located at the end of the wind turbine array is used to increase the voltage to export the power to the main offshore HVDC platform. The other DC/DC converter is required to step–up the voltage and to deliver the power to the shore.

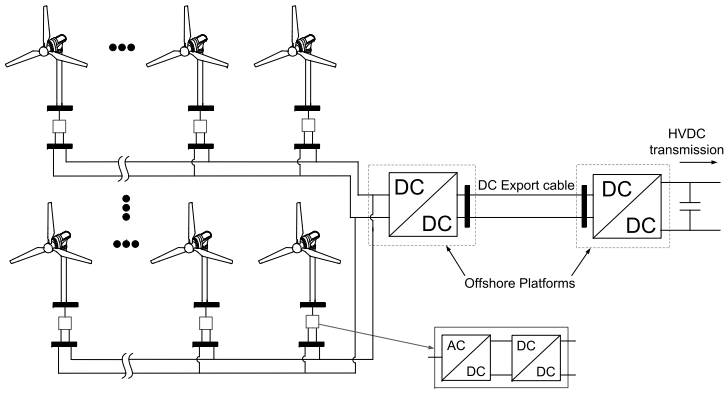

Figure 7.3: Scheme of the DC OWPP configuration 3 proposal (DC3).

This scheme has the advantage of reducing the losses in the export cable due to the voltage increase, which is specially worthwhile if the distance between the collector and the main HVDC offshore platform is significant. However, this topology entails some drawbacks as reliability issues because of lack of redundancy; since if the DC/DC converter fails, the generated power of the whole wind power plant cannot be delivered.

DC OWPP configuration 4 (DC4)

Finally, a schematic representation of DC OWPP configuration 4 is shown in Figure 7.4. As it can be seen, this proposal includes one single step–up DC/DC per wind turbine feeder. This power converter increases the voltage of the system to deliver the power to the main offshore HVDC platform where another step–up DC/DC converter is installed to transmit the generated power to the shore.

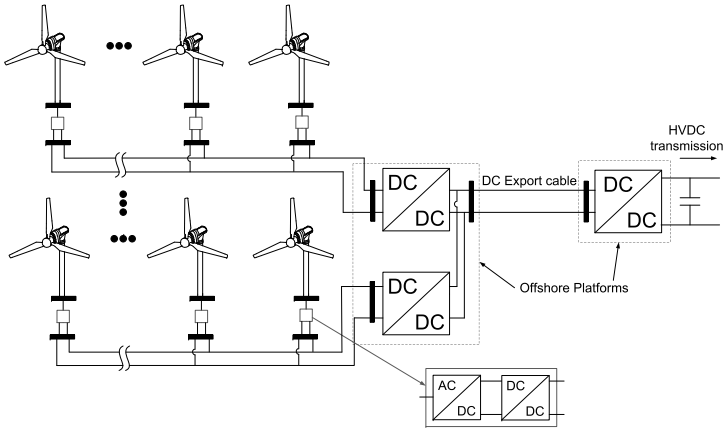

Figure 7.4: Scheme of the DC OWPP configuration 4 proposal (DC4).

Compared to the previous configuration (DC3), the reliability of the system is increased because of the step–up converter redundancy. On the other hand, a disadvantage of this configuration in comparison with the previous one is the lager capital expenditures associated with the higher required number of DC/DC power converters. Moreover, the collector platforms that allocate all the DC/DC converters may be increased in size and cost.

7.2.2 Series / hybrid topologies

For the series topology case, the current of each wind turbine is kept constant and the output voltage increases as the turbines are connected in series [58, 153]. Therefore, the power delivered by the wind power plant (or the single feeder) can be expressed as

$$P_{feeder} = I \sum_{j=1}^{N} V_{wt-j} \tag{7.2}$$

Likewise, the hybrid topology is defined as a mix of both previous topologies. It is designed as a short number of wind turbines electrically connected in series with shunt connected feeders.

Figure 7.5 represents a possible design of both series and hybrid topologies. As it can be noted, in case that only one feeder is considered, the hybrid design represents the series topology case; since all wind turbines are connected in series.

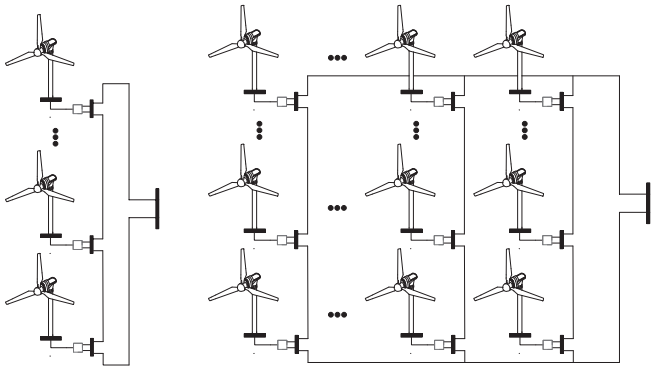

(a) (b)

Figure 7.5: Example of a series (a) and hybrid (b) collection configuration for DC offshore technology

Both series and hybrid topologies present some technical challenges. For example, voltage rating within the collection grid is bounded through voltage limits of the cables, a higher insulation requirement on the wind turbines because of the total voltage to withstand, and the fact that some electrical components of the wind power plant must be oversized to prevent overvoltages in the wind turbines [162]. Moreover, to handle the circumstance that

some turbines are out of operation, the series connected wind turbines should have a bypass designed to short circuit the output of the wind turbines if an internal fault is detected. All these technical issues pose extra uncertainty making it difficult to foresee their short–term feasibility.

7.3 Analysis methodology

Figure 7.6 shows an overview of the methodology used to analyse the possible technical and economic benefits of each DC OWPP configuration considered compared to the AC base case.

As it can be seen, it is divided into four main blocks: first, an initialization process is executed to customize the electrical OWPP collection grid according to the voltage ratings of the elements contained in the input databases (cables and transformers) and the voltage inter–array specification of each study case (set by the user). Next, a cable selection process (similar to that previously explained in Chapter 2) is performed to determine the type of inter–array and export DC cables and the number of parallel lines required. The cables are chosen based on minimizing the cross section available while not overcoming the maximum admissible loading and ensuring a proper and continuous operation under full load. Then, a technical analysis based on load flow simulations is carried out to calculate the energy losses produced within the OWPP. Finally, a cost analysis outputs the capital costs of each component encompassed in the offshore wind power plant, as well as the costs associated to the energy lost over the lifetime of the project.

These two last two processes (technical and economic assessment) are explained in detail below.

7.3.1 Technical analysis

Once the wind power plant is fully configured, the technical analysis can be performed. Thus, the steady state energy losses of each OWPP configuration over a period of time T are computed as

$$E_{losses} = T \sum_{n=1}^{N_s} (P_g(n) - P_{PCC}(n)) \cdot p_{wb}(n) \tag{7.3}$$

where $P_g(n)$ is the power delivered by the OWPP, $P_{PCC}(n)$ is the net active power transferred to the grid at the Point of Common Coupling (PCC), N_s is the maximum number of generation states, which is equivalent to the set

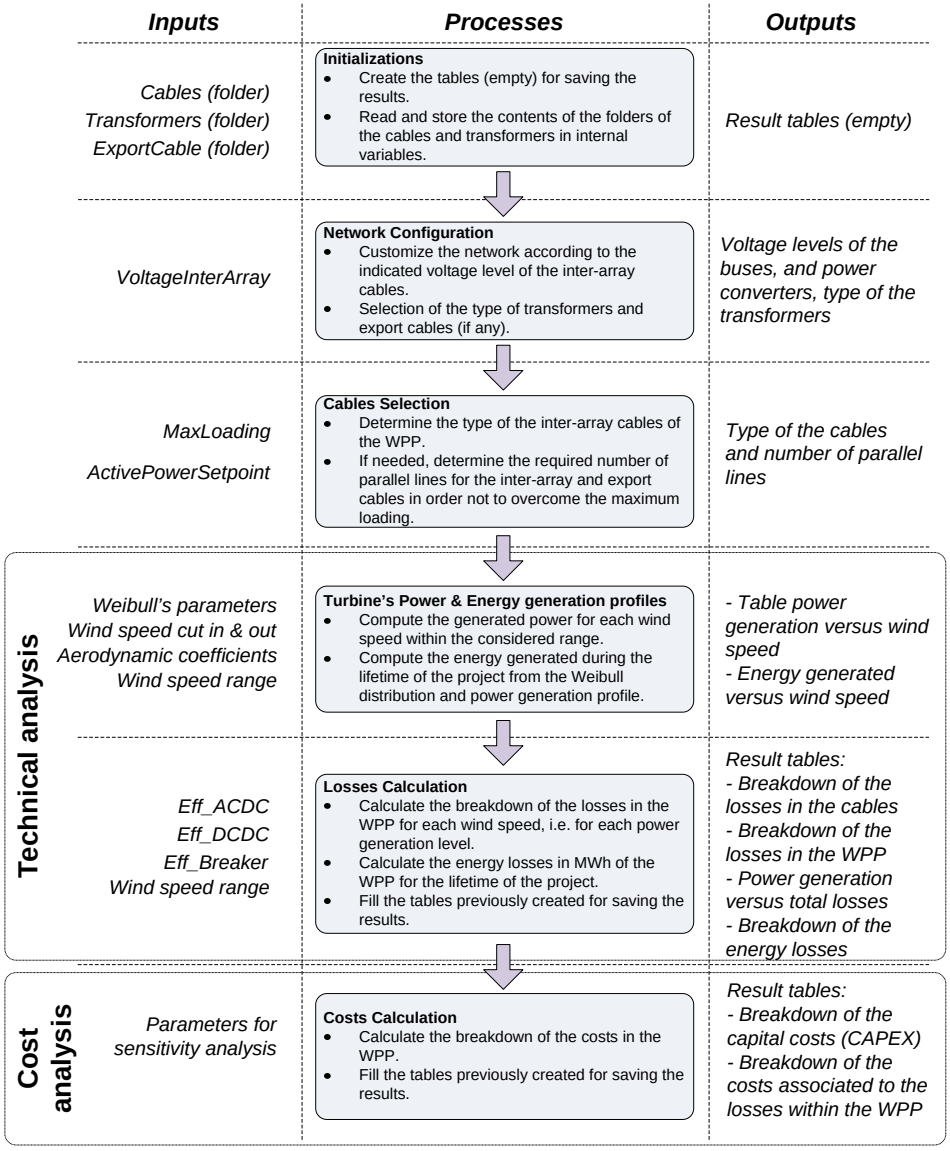

Figure 7.6: General scheme of the methodology used for the technical and economic assessment.

of wind speeds considered, and $p_{wb}(n)$ is probability of occurrence of each state according to the Weibull distribution function used.

The power generated by the OWPP for each state, $P_g(n)$, is computed

by considering the power curves of the wind turbines, while the amount of power received at the PCC, $P_{PCC}(n)$, is calculated by means of multiple load flows (one per each generation state) and depends on the efficiency of the components encompassed within the OWPP collection grid.

Due to the uncertainty existing over DC technology for OWPPs, some parameters such as the efficiency of DC/DC converters or DC protections, are not well defined. Thus, the energy losses previously mentioned in (7.3) are resulted considering only the cable losses. Thereby, the total steady state energy losses (including the power losses produced by the DC/DC converters and DC breakers) are evaluated by means of a sensitivity analysis. Hence, the breakdown of the losses distinguishing between losses in the inter–array cables, export cables, wind turbine power converters, platform converters and protections of both inter-array and export cables, can be finally obtained.

7.3.2 Cost analysis

The cost analysis is based on comparing the total cost of an AC OWPP (base case) to the total cost of each DC OWPP configuration considered in order to assess their cost–effectiveness. To this end, the methodology depicted in Figure 7.7 is applied.

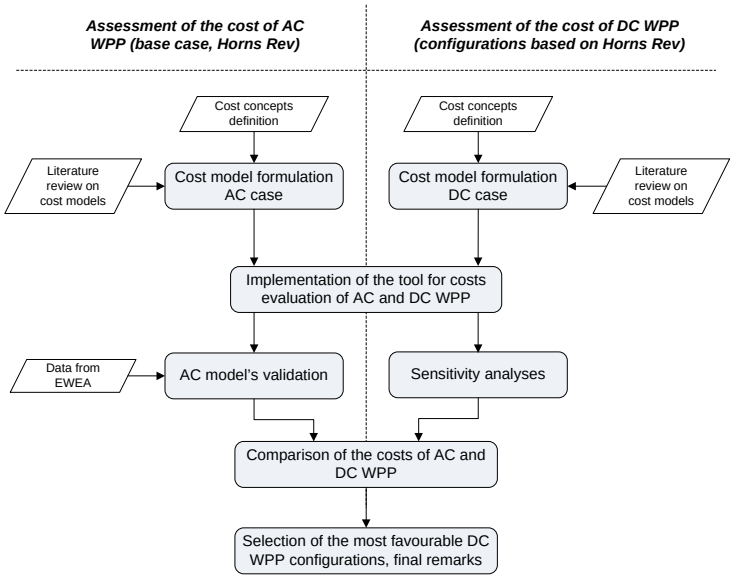

Figure 7.7: Methodology used for the economic analysis.

As it is shown, the results obtained with the AC OWPP cost model are compared to the wide–accepted cost estimations reported by EWEA in order to validate them [90]. Likewise, a sensitivity analysis is performed for the DC OWPP cases to overcome their uncertainty. A comprehensive model considering both the capital expenditures (CAPEX) and the costs associated to the energy losses during the lifetime of the installation is developed to calculate the total cost of each OWPP configuration analysed. Some of the cost functions described below have been previously presented in the previous chapters. However, those are displayed again for the sake of clarity.

Offshore wind power plant investment costs

According to the scope of the study, the investment cost models for both an AC and a DC OWPP are formulated as

$$\begin{aligned} C_{AC\_WPP} &= \sum_{N_{wt}} C_{ACwt} + \sum_{N_{ACcab}} (C_{ACcab} + C_{ca\&inst}) \\ &+ \sum_{N_{ACsg}} C_{ACsg} + \sum_{N_{tr}} C_{tr} + C_{c\_ACDC\_cg} \\ &+ \sum_{N_{Plat}} C_{platAC} \end{aligned} \tag{7.4}$$

$$\begin{aligned} C_{DC\_WPP} &= \sum_{N_{wt}} C_{DCwt} + \sum_{N_{DCcab}} (C_{DCcab} + C_{ca\&inst}) \\ &+ \sum_{N_{DCsg}} C_{DCsg} + \sum_{N_{WT\_DCDC}} C_{WT\_DCDC} \\ &+ \sum_{N_{Plat\_DCDC}} C_{Plat\_DCDC} + \sum_{N_{Plat}} C_{platDC} \end{aligned} \tag{7.5}$$

where N_{wt} is the number of wind turbines within the WPP, N_{ACcab} and N_{DCcab} are the number of MV AC and DC submarine cables, N_{ACsg} and N_{DCsg} are the number of AC and DC switchgears, N_{tr} is the number of MV/HV transformers for the AC WPP, N_{WT_DCDC} and N_{Plat_DCDC} are the number of DC/DC converters in the WT and platforms, respectively, and N_{Plat} represents the number of platforms installed. The calculation of the capital cost of each component is detailed in the following. It is worth noting that all the costs are expressed in k€.

Fully–equipped wind turbines: The cost of a fully–equipped wind turbine for the AC case [122], including the turbine, the back–to–back converter and the LV/MV transformer, can be computed by

$$C_{ACwt} = 1.1 \cdot \underbrace{(2.95 \cdot 10^3 \cdot \ln(P_{wt}) - 375.2)}_{C_{wt}} \tag{7.6}$$

where P_{wt} is the rated power (in MW) of the wind turbine and the coefficient 1.1 includes the costs of transport and installation.

In the DC case, the cost of wind turbines is assumed to be similar to the AC case. The difference relies on the not needing to include a back–to–back power converter nor transformer but only a single AC/DC power converter. Thus, the cost of the power converter and transformer is assumed as a certain percentage of the total cost of the wind turbine and can be expressed as [90]

$$C_{DCwt} = \cdot K_{wt} \cdot C_{ACwt} \tag{7.7}$$

where K_{wt} refers to the sensitivity parameter of the percentage explained above, affecting the capital cost of the DC wind turbine.

AC and DC cables: The cost of MVAC submarine cables within the offshore MV collection grid are calculated through the following cost function [122]

$$C_{ACcab} = \alpha + \beta \exp\left(\frac{\gamma I_n}{10^5}\right) \cdot L \tag{7.8}$$

where I_n is the cable ampacity (in A), L is the cable length (in km) and the coefficients α, β and γ depend on the nominal voltage level. For example, for cables of 30–36 kV they are defined as 52.08 k€/km, 75.51 k€/km and 234.34 1/A, respectively.

DC cable costs can be computed by [123]

$$C_{DCcab} = K_{cab}(A_p + B_p 2 V_{rated} I_{rated})L \tag{7.9}$$

where V_{rated} and I_{rated} are the cable ratings (in A and V respectively), the constants A_p and B_p depend on voltage rating and K_{cab} refers to a sensibility parameter on cable cost.

Finally, the cable transport and installation costs are assumed to be equal in both cases

$$C_{ca\&inst} = K_{cinst} 365 L \tag{7.10}$$

with the only difference that the variable K_{cinst} is a sensitivity parameter for the DC case, but always constant in AC. It is worth noting that this equation provides an average value, and does not reflect particularities of each case study such as seabed composition, water depth, among others.

MV/HV transformers: Referring to [122], the cost of a MV/HV transformer can be expressed as

$$C_{tr} = 42.688 A_t^{0.7513} \tag{7.11}$$

where A_t is the transformer rated power (in MVA).

AC/DC power converter: A single AC/DC power converter cost function which is installed before the HVDC link receiving the total power of the collection grid, has been determined in [123] through comparison of real installation cases. This leads to the following equation

$$C_{c\_ACDC\_cg} = 200P_r \tag{7.12}$$

where P_r is the rated power of converter (in MW).

DC/DC power converters: According to [123], the DC/DC converter cost can be based on Table 7.1 which is suggested by the industry.

Table 7.1: Cost of the DC/DC converters [123].

DC/DC converter type	C_{c_DCDC}
2 MW dc/dc converter to be used with series dc layout	0.33 M€/MW
High power (150 MW and above) to be used in the large DC layout	0.22 M€/MW
2 MW dc/dc converter to be used with small and large DC layout	0.165 M€/MW

To consider a wide–spread power ratings, linear interpolation between points is done (C_{c_DCDC}). Since there are different possible DC/DC converters within the collection grid (wind turbine and offshore platforms), they must be treated separately for the cost analysis. Thus,

$$\begin{aligned} C_{WT\_DCDC} &= K_{WTcon}C_{c\_DCDC} \\ C_{Plat\_DCDC} &= K_{Platcon}C_{c\_DCDC} \end{aligned} \tag{7.13}$$

where C_{c_DCDC} is the cost of the DC/DC converter, K_{WTcon} and $K_{Platcon}$ represent the cost variability of the converters themselves.

AC and DC switchgears: The cost model of the AC switchgears can be found in [122] as

$$C_{ACsg} = 40.543 + 0.76V_n \tag{7.14}$$

where V_n is the nominal voltage in kV. For DC case, according to [123], the cost of the DC breakers is twice the AC switchgears cost, so that

$$C_{DCsg} = K_{CB}(2C_{ACsg}) \tag{7.15}$$

where K_{CB} represents a possible uncertainty on the cost hypothesis.

Offshore platform for AC and DC based OWPPs: The cost of an offshore substation platform for AC OWPPs is computed as [122]

$$C_{pl\_AC} = 2534 + 88.7 N_{wt} P_{wt} \tag{7.16}$$

where N_{wt} is the number of wind turbines within the OWPP and P_{wt} is the wind turbine rated power.

With regard to the DC OWPPs study, there exist various types of offshore platform that could be considered such as feeder, collector and main platform. Thus, the DC offshore platform cost based on the AC case can be expressed as

$$\begin{aligned} C_{pl\_DC} &= K_{Col}\left(2534 + 88.7 N_{wt} P_{wt}\right) \\ &+ K_{Feed}\left(\left(2534 + 88.7 N_{wt} P_{wt}\right) 1.1\right) \\ &+ K_{Plat}\left(2534 + 88.7 N_{wt} P_{wt}\right) \end{aligned} \tag{7.17}$$

where K_{Col}, K_{Feed} and K_{Plat} represent the cost variability depending on the type of platform required. It is worth noting that a cost correction factor is included for the feeder platform cost; since, bigger space is needed when larger number of DC/DC converters are installed, in spite of the amount of power remains the same.

Since the references considered are from diverse years, the cost results is updated to 2013 prices through the Consumer Price Index (CPI) of Spain ($\approx 2\%$).

Cost associated with the energy losses

Energy losses costs associated with those produced within the WPP considering both cases, can be computed as

$$C_{losses} = \sum_{t=1}^{T} (K_e t + C_e) E_{losses} \tag{7.18}$$

where K_e represents the slope of the equation $P_e(n) = K_e t + C_e$, being P_e the energy price for the year t and C_e a fix cost (89.5 €/$(MWh \cdot year)$). T is the lifetime of the OWPP and E_{losses} are the energy lost during this period calculated in (7.3).

7.3.3 Sensitivity analysis

Due to the fact that the novel concept of OWPPs based on DC collection grid are not a reality yet, some uncertainties rise up regarding both electrical

efficiency and their manufacturing cost. With the aim to overcome such problem, a sensitivity analysis is carried out. This is done by modifying several parameters providing a wide range of possible admissible solutions. As it can be seen in Tables 7.2 and 7.3, three different scenarios (S1, S2 and S3) of sensitivity parameters are considered within the study. Such scenarios are mainly related with the expected status of this technologies as positive, average (base case) and negative. S2 parameters values refer to the base case, and correspond to those values presented in literature [122,123,163,164] and industry suggestions.

Table 7.2: Non-cost parameter values used for sensitivity analyses.

Type of analysis	**Sensitivity parameter**	**S1**	**S2**	**S3**
Effect of the rated power of wind turbines (MW)	P_{rated}	2.5	5	7.5
Effect of the export cable distance (km)	D_{export}	10	40	70
Effect of the losses of the DC breakers (%)	P_{loss_b}	0.001	0.05	0.25
Effect of the losses of the DC/DC power converters (%)	P_{loss_DCDC}	1	2	3
Effect of different forecasted energy prices[1] (€/MWh)	K_e	-1.1789	2.1105	5.3
Effect of different maximum admissible cable loading (%)	$MaxLoading$	72	80	88

Table 7.3: Capital cost parameter values used for sensitivity analyses.

Type of analysis	**Sensitivity parameter**	**S1**	**S2**	**S3**
Effect of the cost of DC/DC converters	K_{WTcon} $K_{Platcon}$	0.75	1	1.25
Effect of the cost of the DC breakers	K_{CB}	1	2	3
Effect of the cost of those platforms allocating power converters	K_{Plat} K_{Feed}	0.75	1	1.25
Effect of cost of collector platforms without installing converters	K_{Coll}	0.5	0.75	1
Effect of cable cost	K_{cab}	0.5	1	1.5
Effect of cable transport and installation cost	K_{cinst}	0.5	1	1.5
Effect of the B2B and transformer cost over total WT cost	K_{wt}	0.9	0.925	0.95

[1]These data are obtained from Short–Term Energy Outlook reported by Energy International Agency (EIA) [165].

Aiming to examine the influence of a single parameter on the overall cost of a particular OWPP configuration, several analyses are performed by modifying only one sensitivity parameter while keeping the other in their base value. Alike, in order to determine the maximum cost range admissible for each OWPP scheme, a more general study considering all the sensitivity parameters varying together is also carried out.

7.4 Case study

In this section, the proposed methodology previously described is applied to a particular case study in order to determine which technology (MVAC or MVDC) is most appropriate within the offshore collection system.

The layout of the AC OWPP with which the DC OWPPs configurations considered are compared, is presented in Figure 7.8. It is based on the Horns Rev wind farm composed of 80 wind turbines laid out in a regular matrix form of 10 rows and 8 columns. The spacing among wind turbines is 7 rotor diameters (D) in both directions. A radial design is adopted since it is the most common configuration installed thus far.

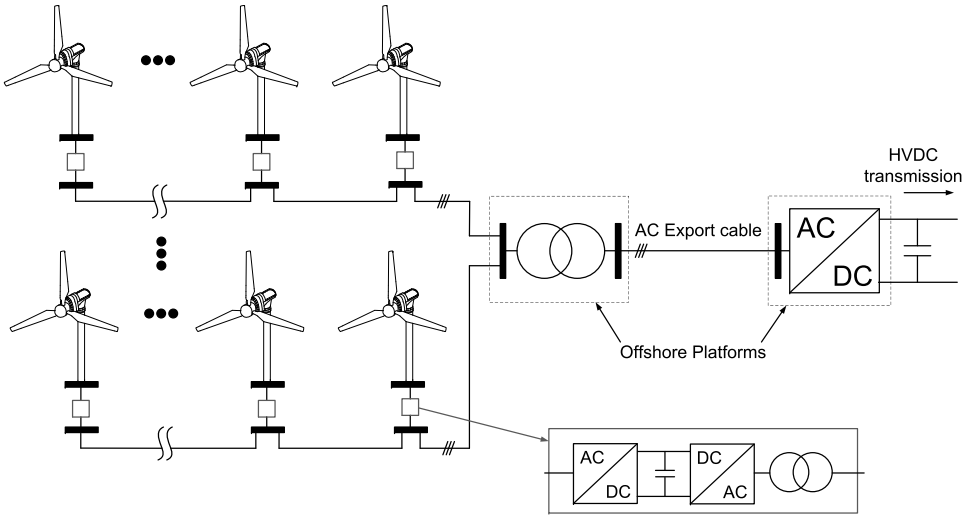

Figure 7.8: Layout of the AC offshore wind power plant considered (base case).

As it is stated previously, the shunt design is the more similar configuration to the radial design for AC cases. To ease the comparison between AC and DC technologies, these wind power plant designs are chosen. Therefore, the

four proposed DC OWPP schemes presented above in section 7.2 related to shunt topology (DC1, DC2, DC3 and DC4) are considered for the study. In order to facilitate the comparison between the AC base case the DC OWPPs design proposals considered, all the DC collector grids analysed present exactly the same characteristics in terms of number and location of wind turbines as the AC scheme. Besides, each DC OWPP topology analysed is studied as two different cases depending on its collection grid voltage rating (case A = $\pm$ 20 kV and case B = $\pm$ 50 kV). The voltage rating at the export cable is $\pm$ 80 kV for DC3 and DC4 configurations.

7.4.1 AC cost function validation

With the aim of validating the AC cost functions used for cost modeling, the values obtained has been compared to the investment cost estimations provided by EWEA for OWPPs [90]. Table 7.4 presents cost predictions for three different scenarios (minimum, average and maximum) according to offshore technology development forecast.

Table 7.4: Capital cost comparison for OWPPs (in M€/MW).

	EWEA estimations			**AC Cost function**
	MIN	**AVG**	**MAX**	
Wind turbine	0.57	0.92	1.26	1.04
Grid connection	0.28	0.50	0.76	0.69
Total CAPEX	1.78	2.08	2.37	1.90

As it can be seen, the obtained cost values lay on these expected ranges; therefore, the AC cost functions are validated. For the grid connection cost calculation, various electrical components of the OWPPs including cables, platforms, converters, switchgears and transformers, are gathered. It is worth noting that although wind turbine and grid connection costs fits in between the average and maximum cost estimations, the total CAPEX results to be among minimum and average scenarios, since not all the costs considered on CAPEX (SCADA, installation costs, among others) are included.

7.4.2 Comparative analysis

After applying the methodology introduced above and considering the sensitivity parameters in Tables 7.2 and 7.3, the results shown in Figures 7.9 and 7.10 are obtained.

Figure 7.9 presents the breakdown of both capital and energy losses costs of all the presented DC OWPP configurations considering a particular case study (wind turbines of 5 MW each and an export cable of 10 km long). The solid line represents the AC cost (base case), while the bars indicate the relative cost of DC OWPP schemes over AC case.

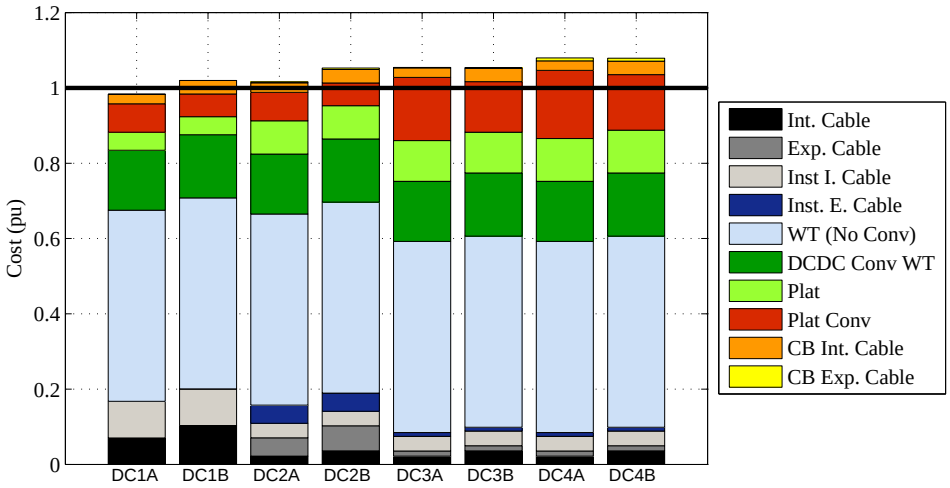

(a) Capital costs (AC base cost = 758.95 M€)

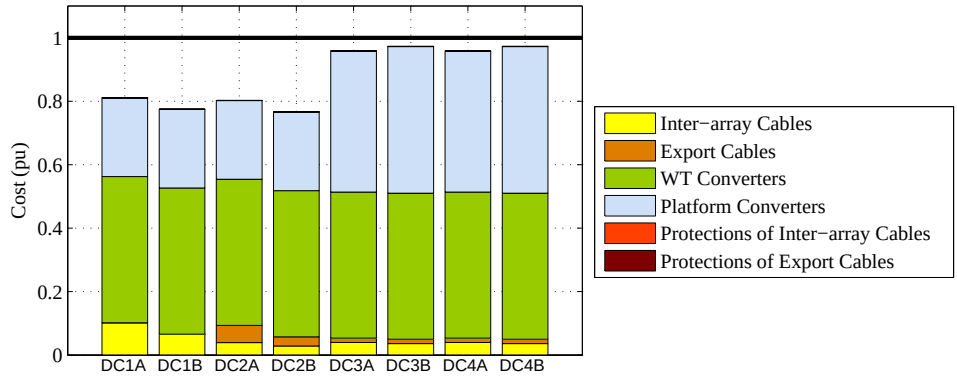

(b) Costs associated with energy losses (AC base cost = 278.37 M€)

Figure 7.9: Breakdown of all the DC OWPP configurations setting all the sensitivity parameters at their base values (S2). The solid black line indicates the cost of the AC base case.

In general terms, it can be seen from Figure 7.9(a) that capital cost for DC OWPPs configurations are slightly higher than AC case. On the other hand,

Figure 7.9(b) shows a reduction on the cost associated to the energy losses for the DC cases, as expected. Concerning investment costs, it should be noted that the most critical expenditures refer to wind turbine and DC/DC converters costs installed on wind turbines and platforms, representing 47–50% and 23–31% of the total capital cost, respectively. With regard to the energy losses costs, it is clear that the crucial components for DC OWPPs are the DC/DC converter losses (considering both wind turbine and platform converters), being about 92–94% of the total losses within the wind power plant.

Finally, Figure 7.10 presents the total relative OWPP costs for all the cases considered for evaluation over its respective AC base case. Table 7.5 shows all the AC base values obtained for different wind turbine power ratings (2.5, 5 and 7.5 MW) and export cable lengths (10, 40 and 70 km) considering base parameters for the sensitivity analysis (S2). It should be mentioned that the distances between wind turbines (7 D) has been adapted for each particular case according to the specific rotor diameter corresponding to each turbine power rating.

Table 7.5: Total cost of AC base cases depending on the wind turbine rating and the export cable length (in M€).

Export cable length	Wind turbine power rating		
	2.5 MW	5 MW	7.5 MW
10 km	538	1037	1402
40 km	685	1192	1567
70 km	840	1354	1735

In Figure 7.10, all possible combinations of sensitivity parameters are taken into consideration. The edges of the blue lines indicates the minimum and the maximum cost for DC OWPPs representing the most optimistic and pessimistic scenarios for these technologies, respectively. According to the results, it can be seen that at short export cable length (10 km), DC1 and DC2 are of interest, since no extra investment must be done for the DC/DC converters; on the other hand, for long export cables (70 km), DC3 and DC4 appear to be economical due to reduced energy losses and lower number of cables needed. Finally, it can be stated that assuming the optimistic case, DC OWPPs are usually more beneficial in terms of costs than AC, but in the pessimistic case they are always the worst option.

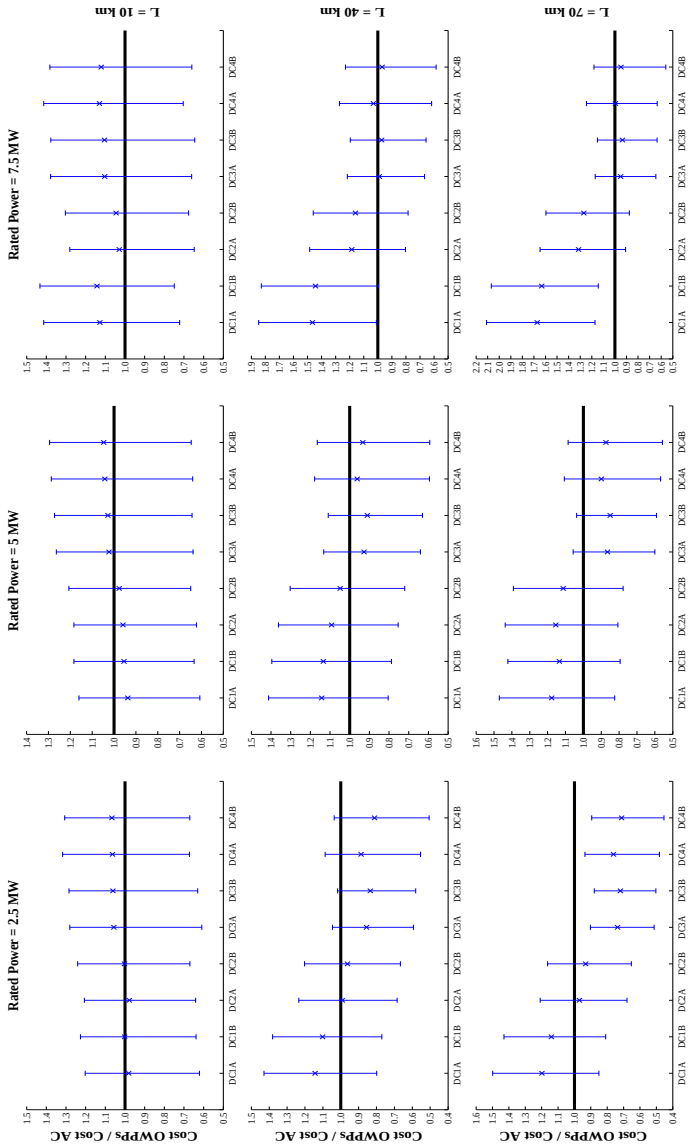

Figure 7.10: Total relative OWPP costs (CAPEX and costs associated with energy losses) for all the cases analysed. The black lines show the AC base case considering a certain export cable length (10, 40 or 70 km) and a particular wind turbine rated power (2.5, 5 or 7.5 MW). The blue line represents the cost sensitivity of DC OWPPs. The $\times$ symbol indicates the DC base values.

7.5 Conclusions of the chapter

In this chapter, an overview of the main topologies for offshore wind power plants with DC collection grids studied in the literature is presented. From those schemes, the four OWPP designs related to the shunt topology are compared to an AC OWPP base case in order to analyse their feasibility. A comprehensive methodology to evaluate the cost of both AC and DC OWPPs has been presented. Since DC technology for DC OWPPs is not well–established yet, a sensitivity analysis has been carried out to consider various scenarios. In general terms, the results show that DC configurations involve higher capital expenditures and lower cost of energy losses, as expected. From this study, the feasibility of DC configurations among current AC systems has been demonstrated. It has been shown that DC OWPPs may be of more interest for cases with longer distances. Likewise, it is not clear (and is extremely sensitive to the DC/DC converter cost) whether the use of DC technologies for larger wind power plants would imply a cost reduction; this is because of the size of DC/DC power converters required. It is worth remarking that the cost of DC OWPPs are mainly affected by the cost of wind turbines, DC/DC converters and platforms, as well as the energy losses cost of such DC/DC converters. Therefore, both cost reduction and efficiency improvement of the electrical components of the DC OWPP (specially DC/DC converters) are required to make this option still more attractive.

8 Conclusions

This thesis deals with the development and the comprehensive analysis of different novel electrical concepts for offshore wind power plants in order to move towards more cost–effective solutions driving the offshore wind industry to a more competitive energy sector within the electricity market. The study performed through out the thesis has covered such issues as the design, optimisation, modelling, operation and control of these new concepts.

All the concepts presented in this thesis, except for the one described in Chapter 3, are motivated by the presence of HVDC technology as an interface between the offshore wind power plants and the onshore electrical grid. Thereby, the nonnecessity of the offshore wind power plant (OWPP) collection grid to be synchronized with the main AC grid (50 or 60 Hz) leads to propose innovative concepts such as the ones presented in this work.

In general terms, all the novel concepts discussed in this thesis can be mainly classified into three groups: First, a new operation control strategy based on properly derating some wind turbines in the attempt of reducing the wake effect within a wind power plant and therefore maximising the total power output, is analysed from the steady state point of view. This control scheme can be applied to any wind power plant (onshore and offshore) with a conventional AC collection grid which is connected to the grid through either an HVAC or an HVDC transmission link. Second, two more disruptive concepts compared to the previous one are presented from Chapter 4 to Chapter 6. Both wind power plant configurations are based on variable frequency operation within the AC collection grid, assuming an HVDC transmission system to shore. Likewise, both concepts are especially worthwhile for OWPPs where the wind flow is assumed to be more uni-

form compared to onshore and maintenance issues have a greater relevance since accessibility to the OWPP may be limited or none at certain times of the year due to bad weather. These OWPP topologies deals with the aim of reducing the LCOE by operating the MVAC collection grid at variable frequency and removing (in Chapters 4 and 5) or reducing the size of (in Chapter 6) the power electronic converters installed in each synchronous or DFIG–based wind turbine, respectively. Finally, the last but not least WPP concept included in this thesis comprehensively investigates the possibility of considering an entire offshore wind power plant in DC, i.e., not only the HVDC transmission system but also the MVDC collection grid.

The main important remarks of each concept analysed are drawn in the following. More detailed conclusions about each specific WPP design can be found at the end of each chapter.

With regard the first concept analysed (presented in Chapter 3), it has been demonstrated its effectiveness, since an increase ranging from 1.86 % up to 6.24 % in the annual energy captured by the wind power plant (depending on the wind rose at the WPP location) can be achieved by operating the upstream turbines slightly away from their optimum point and reducing the wake effect within the wind power plant.

Concerning the second concept discussed in this thesis (detailed in Chapters 4), the results obtained from the exhaustive technical and economic analyis, have been concluded that SLPC–VF is presented as an appealing WPP alternative, since a total cost saving of up to 6 % compared to the conventional MPC WPP topology can be achieved. Thus, although the optimal operation point of each turbine can not be assured due to the inherent configuration of the proposed scheme, the absence of dedicated power converters for each turbine brings a reduction in capital costs, as well as, in maintenance and power flow losses, so that economic benefit can be realized. Moreover, it has been demonstrated that variable frequency operation within the collection grid maximises the energy production in comparison with operating the proposed system (without individual converters) at a constant frequency within the collection grid (SLPC–CF concept).

Likewise, the optimisation model carried out in Chapter 5 indicates that, for the specific case of many large offshore wind power plants connected to a common HVDC hub which transmit their combined power to the onshore grid, it can be more cost–effective to install two smaller offshore collector platforms placing them at their optimal location (rather than just one) and to cluster some wind turbines in the appropriate manner such that the power extraction efficiency is substantially improved.

Regarding Chapter 6, the performance of a coordinated control between

a DFIG–based OWPP and a single VSC–HVDC converter is validated and assessed from both static and dynamic point of view. The results suggest a good performance of the proposed concept in terms of energy capture analysis. Thus, it can be concluded that the size of the power converter installed inside the wind turbine can be potentially reduced. Consequently, improved reliability, increased efficiency due to the lower losses and a cost reduction are expected to be achieved. However, relevant issues such as fault rid through capability or mechanical load reduction should be also considered to fully assert the minimum admissible power converter size.

Finally, the results obtained from Chapter 7 show that MVDC OWPPs may be of more interest for cases with long export cable distances between the offshore collector platform and the main HVDC substation (approximately more than 10 km). In general terms, it is also concluded that DC configurations involves higher capital expenditures and lower cost of energy losses than AC systems. Furthermore, it is worth remarking that the cost of DC OWPPs is mainly affected by the cost of wind turbines, DC/DC converters and platforms, as well as the energy losses cost of such DC/DC converters. Therefore, both cost reduction and efficiency improvement of the electrical components of the DC OWPP (especially DC/DC converters) are required to make this option still more attractive.

To sum up, it can be generally concluded that all the presented concept in this thesis suggest a good potential for future offshore wind power plants by reducing in all the cases the LCOE in comparison with the existing offshore wind power plants. However, it cannot be asserted in a decisive manner that such concepts will be applied in the future offshore wind power plants, since this extremely important decision requires to carry out further investigation on relevant issues such as power system stability analysis, short–circuit fault studies and thorough validation by means of dynamic simulations, scale experimental platforms and field tests.

8.1 Further work

From this thesis, future research lines have arisen, which appear listed in the following:

- Regarding the analysis carried out in Chapter 3 several improvements could be included:
  - To analyse different wind power plant layouts and different wind conditions to better conclude the results obtained.

  - To implement the control strategy proposed in this chapter based on a hierarchical structure with both a central control level (WPP control) and a local control level (each individual WT).

- From the technical and economic assessment performed in Chapter 4, it could be interested to study the following tasks:
  - To improve the wake model used in the tool for evaluating the wind speeds of each wind turbine (i.e., the Jensen's model) by considering a more accurate wake model as, for instance, a Computational Fluid Dynamics (CFD) model.
  - To evaluate the impact of variable frequency operation within the collection grid on power system stability.
  - To validate the proposed concept based on variable frequency operation within a collection grid by means of dynamic simulations and scaled experimental platforms.

- With regard the optimisation problem of Chapter 5, other possible works of interest could be:
  - To include not only the C_P losses but also the power flow losses and the corrective and preventive maintenance losses in the objective function of the optimisation model.
  - To apply the optimisation problem to a very large OWPP layout by using a computer with sufficient computational capacity.

- Further work related to Chapter 6 could be:
  - To carry out a more comprehensive static analysis considering not only the power extraction efficiency losses (C_P losses), but also the power flow and maintenance losses, as well as, the economic indicators to better conclude whether the proposed concept is feasible or not.
  - To validate the simulation results of the implemented control scheme by means of scaled experimental tests.

- Concerning Chapter 6 the technical and economic analysis could be improved by:
  - Obtaining a more reliable data from the industry regarding power converter efficiencies and component costs for DC offshore wind power plants.

- Finally, one possible future research line non–related to any specific chapter could be to analyse the cost–effectiveness of another possible approach in the attempt of reducing the LCOE consisting in stepping–up the voltage level in the OWPP collection grid from the conventional 33–36 kV to 48 kV or 66–72 kV.

Bibliography

[1] United Nations Framework Convention on Climate Change. Kyoto protocol to the united nations framework convention on climate change, 1998. 1

[2] European Commission. Communication from the commision: Energy efficiency: delivering the 20% target, November 2008. 1

[3] EU energy policy to 2050. Achieving 80-95% emissions reductions. Technical report, European Wind Energy Association (EWEA), March 2011. 1

[4] Wind energy: a vision for Europe in 2030. Technical report, European Wind Energy Technology Platform (TPWind), September 2006. 1

[5] Global wind statistics 2013. Technical report, Global Wind Energy Council (GWEC), February 2014. 1

[6] 2012 Annual Report. Technical report, The World Wind Energy Association (WWEA), 2013. 1, 2, 3, 13

[7] Renewables 2013 Global status report. Technical report, Renewable Energy Policy Network for the 21st Century (REN21), 2013. 2

[8] J. Wilkes and J. Moccia. Wind in power: 2012 European statistics. Technical report, European Wind Energy Association (EWEA), 2013. 2, 13

[9] R. Berger. Offshore wind toward 2020. on the pathway to cost competitiveness. Technical report, Roland Berger Strategy consultants GmbH, April 2013. 2, 3

[10] Europe's onshore and offshore wind energy potential. An assessment of environmental and economic constraints. Technical Report 6, European Environment Agency (EEA), 2009. XV, 2

[11] The European offshore wind industry - key trends and statistics 2013. Technical report, European Wind Energy Association (EWEA), January 2014. XIII, XV, 2, 3, 14

[12] B. Snyder and M.J. Kaiser. A comparison of offshore wind power development in europe and the us: Patterns and drivers of development. *Applied Energy*, 86(10):1845–1856, October 2009. 3

[13] Deep water. the next step for offshore wind energy. Technical report, European Wind Energy Association (EWEA), July 2013. 3

[14] N. Barberis Negra, J. Todorovic, and T. Ackermann. Loss evaluation of hvac and hvdc transmission solutions for large offshore wind farms. *Electric Power Systems Research*, 76(11):916–927, 2006. 3

[15] N. M. Kirby, M. J. Luckett, L. Xu, and W. Siepmann. HVDC transmission for large off shore wind farms. IEE AC-DC Power Transmission. Number 485, London, November 2001. IEE ACDC Power Transmission. 3

[16] R. L. King. *Electrical Transmission systems for large offshore wind farms.* PhD thesis, Cardiff University, February 2011. 3, 159

[17] T. Ackermann. *Wind Power in Power Systems.* Wiley, 2005. 4, 15, 16, 18, 26, 51

[18] B. Wu, Y. Lang, N. Zargari, and S. Kouro. *Power Conversion and Control of Wind Energy Systems.* John Wiley & Sons, 2011. 4

[19] E. Pouresmaeil, O. Gomis-Bellmunt, D. Montesinos-Miracle, and J. Bergas-Jané. Multilevel converters control for renewable energy integration to the power grid. *Energy*, 36(2):950–963, February 2011. 4, 131

[20] B. Fox, D. Flynn, L. Bryans, N. Jenkins, D. Milborrow, M. O'Malley, R. Watson, and O. Anaya-Lara. *Wind Power Integration: Connection*

and system operational aspects. The Institution of Engineering and Technology, 2007. 4

[21] S. Heier. *Grid Integration of Wind Energy Conversion Systems*. John Wiley and Sons, 1998. 4, 44, 76

[22] L. Trilla. *Power converter optimal control for wind energy conversion systems*. PhD thesis, Catalonia Institute for Energy Research, September 2013. 4

[23] R. Villafáfila, A. Sumper, A. Suwannarat, B. Bak-Jensen, R. Ramírez, O. Gomis, and A. Sudrià. On wind power integration into electrical power system: Spain vs. Denmark. International Conference on Renewable Energies and Power Quality (ICREPQ), Sevilla, Spain, March 2007. 4

[24] Gabriel G. Michalke and A. D. Hansen. Modelling and control of variable speed wind turbines for power system studies . *Wind*, 13(4):307–322, 2010. 4

[25] C. Jauch. Transient and dynamic control of a variable speed wind turbine with synchronous generator. *Wind Energy*, 10:247–269, 2007. 4

[26] E. Muljadi, C. P. Butterfield, B. Parsons, and A. Ellis. Effect of variable speed wind turbine generator on stability of a weak grid. *IEEE Transactions on Energy Conversion*, 22:29–36, 2007. 4

[27] R. Pena, J. C. Clare, and G. M. Asher. Doubly fed induction generator using back-to-back PWM convertersand its application to variable-speed wind-energy generation. *IEE Proceedings Electric Power Applications*, 143(3):231–241, 1996. 4, 45, 76, 133, 136, 137

[28] A. Sumper, O. Gomis-Bellmunt, A. Sudrià-Andreu, R. Villafafila-Robles, and J. Rull-Duran. Response of Fixed Speed Wind Turbines to System Frequency Disturbances. *IEEE Transactions on Power Systems*, 24:181–192, 2009. 4

[29] S. Papathanassiou and P. Papadopoulos. Mechanical stresses in fixed-speed wind turbines due to network disturbances. *IEEE Transactions on Energy Conversion*, 16:361–367, 2001. 4

[30] L. R. Chang-Chien and Y. C. Yin. Strategies for operating wind power in a similar manner of conventional power plant. *IEEE Transaction on Energy Conversion*, 24(4):926–934, December 2009. 4

[31] M. Tsili, Ch. Patsiouras, and S. Papathanassiou. Grid code requirements for large wind farms: A review of technical regulations and available wind turbine technologies. In *Proc. of the European Wind Energy Conference & Exhibition (EWEC'08)*, 2008. 4

[32] O. Gomis-Bellmunt, A. Junyent-Ferre, A. Sumper, and J. Bergas-Jane. Ride-through control of a doubly fed induction generator under unbalanced voltage sags. *IEEE Transactions on Energy Conversion*, 23:1036–1045, 2008. 4, 123, 137, 138

[33] A. D. Hansen and G. Michalke. Fault ride-through capability of DFIG wind turbines. *Renewable Energy*, 32(9):1594–1610, July 2007. 4, 123

[34] G. Ramtharan, J.B. Ekanayake, and N. Jenkins. Frequency support from doubly fed induction generator wind turbines. *IET Renewable Power Generation*, 1:1–9, 2007. 4

[35] F. Díaz-González. *Contributions of Flywheel Systems in Wind Power Plants*. PhD thesis, Catalonia Institute for Energy Research (IREC), July 2013. 4

[36] I. Errasti Salaberri, M. Santos Múgica, and M. A. Rodríguez Vidal. Wind farms and conventional plants primary frequency control interaction. Milan, May 2007. European Wind Energy Conference & Exhibition (EWEC) . 4

[37] P. Kundur. *Power System Stability and Control*. McGraw-Hill, 1994. 4

[38] F. Wu, Z.P. Zhang, K. Godfrey, and P. Ju. Small signal stability analysis and optimal control of a wind turbine with doubly fed induction generator. *IET Generation. Transmission and Distribution*, 1:751–761, 2007. 4

[39] J. Machowski, J. W. Bialek, and J. R. Bumby. *Power System Dynamics: Stability and Control*. Wiley, 2008. 4

[40] C. Jauch. *Stability and Control of Wind Farms in Power Systems*. PhD thesis, Aalborg University - Risø, 2006. 4

[41] J. L. Domínguez-García. *Analysis of the contribution of wind power plants to damp power system oscillations.* PhD thesis, Catalonia Institute for Energy Research (IREC), April 2013. 4

[42] P. Breseti, W.L. Kling, R.L. Hendriks, and R. Vailati. HVDC Connection of Offshore Wind Farms to the Transmission System. *IEEE Transactions on Energy Conversion*, 22 (1):37–43, 2007. 4

[43] O. Gomis-Bellmunt, J. Liang, J. Ekanayake, R. King, and N. Jenkins. Topologies of multiterminal HVDC-VSC transmission for large offshore wind farms. *Electric Power Systems Research*, 81:271–281, 2011. 4

[44] J. Glasdam, L. Zeni, M. Gryning, J. Hjerrild, L. Kocewiak, B. Hesselbaek, K. Andersen, T. Sørensen, M. Blanke, P. E. Sørensen, A. D. Hansen, C. L. Bak, and P. C. Kjær. HVDC Connected Offshore Wind Power Plants: Review and Outlook of Current Research. 12th International Workshop on Large-Scale Integration of Wind Power into Power Systems as well as on Transmission Networks for Offshore Wind Power, October 2013. London, UK. XIII, 4, 131

[45] DolWin 3. 162 kilometre grid connection for offshore wind energy. Technical report, Tennet, February 2013. XIII, 4

[46] Levelized cost of electricity renewable energy technologies. Technical report, Fraunhofer ISE, November 2013. 5

[47] L. Trilla, O. Gomis-Bellmunt, A. Sudrià-Andreu, and J. Liang. Control of SCIG wind farm using a single VSC. pages 1–9. Power Electronics and Applications (EPE 2011), Proceedings of the 2011–14th European Conference, 2011. 5, 66, 142

[48] O. Gomis-Bellmunt, A Junyent-Ferré, A. Sumper, and J. Bergas-Jané. Control of a Wind Farm Based on Synchronous Generators With a Central HVDC-VSC Converter. *IEEE Transactions on Power Systems*, 26(3):1632–1640, August 2011. 5, 66

[49] D. Jovcic. Offshore wind farm with a series multiterminal csi hvdc. *Electric Power Systems Research*, 78:747–755, 2008. 5, 66

[50] D. Jovcic and N. Strachan. Offshore wind farm with centralised power conversion and DC interconnection. *IET Generation, Transmission & Distribution*, 3(6):586–595, 2009. 5, 66, 75, 92, 104, 142

[51] T. Vrionis, X. Koutiva, N. Vovos, and G. Giannakopoulos. Control of an hvdc link connecting a wind farm to the grid for fault ride-through enhancement. *IEEE Transactions on Power Systems*, 22(4):2039–2047, 2007. 5, 66

[52] M. De-Prada-Gil, O. Gomis-Bellmunt, A. Sumper, and J. Bergas-Jané. Analysis of a multi turbine offshore wind farm connected to a single large power converter operated with variable frequency. *Energy*, 36:3272–3281, 2011. 5, 66

[53] O. Gomis-Bellmunt, A. Junyent-Ferré, A. Sumper, and S. Galceran-Arellano. Maximum generation power evaluation of variable frequency offshore wind farms when connected to a single power converter. *Applied Energy*, 87:3103–3109, 2010. 5, 66

[54] V. Gevorgian, M. Singh, and E. Muljadi. Variable frequency operations of an offshore wind power plant with hvdc-vsc. San Diego, California. IEEE Power and Energy Society General Meeting (PES). 5, 66, 88

[55] M. Alexander Parker and O. Anaya-Lara. Cost and losses associated with offshore wind farm collection networks which centralise the turbine power electronic converters. *IET Renewable Power Generation*, 7(4):390–400, 2013. 5, 27, 66, 159

[56] M. De-Prada-Gil, O. Gomis-Bellmunt, A. Sumper, and J. Bergas-Jané. Power generation efficiency analysis of offshore wind farms connected to a SLPC (single large power converter) operated with variable frequencies considering wake effects. *Energy*, 37(1):455–468, January 2012. 5, 47, 66, 71, 75, 104, 212

[57] J. L. Domínguez-García, D.J. Rogers, C.E. Ugalde-Loo, J. Liang, and O. Gomis-Bellmunt. Effect of non-standard operating frequencies on the economic cost of offshore AC networks. *Renewable Energy*, 44:267–280, 2012. 5, 86

[58] N. Holtsmark, H. J. Bahirat, M. Molinas, B. A. Mork, and H. K. Hoidalen. An All-DC Offshore Wind Farm With Series-Connected Turbines: An Alternative to the Classical Parallel AC Model? *IEEE Transactions on Industrial Electronics*, 60:2420–2428, 2013. 5, 159, 164

[59] J. Serrano-González, M. Burgos-Payán, and J. Riquelme-Santos. A New and Efficient Method for Optimal Design of Large Offshore Wind

Power Plants. *IEEE Transactions on Power Systems*, 28(3):3075–3084, August 2013. XVIII, 5, 87, 105

[60] R. Allen-Walling, E. Vaughn-Larsen, and R. William-Delmerico. General Electric Company. Variable frequency wind plant, May 2011. US 7,939,970 B1. 5

[61] M. Jakobsson. 2-B Energy Holding B.V. Method and system for controlling wind power plants, January 2013. EP 2 232 667 B1. 5

[62] R. Mc Dermott. Investigation of Use of Higher AC Voltages on Offshore Wind Farms. In *European Wind Energy Conference and Exhibition (EWEC)*, Marseille, March 2009. 5

[63] A. Ferguson, P. de Villiers, B. Fitzgerald, and J. Matthiesen. Benefits in moving the inter-array voltage from 33 kV to 66 kV AC for large offshore wind farms. European Wind Energy Conference & Exhibition (EWEC), Copenhagen, Denmark, April 2012. 5

[64] D. Saez, J. Iglesias, E. Giménez, and M. Reza I. Romero. Evaluation of 72 kV collection grid on Offshore Wind Farms. European Wind Energy Conference & Exhibition (EWEC), Copenhagen, Denmark, April 2012. 5

[65] P. K. Steimer, O. Apeldoorn, L. Dalessandro, R. Grinberg, and S. Ebner. Efficient medium voltage power collection windparks. European Wind Energy Conference & Exhibition (EWEC), Copenhagen, Denmark, 16–19 April 2012. 5, 26, 27

[66] L. H. Hansen, L. Helle, F. Blaabjerg, E. Ritchie, S. Munk-Nielsen, H. Bindner, P. Sørensen, and B. Bak-Jensen. Conceptual survey of Generators and Power Electronics for Wind Turbines. Technical report, Risø National Laboratory, December 2001. 16

[67] National Grid Electricity Transmission. Offshore developement information statement 2010. Technical report, National Grid, 2010. XVI, 19, 29, 30, 31

[68] Prysmian Group Cables and Systems. Submarine energy systems. 20

[69] J. Declercq and R. Van Schevensteen. Challenges for Reliable Offshore Transformers. *Windtech International*, 2008. 21

[70] R. MacLean. Electrical System Design for the Proposed One Gigawatt Beatrice Offshore Wind Farm. Master's thesis, University of Strathclyde, 2004. 21

[71] P. Gardner, L. M. Craig, and G. J. Smith. Electrical Systems for Offshore Wind Farms. In *Twentieth BWEA Wind Energy Conference Wind Energy*, 1998. 21, 26

[72] J. D. McDonald, editor. *Electric Power Substations Engineering*. CRC, 2003. 22

[73] ABB. ABB's super-slim switchgear for wind turbines. www.abb.com, Accessed on 08/01/2014. XV, 22

[74] S&C Electric Company. Wind Turbine Manufacturer Turns to S&C for Special Vista Switchgear. http://www.sandc.com, Accesed on 08/01/2014. XV, 22

[75] Offshore Transformer Platform: Earthing, Bonding and Lightning Protection. 22, 23

[76] ABB HVDC Reference Projects in Europe: BorWin1. 23

[77] DNV-GL. A plug–in solution. http://www.dnv.com, Accesed on 12/01/2014. XV, 24

[78] IEEE Wind and Solar Plant Collector Design Working Group. Wind Power Plants SCADA and Controls. 25

[79] Business Technology Consulting (BTC) SCADA control center. http://blogs.msdn.com/b/mspowerutilities/archive/2012/04/05/wind-variability-addressed-by-btc-s-sera-based-solution.aspx, Accesed on 14/01/2014. XV, 25

[80] DEIF Wind Power Technology. SCADA for remote supervision and control of wind turbines and wind parks. http://www.deifwindpower.com/scada.aspx, Accesed on 14/01/2014. XV, 25

[81] C. Nicolae. SCADA-Supervisory Control and Data Acquisition. *Journal of Sustainable Energy*, 2(4):1–5, 2011. 25, 26

[82] WindAcWind- Alstom's SCADA for onshore and offshore applications. 26

[83] The REpower SCADA System. End-to-end management of wind turbines. 26

[84] GH SCADA. http://www.gl-garradhassan.com/en/software/scada.php, Accesed on 15/01/2014. 26

[85] S. Lumbreras and A. Ramos. Optimal Design of the Electrical Layout of an Offshore Wind Farm Applying Decomposition Strategies. *IEEE Transactions on Power Systems*, 28(2):1434–1441, May 2013. 26, 103

[86] T. Haugsten Hansen. Offshore Wind Farm Layouts. Performance Comparison for a 540 MW Offshore Wind Farm. Master's thesis, Norwegian University of Science and Technology. Department of Electric Power Engineering, July 2009. 26, 27

[87] A. Sannino, H. Breder, and E. K. Nielsen. Reliability of collection grids for large offshore wind parks. In *9th International Conference on Probabilistic Methods Applied to Power Systems*, KTH, Stockholm, Sweden, June 11–15 2006. 26, 27

[88] J. T. G. Pierik, M. E. C. Damen, P. Bauer, and S. W. H. de Haan. Steady state electrical design, power performance and economic modeling of offshore wind farms. *EPE Journal*, 16:44–49, 2006. 26, 27

[89] N. Barberis-Negra, J. Todorovic, and T. Ackermann. Loss evaluation of HVAC and HVDC transmission solution for large offshore wind farms. *Electric Power Systems Research*, 76:916–927, 2006. 28, 159

[90] The economics of wind energy. Technical report, European Wind Energy Association (EWEA), March 2009. 37, 92, 117, 168, 169, 174

[91] C. B. Hasager, A. Pena, M. B. Christiansen, P. Astrup, M Nielsen, F. Monaldo, D. Thompson, and P. Nielsen. Remote Sensing Observation Used in Offshore Wind Energy. *IEEE Journal of Selected Topics in Applied Earth Observations and Remote Sensing*, 1(1):67–79, March 2008. XIII, XVIII, 40, 63, 64, 87, 98, 125

[92] L. Anatoly, F. Ilia, and D. Yi. *Multi-state System Reliability Analysis and Optimization for Engineers and Industrial Managers.* Springer, 1st edition, 2010. 41, 79, 222

[93] J. H. M. Larsen, H. C. Soerensen, E. Christiansen, S. Naef, and P. Vølund. Experiences from Middelgrunden 40 MW Offshore Wind

Farm. In *Copenhagen Offshore Wind Conference*, October 2005. 42, 79

[94] P. Volund, P. H. Pedersen, and P. E. Ter-Borch. 165 MW Nysted Offshore Wind Farm. First year of operation - performance as planned. Technical report, 2004. 42, 79

[95] J. Serrano González, M. Burgos Payán, and J. Riquelme Santos. Optimum Wind Turbines Operation for Minimizing Wake Effect Losses in Offshore Wind Farms. 13th International Conference on Environment and Electrical Engineering (EEEIC), Wroclaw, Poland, November 2013. 44

[96] J. Annoni, P. Seiler, K. Johnson, P. Fleming, and P. Gebraad. Evaluating Wake Models for Wind Farm Control. In *Accepted to the 2014 American Control Conference*, June 2014. 44

[97] C. Guillén Alías. Optimización de la generación de un parque eólico considerando efectos de estela. Master's thesis, UB-UPC dEnginyeria en Energia, June 2013. 44, 51

[98] J. R. Marden, S. Ruben, and L. Pao. A model-free approach to wind farm control using game theoretic methods. *IEEE Transactions on Control Systems Technology*, pages 1207–1214, 2013. 44

[99] E. Bitar and P. Seiler. Coordinated control of a wind turbine array for power maximization. In *American Control Conference*, Washington, DC, USA, 2013. 44

[100] K. E. Johnson and G. Fritsch. Assessment of extremum seeking control for wind farm energy production. *Wind Engineering*, 36(6):701–716, 2012. 44

[101] P. M. O. Gebraad, F. C. van Dam, and J. W. van Wingerden. A model-free distributed approach for wind plant control. In *American Control Conference*, pages 628–633, 2013. 44

[102] Z. Lubosny. *Wind Turbine Operation in Electric Power Systems*. Springer, 2003. 44, 76

[103] F. D. Bianchi, H. D. Battista, and R. J. Mantz. *Wind Turbine Control Systems*. Springer, 2007. 45, 76, 134, 137

[104] M. Ali, J. Matevosyan, J. V. Milanović, and L. Söder. Effect of Wake Consideration on Estimated Cost of Wind Energy Curtailments. In *8th International Workshop on Large-Scale Integration of Wind Power into Power Systems as well as on Transmission Networks for Offshore Wind Farms*, Bremen, Germany, 14–15 Nov 2009. 46, 48, 49

[105] R. J. Barthelmie, L. Folkerts, G. C. Larsen, K. Rados, S. C. Pryor, S. T. Frandsen, B. Lange, and G. Schepers. Comparison of Wake Model Simulations with Offshore Wind Turbine Wake Profiles Measured by Sodar. *Journal of Atmospheric and Oceanic Technology*, 23:888–901, 2005. 46, 47

[106] J. F. Ainslie. Calculating the flowfield in the wake of wind turbines. *Journal of Wind Engineering and Industrial Aerodynamics*, 27:213 – 224, 1988. 47

[107] S. Frandsen, R. J. Barthelmie, S. C. Pryor, O. Rathmann, S. Larsen, J. Højstrup, and M. Thøgersen. Analytical modelling of wind speed deficit in large offshore wind farms. *Wind Energy*, 9(1–2):39–53, January 2006. 47

[108] O. Rathmann, S. Frandsen, and R. J. Barthelmie. Wake Modelling for intermediate and large wind farms. Wind Energy Conference & Exhibition (EWEC), Milan, Italy, May 2007. 47

[109] N. O. Jensen. A note on wind generator interaction. Technical report, RISØ-M-2411, 1983. Denmark. 47, 48, 71, 212

[110] P. E. Réthoré, A. Bechmann, N.N. Sørensen, S. T. Frandsen, J. Mann, H. E. Jørgensen, O. Rathmann, and S. E. Larsen. A CFD model of the wake of an offshore wind farm: using a prescribed wake inflow. *Journal of Physics: Conference Series*, 75(1):12–47, 2007. 47

[111] M. Youjie, Y. Haishan, Z. Xuesong, L. Ji, and W. Hulong. The Dynamic Modeling of Wind Farms Considering Wake Effects and its Optimal Distribution. In *World Non-Grid-Connected Wind Power and Energy Conference, WNWEC 2009*, pages 1–4, Nanjing, Sept 2009. 49, 212

[112] B. Zhaohong, B. Xin, W. Zijing, and W. Xifan. Studies on Models and Algorithms of the Power System Probabilistic Production Simulation Integrated With Wind Farm. In *Power & Energy Society General*

Meeting, 2009. PES IEEE, pages 1–7, Calgary, AB, 26-30 July 2009. 50, 212

[113] R. J. Barthelmie and S. C. Pryor. Can satellite sampling of offshore wind speeds realistically represent wind speed distributions? *Journal of Applied Meteorology*, 42(1):83–94, January 2003. 57

[114] S. C. Pryor, M. Nielsen, R. J. Barthelmie, and J. Mann. Can satellite sampling of offshore wind speeds realistically represent wind speed distributions? part ii: Quantifying uncertainties associated with distribution fitting methods. *Journal of Applied Meteorology*, 43(5):739–750, May 2004. 57

[115] Comisión Nacional de la Energía (CNE). Resultados del Mercado de Producción de Energía Eléctrica 2013. http://www.cne.es., Accessed on 04/02/2014. 64

[116] European Central Bank (ECB). Money market interest rates. http://sdw.ecb.europa.eu, Accessed on 04/02/2014. 64

[117] Energy Information Administration (EIA). Annual Energy Outlook 2014. http://www.eia.gov/forecasts/aeo/er/index.cfm, Accessed on 04/02/2014. 64

[118] C. Feltes and I. Erlich. Variable Frequency Operation of DFIG based Wind Farms connected to the Grid through VSC-HVDC Link. In *IEEE Power Engineering Society General Meeting*, pages 1–7, June 2007. 73, 120

[119] M. De-Prada-Gil, O. Gomis-Bellmunt, and A. Sumper. Technical and economic assessment of offshore wind power plants based on variable frequency operation of clusters with a single power converter. *Applied Energy*, 125:218–229, July 2014. 75

[120] A. Junyent-Ferré, O. Gomis-Bellmunt, A. Sumper, M. Sala, and M. Mata. Modeling and control of the doubly fed induction generator wind turbine. *Simulation Modelling Practice and Theory*, 18(9):1365–1381, October 2010. 76

[121] OceanWind. Offshore wind experiences. a bottom–up review of 16 projects. Technical report, 2010. 79

[122] M. Dicorato, G. Forte, M. Pisani, and M. Trovato. Guidelines for assessment of investment cost for offshore wind generation. *Renewable Energy*, 36 (8):2043–2051, 2011. 84, 85, 111, 114, 168, 169, 170, 171, 172

[123] G. Stamatiou. Techno-Economical Analysis of DC Collection Grid for Offshore Wind Parks. Master's thesis, University of Nottingham, 2010. XIV, 84, 85, 111, 114, 169, 170, 172

[124] G. Daelemans, K. Srivastava, M. Reza, S. Cole, and R. Belmans. Minimization of Steady–State Losses in Meshed Networks using VSC HVDC. In Proceedings of IEEE Power & Energy Society General Meeting, 2009. 89, 221

[125] R. W. De. Doncker. Future DC Grid Technology for more Decentralized Power Production and Renewable Power Supplies. Aalborg, 2012. In Proceedings of 3rd IEEE International Symposium on Power Electronics for distributed Generation Systems. 89, 221

[126] A. Underbrink, J. Hanson, A. Osterholt, and W. Zimmermann. Probabilistic Reliability Calculations for the Grid Connection of an Offshore Wind Farm. KTH, Stockholm, Sweden, June 11–15 2006. 9th International Conference on Probabilistic Methods Applied to Power Systems. 90

[127] E. Spahić, A. Underbrink, V. Buchert, J. Hanson, I. Jeromin, and G. Balzer. Reliability Model of Large Offshore Wind Farms. Bucharest, Romania, June 28th–July 2nd 2009. IEEE Bucharest Power Tech Conference. 90

[128] P. Sørensen, D. A. Hansen, F. Iov, F. Blaabjerg, and M. H. Donovan. Wind farm models and control strategies. Technical Report Risø-R-1464, 2005. 96

[129] M. Lindahl, N.C. Fink Bagger, T. Stidsen, S. Frost Ahrenfeldt, and I. Arana. OptiArray from DONG Energy. In *12th Workshop on Large–Scale Integration of Wind Power into Power Systems*, London, 22–24 Oct 2013. 103

[130] A. Brooke, D. Kendrick, and A. Meeraus. Release 2.25 GAMS Users Guide. The Scientific Press. South Francisco, USA, 1992. 112

[131] D. Lane. Round 3 Offshore Wind Farm Connection Study. Technical report, The Crown State, 2010. 114

[132] E. Muljadi, M. Singh, and V. Gevorgian. Doubly Fed Induction Generator in an Offshore Wind Power Plant Operated at Rated V/Hz. *IEEE Transactions on Industry Applications*, 49(5):2197–2205, 2013. 120, 142

[133] K. E. Okedu. Impact of Power Converter Size on Variable Speed Wind Turbine. *The Pacific Journal of Science and Technology*, 13(1):176–181, May 2012. 122

[134] B. Barahona, N. A. Cutululis, A. D. Hansen, and P. Sørensen. Unbalanced voltage faults: the impact on structural loads of doubly fed asynchronous generator wind turbines. *Wind Energy*, June 2013. 123

[135] B. Barahona, R. You, A. D. Hansen, N. A. Cutululis, and P. Sørensen. Assessment of the impact of frequency support on DFIG wind turbine loads . 12th International Workshop on Large-Scale Integration of Wind Power into Power Systems as well as on Transmission Networks for Offshore Wind Power Plants, London, 2013. 123

[136] A. D. Hansen, N. A. Cutululis, F. Iov, P. E. Sørensen, and T. J. Larsen. Grid faults' impact on wind turbine structural loads. 4th Nordic Wind Power Conference, Roskilde, 2007. Risø National Laboratory. 123

[137] A. Zohoori, A. Kazemi, and R. Shafaie. Fault Ride through Capability Improvement of Wind Turbine Based DFIG Considering an Optimized Crowbar Along with STATCOM under Grid Fault Condition. *Research Journal of Applied Sciences, Engineering and Technology*, 5(7):2297–2302, 2013. 123

[138] A. D. Hansen, N. A. Cutululis, B. Barahona, and H. Markou. Impact of fault ride-through requirements on wind turbine structural loads. European Wind Energy Conference and Exhibition (EWEC), Warsaw, Poland, 2010. 123

[139] B. Bak-Jensen, T.A. Kawady, and M. H. Abdel-Rahman. Coordination between Fault-Ride-Through Capability and Over-current Protection of DFIG Generators for Wind Farms. *Journal of Energy and Power Engineering*, 4(4):20–29, April 2010. 123

[140] N. A. Cutululis, A. D. Hansen, T. J. Larsen, P. E. Sørensen, and F. Iov. Wind turbines structural loads during fault ride-through operation. pages 77–80, European Wind Energy Conference and Exhibition (EWEC), Brussels, Belgium, 2008. 123

[141] A. D. Hansen, P. E. Sørensen, F. Iov, and F. Blaajberg. Centralised power control of wind farm with doubly fed induction generators. *Renewable Energy*, 32(7):935–951, 2006. 130

[142] D. Xiang, L. Ran, J. R. Bumby, P. J. Tavner, and S. Yang. Coordinated Control of an HVDC Link and Doubly Fed Induction Generators in a Large Offshore Wind Farm. *IEEE Transaction on Power Delivery*, 21(1):463–471, Janurary 2006. 130

[143] M. Santos, M. Rodriguez, and I. Errasti. Centalised control of a wind farm based on DFIG variable speed wind turbines. Athens, March 2006. European Wind Energy Conference & Exhibition (EWEC) . 130

[144] F. Díaz-González, A. Sumper, O. Gomis-Bellmunt, and R. Villafáfila-Robles. A review of energy storage technologies for wind power applications. *Renewable and Sustainable Energy Reviews*, 16(4):2154–2171, 2012. 131

[145] M. Merlin, T. Green, P. Mitcheson, D. Trainer, D. Critchley, and R. Crookes. A new hybrid multi-level voltage-source converter with dc fault blocking capability. In *Proceedings of the 9th IET International Conference on AC and DC Transmission (ACDC)*, 2010. 131

[146] M. Davies, M. Dommaschk, J. Dorn, J. Lang, D. Retzmann, and D. Soerangr. HVDC PLUS Basics and Principle of Operation. Technical report, Siemens, 2008. 131

[147] N. Flourentzou, V. G. Agelidis, and G. D. Demetriades. VSC-Based HVDC Power Transmission Systems: An Overview. *IEEE Transactions on Power Electronics*, 24(3):592–602, March 2009. 131

[148] N. Mohan. *Advanced Electric Drives*. MNPERE, 2001. 132

[149] E. Valsera-Naranjo, A. Sumper, O. Gomis-Bellmunt, A. Junyent-Ferré, and M. Martínez-Rojas. Design of a pitch control of a wind turbine to improve system frequency response. pages 1–11. Power Electronics and Applications, 2009. EPE '09. 13th European Conference, 2009. 137

[150] C. De-Prada. PID controllers and tuning. Universidad de Valladolid. 138

[151] V. Gevorgian, M. Singh, and E. Muljadi. Variable Frequency Operations of an Offshore Wind Power Plant with HVDC-VSC. IEEE Power and Energy Society General Meeting San Diego, California, 22–26 July 2012. 142

[152] National Renewable Energy Laboratory (NREL) webpage. http://www.nrel.gov/, Access data: 24/09/2013. XX, 153

[153] G. Stamatiou, K. Srivastava, M. Reza, and P. Zanchetta. Economics of DC wind collection grid as affected by cost of key components. In *World Renewable Energy Congress*, 2011. 159, 164

[154] M. De Prada-Gil, J.L. Domínguez-García, F. Díaz-González, M. Aragüés-Peñalba, O. Gomis-Bellmunt, D. Berenguel-Centeno, M. Martins, and G. Fullana. Analysis of DC collector grid for offshore wind power plants. In *12th Workshop on Large–Scale Integration of Wind Power into Power Systems*, London, 22–24 Oct 2013. 159

[155] D. M. Valcan, P. C. Kjaer, L. Helle, S. Sahukari, M. Haj-Maharsi, and S. Singh. Cost of energy assessment methodology for offshore AC and DC wind power plants. 13th International Conference on Optimization of Electrical and Electronic Equipment (OPTIM), Brasso, Romania, May 2012. 159

[156] C. Meyer, S. Schröder, and R. W. De Doncker. Solid-State Circuit Breakers and Current Limiters for Medium-Voltage Systems Having Distributed Power Systems. *IEEE Transactions on Power Electronics*, 19(5):1333–1340, September 2004. 160

[157] M. Steurer, K. Fröhlich, W. Holaus, and K. Kaltenegger. A Novel Hybrid Current-Limiting Circuit Breaker for Medium Voltage: Principle and Test Results. *IEEE Transactions on Power Delivery*, 18(2):460–467, April 2003. 160

[158] J. Häfner and B. Jacobson. Proactive Hybrid HVDC Breakers - A key innovation for reliable HVDC grids. In *Proceedings of The Electric Power System of the Future, Cigré 2011, Bologna Symposium*, 2011. 160

[159] TWENTIES project– Alstom Grid Technologies. Feasibility tests of Direct Current Circuit Breaker prototype in DEMO3-DCGRID: breaking test demonstration. 160

[160] D. Jovcic. Step–up DC–DC converter for megawatt size applications. *IET Power Electronics*, 2 (6):675–685, 2008. 160

[161] D. Jovcic. Bidirectional, High–Power DC Transformer. *IEEE Transactions on Power Delivery*, 24 (4):2276–2283, 2009. 160

[162] E. Veilleux. Interconnection of Direct-Drive Wind Turbines Using a Series Connected DC Grid. Master's thesis, University of Toronto, 2009. 164

[163] The High voltage DC breaker: The power grid revolution. Technical report, ABB, 2012. 172

[164] L. MacLeod. 2010 offshore development information statement. Technical report, National Grid, 2010. 172

[165] Short term energy outlook. Technical report, Energy International Agency (EIA), August 2013. 172

[166] M. H. Ali, M. Park, I.K. Yu, T. Murata, and J. Tamura. Improvement of Wind-Generator Stability by Fuzzy-Logic-Controlled SMES. *IEEE Transactions on Industry Applications*, 45:1045–1051, 2009. 212

[167] L. Jensen, C. Mørch, P. Sørensen, and K. H. Svendsen. Wake measurements from the Horns Rev wind farm. European Wind Energy Conference & Exhibition (EWEC), London, United Kingdom, 22–25 Nov 2004. 212

A

List of Publications

In this chapter, the list of publications both journals and conferences papers, derived from the development of the thesis are presented.

A.1 Journal articles

[J1] M. De-Prada-Gil, O. Gomis-Bellmunt, A. Sumper, J. Bergas-Jané. Analysis of a multi turbine offshore wind farm connected to a single large power converter operated with variable frequency. Energy. May 2011; 36(5):3272-81.
DOI: http://dx.doi.org/10.1016/j.energy.2011.03.020

[J2] M. De-Prada-Gil, O. Gomis-Bellmunt, A. Sumper, J. Bergas-Jané. Power generation efficiency analysis of offshore wind farms connected to a SLPC (single large power converter) operated with variable frequencies considering wake effects. Energy. January 2012; 37(1):455-68.
DOI: http://dx.doi.org/10.1016/j.energy.2011.11.010

[J3] M. De-Prada-Gil, O. Gomis-Bellmunt, A. Sumper. Technical and economic assessment of offshore wind power plants based on variable frequency operation of clusters with a unique power converter. Applied energy. July 2014; 125:218-229.
DOI: http://dx.doi.org/10.1016/j.apenergy.2014.03.031

[J4] M. De-Prada-Gil, L. Igualada, C. Corchero, O. Gomis-Bellmunt, A. Sumper. Hybrid AC-DC offshore wind power plant topology: optimal design Energy. Submitted to IEEE Transaction on Power Systems.

[J5] M. De-Prada-Gil, J. L. Domínguez-García, F. Díaz-González, M. Aragüés-Peñalba, O. Gomis-Bellmunt. Feasibility analysis of offshore wind power plants with DC collection grid. Submitted to Renewable Energy.

[J6] M. De-Prada-Gil, F. Díaz-González, O. Gomis-Bellmunt, A. Sumper. DFIG–based offshore wind power plant connected to a single VSC–HVDC operated at variable frequency: Energy yield assessment. Submitted to Applied Energy.

[J7] M. De-Prada-Gil, C. Guillén Alías, O. Gomis-Bellmunt, A. Sumper. Optimal wind power plant operation by reducing the wake effect. Submitted to Applied Energy.

A.2 Conference articles

[C1] M. De-Prada-Gil, O. Gomis-Bellmunt, A. Sumper. Power extraction efficiency analysis of a multi turbine offshore wind farm connected to a single power converter. In: European Wind Energy Conference & Exhibition (EWEC). Brussels, Belgium. March 2011.

[C2] M. De-Prada-Gil, A. Sumper, O. Gomis-Bellmunt. Modeling and control of a pitch-controlled variable-speed wind turbine driven by a DFIG with frequency control support in PSS/E. IEEE Power Electronics and Machines in Wind Applications (PEMWA). Denver CO, USA, July 2012. DOI: http://dx.doi.org/10.1109/PEMWA.2012.6316406

[C3] M. De-Prada-Gil, J.L. Domínguez-García, F. Díaz-González, M. Aragüés-Peñalba, O. Gomis-Bellmunt, D. Berenguel-Centeno, M. Martins, G. Fullana. Analysis of DC collector grid for offshore wind power plants. In: 12th International Workshop on Large-Scale Integration of Wind Power into Power Systems as well as on Transmission Networks for Offshore Wind Power Plants. London, UK. October 2013.

[C4] M. De-Prada-Gil, J.L. Domínguez-García, O. Gomis-Bellmunt, A. Sumper. Technical and economic assessment tool for OWPPs based on a collector grid connected to a single VSC-HVDC converter. In: European Wind Energy Conference & Exhibition (EWEC). Barcelona, Spain. March 2014.

A.3 Other publications

Other relevant publications not directly related to the thesis are listed in this section.

A.3.1 Journal and conference articles

[O1] D. Berenguel, M. De-Prada-Gil, O. Gomis-Bellmunt, M. Martins. Electrical interconnection options analysis for offshore wind farms. In: European Wind Energy Conference & Exhibition (EWEC). Vienna, Austria. February 2013.

[O2] M. De-Prada-Gil, J.L. Domínguez-García, F. Mancilla-David, E. Muljadi, M. Singh, O. Gomis-Bellmunt, A. Sumper. Type-2 Wind Turbine with Additional SubSynchronous Resonance Damping. In: Green Technologies Conference, 2013 IEEE. Denver CO, USA. April 2013. DOI: http://dx.doi.org/10.1109/GreenTech.2013.42

[O3] G. Perez, J. Lopez-Mendia, L. Val, A. Sumper, F. Schuon, M. De-Prada-Gil, M. Aragüés, H. Lopes, H. Ergun, D. Van-Hertem. Deep offshore wind farm planning and cost calculation tools. In: European Wind Energy Conference & Exhibition (EWEC). Frankfurt, Germany. November 2013.

[O4] M. De-Prada-Gil, F. Mancilla-David, J.L. Domínguez-García, E. Muljadi, M. Singh, O. Gomis-Bellmunt, A. Sumper. Contribution of type-2 wind turbines to sub-synchronous resonance damping. International Journal of Electrical Power & Energy Systems (IJEPES). Feb. 2014; 55(1):714-722. DOI: http://dx.doi.org/10.1016/j.ijepes.2013.10.025

A.3.2 Book chapters

[B1] M. De-Prada-Gil, J.L. Domínguez-García, F. Díaz-González, A. Sumper. Offshore Wind Power Plants (OWPPs). Building the grid of the future using HVDC. Offshore grids and the supergrid. Accepted for publication in John Wiley & Sons. 2014.

A.3.3 Patent

[P1] Inventors: O. Gomis-Bellmunt, M. De-Prada-Gil, F. Díaz-González, E. Prieto-Araujo. Harmonics mitigation in multiphase generator-con-

version systems. Application number: EP13382510.9. Requested in December, 2013.

B

Description of the tool used for Chapter 4: user guide

B.1 Introduction

The aim of this chapter is to present the technical and economic assessment tool employed for Chapter 4. This tool has been implemented in MATLAB using a Graphical User Interface (GUI). Figure B.1 displays the executable file and the cover screen of the Wind Energy Assessment (WEA) tool. As it can be noted, it contains a HELP button for user's assistance.

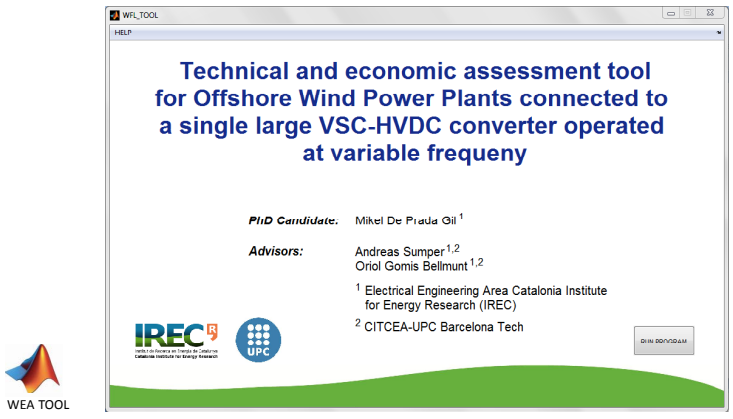

(a) (b)

Figure B.1: Executable file (a) and cover screen (b) of the tool.

B.2 Program menu

A snapshot of the program menu is shown in Figure B.2. As it can be seen, it is divided into seven buttons. The first button is only introduced for informative purposes, whilst the others correspond to each of the steps involved in the methodology used in Chapter 4 for the technical and economic assessment of the proposed SLPC–VF topology based on removing the individual power converters of each turbine and connecting a cluster of wind turbines or an entire OWPP to a single large power converter which operates at variable taking advantage of HVDC technology and its ability to operate the wind farm collection grid out of synchronism with the onshore electrical network (50 or 60 Hz). All theses steps (from 1 to 6) must be executed by the user in a sequential manner.

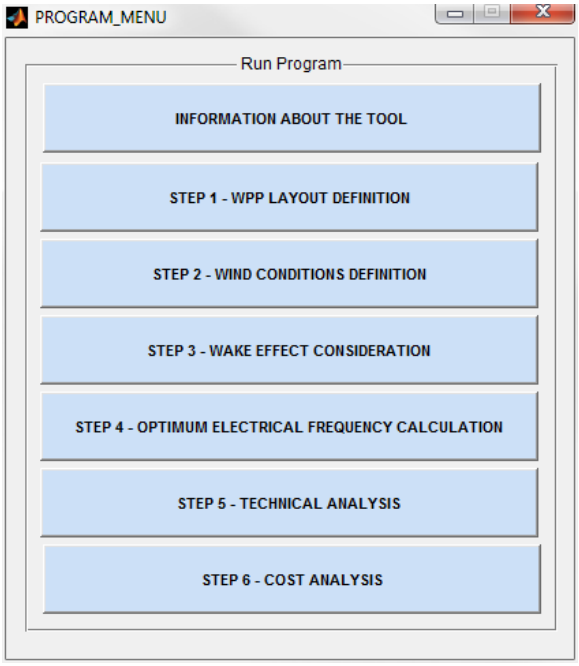

Figure B.2: Program menu of the tool.

Next, all the buttons encompassed in the tool are explained:

- **Information about the tool:** As it has been mentioned, the aim of this button is purely explanatory. It highlights the main objective of the tool and describes the two OWPP topologies analysed which have been described in detail in Chapter 4.

- **Step 1 – WPP layout definition:** In this step, the layout of a specific wind power plant has to be defined in order to compare both WPP topologies (conventional and proposed) in a same scenario. As it is a generic tool, any hypothetical WPP layout can be set by the user. The program enables to define the arrangement of the wind turbines in the WPP not only by a matrix rectangle form (Figure B.3(a)), but also by specifying the coordinates of each wind turbine (Figure B.3(b)).

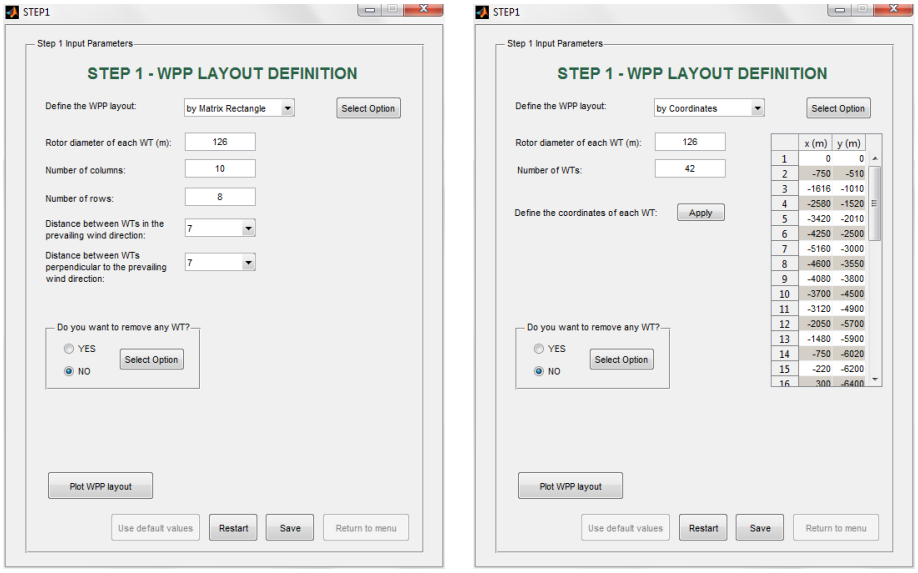

(a) (b)

Figure B.3: Visualization of step 1 – WPP layout definition. On the left (a), the input parameters required to define a WPP layout composed of 80 wind turbines and defined by a matrix rectangle form. On the right (b), the data needed to define a WPP comprised of 42 wind turbines by coordinates.

The former option requires to introduce as input data the following parameters: the rotor diameter (D) of the wind turbines, the number of rows and columns of the WPP, the distance between two nearby wind turbines in the prevailing wind direction and the crosswind spacing among wind turbines within a same row. Otherwise, if the WPP layout is defined by coordinates, the user must indicate the rotor diameter of the wind turbines and their position (x,y) in meters. Figures B.4(a) and B.4(b) show the layout of two WPPs defined by a matrix rectangle form and by coordinates, respectively.

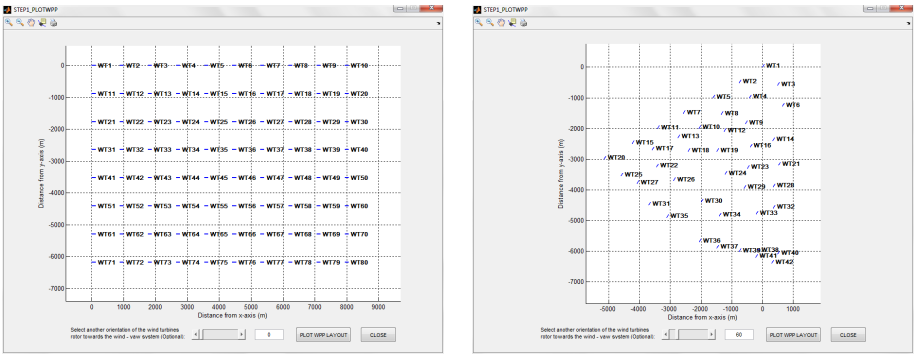

(a) (b)

Figure B.4: Example of two WPP layouts defined by a matrix rectangle form (a) and by coordinates (b).

- **Step 2 – Wind conditions definition:** In this step, certain wind conditions are established for the WPP whose layout has been previously defined. These wind conditions are characterized by specific wind speeds and wind directions. The wind speeds are obtained from the Weibull distribution function at the wind power plant location, while the wind directions are computed according to the wind rose function. It is assumed that the wind strikes the blades of each turbine under the same wind direction. The program allows the user to decide whether to estimate the incoming wind speed of each turbine using an unique Weibull distribution function which is independent of wind direction or considering a more realistic scenario with different Weibull distribution functions which depend on wind direction. The number of wind direction sectors used is defined by the user.

  Figure B.5 shows two different wind conditions (Weibull and wind rose distribution functions) considered for two particular examples. In Figure B.5(a) it has been assumed an unique Weibull distribution function regardless of the wind direction, whilst in Figures B.5(b) and B.5(c) it has been considered that the incoming wind speeds depends on the wind direction. For this particular case, it is characterized into four different sectors: North–West [N–W) 0°, South–West [W–S) 90°, South–East [S–E) 180° or North–East [E–N) 270°. Thereby, four different sets of Weibull parameters (dimensionless shape–k and scale–c) have been taken into consideration.

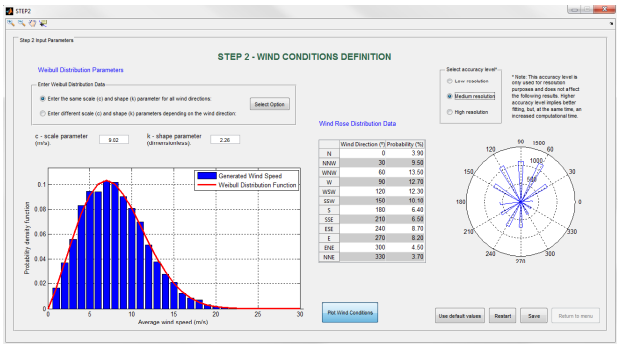

(a)

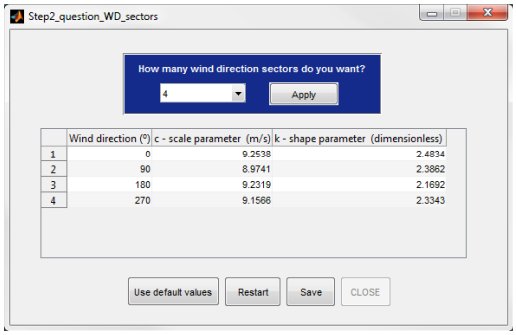

(b)

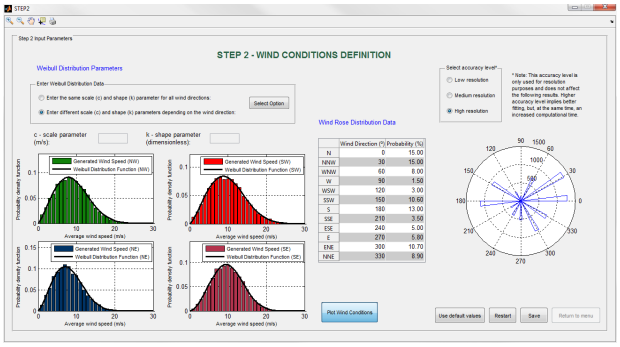

(c)

Figure B.5: Graphical User Interface (GUI) of the step 2 – Wind conditions definition: (a) Weibull is independent of wind direction. (b) and (c) Four Weibull distribution functions are considered depending on four wind direction sectors.

- **Step 3 – Wake effect consideration:** Once the WPP layout and its wind conditions are defined, the next step consists in computing the wind speeds of each wind turbine. In order to obtain more realistic values of wind speeds, the wake effect amongst wind turbines is considered [56,109,111,112,166]. A comprehensive wake model considering single, partial and multiple wakes within a wind power plant and taking into account different wind directions, is used. The Jensen's wake model [109] has been chosen for this study, as it provides adequate accuracy and reduced computational time. It is based on global momentum conservation in the wake downstream of the wind turbine and assumes that the wake downstream of the turbine expands linearly. According to this, the wind speeds facing the first turbines affected by the wake effect (v_1) can be computed as

$$v_1 = u\left[1 - \left(\frac{D}{D + 2mx_0}\right)^2 (1 - \sqrt{1 - C_t})\right] \tag{B.1}$$

where u is the free–stream wind, C_t is the thrust coefficient, m is the wake decay constant or opening angle which represents the effects of atmospheric stability, D is the rotor diameter of the wind turbine and x_0 indicates the distance between two turbines in the prevailing wind direction. These last two parameters have been defined previously in step 1. The program allows the user to decide how to enter the required data, whether manually or by using the default values. This option is available for all the steps. For instance, the thrust coefficient dependent on the free–stream wind speed ($C_t = f(v_1)$) data, shown in Figure B.6, correspond to those reported in [167] for a Vestas V80 turbine operating at Horns Rev wind farm. The wind speeds of the upstream turbines (free–stream wind) are randomly generated by means of a normal distribution function – $\mathcal{N}(\mu, \sigma^2)$, where the mean value ($\mu$) is obtained from step 2 using the Weibull distribution function.

Figures B.7(a) and B.7(b) show two examples of how the wake effect affects the wind turbines of both WPPs previously defined in step 1, when the wind comes from 0° (a) or 12° (b). It is worth noting that these specific wind directions are for visualization purposes only, since all the wind directions are taken into account.

Similarly, the wind speed of each wind turbine for the particular case shown in Figure B.7(b), is displayed in Figure B.8. Green boxes indicate the average wind speed of each row. As it can be seen, the wake

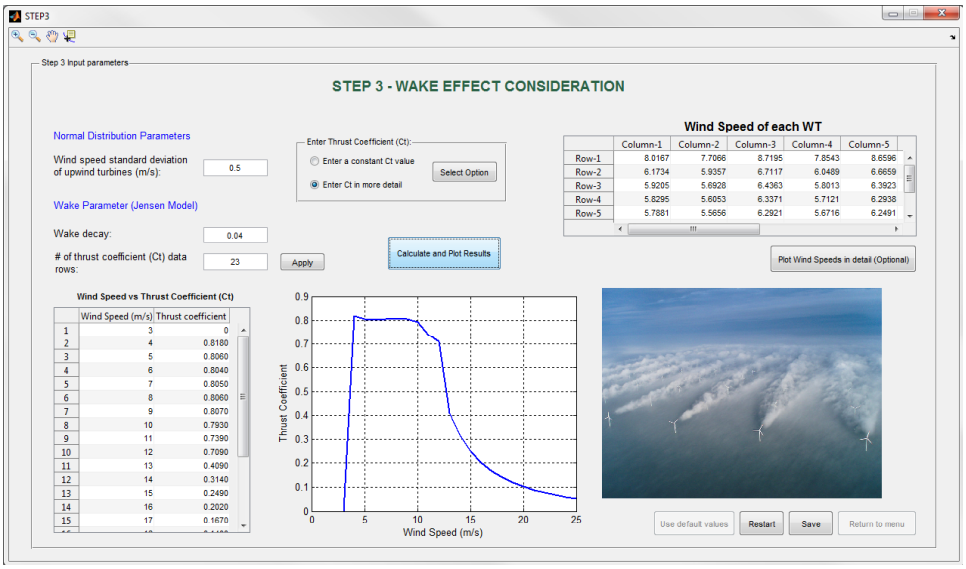

Figure B.6: Screenshot of the step 3 – Wake effect consideration.

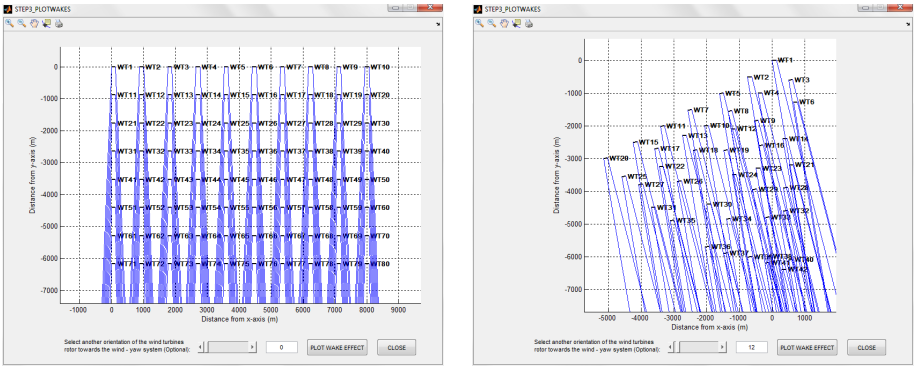

(a) (b)

Figure B.7: Example of how the wake effect affects the wind turbines of two WPPs when the wind is coming from 0° (a) or 12° (b).

effect shows a significant average wind speed reduction from the upwind turbines to those located at the second row (as it is the general tendency). The rest of turbines located from the third to the eighth row have similar wind speeds (slightly lower) than the turbines of the second row. It should be noted that the wind speeds of each turbine

are computed for all the wind directions and average wind speeds of the OWPP considered.

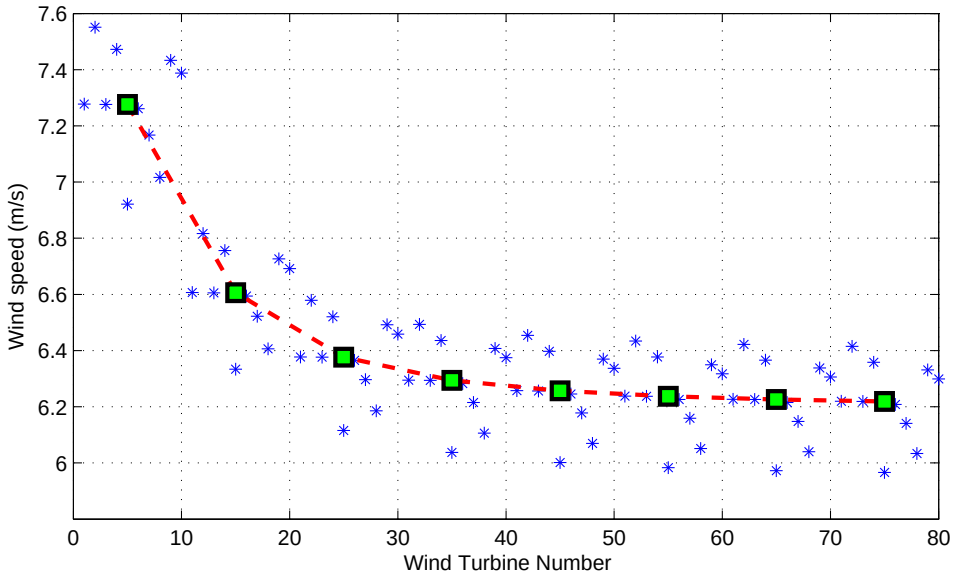

Figure B.8: Wind speeds of each turbine for a particular case example. Green boxes indicate the average wind speed of each row.

- **Step 4 – Optimum electrical frequency calculation:** A screenshot of the step 4 of the tool is displayed in Figure B.9. This step is only applied for the proposed SLPC–VF concept. As it has been previously mentioned, the set of optimum electrical frequencies imposed by the common SLPC are calculated to maximize the power generation of the aforementioned scheme. The optimization algorithm is explained in detail in Chapter 4. As it can be seen from Figure B.9, it depends on technical information, such as the air density, the cut–in, the rated and the cut–out speed of the wind turbines, the pair of poles of the synchronous generator, the gearbox ratio and the power coefficient C_P. It also depends on the wind speeds of each wind turbine computed in the previous step. It should be noted that a polynomial of degree N_{pol}, which is only dependent on the tip speed ratio λ, is considered to approximate the C_P coefficient. Figure B.9 also indicates an example of the resulting optimum electrical frequencies for a particular case study, according to their probability of occurrence.

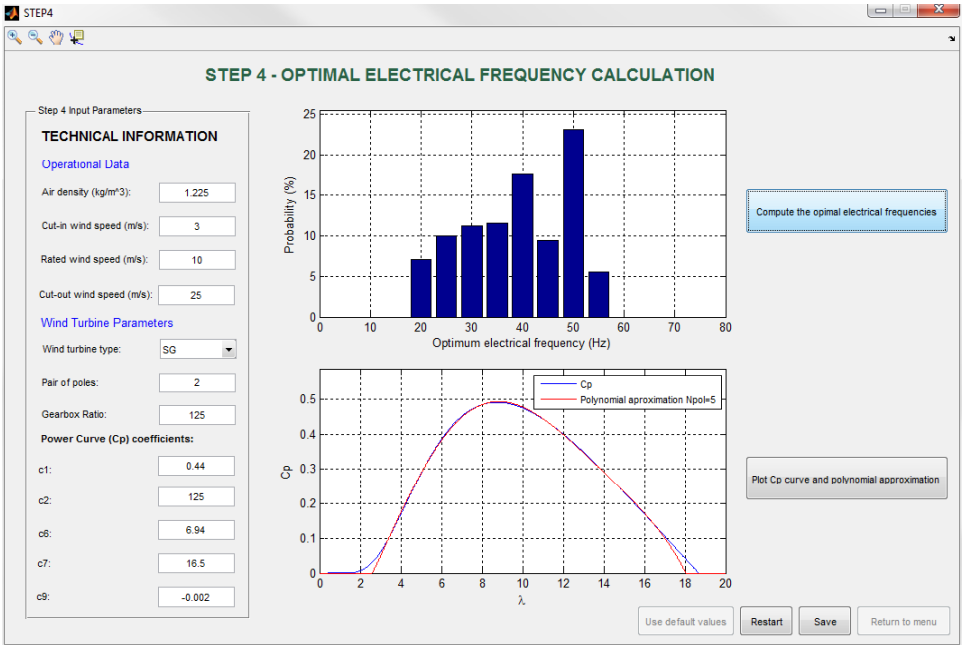

Figure B.9: Visualization of the step 4 – Optimum electrical frequency calculation.

Once the user have entered all the input parameters and the program has calculated the optimal set of frequencies as a function of the generation state of each turbine, the question dialog box of Figure B.10 appears asking the user to recalculate the wind speed values of each turbine and the optimum electrical frequencies according to a more realistic C_t based on the operational point of each wind turbine. Thus, the thrust coefficient is based on a tip–speed ratio dependence ($C_t = f(\lambda)$) rather than relying on the incoming wind speed ($C_t = f(v)$) as in step 3.

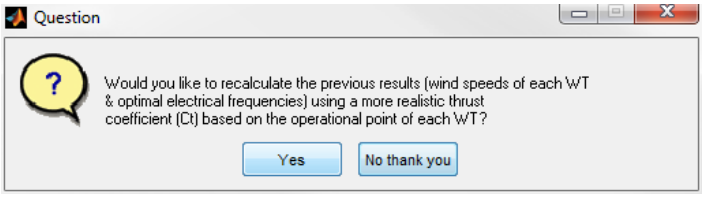

Figure B.10: Question dialog box displayed in step 4.

This process can not be executed previously in step 3 due to the unavailability of tip–speed ratio value upon the start of the steady state calculation (it is not possible to compute the operating point of each wind turbine without knowing its corresponding wind speed (step 3) and the electrical frequency of the collection grid (step 4)). Therefore, an iterative process needs to be carried out to find the proper operational point of each wind turbine.

- **Step 5 – Technical analysis:** According to the output data resulted from step 1 to 4, this button of the program menu carries out a technical analysis to evaluate the suitability of the proposed SLPC–VF topology in comparison to the conventional OWPP scheme. In order to provide an accurate assessment, different types of losses have been taken into consideration. As it can be seen in Figure B.11, these losses can be classified into two main groups: the steady-state losses (C_P losses and power flow losses) and the unavailability losses of the system due to the failure of certain equipment (corrective maintenance losses) or the partial or total stop of the installation during a fixed time for preventive maintenance purposes (preventive maintenance losses). All type of energy losses are calculated for several cases (varying the average wind speed and the wind direction) taking into account their probability of occurrence (according to the Weibull and Wind Rose distribution functions).

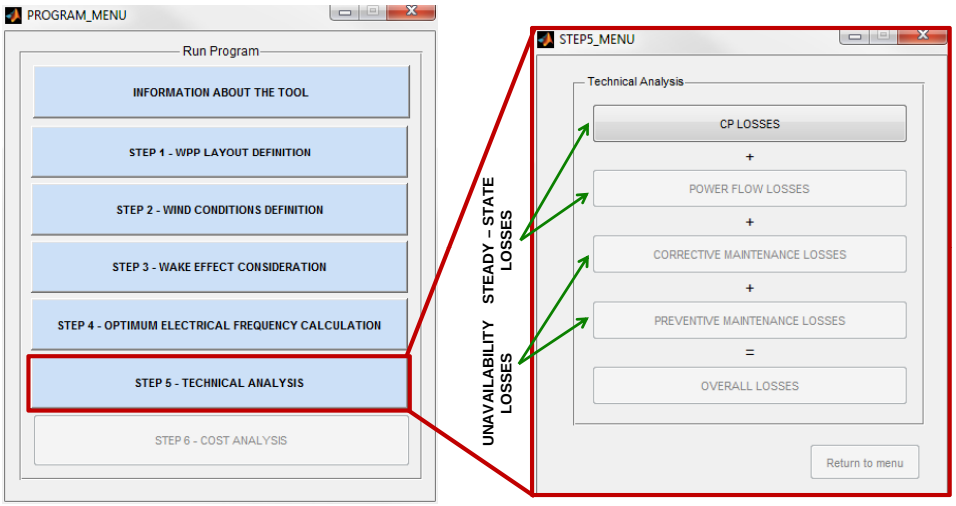

Figure B.11: Detailed menu of step 5 – Technical analysis.

– **C_P losses:** The C_P losses are explained in detail in Chapter 4 and refer to the inherent limitation of the proposed SLPC–VF topology. This type of losses are computed as the difference between the maximum available power a wind turbine could generated if it had a dedicated power converter ensuring its optimal operation and the actual power generated by such turbine. Figure B.12 shows the energy and power produced by the WPP as a function of the wind speed, as well as, the operational points of each wind turbine, for all the topologies analysed (MPC, SLPC–VF and SLPC–CF). As it is shown, the tool allows the user to choose between a constant frequency of 50 or 60 Hz for the analysis.

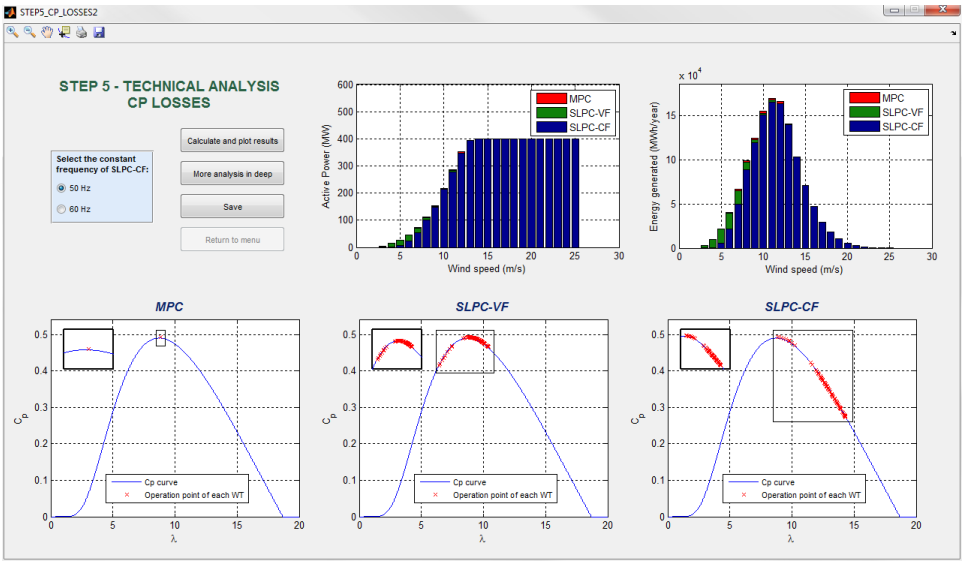

Figure B.12: Results of C_P losses calculation procedure (step 5).

In case the user desires to carry out further analysis regarding the C_P losses, an additional module is provided by the tool. Figure B.13 is displayed when clicking this optional button.

Thereby, the tool allows to study in detail the three following items:

1. Influence of wind speed variability on power generation efficiency analysis.
2. Influence of wind direction on power generation efficiency analysis.

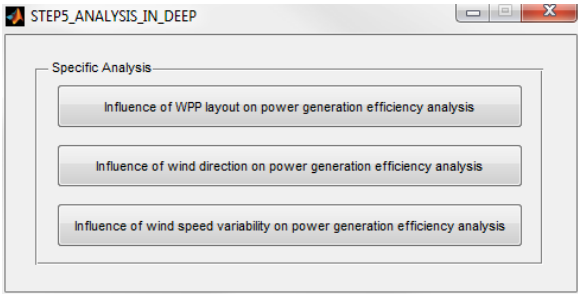

Figure B.13: Further analysis regarding the C_P losses calculation procedure (step 5).

3. Influence of WPP layout on power generation efficiency analysis.

The results of applying these specific analysis to a different study cases is shown in Figures B.14, B.15 and B.16. In order to assess the influence of wind speed variability within the WPP, different standard deviation from 0 to 3 m/s for the upstream wind turbines has been considered in Figure B.14. The WPP layout consists of a matrix rectangle of 4 columns and 5 rows of wind turbines spaced 7 D in both directions.

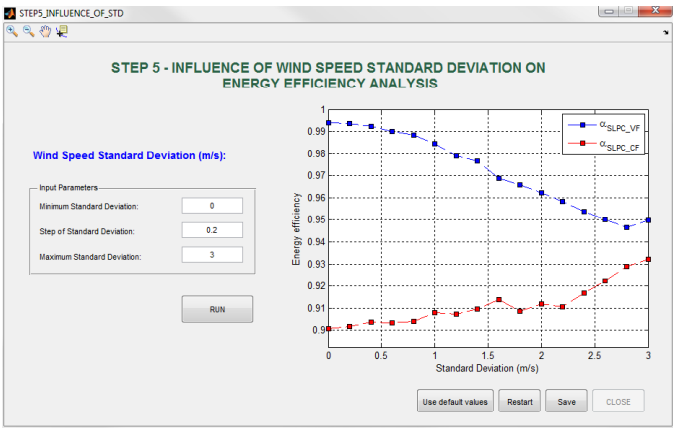

Figure B.14: Influence of wind speed variability on power generation efficiency analysis.

As it can be expected, the results show that the more wind speed

variability, the lower power generation efficiency achieved for the proposed SLPC–VF concept.

Regarding the second analysis in deep (influence of wind direction on power generation efficiency analysis), the four different wind roses shown in Figure B.15 has been considered for the same WPP layout of the previous case.

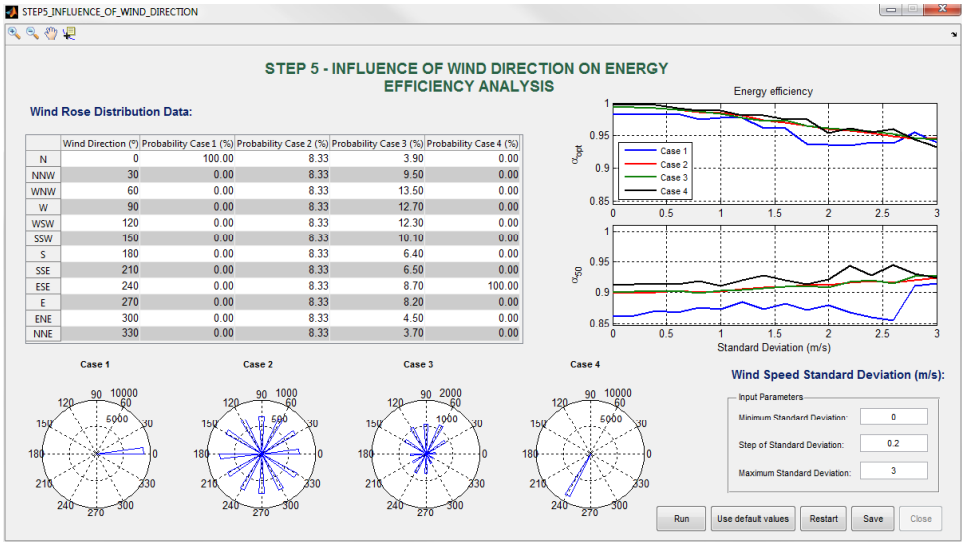

	Wind Direction (°)	Probability Case 1 (%)	Probability Case 2 (%)	Probability Case 3 (%)	Probability Case 4 (%)
N	0	100.00	8.33	3.90	0.00
NNW	30	0.00	8.33	9.50	0.00
WNW	60	0.00	8.33	13.50	0.00
W	90	0.00	8.33	12.70	0.00
WSW	120	0.00	8.33	12.30	0.00
SSW	150	0.00	8.33	10.10	0.00
S	180	0.00	8.33	6.40	0.00
SSE	210	0.00	8.33	6.50	0.00
ESE	240	0.00	8.33	8.70	100.00
E	270	0.00	8.33	8.20	0.00
ENE	300	0.00	8.33	4.50	0.00
NNE	330	0.00	8.33	3.70	0.00

Figure B.15: Influence of wind direction on power generation efficiency analysis.

As it can be seen, the wind rose referred to case 4 presents lower power generation efficiency compared to the other cases. This is because the wake effect that occurs for this particular WPP layout and the specific wind direction of 240° does not practically affects the downstream turbines.

Finally, Figure B.16 depicts the power generation efficiency obtained for the two different WPP layouts displayed in Figures B.16(a) and B.16(b). The WPP layout of Figure B.16(a) consists of 25 wind turbines laid out in a matrix rectangle form of 5 columns and 5 rows, while the WPP layout of Figure B.16(b) is based on the previous wind turbine arrangement, but removing the downstream wind turbines. The spacing between two nearby wind turbines for both cases is 7 rotor diameters (D) in both

directions.

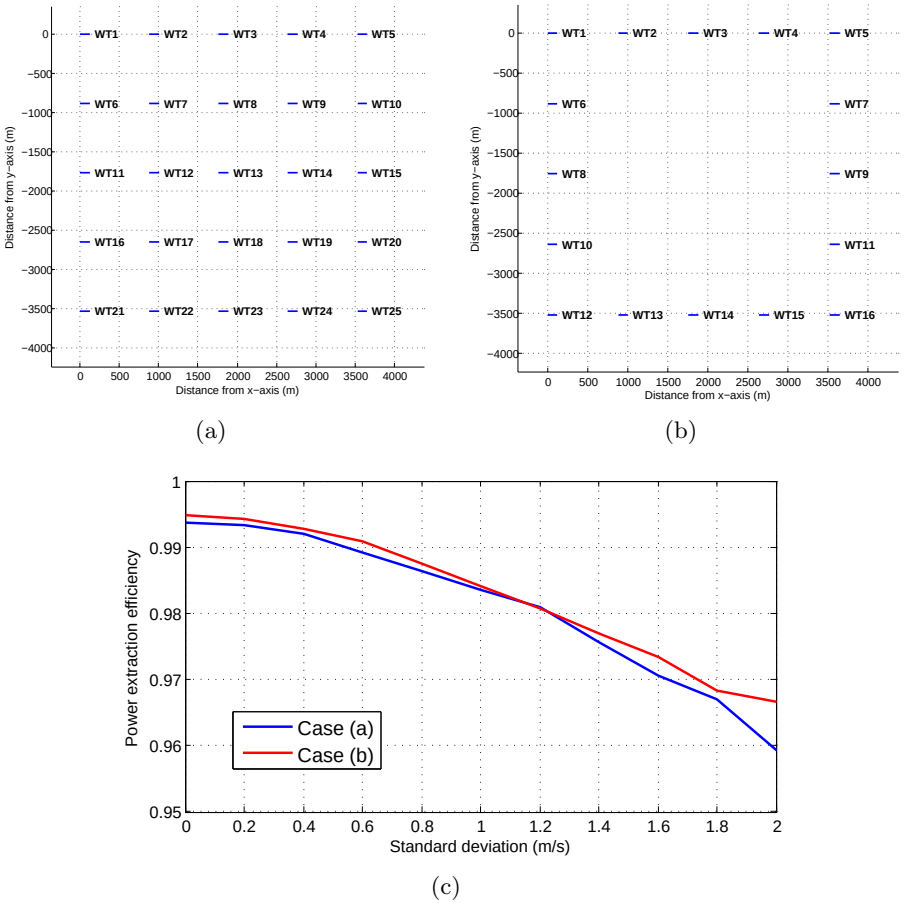

Figure B.16: (a) and (b) Two different WPP layouts analysed. (c) Influence of WPP layout on power generation efficiency analysis.

As it is shown, the C_P losses resulting for the WPP layout of Figure B.16(b) are the lowest, since its wake effect is reduced due to the avoidance of the downstream wind turbines.

– **Power flow losses:** The power flow or load flow losses occur as a result of the energy dissipated as a heat in the components encompassed within the wind power plant, such as cables, converters, transformers, among others. As in the previous case, this type of losses refers to steady–state losses, since the energy lost is

produced throughout the lifetime of the installation. This losses are obtained by means of load flow calculations considering the total energy generated by all the wind turbines of a WPP and the net energy measured at its grid connection point or Point of Common Coupling (PCC).

Figure B.17 presents the results obtained for both OWPP topologies analysed (conventional and SLPC–VF). Due to the current uncertainty of the power converters efficiency [124, 125], a sensitivity analysis is carried out to assess its influence on the power flow losses. Thus, three different scenarios (for the conventional case) are evaluated considering a back–to–back power converter efficiency (AC/DC and DC/AC) of 97%, 98% and 99%, respectively.

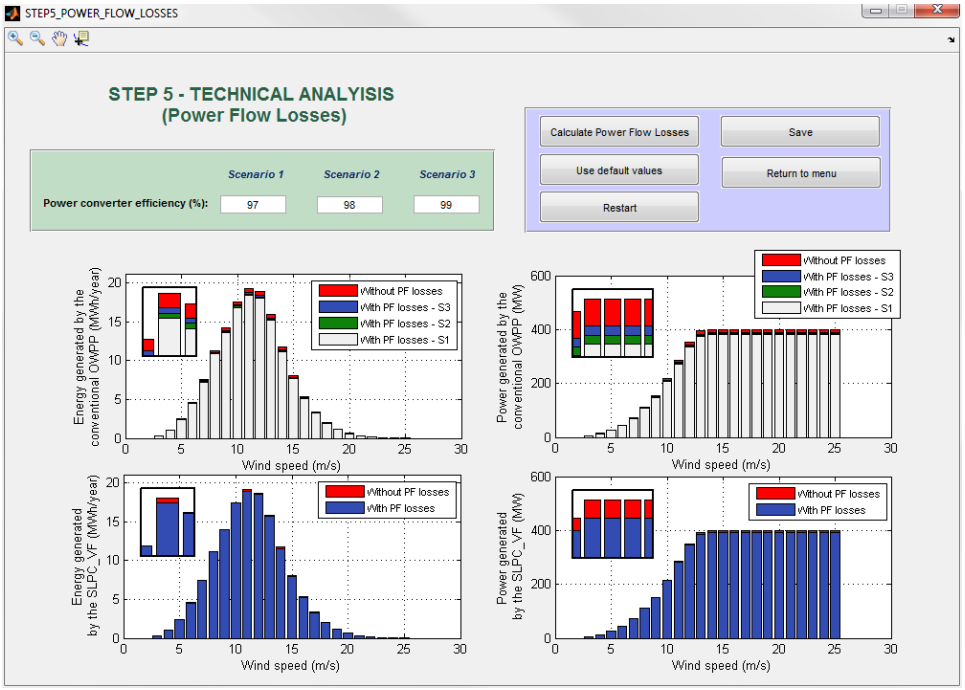

Figure B.17: Results of power flow losses calculation procedure (step 5).

– **Corrective maintenance losses:** Once the steady–state losses are computed, the next step of the tool is to consider the stoppages produced in the system due to corrective and preventive maintenance actions. Regarding the corrective maintenance losses

or unexpected losses, they occur as a result of unforeseen equipment failures, so that they are extremely important in offshore, since severe weather seasons can lead to long downtimes. The calculations of this type of losses are based on the reliability multi–state models [92]. These models considers that each component has several states of service and has a probability of malfunction in each state per year, which can be computed as

$$P_k = \binom{n}{k} \cdot A^{n-k} \cdot (1-A)^k \tag{B.2}$$

where n is the maximum number of states and A is the availability of the component given by

$$A = \frac{1}{1+\lambda \cdot MTTR} \tag{B.3}$$

where λ is the failure rate and MTTR the mean time to repair the fault of a particular component. Likewise, the unavailability or forced outage rate (FOR) is computed as $U = 1-A$. Analogously to the previous cases, the tool allows the user to enter data by two possible ways: by introducing the failure rate and MTTR of each component or by directly entering its unavailability.

Once the probability of occurrence of each state is known, the corrective maintenance losses can be obtained as follows:

$$E_{cml} = T \sum_{k=1}^{n} P_k^{cons} \; P_k \tag{B.4}$$

where P_k^{cons} is the power constrained or not delivered in each state due to the equipment failures and T is the period of time considered for the study.

Figure B.18 shows the power generated and the energy yield per year by the OWPP with and without considering the corrective maintenance or reliability losses, for the three OWPP topologies analysed: MPC, SLPC–VF and SLPC–CF.

It is worth pointing out that the model implemented in this tool computes the corrective maintenance losses for any generic OWPP layout with any wind conditions and taking into account the wake effect between wind turbines. Thus, it is necessary to identify which turbine is failing in each state, since each of them sees a different wind speed and, therefore, generates a distinct power.

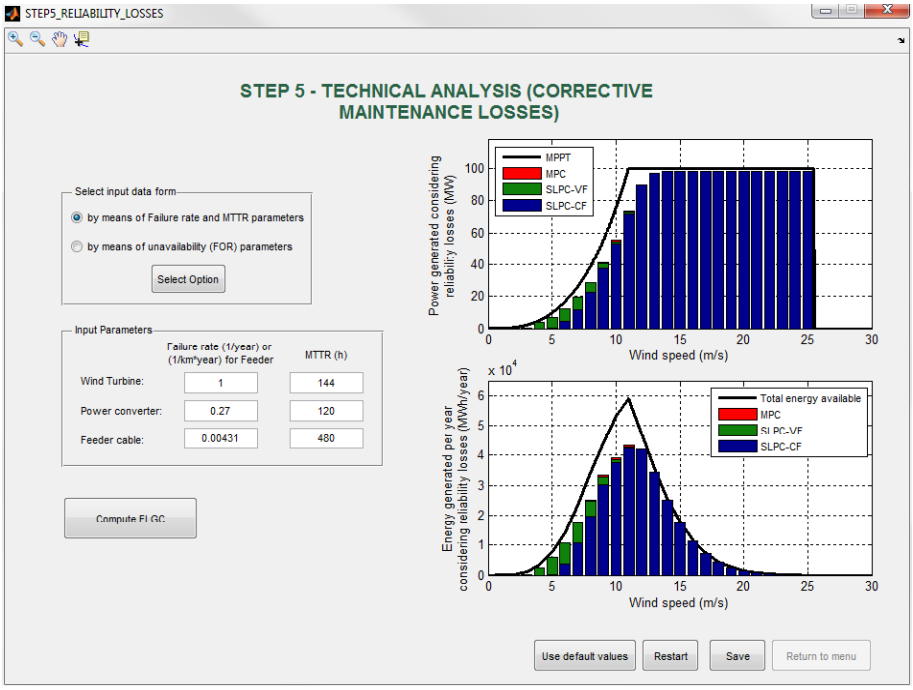

Figure B.18: Results of corrective maintenance losses calculation procedure (step 5).

  - **Preventive maintenance losses:** Finally, the preventive or planned maintenance losses are those that occur due to partial or total expected outages in the OWPP with the aim to extend the lifetime of its components. These interruption of service tend to be carried out in low wind periods to minimize the losses. A snapshot of this step is depicted in Figure B.19, considering 2400 hours of planned maintenance per year.
  - **Overall losses:** An example of the resulting breakdown of energy losses within the WPP, for the technical analysis performed in this step 5, is presented in Figure B.20. Five scenarios are considered for this study: MPC - S1, S2 or S3 (considering three different efficiencies of the individual power converters of each wind turbine), SLPC–VF and SLPC–CF.

- **Step 6 – Cost analysis:** Finally, in the step 6, this tool performs a cost assessment to evaluate the total cost of the three OWPP topolo-

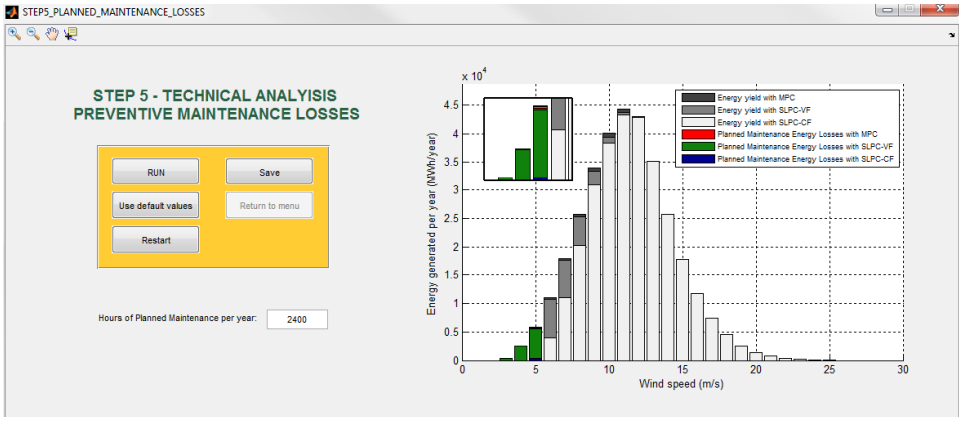

Figure B.19: Results of preventive maintenance losses calculation procedure (step 5).

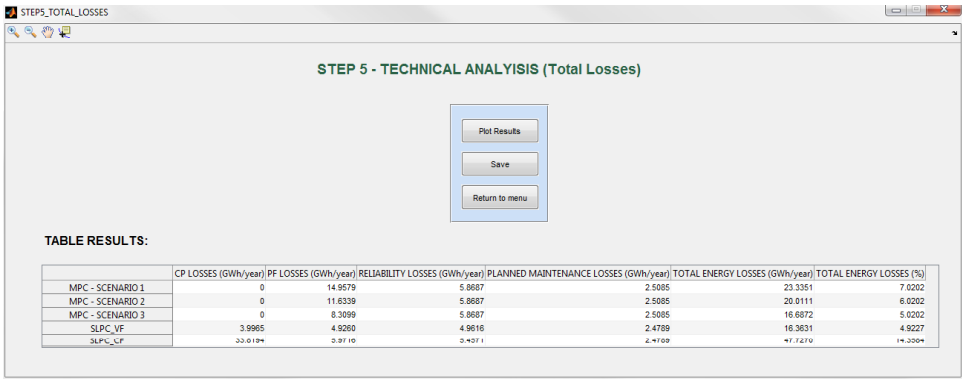

	CP LOSSES (GWh/year)	PF LOSSES (GWh/year)	RELIABILITY LOSSES (GWh/year)	PLANNED MAINTENANCE LOSSES (GWh/year)	TOTAL ENERGY LOSSES (GWh/year)	TOTAL ENERGY LOSSES (%)
MPC - SCENARIO 1	0	14.9579	5.8687	2.5085	23.3351	7.0202
MPC - SCENARIO 2	0	11.6339	5.8687	2.5085	20.0111	6.0202
MPC - SCENARIO 3	0	8.3099	5.8687	2.5085	16.6872	5.0202
SLPC_VF	3.9965	4.9260	4.9616	2.4789	16.3631	4.9227
SLPC_CF	33.0184	3.3719	5.4371	2.4708	47.7270	14.3564

Figure B.20: Visualization of step 5 – Technical analysis.

gies analysed: MPC, SLPC–VF and SLPC–CF. The cost functions used for this step (both for CAPEX and O&M cost) are detailed in Chapter 4. The total cost of an OWPP example is obtained in Figure B.21 considering both the capital costs of all the components involved in the OWPP (CAPEX), as well as, the energy cost produced during the lifetime of the installation. As it is concluded in Chapter 4, the proposed SLPC–VF reduces the total OWPP costs and, therefore, it is presented as an appealing WPP alternative compared to the conventional MPC topology.

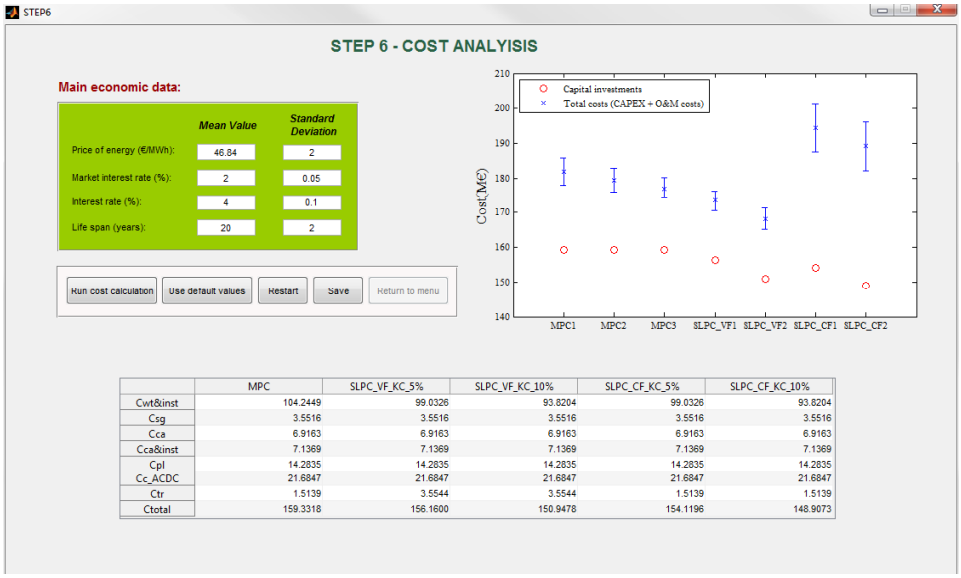

Figure B.21: Visualization of step 6 – Cost analysis.

B.3 Error handling

This section aims to show the robustness of the tool. Figure B.22 displays several examples of different error messages that automatically appear if the user is not entering the input data in the required format.

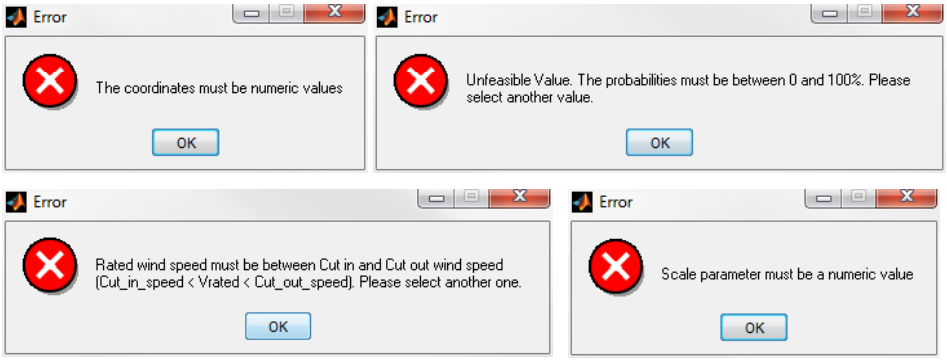

Figure B.22: Example of several error messages encountered by not entering the input data in the required format.

C

Notation of Chapter 5

Sets

$\mathcal{C}$	Set of submarine cables $c \in \mathcal{C}$
$\mathcal{I}$	Set of wind turbines $i, j \in \mathcal{I}$
$\mathcal{K}$	Set of power converters $k \in \mathcal{K}$
$\mathcal{S}$	Set of offshore platforms $s \in \mathcal{S}$

Parameters

$A_{k,s}$	Adjacency matrix between AC/DC converters $k \in \mathcal{K}$ and intermediate platforms $s \in \mathcal{S}$
C^E	Cost of energy [€/MWh]
C^C	Offshore cable installation cost [M€/km]
C^I	Cost of the AC inter–array cables [M€/km]
C^X	Cost of the DC export cables [M€/km]
C^K	Cost of an AC/DC power converter [M€/MW]
C^S	Cost of the offshore collector platforms [M€]
$D^{TT}_{i,j}$	Distance between wind turbines $i, j \in \mathcal{I}$ [km]
$D^{TC}_{i,k}$	Distance between wind turbines $i \in \mathcal{I}$ and AC/DC converters $k \in \mathcal{K}$ [km]
D^{PP}_{s}	Distance between collector platforms $s \in \mathcal{S}$ and the HVDC offshore platform [km]
$\overline{f}$	Maximum admissible electrical frequency [Hz]
$\underline{f}$	Minimal admissible electrical frequency [Hz]
$\overline{L}$	Lifetime of an offshore wind power plant [h]
N	Number of wind turbines
$\overline{N}_c$	Maximum number of wind turbines that can be connected to an

inter–array cable $c \in \mathcal{C}$

$\overline{P}_i$ Maximum available power of each wind turbine $i \in \mathcal{I}$ [MW]

$P_{i,k}$ Power generated by each wind turbine $i \in \mathcal{I}$ controlled by converter $k \in \mathcal{K}$ [MW]

P^N Nominal power of each wind turbine $i \in \mathcal{I}$ [MW]

Variables

- *Continuous positive variables:*

f_k Electrical frequency operated in each converter $k \in \mathcal{K}$ [Hz]

- *Binary decision variables*

h_s Offshore collector platform $s \in \mathcal{S}$

q_k Power converter $k \in \mathcal{K}$

$u_{i,j,k,c}$ Wind turbine $i \in \mathcal{I}$ connected to wind turbine $j \in \mathcal{I}$ controlled by converter $k \in \mathcal{K}$ through cable $c \in \mathcal{C}$

$x_{i,k,c}$ Wind turbine $i \in \mathcal{I}$ connected to converter $k \in \mathcal{K}$ by cable $c \in \mathcal{C}$

$y_{i,k}$ Wind turbine $i \in \mathcal{I}$ controlled by converter $k \in \mathcal{K}$

$z_{k,c}$ Converter $k \in \mathcal{K}$ connected to cable $c \in \mathcal{C}$

D

Parameters related to Chapter 6

Table D.1 depicts the parameters of the network used in Chapter 6 for modelling the overall system presented in Figure 6.8.

Table D.1: Parameters of the network presented in Figure 6.8 for the case study of Chapter 6.

Element	Parameter	Value	Unit
Line 1-0	L_{10}	1.5	km
	r_{10}	$0.0212 \cdot L_{10}$	Ω
	x_{10}	$0.1162389 \cdot L_{10}$	Ω
Line 2–0	L_{10}	1.0	km
	r_{20}	$0.0212 \cdot L_{20}$	Ω
	x_{20}	$0.1162389 \cdot L_{20}$	Ω
Line 3–0	L_{10}	1.5	km
	r_{30}	$0.0212 \cdot L_{30}$	Ω
	x_{30}	$0.1162389 \cdot L_{30}$	Ω
Transformer 1–0	r_{t10}	0.0484	Ω
	x_{t10}	0.726	Ω
Transformer 2–0	r_{t20}	0.0484	Ω
	x_{t20}	0.726	Ω
Transformer 3–0	r_{t30}	0.0484	Ω
	x_{t30}	0.726	Ω

Likewise, Table D.2 shows the parameters of each DFIG–base wind turbine used for the study.

Table D.2: Parameters of the DFIG–based wind turbines presented in Figure 6.8 for the case study of Chapter 6.

Element	**Parameter**	**Value**	**Unit**
DFIG	P_{rated}	1.5	MW
	r_s	$2.65{\cdot}10^{-3}$	Ω
	$r_r^{'}$	$2.63{\cdot}10^{-3}$	Ω
	x_{ls}	0.0530	Ω
	$x_{lr}^{'}$	0.0420	Ω
	x_m	1.72	Ω
	D	83.4	m
	N_{gr}	105	-
Wind Turbine	v_{rated}	10.1	m/s
	J_g	100	kg·m^2
	J_t	$3{\cdot}10^6$	kg·m^2
	c_1	0.73	-
	c_2	151	-
	c_3	0.58	-
	c_4	0.0002	-
	c_5	2.14	-
	c_6	13.2	-
	c_7	18.4	-
	c_8	-0.02	-
	c_9	-0.003	-